29 May 2009 | $10

Science

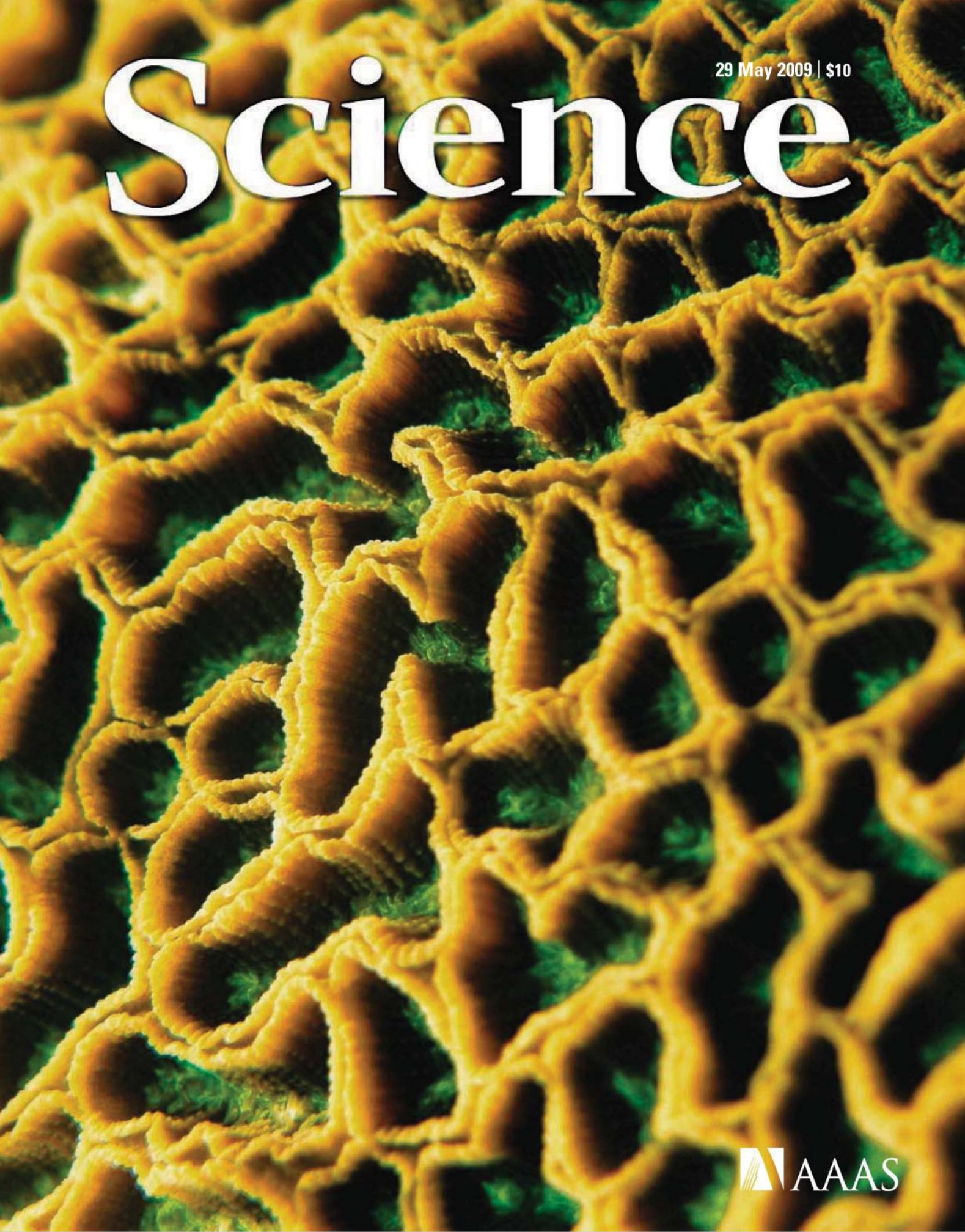

AAAS

Automated sample and assay technologies by QIAGEN

Free up your time

Automated solutions from sample to result:

- **The widest choice of sample processing protocols**
- **Low-, medium-, and high-throughput automation**
- **Leading solutions for molecular diagnostics**
- **Plug-and-play automated sample preparation**
- **Quantitative, real-time PCR detection**
- **Automated analysis of DNA fragments and RNA**
- **High-resolution sequence-based DNA detection and quantification**
- **HPV testing**

Making improvements in life possible — www.qiagen.com

QIAGEN®

Sample & Assay Technologies

AUTOprd1109S1WW

Submission deadline August 1

"It's truly exhilarating to be recognized for your hard work. This prize will motivate young generations of scientists and encourage new discoveries."

Dr. Christine Jacobs-Wagner
Grand Prize winner 1997

The GE & Science Prize for Young Life Scientists. Rewarding brilliance since 1995.

Imagine standing on the podium at the Grand Hotel in Stockholm, making your acceptance speech. Imagine joining the ranks of those published in Science magazine and having your essay on your work in molecular biology read by your peers around the world. Imagine taking part in a seminar with the other Prize winners and Nobel Prize laureates and discussing your work with leaders in the field. Imagine what you could do with the US$25,000 prize money. Imagine this brilliant start to your career and where it could lead you. Now stop imagining, and make it a reality.

Dr. Christine Jacobs-Wagner did just that. In 1997, she entered in the GE & Science Prize for Young Life Scientists and won the grand prize. So why not you? If you are one of those who were awarded a Ph.D in 2008, then submit your 1000-word essay by August 1, 2009. Your brilliant idea could well be on its way to building a better reality, for you and for those around you.

All the information you need awaits you at: www.gelifesciences.com/science

GE & Science Prize for Young Life Scientists

imagination at work

Science AAAS

For the purpose of this prize, molecular biology is defined as "that part of biology which attempts to interpret biological events in terms of the physico-chemical properties of molecules in a cell".

(McGraw-Hill Dictionary of Scientific and Technical Terms, 4th Edition).

GE Healthcare

Coordinate your application focus. Achieve greater operational efficiency.

GE Healthcare is focused on helping you develop efficient biopharmaceutical process flows and eliminating wasteful practices, taking your value stream to new frontiers. Through our wide range of technology platforms and services, upstream and downstream from process development to final manufacturing scale, GE Healthcare can connect you to the power of operational excellence.

Learn more about operational excellence at: www.gelifesciences.com/opex

imagination at work

GE Healthcare Bio-Sciences AB, a General Electric Company
Björkgatan 30, 751 84 Uppsala, Sweden

GE04-09. First printetd 09/2008.

EDITORIAL

NEWS OF THE WEEK

NEWS FOCUS

LETTERS

BOOKS *ET AL.*

EDUCATION FORUM

PERSPECTIVES

CONTENTS continued >>

page 1134

page 1146

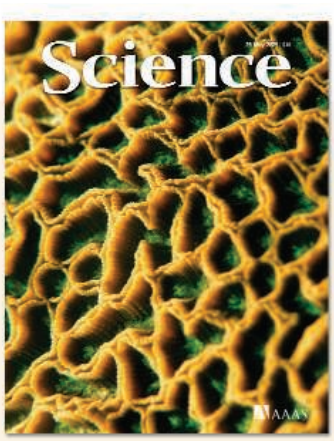

COVER

A close-up of the tropical coral *Favia speciosa*. The position and age of related fossil corals have been used to constrain the timing of sea-level rise during the penultimate deglacial period. The timing of past sea-level change, relative to potential forcings, can help determine the mechanisms of climate change and the speed of ice sheet collapse. See page 1186.

Photo: Getty Images

DEPARTMENTS

Published by AAAS

ACROSS THE HALL OR ACROSS THE GLOBE, REFMAN KEEPS EVERYBODY ON THE SAME PAGE.

No matter where you or your colleagues are in the world, so are your references. With Reference Manager,® you can collaborate with others on a network—or even the Web. Simplify your publishing with Reference Manager where you can search Internet databases, organize your references and create instant bibliographies. Plus, with newly added features you can do even more.

- Attach any file to a record and create a single Reference Manager repository
- Cite While You Write™ with a Reference Manager tab on the Word 2007 ribbon
- Use Web Publisher to collaborate with colleagues

Reference Manager 12

Download a free trial
www.refman.com

Simplify your life and keep everybody on the same page today.
800-722-1227 • 760-438-5526 • rs.info@thomson.com

THOMSON REUTERS

REVIEW

BREVIA

REPORTS

CONTENTS continued >>

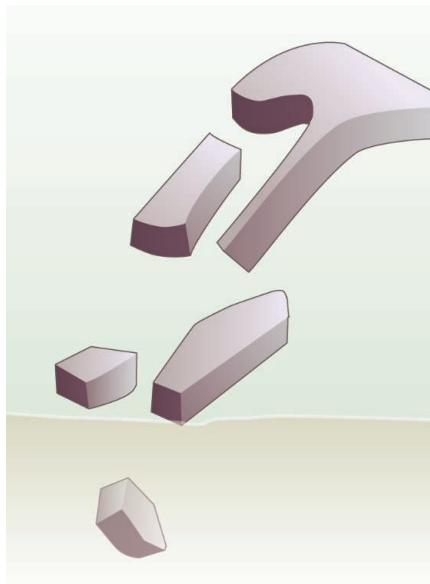

pages 1152 & 1173

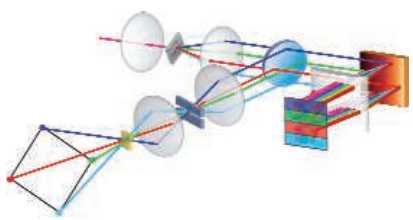

page 1169

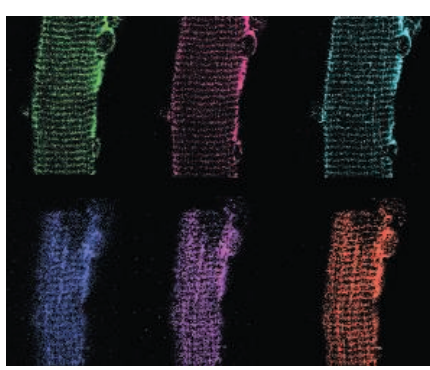

pages 1155 & 1192

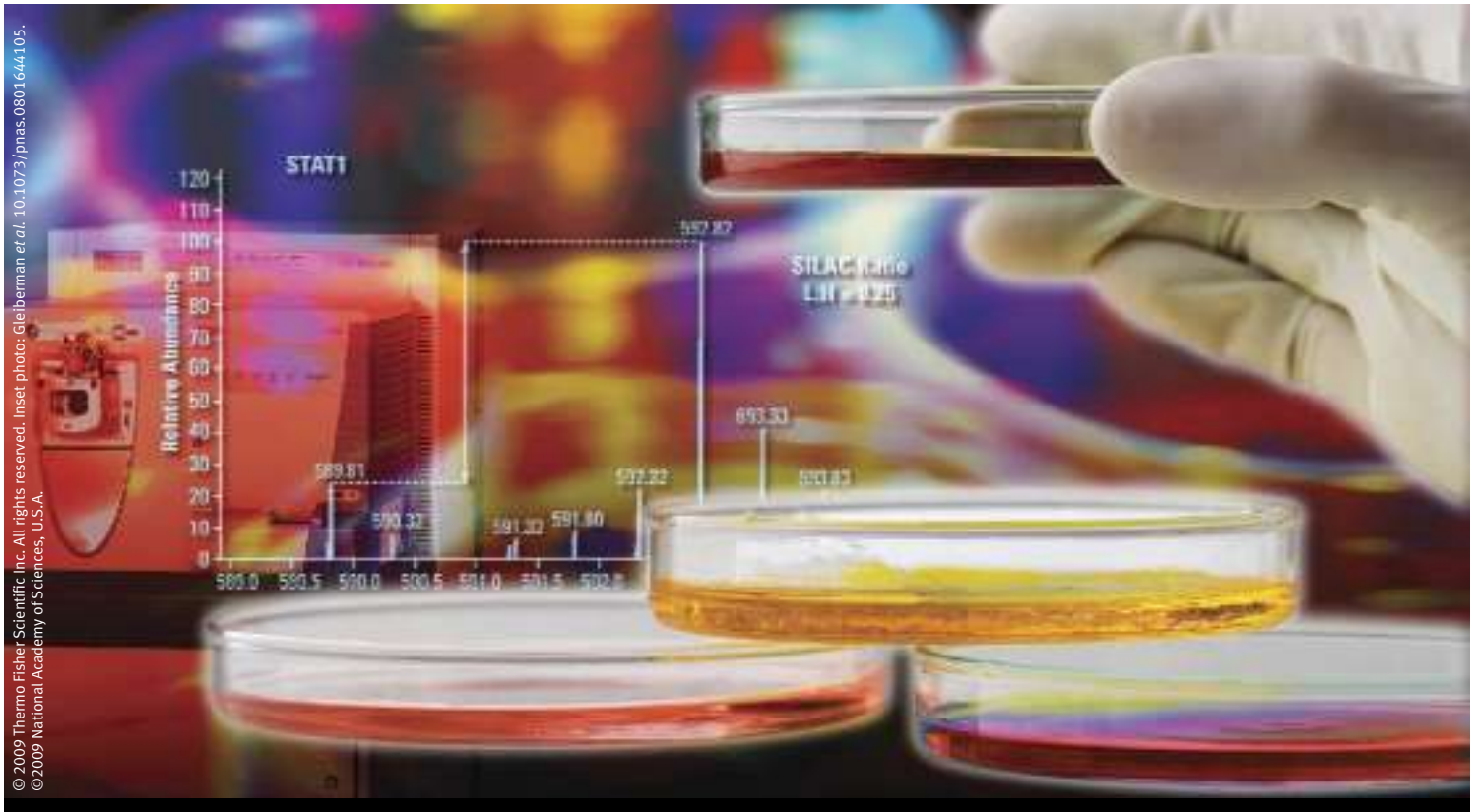

What's up (or down) with your protein? SILAC can tell you, even in your stem cells.

New Thermo Scientific Pierce SILAC (stable isotope labeling using amino acids in cell culture) Kits identify and quantify relative differential changes in protein samples. These kits and Thermo Scientific Mass Spectrometry Instruments provide a complete and validated workflow, making protein quantitation easier, faster and more reproducible.

SILAC applications:

- Quantitative analysis of protein changes and proteins for which there are no antibodies available
- Proteomic profiling in normal and diseased cells
- Quantitative identification of 100s to 1,000s of proteins in one experiment

Visit www.thermo.com/silac or call 800-874-3723 or +1-815-968-0747 to request our SILAC technical brochure.

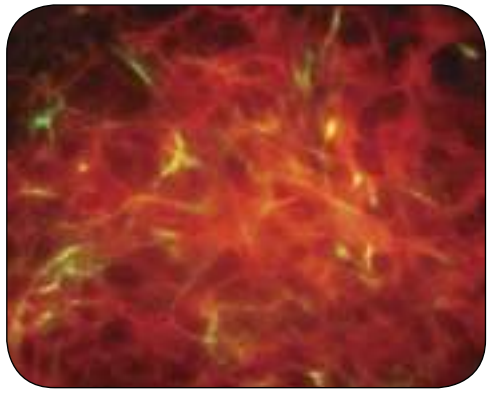

Now available for stem cells!
Pierce SILAC Kits are ideal for quantitative analysis of differential protein expression for tissue culture and stem cell lines.

Moving science forward

Thermo SCIENTIFIC
Part of Thermo Fisher Scientific

SCIENCEONLINE

SCIENCEXPRESS
www.sciencexpress.org

Antigenic and Genetic Characteristics of Swine-Origin 2009 A(H1N1) Influenza Viruses Circulating in Humans
R. J. Garten et al.

Evolutionary analysis suggests a triple reassortant avian-to-pig origin for the 2009 influenza A(H1N1) outbreak.
10.1126/science.1176225
>> News story p. 1127

Essential Role of the Glycosyltransferase Sxc/Ogt in Polycomb Repression
M. C. Gambetta et al.

The Polycomb-group protein super sex combs acts to glycosylate a second Polycomb repressor protein.
10.1126/science.1169727

IL-21R on T Cells Is Critical for Sustained Functionality and Control of Chronic Viral Infection
A. Fröhlich et al.

Thymus cells of the immune system require the cytokine interleukin-21 to control chronic viral infections.
10.1126/science.1172815

Structure and Mechanism of an Amino Acid Antiporter
X. Gao et al.

The architecture of a membrane protein channel helps explain how *Escherichia coli* survive the acidic conditions of the stomach.
10.1126/science.1173654

Ventral Tegmental Area BDNF Induces an Opiate-Dependent–Like Reward State in Naïve Rats
H. Vargas-Perez et al.

A growth factor involved in neuronal plasticity alters neurons in a specific area of the brain after chronic exposure to opioid drugs.
10.1126/science.1168501

Venezuelan Science at Risk
C. Bifano
10.1126/science.1176733

TECHNICALCOMMENTS

Comment on "A Large Excess in Apparent Solar Oblateness Due to Surface Magnetism"
J. R. Kuhn et al.

full text at www.sciencemag.org/cgi/content/full/324/5931/1143-b

Response to Comment on "A Large Excess in Apparent Solar Oblateness Due to Surface Magnetism"
M. D. Fivian et al.

full text at www.sciencemag.org/cgi/content/full/324/5931/1143-c

SCIENCENOW
www.sciencenow.org
Highlights From Our Daily News Coverage

Compact Discs Enter the Fifth Dimension
A new technology could boost the storage capacity of conventional optical discs 10,000-fold.

Martian Water Had Antifreeze
Dissolved minerals might have kept liquid flowing on the Red Planet.

Tumors Trigger Cancer Blues
Biochemical signals from tumors cause anxiety and depression in rats.

SCIENCESIGNALING
www.sciencesignaling.org
The Signal Transduction Knowledge Environment

EDITORIAL GUIDE: "Omic" Risk Assessment
M. B. Major and R. T. Moon
Integration of multiple data sets is the key to hit validation.

RESEARCH ARTICLE: System-Wide Changes to SUMO Modifications in Response to Heat Shock
F. Golebiowski et al.
SUMO is redistributed among many targets to mediate both short- and long-term signaling events.

RESEARCH ARTICLE: Bruton's Tyrosine Kinase Revealed as a Negative Regulator of Wnt–β-Catenin Signaling
R. G. James et al.
Combining an siRNA screen with a small-molecule screen reveals a negative pathway regulator.

REVIEW: CD36, a Scavenger Receptor Involved in Immunity, Metabolism, Angiogenesis, and Behavior
R. L. Silverstein and M. Febbraio
Signaling by CD36 is ligand and cell specific and is implicated in multiple human diseases.

EVENTS
Plan your travel with this list of meetings, conferences, and workshops related to cell signaling.

SCIENCECAREERS
www.sciencecareers.org/career_magazine
Free Career Resources for Scientists

In Person: Breaking All the Rules
R. Ley
Two-scientist couples do not have to compromise their research careers.
>> News story p. 1136

A Tale of Two Pathologists
A. Sasso
Terrill Topps and Dorkina Myrick have two careers, three doctoral degrees, and one life together.

Finding His Voice by Silencing Genes
E. Pain
Molecular biologist Olivier Voinnet early on bet his career on gene silencing—and won.

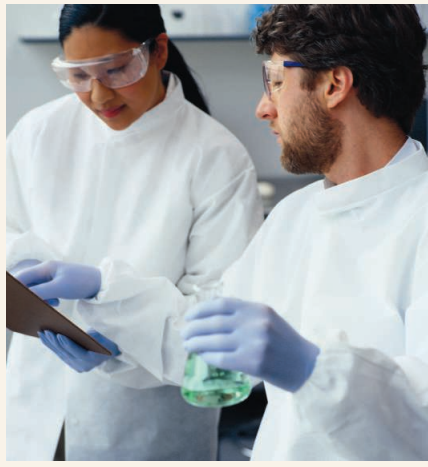

SCIENCECAREERS
Balancing two science careers in one family.

SCIENCEPODCAST
www.sciencemag.org/multimedia/podcast
Free Weekly Show

Download the 29 May *Science* Podcast to hear about assessing Arctic oil and gas reserves, bat white-nose syndrome, your letters to *Science*, and more.

ORIGINSBLOG
blogs.sciencemag.org/origins
A History of Beginnings

SCIENCEINSIDER
blogs.sciencemag.org/scienceinsider
Science Policy News and Analysis

SCIENCE (ISSN 0036-8075) is published weekly on Friday, except the last week in December, by the American Association for the Advancement of Science, 1200 New York Avenue, NW, Washington, DC 20005. Periodicals Mail postage (publication No. 484460) paid at Washington, DC, and additional mailing offices. The title SCIENCE is a registered trademark of the AAAS. Domestic individual membership and subscription (51 issues): $146 ($74 allocated to subscription). Domestic institutional subscription (51 issues): $835; Foreign postage extra: Mexico, Caribbean (surface mail) $55; other countries (air assist delivery) $85. First class, airmail, student, and emeritus rates on request. Canadian rates with GST available upon request, GST #1254 88122. Publications Mail Agreement Number 1069624. **Printed in the U.S.A.**

Change of address: Allow 4 weeks, giving old and new addresses and 8-digit account number. **Postmaster:** Send change of address to AAAS, P.O. Box 96178, Washington, DC 20090–6178. **Single-copy sales:** $10.00 current issue, $15.00 back issue prepaid includes surface postage; bulk rates on request. **Authorization to photocopy** material for internal or personal use under circumstances not falling within the fair use provisions of the Copyright Act is granted by AAAS to libraries and other users registered with the Copyright Clearance Center (CCC) Transactional Reporting Service, provided that $20.00 per article is paid directly to CCC, 222 Rosewood Drive, Danvers, MA 01923. The identification code for *Science* is 0036-8075. *Science* is indexed in the *Reader's Guide to Periodical Literature* and in several specialized indexes.

AAAS
ADVANCING SCIENCE, SERVING SOCIETY

CREDIT: (*SCIENCE* CAREERS) PHOTODISC

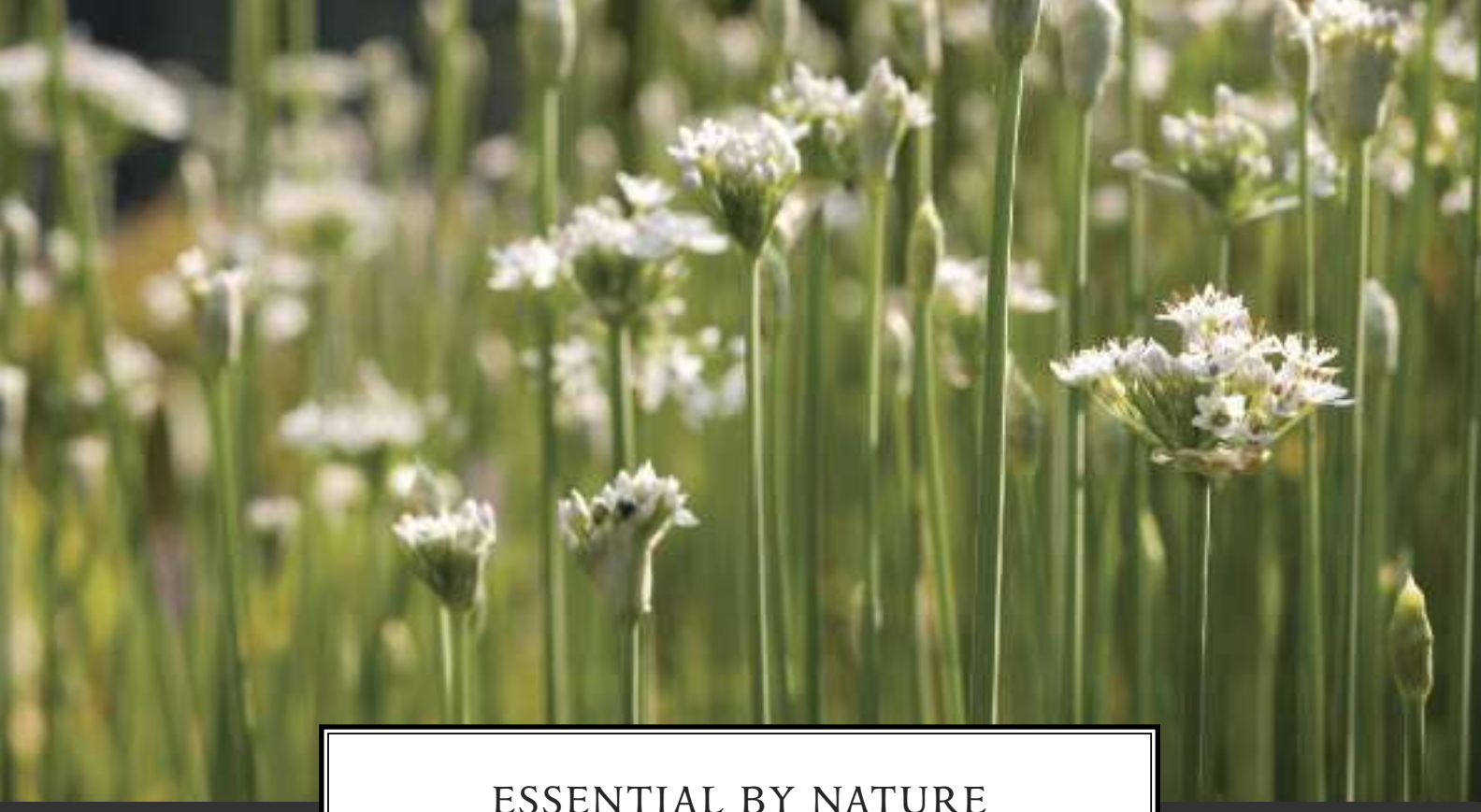

ESSENTIAL BY NATURE

The 2009|10 NEB Catalog & Technical Reference

This year's catalog features minireviews focused on renewable energy generated from natural resources.

Highlights

- High Fidelity (HF) Restriction Enzymes - the next generation in restriction enzyme technology
- A comprehensive offering of PCR reagents
- The latest innovation in competent cells for protein expression
- An extensive selection of markers and ladders for DNA, RNA and protein
- A new gene expression and cellular analysis section showcasing a powerful protein labeling technology unique to NEB
- A range of expression systems, including a novel kit for cell-free expression
- Tools for glycobiology
- Tools to enable RNA research
- A substantial technical reference section

To request a copy, visit www.neb.com

NEW ENGLAND BioLabs® Inc.
enabling technologies in the life sciences

CLONING & MAPPING	DNA AMPLIFICATION & PCR	RNA ANALYSIS	PROTEIN EXPRESSION & ANALYSIS	GENE EXPRESSION & CELLULAR ANALYSIS

www.neb.com

Arctic Energy Reserves >>

The Arctic consists of approximately equal fractions of terrain above sea level, continental shelves with depths less than 500 meters, and deep ocean basins that have been mostly covered in ice. While the deep ocean regions probably have limited petroleum reserves, the shelf areas are likely to contain abundant ones. Based on the limited amount of exploration data available, **Gautier *et al.*** (p. 1175) have constructed a probabilistic, geology-based estimate of how much oil and gas may be found. Approximately 30% of the world's undiscovered gas, and 13% of its undiscovered oil, may be found north of the Arctic Circle. Advances in the technology of hydrocarbon recovery, as well as vanishing ice cover around the North Pole, make the Arctic an increasingly attractive region for energy source development, although the existing reserves are probably not large enough to shift current production patterns significantly.

Quantum-Enhanced Measurement

The single electron spin in a molecule, atom, or quantum dot precesses in a magnetic field and so can be used as a magnetic field sensor. As the number of spins in a sensor increases, so too does the sensitivity. Quantum mechanical entanglement of the spin ensemble should then allow the sensitivity to increase much more than would be expected from a simple increase in the number of individual spins in the ensemble. Using the highly symmetric molecule, trimethyl phosphite, a molecule containing a central P atom surrounded by nine hydrogen atoms, **Jones *et al.*** (p. 1166, published online 23 April) quantum mechanically entangled the 10 spins (or qubits) to generate a nearly 10-fold enhancement in the magnetic field sensitivity. The results pave the way for the further development of quantum sensors.

The Power of Green

Carbon dioxide is produced both by fossil fuel burning and by deforestation and other land-use changes. Limiting both sources of CO_2 is necessary if we are to curb global warming. **Wise *et al.*** (p. 1183) use an integrated assessment model to explore the consequences of limiting atmospheric CO_2 concentrations at levels between 450 and 550 parts per million through a combination of fossil-fuel emissions reductions and land-use modification. Land-use modification strategies reduce the cost of limiting atmospheric CO_2 concentrations, but can make crop prices rise and transform human diets, for example, when people consume less beef and other carbon-intensive protein sources. The rate at which crop productivity is improved has a strong influence on emissions from land-use change. Thus, the technology used for growing crops is potentially as important for limiting atmospheric CO_2 as are approaches like CO_2 capture and storage.

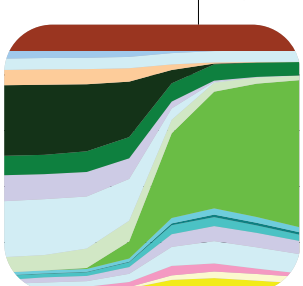

CREDITS (TOP TO BOTTOM): DAVID W. HOUSEKNECHT/USGS; WISE *ET AL.*

The Close and Personal Biome

Fortunately, our skin is readily accessible for ecological studies of the microbial communities that influence health and disease states. **Grice *et al.*** (p. 1190) present a metagenomic survey of body sites from 10 healthy human individuals sampled over time. Although, altogether 18 phyla were discovered, only a few predominated. The most diverse communities were found on the forearm and the least behind the ear, but between people the microorganisms living behind the knees, in the elbow, and behind the ear were most similar. This finding might have some bearing on the common occurrence of atopic dermatitis in these zones, although no similar relationship was discerned between skin microbial flora and psoriasis.

Tearing the Plate

Recent seismic data show a widely variable geometry of subduction: Some plates penetrate deep into the mantle; others bend and become horizontal at 670 kilometers near a prominent phase boundary. **Obayashi *et al.*** (p. 1173; see the Perspective by **Nolet**) provide a detailed view of a situation where subduction of juxtaposed plates in the western Pacific, in somewhat different directions, seems to have ripped a gash in the plates starting at a depth of about 300 kilometers. The geometry of the gash provides information on the past evolution of this plate boundary.

Middle Permian Extinction

A major extinction in the Middle Permian 260 to 270 million years ago preceded the huge end-Permian extinction. **Wignall *et al.*** (p. 1179) present a detailed analysis of the Middle Permian event from rocks in southwest China. The extinction coincided with extensive nearby volcanic eruptions. A major drop in carbon isotope values followed the extinction event, implying massive disruption of the carbon cycle.

Early Riser

How glacial-interglacial cycles and the long-term variability of sea level depend on the amount of energy received by Earth from the Sun is unclear. **Thomas *et al.*** (p. 1186, published online 23 April; see the cover) report results from fossil corals found in Tahiti that indicate that sea level began to rise when insolation at 65° North latitude was near a minimum, not after it had begun to rise, as predicted by the Milankovitch theory. In contrast, the timing of the last deglaciation agrees well with the Milankovitch theory. Thus, glacial cycles do not behave as simply as the Milankovitch theory suggests.

Continued on page 1116

Published by AAAS

Continued from page 1115

GLUT4, Clathrin, and Glucose

In human muscle, the GLUT4 glucose transport pathway responds to insulin and is responsible for 70 to 90% of human glucose clearance. In the basal metabolic state, GLUT4 is sequestered away from the cell surface and is released from an intracellular membrane compartment in response to insulin. This GLUT4 membrane pathway is defective in type II diabetes. **Vassilopoulos *et al.*** (p. 1192; see the Perspective by **Orme and Bogan**) now describe a function for CHC22 clathrin, a second isoform of clathrin that is present in humans and not in mice. CHC22 participates in the biogenesis of the intracellular compartment that sequesters the GLUT4 glucose transporter for insulin-stimulated release. Because CHC22 is restricted to humans, mice differ in their pathways that control glucose metabolism, which may restrict the utility of the mouse as a model system in assessing glucose metabolism and diabetes.

Anti-Aging

Several human neurodegenerative diseases, such as Alzheimer's and Huntington's, are caused by aberrant protein aggregation. These disorders typically develop after the fifth decade of life, suggesting a connection with the aging process. In a number of different species, life span can be extended by dietary restriction and reduced insulin and insulin-like growth factor–1 (IGF-1) signaling. These pathways can also decrease toxic protein aggregation, mechanistically linking aging with proteotoxic diseases. While searching for regulators of proteotoxicity in *Caenorhabditis elegans*, **Mehta *et al.*** (p. 1196, published online 16 April) found that reduction of the von Hippel–Lindau tumor suppressor homolog VHL-1 significantly increased life span and enhanced resistance to proteotoxicity. VHL-1 is an E3 ubiquitin ligase that negatively regulates the hypoxic response, and animals grown under hypoxic conditions lived longer. This alternative longevity pathway was distinct from both dietary restriction and insulin/IGF-1–like signaling.

One, Two, Three

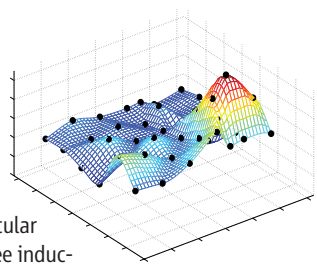

Synthetic biologists take much of their inspiration from computing and electrical engineering, attempting to gain programmability in cells using analogous genetic circuits. **Friedland *et al.*** (p. 1199; see the Perspective by **Smolke**) have constructed complementary *Escherichia coli* synthetic gene networks that keep track of prior molecular events to function as counters. These modular devices count up to three induction events over a range of frequencies and could be extended to higher numbers. Similar devices may find application in multi-event processes of cell biology, bioengineering, and, potentially, therapeutics.

Stepping Back to Go Forward

Insight into the mechanism of transcription has come from crystal structures of actively transcribing RNA polymerase II complexes in the pre- and posttranslocation states. RNA polymerase also backtracks on the DNA template. Backtracking by only a few residues is reversible, but longer backtracking leads to arrest that is relieved by cleavage of the transcript by the transcription elongation factor SII (TFIIS). Now **Wang *et al.*** (p. 1203) report x-ray structures of backtracked ternary complexes and of a backtracked complex bound to a noncleaving mutant of TFIIS. The structures show a defined one-residue, backtracked state supporting the idea that RNA polymerase oscillates between backward and forward motion during active transcription. Mismatched residues disfavor forward translocation, increasing the lifetime of the backtracked state and facilitating cleavage by TFIIS. Thus, TFIIS-induced cleavage is likely to provide an important proofreading function during transcription.

Attention and Synchrony

Neural activity in the visual cortex becomes synchronized with attention and other behavioral states. However, the source of this synchrony is still unknown. **Gregoriou *et al.*** (p. 1207) tested the hypothesis that synchronized activity from the frontal eye field is one of the causes of the synchrony in monkey visual cortical area V4 during attention. With attention, neural activity in area V4 synchronized with frontal eye field activity when a stimulus fell in a joint receptive field, but did not do so when the fields were not overlapping.

CREDIT: FRIEDLAND *ET AL.*

Published by AAAS

Kavita M. Berger is project director for the Center for Science, Technology, and Security Policy at AAAS.

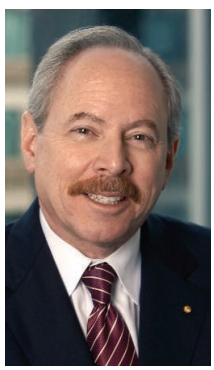

Alan I. Leshner is chief executive officer of AAAS and executive publisher of *Science*.

New Rules for Biosecurity

BIOSECURITY REGULATIONS ARE BACK ON THE TABLE AGAIN, AND REVISED POLICIES COULD have broad implications for the entire scientific enterprise. In response to an Executive Order by President Bush on 9 January 2009, an interagency working group is reviewing all U.S. laws and regulations governing the conduct of research with biological materials that are potential security threats—so-called select agents. The issue at hand concerns how to balance the risks associated with select agents against ensuring that the public can reap the full potential benefits of research on them. The report of the working group is expected in July, and it will propose an array of policies for improving laboratory biosafety and security, from defining what select agents are and who has access to them, to specifying the oversight of laboratories that handle them. Done well, the review could greatly improve biosecurity and the climate for biological research in the United States and abroad. Done poorly, there could be a variety of unintended negative consequences, including over-restricted access to vital resources and a constrained ability to collaborate internationally on a broad range of topics.

The existing U.S. biosecurity policies have hindered international collaboration and they need revision. For example, in 2003, expert scientists had to plead with the U.S. government to keep the virus responsible for severe acute respiratory syndrome (SARS) off the select agent list, so as to facilitate international collaboration. This resulted in rapid identification of the causative agent and the development of the first vaccine against SARS. Most recently, Mexican officials sent the first 200 samples of H1N1 influenza to Canada for identification rather than to the U.S. Centers for Disease Control and Prevention, because of the U.S. rules on importing biological materials.

The interagency working group is not operating in a vacuum. For example, in 2008, the National Science Advisory Board for Biosecurity (NSABB) issued recommendations for adjusting the existing select agent classification system to accommodate scientific advances. Last month, the NSABB released recommendations for determining who can get access to select agents; that is, the rules for "personnel reliability." The U.S. National Academies have also charged a committee to review personnel reliability, and its report is expected in September.

The Executive Branch is not alone in worrying about biosecurity; Congress is considering several bills. Among them is one in preparation by the Senate Homeland Security and Governmental Affairs Committee that addresses security concerns of high-containment laboratories. Other bills governing criteria for including agents on the select agent list, biosafety training, and developing a voluntary reporting system for laboratory exposures to these agents have also been introduced in Congress.

The definitions, rules, and regulations that emerge from these activities will not only affect the accessibility, handling, and transport of almost 80 select agents. New policies may also affect both the climate for U.S. science and how inviting America will be to international scientific guests. The ability to perform beneficial research on many materials beyond known select agents that could have both positive and ill-intended uses—such as nanomaterials, immunomodulatory molecules, or the products of synthetic biology—could also be severely constrained.

The White House Office of Science and Technology Policy (OSTP) and the interagency working group are seeking input from the scientific community and the broader public as they carry out their review, and it is critical that scientists respond as quickly as possible, well before the report is finalized in early July.* This is the most comprehensive review of biosecurity research policies since 2001, when biodefense funding and programs substantially increased. The scientific community should seize this opportunity to help guide policy decisions that will have broad ramifications for both national security and the climate for science in the United States and globally.

– Kavita M. Berger and Alan I. Leshner

*Recommendations to OSTP and the interagency working group can be made before 12 June 2009 at http://cstsp.aaas.org/BiosecurityComment.html, a Web site created by the American Association for the Advancement of Science (AAAS), the publisher of *Science*.

10.1126/science.1176543

Published by AAAS

GEOLOGY

Fighting for Exposure

Geologic maps provide information on the distribution of rocks and deposits currently exposed on Earth's surface. It has been recognized for some time that fewer older rocks are exposed than younger ones; only a few outcrops remain from Earth's earliest history, more than 3.5 billion years ago. Wilkinson *et al.* separate out rocks deposited at the surface (volcanic and sedimentary rocks) from those that form in the crust (metamorphic and intrusive rocks representing chilled magma bodies) and show how the exposures today of rocks of different ages and origination depth reflect geologic history and processes. On average, about 6.5% of continental land is covered by new sediments or volcanic deposits every million years. Young metamorphic and plutonic rocks are rare; the average age of metamorphic rocks (nearly 1 billion years) is older than that of intrusive rocks (about 200 million years), reflecting the greater difficulty in exposing deeper rocks. Together, the data imply that long-term rates of burial and uplift are about equal at roughly 0.5 km per million years, in reasonable agreement with rates measured by other techniques in many specific orogenic belts. — BH

Geol. Soc. Am. Bull. **121**, 760 (2009).

CELL BIOLOGY

Sorting Out Rafts

During membrane trafficking within eukaryotic cells, lipids and membrane-bound proteins are sorted and transported to their intracellular destinations, generating organelles with distinctive compositions of proteins and lipids. One major trafficking nexus is the trans-Golgi network (TGN), where proteins that have traversed the early stages of the secretory pathway are collected before transport to the plasma membrane. The plasma membrane is enriched in sphingolipids and sterols in comparison to internal membranes; how this sorting of lipid components occurs remains poorly understood, although lipid rafts—organized microdomains that include sterols, sphingolipids, saturated glycerophospholipids, and proteins—have been proposed to play a role.

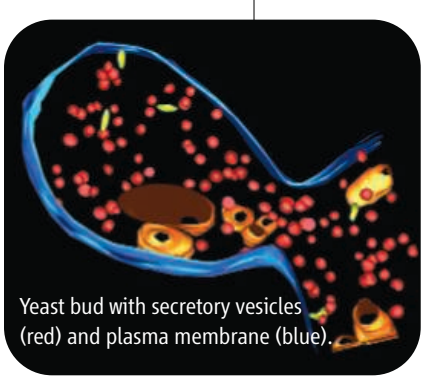

Yeast bud with secretory vesicles (red) and plasma membrane (blue).

Klemm *et al.* recovered post-Golgi secretory vesicles from yeast cells that had been modified so as to accumulate these vesicles in the bud. These vesicles were then subjected to a shotgun lipidomics procedure, which confirmed that the vesicles were enriched in ergosterol and sphingolipids. Thus, the TGN, in addition to acting as a sorting station for proteins, can indeed sort lipids. The vesicles also exhibited a more ordered lipid structure than the Golgi membrane, consistent with the idea that lipid rafts contribute to lipid sorting. — SMH

J. Cell Biol. **185**, 601 (2009).

APPLIED PHYSICS

Cloud Gazing

For persons deep in thought, or perhaps simply wishing to pass time peacefully, looking up at the clouds has been an idle pursuit practiced for millennia. To those in the communication business, though, cloud gazing and characterization are serious issues. There is an increasing demand for higher data transfer rates between Earth-based communication stations and space-based satellites. Optical signals provide the fastest possible route of communication between two points. However, Earth-to-space optical links can be hampered by signal attenuation or obstruction from cloud cover. Nugent *et al.* have developed a thermal infrared cloud imaging system that can characterize and classify clouds above a communication station. With this established ability to determine the optical depth of particular clouds, they can apply their technique toward keeping the communication channels open even when there is partial or thin cloud cover. — ISO

Opt. Express **17**, 7862 (2009).

BIOTECHNOLOGY

A Bright Idea

The identification of single-nucleotide polymorphisms (SNPs) across individuals can contribute to characterizing underlying genetic variation in humans, DNA damage, and potential biomarkers of disease. However, it is currently challenging to detect SNPs in real time at room temperature and without the addition of a battalion of exogenous reagents.

Xiao *et al.* have engineered a detection system consisting of a single strand of DNA, which folds into a discontinuous double helix composed of three seven–base pair stems and incorporates both a fluorescent moiety and a quencher. When this molecule finds a perfectly complementary piece of DNA, it forms a detector-target hybrid, disrupting the proximity of

CREDITS (TOP TO BOTTOM): MICHAEL MISCHENKO (NASA/GISS); KLEMM *ET AL.*, *J. CELL BIOL.* **185**, 601 (2009)

Published by AAAS

the fluorophore and quencher, and yielding a fluorescent burst. It can discriminate between targets differing by only a single nucleotide, and hybridization to the target occurs within 30 min at room temperature and in the presence of a 64-fold excess of a singly mismatched competitor. — LMZ

Angew. Chem. Int. Ed. **48**, 10.1002/anie.200900369 (2009).

MOLECULAR BIOLOGY

Start and Stop Signals

Human sleeping sickness is caused by the parasitic protozoan *Trypanosoma brucei*, which is transmitted when the tsetse fly bites. As in prokaryotes, the genes in this microorganism are arrayed in large polycistronic transcription units. Despite this unusual organization relative to what is seen in most other eukaryotes, the promoter elements where RNA polymerase II and its associated transcription factors bind have largely eluded identification.

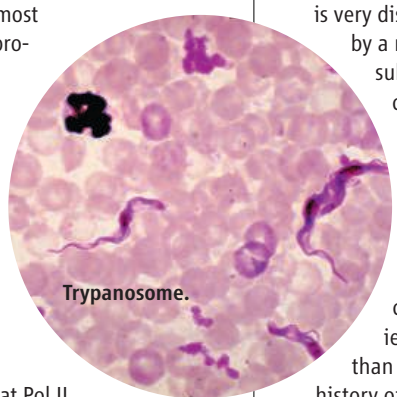

Trypanosome.

Using the ChIP-seq method, which involves DNA sequencing of chromatin immunoprecipitations, Siegel *et al.* suggest that Pol II transcription factors look for histone modifications and histone variants. Levels of acetylated histone H4 (H4K10ac) are higher at Pol II transcription start sites. In addition, histone variants H2BV and H2AZ, as well as the bromodomain protein BDF3, colocalize with H4K10ac. The authors also show that decoration with these histone variants correlates with less stable nucleosomes, which would allow for their displacement by transcription initiation complexes. A third feature defined by histone variants, in this instance H3V and H4V, is the transcription termination regions. Finally, G-rich stretches in the sense strand upstream of H4K10ac sites may serve as directional signposts for transcription. Hence, *Trypanosoma* appears to use nucleotide sequence and chromatin structure to mark starts and stops. — BAP

Genes Dev. **23**, 1063 (2009).

ASTRONOMY

Signs of Old Age

Researchers believe that most of the stars we see today were formed during short but very vigorous bursts in early dusty galaxies. Although the starlight emanating from these galaxies is concealed by dust, bright submillimeter emission, which traces dust heated by the ultraviolet light from newly formed stars, can be detected at great distances. Using data from a new submillimeter survey combined with radio, infrared, and optical observations, Coppin *et al.* found the most distant submillimeter galaxy yet detected: Its redshift of 4.76 suggests that intense star formation occurred in galaxies within 1 billion years of the Big Bang. In a different study, Cowie *et al.* used a submillimeter interferometer to determine an accurate position for HDF 850.1, a submillimeter galaxy discovered in 1998. Their data are not consistent with any previous optical identifications; no counterpart can be found even in the Hubble Deep Field, one of the deepest optical images available. Combined with information at other wavelengths, this result implies that HDF 850.1 is very distant, most probably characterized by a redshift greater than 4. Very few submillimeter galaxies have been confirmed at these high redshifts, but their absence could simply be the result of the observational difficulties involved in determining their positions. Both groups of authors suggest that galaxy formation models could be challenged if such galaxies proved to be more common than anticipated at early times in the history of the universe. — MJC

Mon. Not. R. Astron. Soc. **395**, 1905 (2009); *Astrophys. J.* **697**, L122 (2009).

MICROBIOLOGY

Surely Something Is Missing

Cell division in the parasitic protozoan *Entamoeba histolytica* is an olio of polyploidy, multiple nuclei, and failed cell division. In the latest of a series of studies, Mukherjee *et al.* show that multiple genome complements arise because the amoeba lacks the regulatory components present in higher eukaryotes that not only control the structure of the microtubule organizing centers but also couple cytokinesis with nuclear division. The result in *Entamoeba* is the formation of multipolar spindles, which segregate multiple copies of the chromosomes simultaneously into unequal daughter cells. This phenomenon can be observed both in vitro and within the intestine, and there does not appear to be strong selective pressure to constrain genomic exuberance, possibly because having such lax controls is an advantage for a parasite that may encounter sudden shifts in its environment. — CA

PLoS Negl. Trop. Dis. **3**, 3409 (2009).

CREDIT: DR. MAE MELVIN/CDC

Published by AAAS

www.sciencemag.org

Science

1200 New York Avenue, NW
Washington, DC 20005
Editorial: 202-326-6550, FAX 202-289-7562
News: 202-326-6581, FAX 202-371-9227
Bateman House, 82-88 Hills Road
Cambridge, UK CB2 1LQ
+44 (0) 1223 326500, FAX +44 (0) 1223 326501

Subscription Services For change of address, missing issues, new orders and renewals, and payment questions: 866-434-AAAS (2227) or 202-326-6417, FAX 202-842-1065. Mailing addresses: AAAS, P.O. Box 96178, Washington, DC 20090-6178 or AAAS Member Services, 1200 New York Avenue, NW, Washington, DC 20005

Institutional Site Licenses please call 202-326-6755 for any questions or information

Reprints: Author Inquiries 800-635-7181
Commercial Inquiries 803-359-4578

Permissions 202-326-7074, FAX 202-682-0816

Member Benefits AAAS/Barnes&Noble.com bookstore www.aaas.org/bn; AAAS Online Store www.apisource.com/aaas/ code MKB6; AAAS Travels: Betchart Expeditions 800-252-4910; Apple Store www.apple/eppstore/aaas; Bank of America MasterCard 1-800-833-6262 priority code FAA3YU; Cold Spring Harbor Laboratory Press Publications www.cshlpress.com/affiliates/aaas.htm; GEICO Auto Insurance www.geico.com/landingpage/go51.htm?logo=17624; Hertz 800-654-2200 CDP#343457; Office Depot https://bsd.officedepot.com/portalLogin.do; Seabury & Smith Life Insurance 800-424-9883; Subaru VIP Program 202-326-6417; VIP Moving Services www.vipmayflower.com/domestic/index.html; Other Benefits: AAAS Member Services 202-326-6417 or www.aaasmember.org.

science_editors@aaas.org	(for general editorial queries)
science_letters@aaas.org	(for queries about letters)
science_reviews@aaas.org	(for returning manuscript reviews)
science_bookrevs@aaas.org	(for book review queries)

Published by the American Association for the Advancement of Science (AAAS), *Science* serves its readers as a forum for the presentation and discussion of important issues related to the advancement of science, including the presentation of minority or conflicting points of view, rather than by publishing only material on which a consensus has been reached. Accordingly, all articles published in *Science*—including editorials, news and comment, and book reviews—are signed and reflect the individual views of the authors and not official points of view adopted by AAAS or the institutions with which the authors are affiliated.

AAAS was founded in 1848 and incorporated in 1874. Its mission is to advance science, engineering, and innovation throughout the world for the benefit of all people. The goals of the association are to: enhance communication among scientists, engineers, and the public; promote and defend the integrity of science and its use; strengthen support for the science and technology enterprise; provide a voice for science on societal issues; promote the responsible use of science in public policy; strengthen and diversify the science and technology workforce; foster education in science and technology for everyone; increase public engagement with science and technology; and advance international cooperation in science.

Information for Authors
See pages 807 and 808 of the 6 February 2009 issue or access www.sciencemag.org/about/authors

Learn how current events are impacting your work.

***Science*Insider, the new policy blog from the journal *Science*,** is your source for breaking news and instant analysis from the nexus of politics and science.

Produced by an international team of science journalists, *Science*Insider offers hard-hitting coverage on a range of issues including climate change, bioterrorism, research funding, and more.

Before research happens at the bench, science policy is formulated in the halls of government. Make sure you understand how current events are impacting your work. Read *Science*Insider today.

www.ScienceInsider.org

*Science*Insider

Breaking news and analysis from the world of science policy

Science
AAAS

Working toward a better future?

So are we.

quality health selection delivery support

Diabetes. Heart disease. Cancer.

Every dollar spent on JAX® Mice & Services is an investment in our shared future. It supports our common research goals and helps to sustain the many valuable mouse models and resources available only from The Jackson Laboratory.

Ask for the J.

www.jax.org
1-800-422-6423

The Jackson Laboratory

SPECIAL CAREER FEATURE

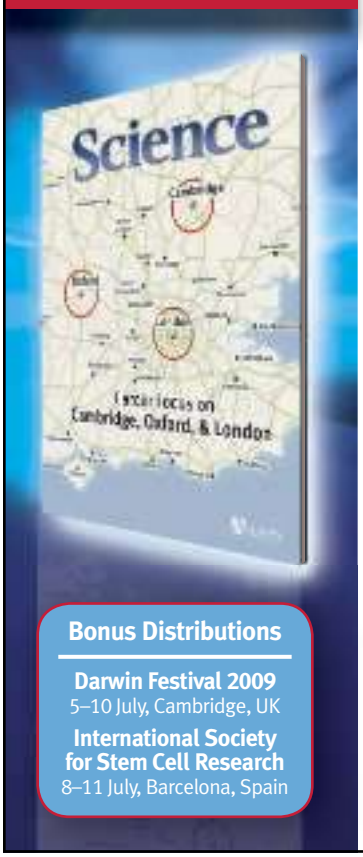

Bonus Distributions

Darwin Festival 2009
5–10 July, Cambridge, UK

International Society for Stem Cell Research
8–11 July, Barcelona, Spain

Career Focus on Cambridge, Oxford, and London

Issue date
26 June
Reserve ad space by 9 June

The power of *Science* is in the journal's 131,000 weekly subscribers and 700,000 weekly readers. In our 26 June issue we will use this power to highlight the state of the scientific job market in and around these renowned British seats of learning.

Contact: Alex Palmer
Telephone:
+44 (0) 1223 326 500
E-mail:
ads@science-int.co.uk

Science Careers
From the journal *Science* AAAS

ScienceCareers.org

Scientific-Grade Spectroscopy for Life Sciences

QUANTUM EFFICIENCY TO 90% IN MINIMAL FOOTPRINT

The Ocean Optics QE65000 is a scientific-grade spectrometer that combines enhanced UV response and high sensitivity in a robust, low-noise instrument.

Its proprietary BRDF bench coating improves stray light performance and helps make the QE65000 more sensitive for demanding applications such as fluorescence, Raman, DNA sequencing and tissue analysis.

The QE65000 features a back-thinned FFT-CCD detector and TE-cooling, which enables integration times from 8 milliseconds to as long as 1,500 seconds.

The QE65000 can be configured with a choice of gratings, entrance aperture sizes, order-sorting filters and other optical bench accessories.

The QE65000 starts at under $12,000 and you can find more information at www.oceanoptics.com/products/qe65000.asp .

Ocean Optics

www.oceanoptics.com | info@oceanoptics.com | +1 727-733-2447

Eppendorf & Science Prize for

Neurobiology

$25,000 Prize

Get recognized!

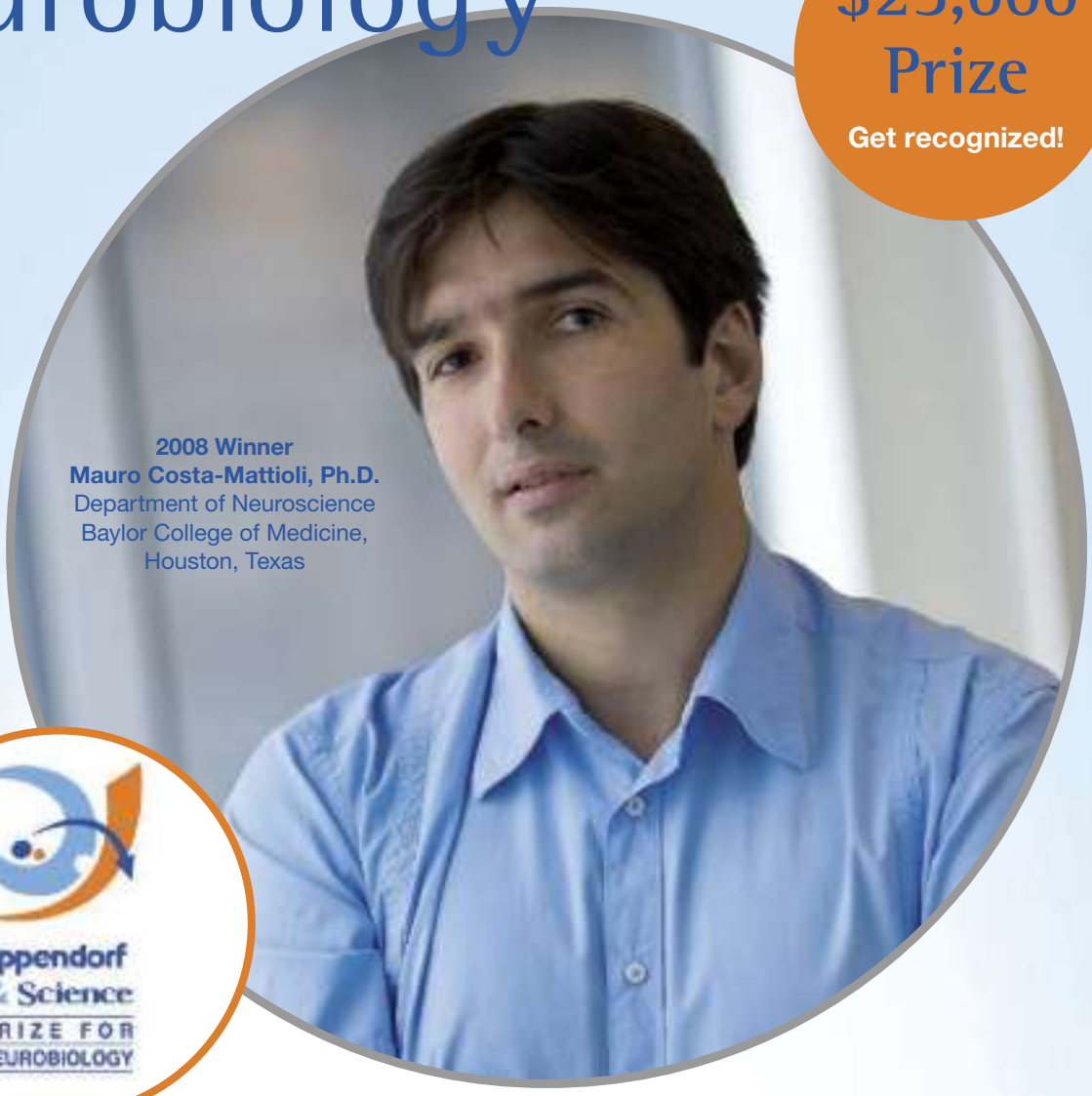

2008 Winner
Mauro Costa-Mattioli, Ph.D.
Department of Neuroscience
Baylor College of Medicine,
Houston, Texas

eppendorf & Science PRIZE FOR NEUROBIOLOGY

Deadline for entries
June 15, 2009

For more information
www.eppendorf.com/prize

This annual international research prize recognizes accomplishments in neurobiology research based on methods of molecular and cell biology. The winner and finalists are selected by a committee of independent scientists, chaired by the Editor-in-Chief of *Science*. Past winners include postdoctoral scholars and assistant professors.

To be eligible, you must be 35 years of age or younger. If you´re selected as this year´s winner, you will receive $25,000, have your work published in the prestigious journal *Science* and be invited to visit Eppendorf in Hamburg, Germany.

eppendorf
In touch with life

Science AAAS

Kurstin Roe Photography

Shockley Dilemma

Some citizens in Auburn, California, are riled by plans to name a park after William Shockley. Shockley, who died in 1989, won the Nobel Prize for coinventing the transistor. However, he also proclaimed the intellectual inferiority of black people and favored voluntary sterilization for people with low IQs.

This has put the board of Auburn's park district in a dilemma. On 28 April, it voted to accept a donation by Shockley's wife—who died in 2007—of an 11-hectare wooded area to be called "Nobel Laureate William B. Shockley and His Wife Emmy L. Shockley Memorial Park." Environmentalists want the park, but social activists are up in arms. "I don't want to honor a despicable man," says Karen Tajbl, chair of the social action committee of the Sierra Foothills Unitarian Universalist Church. Tajbl points out that last year in Sacramento, the citizens "cleansed" the name of Charles M. Goethe, a philanthropist but also founder of the Eugenics Society of Northern California, from several public places.

If the name can't be removed, says district administrator Kahl Muscott, alternate suggestions include adding a sign that reads: "This park is dedicated to people of all races, ethnicities, beliefs, education levels, intelligences, and walks of life who wish to live together in peace & harmony. Dedicated in 2009, the year when Barack Obama, a man of Black African heritage, took office as President of the United States."

Deconstructing Halitosis

"Even your best friends won't tell you," a classic mouthwash ad warned. But OkayToKiss will bluntly let you know if your mouth is foul.

The new, patent-pending saliva test, developed by microbiologist Mel Rosenberg of Tel Aviv University in Israel and colleagues, turns blue if it senses high quantities of certain enzymes. The research behind the product is reported in the latest *Journal of Breath Research*. In the past, Gram-negative bacteria have been held solely responsible for dragon breath. But Rosenberg and his team analyzed bacteria in incubated saliva samples and found that Gram-positive bacteria help out by producing enzymes that make it easier for Gram-negative bacteria to break proteins into stinky compounds.

OkayToKiss is one byproduct of a boom in research on the microbiology of odors, says Rosenberg. At the first-ever symposium on the field, held last week at the meeting of the American Society for Microbiology in Philadelphia, he and about 150 other scientists discussed the tiny lives that underlie flatulence, manure, livestock, and pet odors.

"You need to know who's living there first in order … to try and inhibit these bacteria, whether in the mouth, in manure, or in the intestinal tract," says the symposium's co-organizer, Terence Whitehead, a microbiologist with the U.S. Department of Agriculture in Peoria, Illinois. Whitehead notes that when he and colleagues recently analyzed the bacteria in swine manure, they found that "probably 90% of them had never been seen before."

The Genes Behind the Beard

Julia Pastrana, history's most famous bearded lady, fascinated audiences in a 19th century traveling circus, for which she danced and sang in clothes that showed off her hairy limbs. Pastrana, a Mexican Indian, suffered from a rare but highly heritable disorder called congenital generalized hypertrichosis terminalis (CGHT). Now, Chinese scientists have begun to unravel the genetic story behind her condition.

Sometimes called "wolfman syndrome," the disorder causes excessive dark hair across the body and face as well as enlargement of the head and facial features. There are at least 30 cases in China, estimates geneticist Xue Zhang of Peking Union Medical College in Beijing. In a study reported 21 May in the *American Journal of Human Genetics*, Zhang found 16 cases in three families and analyzed DNA from them and from 19 unaffected family members. All of the CGHT sufferers had mutations—called copy number variations (CNVs)—in which chunks of DNA were deleted in four genes. In one case, DNA was also duplicated across the same region. No such mutations showed up in unaffected family members.

Zhang speculates that the CNVs are "chang[ing] the local structure of the chromosome, interfering with the production of genes farther down." One nearby gene that might be affected has been linked to hair production in mice. Although the mechanism is still unclear, the study marks "a first and important step" toward solving the puzzle of CGHT, says Eli Sprecher, a dermatologist at the Rappaport Institute in Haifa, Israel.

This photograph, "Wings of newly emerged dragonfly," is a finalist in the second annual competition for International Garden Photographer of the Year of the Royal Botanic Gardens, Kew. It's by Lancashire resident Jason Smalley. See more stunning photos at www.igpoty.com.

CREDITS (TOP TO BOTTOM): AP; H. N. HUTCHINSON, J. W. GREGORY, AND R. LYDEKKER, *THE LIVING RACES OF MANKIND* (1900); JASON SMALLEY/IGPOTY.COM

Published by AAAS

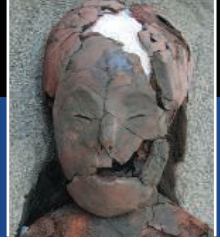

Arsenic and the first mummies
1130

The Soviet Union's legacy of illegal whaling
1132

Rock star. The University of Oslo's Jørn Hurum took Ida on a world tour.

PALEONTOLOGY

Celebrity Fossil Primate: Missing Link or Weak Link?

It's not every day that a 47-million-year-old fossil primate is the star guest on *Good Morning America*. "Ida is so big, she's even made the Google home page," anchor Robin Roberts said on 20 May as she introduced TV viewers to the cat-size skeleton from Germany. Ida is so big, in fact, that "missing link found" was the hottest search term on Google that morning, the day after New York City Mayor Michael Bloomberg helped unveil the fossil at a press conference at the American Museum of Natural History in New York City. Within days, Ida had appeared in *People* magazine, and she had her own book, Web site, and documentary film for the History Channel and BBC. "This little creature is going to show us our connection with the rest of all mammals," pronounces narrator David Attenborough in the film. "The link they would have said until now is missing is no longer missing."

The man behind the fossil is paleontologist Jørn Hurum of the Natural History Museum at the University of Oslo. With a lock of long hair falling boyishly over his face, a photogenic smile, and a Nordic accent, Hurum—who stars in a weekly children's science show on Norwegian television—makes the dusty science of primate origins come alive as he describes Ida. "This is like finding the Holy Grail for paleontologists," he enthused. "This is the first link to all humans."

Maybe so—but probably not. Many of the leading scientists who study primate evolution don't think Ida lives up to Hurum's billing as a human ancestor; most think she's a relative of lemurs instead. After looking at photos and a description that Hurum and his collaborators published in an online paper last week, most researchers think the skeleton—though stunning—reveals little new information about ancient primates, much less human origins. Some worry that the publicity framing Ida as a human ancestor will backfire as her true identity and lowly origins are revealed. "A lot of articles say it is a missing link. That is wrong," says paleoanthropologist Elwyn Simons of Duke University in Durham, North Carolina. "It has no convincing links to monkeys, apes, and humans."

Ida is indeed a special find—perhaps the most complete skeleton of an ancient primate ever found. About 95% of her bones are intact, as well as the outline of her furry body and even fruit and leaves from her gut. Private collectors dug the fossil out of the famed Messel pit near Frankfurt, Germany, in 1983, even though it was illegal to collect there. They split the fossil in half and sold one slab, with falsified features, to the Wyoming Dinosaur Center in Thermopolis. The other, better half was framed and hung as décor on the wall of an unnamed collector's home until 2006, when a dealer offered it to Hurum at a fossil show. At that time, Germany had an amnesty period when illegally collected fossils could be sold legally. The asking price was $1 million. Hurum returned to Oslo and, to his surprise, persuaded the board of his museum to buy it. He negotiated a lower, undisclosed price, and an armed escort delivered Ida to Oslo in September 2007.

Hurum then put together what he calls a "dream team" of scientists who studied the fossil under a veil of secrecy for 2 years. The result of their scrutiny was published on 19 May in the online journal *PLoS One*. In the paper, they named the fossil *Darwinius masillae* to honor the bicentennial of Charles Darwin's birth. (Hurum dubbed it Ida, after his 6-year-old daughter.)

Darwinius's identity is undisputed as a member of an extinct primate group known as the Adapiformes. Researchers have long known that some adapids share some features with higher primates, including anthropoids (monkeys, apes, and humans). Thus, a few have argued that adapids might be primitive relatives of anthropoids—and us. Most experts, however, think adapids should be grouped with lower primates, lemurs and lorises, in a suborder called Strepsirrhini (*Science*, 19 October 2001, p. 587).

In their paper, Hurum, paleontologist Philip Gingerich, and colleagues propose that Ida is not on the primitive lemur line but belongs with more advanced primates, as a member of the so-called haplorrhine suborder. They also suggest that Ida could be a member of a stem group of adapids that gave rise to the earliest anthropoids, a role often assigned to another group of primitive primates, the small, nocturnal tarsiers. The team bases that conclusion on a dozen traits, the most significant of which is the surprising discovery that Ida lacks a key characteristic shared by lemurs and tarsiers: a grooming claw on her second toe. Gingerich also says Ida's spatulate front teeth, her interlocking canines, and the talus bone in her ankle resemble those of higher primates. He argues that Ida might be a direct ancestor of anthropoids—and, hence, humans.

Not so fast, say many paleontologists who specialize in this early chapter of primate evo-

CREDIT: ANDREW H. WALKER/IMAGE.NET

On the trail of the bat killer
1134

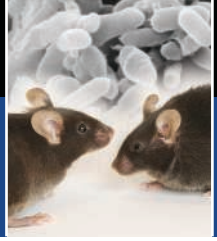

Probing the ecology of the gut
1136

lution. Paleontologist Erik Seiffert of Stony Brook University in New York state points out that many of the traits used to link Ida with haplorrhines are not found in some of the earliest universally accepted anthropoids, which lived as long as 37 million years ago in what is now the Fayum province of Egypt. Ida is crushed, Simons says, and lacks a key feature that all other anthropoids share: a wall of bone at the back of the eye socket.

Simons and others say Ida's most convincing feature is the absence of a grooming claw, but that trait alone doesn't sway them. Several also grumble that the team cherry-picked the traits and the species of fossils it compared with Ida. The analysis left out many traits and extinct primates, including the well-known Fayum anthropoids and *Eosimias*, a tiny 45-million-year-old Asian primate that most researchers think may be the earliest known anthropoid. "Smoke could be coming out of my ears," says paleontologist K. Christopher Beard of the Carnegie Museum of Natural History in Pittsburgh, Pennsylvania, who found the first fossils of *Eosimias* in 1994. "It's like going back to 1994. They've ignored 15 years of literature."

Sought-after. Google's home page celebrated the fossil.

Gingerich, who did the analysis to compare Ida with haplorrhines, responds that this is just the first description of *Darwinius* and that the team was trying to make the data public as quickly as possible. "If the critics want to do more, they can do more, and we will do more," he says.

Perhaps fewer paleontologists would be smoldering if the fossil had not been promoted as a direct ancestor of humans. The paper itself is "a very reasonable, very cautiously presented hypothesis," says paleontologist D. Tab Rasmussen of Washington University in St. Louis, Missouri, who is among the handful who think adapids are haplorrhines and that Ida is "a reasonable candidate as our earliest anthropoid kin."

The "missing link" hyperbole in newspaper and Web stories—and Google—was a different story. "Since there's nothing very surprising about this specimen, the amount of media attention that it has gotten is just flabbergasting," says paleoanthropologist Matt Cartmill of Boston University. As for its being an ancestor, "amoebas also are in our ancestry in a primitive sense," says Stony Brook University paleoanthropologist John Fleagle.

Hurum, who signed off on the text in the film and on the Web site and has compared Ida to the Rosetta stone and the *Mona Lisa*, is unrepentant: "It's hard to discuss haplorrhine and strepsirrhines in a press release. You need to link it to us." He is proud of using multimedia to promote interest in fossils: "Yes, I am shaking things up. If you want kids to be interested in science, we need to start packaging it in many different ways."

Other researchers think rollouts like this one are just too risky. "On the one hand, I view it as a major task for scientists to translate their work for the public at large," says Beard. "On the other hand, when you make these breathless statements, you have to have the goods to back it up. Otherwise, we all lose credibility with the public. The only thing we have going for us that Hollywood and politicians don't is objectivity." **–ANN GIBBONS**

APPOINTMENTS

Obama Turns to NASA Veterans to Lead Space Agency

President Barack Obama has chosen two longtime advocates of human space flight to lead NASA. On 23 May, the White House nominated former astronaut Charles Bolden Jr. and Washington lobbyist Lori Garver to take the positions of administrator and deputy administrator, respectively, for the space agency.

If confirmed by the Senate, Bolden and Garver will confront a series of momentous decisions on where to take NASA in the coming decade. An expensive new launcher is now in the works to replace the space shuttle, due to retire next year, but its projected costs are rising rapidly. Meanwhile, the new Administration wants to spend more money on Earth observation at a time when the overall science program is suffering from delays and overruns. Yet Obama has proposed only small increases to NASA's $18 billion budget in the coming 5 years.

The situation is so urgent that the White House last month appointed a 90-day blue-ribbon panel led by former aerospace manager Norman Augustine to come up with options for the future human space-flight effort, which now is focused on a return to the moon by 2020 (*Science*, 22 May, p. 999). Given that the overall agency budget is unlikely to increase substantially in coming years, the outcome will have a profound effect on science as well. "NASA is facing a crisis that many of us knew would come," says Charles Kennel, a former NASA advisory council chair and director emeritus of the Scripps Institution of Oceanography in San Diego, California. Kennel says that the rush to get the new launcher in operation by 2015 has already caused "a slowdown in science funding."

A new mission. President Obama met with Bolden (*right*) on 19 May to talk about the top job at NASA.

Bolden is a 62-year-old retired African-American Marine brigadier general who flew on four shuttle missions. Garver is a former director of a pro–space-flight group called the National Space Society and also served as a senior NASA manager. Both are likely to get a warm reception in the Senate. Senator Bill Nelson (D–FL) pushed hard for Bolden's nomination, derailing other candidates favored by the White House, according to congressional and Administration sources. And Senator Barbara Mikulski (D–MD), who chairs the panel that funds NASA, said, "I will certainly support their nominations."

–ANDREW LAWLER

With reporting by Yudhijit Bhattacharjee.

CREDIT (BOTTOM): PETE SOUZA/MAI/LANDOV

Published by AAAS

Comrades. Chávez (dark shirt), during the 2008 regional elections with candidate, now science minister, Jesse Chacón (third from left).

VENEZUELA

As Research Funding Declines, Chávez, Scientists Trade Charges

Venezuelans have grown accustomed to blunt remarks from their president, Hugo Chávez, elected in 1998 with an agenda of empowering the poor. Still, academics were taken aback this month when Chávez turned his scorn on them: During his weekly television program on 3 May, *Aló Presidente*, Chávez said that researchers should stop working on "obscure projects," such as whether life exists on Venus, and instead go into the barrios to make themselves useful. The words sent a chill through the scientific community, as did Chávez's comment that his recently appointed minister for science, technology, and intermediate industry, Jesse Chacón Escamillo, should "put the screws" on "feeble scientists" to get better results.

To many observers, it was another sign of the growing tension between Chávez and the academic establishment, particularly involving well-established research centers in Caracas. Nerves were already on edge following Chávez's dismissal in April of science minister Nuris Orihuela, a geophysical engineer, and her replacement by Chacón, an engineer and Army lieutenant. Critics say Chacón has scant scientific credentials but has been close to Chávez since at least 1992, when he backed Chávez's failed coup attempts.

Disaffected researchers say they fear that science funding is becoming more politicized. This is one of many concerns they've added to a growing catalog of perceived government failures or threats. Heading this list is a complaint that the government has made broad cuts in funding for institutions that support research. This has come partly in response to declining government petroleum revenues. But critics say the trouble runs deeper—that research is being mismanaged, and that the government has fired, demoted, or blacklisted dissidents.

Claudio Bifano, president of the Venezuelan Academy of Physical, Mathematical and Natural Sciences in Caracas, sent a letter with outstanding grievances to *Science* this month (www.sciencemag.org/cgi/content/abstract/1176733). They are, he wrote, "just a fraction of the many actions that clearly reveal an aim of the government to control all of the national scientific activity and the higher education system, putting Venezuela's scientific activities at risk." Bifano says that the government recently decreed the creation of about 40 new universities—on top of 51 existing public and private institutions. He says that Venezuela has insufficient academic resources for 90-odd universities and does not need that many.

"We are worried about the dilution of funding, which could lead to the closure of universities not aligned to government policies," adds biologist Roberto Cipriani, head of environmental studies at the Simón Bolívar University (USB) in Caracas. Scientists also view a 3-year-old program called LOCTI, which taxes companies to create a fund for research and innovation, as a disappointment. Publication indexes show that peer-reviewed publications from Venezuela have declined recently, says Cipriani. He notes that the ISI Web of Knowledge shows that science and technology articles written by Venezuelans dropped 15%, from 968 in 2006 to 831 last year.

Other groups are protesting what they view as threats to research. A petition by the Caracas chapter of the Venezuelan Academy for the Advancement of Science, posted last week for comment (http://asovac.net/bitacora/?p=3372), states that the "fundamental pillars of Venezuelan science are in grave danger."

It claims that a key government science program—Misión Ciencia—has produced few tangible results despite massive spending and deplores budget cuts ordered in March that, it says, translate into a 33% reduction in operating budgets for the Central University of Venezuela (UCV), in Caracas, and several other institutions. These are having "a severe effect on [UCV's] basic scientific and technological research programs," the declaration adds.

On 14 May, about 20 scientists stood in silence for 5 minutes during a meeting of some 250 researchers at UCV to protest Chávez's statements on *Aló Presi-*

In the streets. University of Simón Bolívar students protested budget cuts in Caracas earlier this month.

CREDITS (TOP TO BOTTOM): JORGE SILVA/REUTERS/LANDOV; AP PHOTO

dente and the government's withdrawal of certain awards funded by LOCTI. The protesters from the Venezuelan Institute for Scientific Research remained silent because the ministry had told them to make no public statements, say sources in Caracas who did not want to be identified.

Whatever its flaws, LOCTI has been helpful to some institutions, researchers say. USB, the largest single recipient of LOCTI cash, received about 100 grants a year from 2006 through 2008, about 20% of the amount given to universities and agencies, says USB president and chemist Benjamin Scharifker. USB marine resources manager Eduardo Klein, a professor in the department of environmental studies, says he has been able to build labs and buy equipment that would not have been possible without LOCTI—including a 4000-square-meter, $7 million center for marine biodiversity now under construction. But Klein adds that funding needs are determined at the top: "The ministry decides on projects without our participation."

While some institutions have done well, scientists say that critics of government policy rarely escape punishment. A widely cited example this year is biologist Jaime Requena, a Cambridge, U.K.–educated professor at the government's Institute for Advanced Studies (IDEA) in Caracas. Requena and his supporters say that IDEA's director stripped Requena of his professorship just before his retirement, costing him his pension rights. IDEA took this step, according to an independent group, the Human Rights Commission of the Venezuelan Association for the Advancement of Science, after Requena published a letter in *Nature* criticizing the government for restricting support of the social sciences. Requena wrote that this government decision was one reason why Venezuela's scientific publications have fallen to a 25-year low point.

Speaking for the science minister, IDEA president Prudencio Chacón, who is not related to the minister, denied that the government is imposing political control over science, stifling dissent, or cutting research budgets. He also said that Requena was dismissed because "he worked in two places simultaneously," left work "several times without permission from his supervisor," and because IDEA requested the purchase of software that Requena had developed. Requena and his backers deny the charges. IDEA's statement recognizes the significance of the dispute, however, saying it has become one of the "political flags" of government critics.

–BARBARA CASASSUS

Barbara Casassus is a writer in Paris.

SWINE FLU OUTBREAK

New Details on Virus's Promiscuous Past

An international team of scientists working at breakneck speed has provided the most detailed description yet of the origins of the novel H1N1 swine flu virus now causing a global outbreak. The study, published online by *Science* on 22 May (www.sciencemag.org/cgi/content/abstract/1176225), has good news about the prospects for making a vaccine against the virus. It also raises the intriguing possibility that a species other than pigs might have harbored a precursor to the virus.

Much of the data have already dribbled out, released as soon as it was generated. But this new study, which involved a team of 59 researchers led by investigators from the U.S. Centers for Disease Control and Prevention (CDC) and the University of Cambridge, U.K., is the first to pull it all together. "The people at CDC deserve to have this published," says leading flu expert Robert Webster of St. Jude Children's Research Hospital in Memphis, Tennessee. "They bust their butts and have done the lion's share of the work and tried to be as open as possible."

The authors reconstructed the puzzling past of what's known as influenza A 2009 (H1N1) by analyzing 76 isolates from people in Mexico and the United States. The paper begins the somewhat operatic and knotty story of this outbreak's origins with an H1N1 first isolated in swine in 1930, which itself was a close relative of the virus that caused the 1918 pandemic in humans. Unlike flu viruses that affect humans, the eight influenza genes in this swine H1N1 changed very little for 6 decades. In 1998, researchers discovered that this rock-steady swine H1N1 had combined with a human H3N2 and a U.S. avian virus. This so-called triple reassortant spread to Asian pigs, and many different variants soon began popping up in swine all over the world.

In a separate drama, related but distinct H1N1 strains have long circulated in humans. An H1N1 caused the 1918 pandemic and remained the predominant strain until it was replaced by an H2N2 that caused a new pandemic in 1957. The human H1N1 then suddenly reappeared in 1977 and has been making the *Homo sapiens* rounds ever since. Then an H3N2 strain that caused the 1968 pandemic replaced the H2N2. So today, both H3N2 and a human H1N1 cocirculate, along with two strains of influenza B.

Now along comes the swine flu outbreak of April. The paper explains that this novel H1N1 has two genes from avian influenza that entered Eurasian swine in 1979, three from the old-fashioned H1N1 in North American swine, two from the triple reassortants in North American swine, and the final one from humans transmitted to us from birds in 1968. That head-spinning mix has never been seen before, and given its genetic distance between known strains, CDC chief influenza investigator and co-author Nancy Cox said the virus was likely lurking around somewhere long before it jumped into humans. "We do not know if the virus entered the human population directly from swine or via an intermediate host," said Cox.

The encouraging news for vaccine development is that the many isolates of the new viruses analyzed in this report showed little variation, much less than typical seasonal influenza viruses. This makes it "much, much easier" to make a vaccine, said Cox.

–JON COHEN

Gene Segments, Hosts, and Years of Introduction

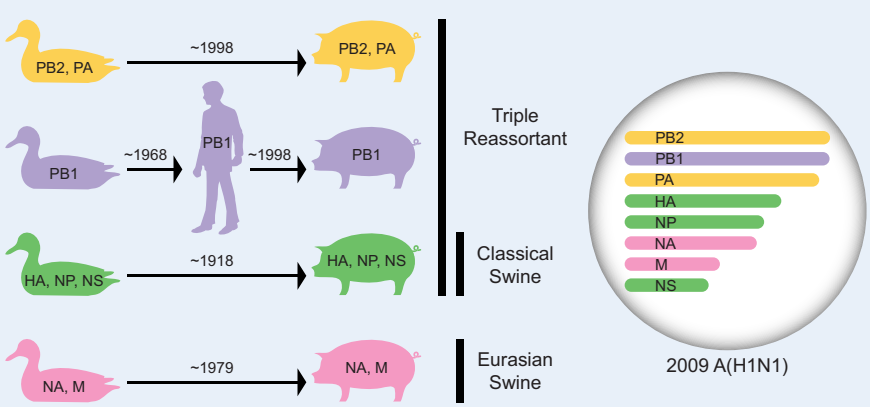

CREDIT: GARTEN *ET AL.*

Published by AAAS

NATIONAL SCIENCE FOUNDATION

The Money to Meet the President's Priorities

Money talks. But this year it's on the move at the National Science Foundation (NSF), which has turned recent actions by Congress and the priorities of a new president into an array of programs to strengthen the scientific work force, tackle pressing societal problems, and foster collaborations across disciplines.

The initiatives are made possible by the brightest budget picture in NSF's 60-year history. Some $3 billion from the one-time stimulus package, combined with a 6.5% boost to its regular 2009 budget, has brought spending to a record $9.5 billion this year. Its 2010 budget, excluding stimulus funds, would rise by 8.5%, to just over $7 billion, if Congress approves President Barack Obama's request.

"This Administration has made clear its priorities in science," notes NSF Director Arden Bement Jr., "and they include all the things we're doing." In particular, that translates into an increase of $197 million in 2010 for all manner of climate research, plus $20 million over 2 years for climate change education; $31 million more for research on improved silicon technology to push beyond Moore's Law; $12 million more for technology training at community colleges; $50 million for high-speed networks in low-intensity research states; and $92 million for novel ways to fund out-of-the-box research ideas.

Although Congress passed the stimulus package in February and the 2009 budget in March, it was only last week that NSF revealed in detail how that money will be allocated, along with the specifics of its 2010 request. That additional information fleshes out why research gets an 11% increase, education only 1.5%, and funding for major new facilities drops 23%.

For example, Obama has promised to triple the number of NSF's prestigious graduate research fellowships by 2013. But after getting a 20% boost in 2009, NSF has asked for only a 6% increase in 2010, to $122 million. Why so low? The answer is the $45 million in stimulus funding that Bement allocated to the program. That influx will allow NSF to grow this year's class by roughly one-third and make good progress toward Obama's goal of 3000 new awardees.

The faculty early career development

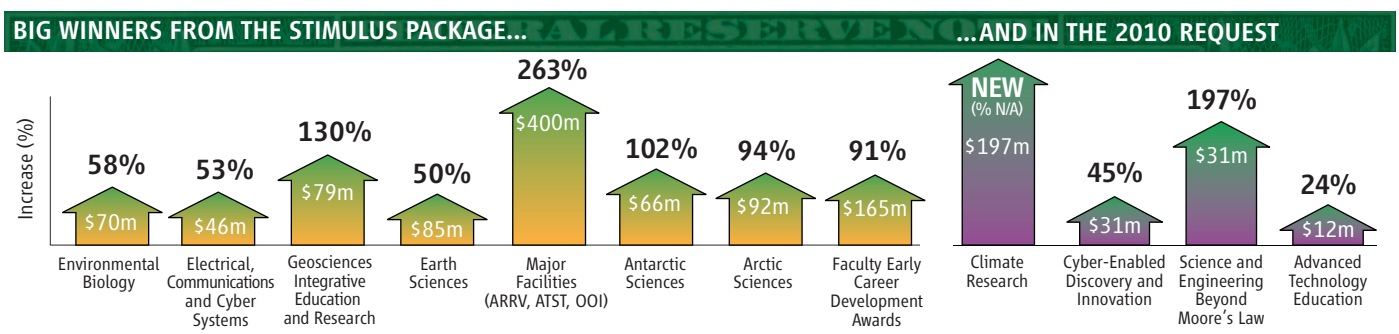

Digging for Fresh Ideas in the Sandpit

Does the idea of writing a grant proposal that's been all but approved before it's even sent in sound appealing? Then play in the sandpit.

That's what 30 scientists did this spring, meeting outside Washington, D.C., for 5 days of intense discussion about synthetic biology under the auspices of the U.S. National Science Foundation (NSF) and the U.K. Engineering and Physical Sciences Research Council. But instead of simply discussing where the burgeoning field is headed and then waiting for a possible funding solicitation down the road, the scientists—equally split between the United States and the United Kingdom and drawn from several disciplines—assembled into 10 teams and came up with specific research proposals.

That's when the fun began, at least for some participants. Each team presented its idea to the larger group, received instant feedback, made revisions, and presented it again—six times in all. By the end of the week, officials from the two government agencies—each of which had agreed to put up $5 million to fund the best ideas—verbally signed off on five of the 10 proposals. The two agencies also split the $200,000 cost of the workshop, held in Warrenton, Virginia.

The exercise, conceived in 2004 by the U.K. research council and labeled a sandpit (the British term for sandbox), is the latest attempt by governments to fund so-called transformative research. Joanne Tornow of NSF's biology directorate told the participants—chosen from among 170 applicants—that she and her U.K. counterpart, Paula Duxbury, "didn't want to hear anything that had more than a 10% chance of succeeding." The week began with team-building exercises designed to help participants "strip off their preconceived notions," says Duxbury, before choosing partners and getting down to the science. "The talent in the room was just amazing," says Joseph Ayers, a neurophysiologist at Northeastern University Marine Science Center in Nahant, Massachusetts, who had spent 15 years working on biomimetic marine robots. "You'd ask a question, and people would respond with a lecture."

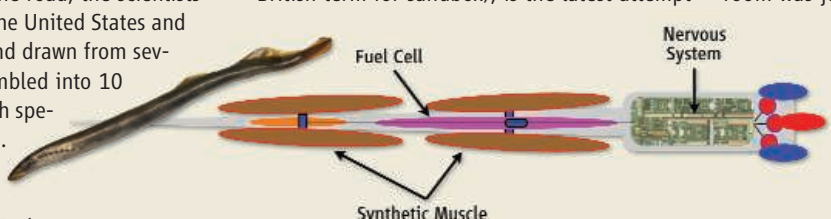

Water works. This "cyberplasm" will try to mimic the undulations of the lamprey.

Andy Ellington, a self-

SOURCE: NSF; CREDITS: JOSEPH AYERS; JUPITERIMAGES

Published by AAAS

(CAREER) program is an even more dramatic example of the interplay between stimulus funding and NSF's regular budget. Despite strong interest from both Congress and the White House, NSF requested only enough money in 2010 to restore the program to its 2008 level of $203 million. However, those numbers do not include a whopping $165 million increase for the program this year, using stimulus money spread across all six of the foundation's research directorates.

Some priorities come courtesy of Congress. As part of the stimulus package, legislators designated $60 million more for scholarships to undergraduates majoring in science and engineering. That jump will enable NSF to expand the program while holding its 2010 request flat at $55 million.

The stimulus package also added $400 million to NSF's major facilities account, which typically contains a half-dozen big projects in various stages of construction. Bement has divvied the money among three projects—the Alaska Region Research Vessel (ARRV), the Advanced Technology Solar Telescope, and the Ocean Observatories Initiative—that have been in the pipeline for years but were held out of the 2009 request for various reasons. Bement says the $148 million for ARRV should be enough to finish the ship, so nothing is being requested for it in the 2010 construction budget. One big facility still awaiting a green light from NSF is the National Ecological Observatory Network, first proposed a decade ago but still awaiting approval of its final design.

Bement promises that the bolus of new funding will enable NSF to be more innovative, and he's asking each of the foundation's 46 divisions to spend $2 million next year on innovative research ideas chosen outside the normal grants-making procedures. "We hope to stretch the culture of what's acceptable," explains Jim Collins, head of the biology directorate, which this spring sponsored a weeklong workshop in synthetic biology that featured real-time peer review (see sidebar). "We don't want to put too many boundaries on people."

One effort to break down disciplinary boundaries is already under way, as 17 program managers from the biology and geosciences directorates are being formed into an "integrated global system science" team. "The phrase 'earth system science' has been around since the 1970s," says geosciences chief Timothy Killeen. "But it didn't bring in the human dimension of these processes." NSF has already set aside money for proposals in three areas that will funnel into this new "node"—emerging topics in biogeochemical cycles, multiscale modeling, and environment, economics, and society. "It's not enough to talk the talk," says Killeen. "We also have to walk the walk."

–JEFFREY MERVIS

described evolutionary engineer at the University of Texas, Austin, admits that it took him a while to embrace the sandpit approach: "It was like nothing I've ever done before." He says the most important lesson he learned "is shutting the heck up … and letting others put their ideas forward." Ellington says that the sandpit approach "is more like Twitter" than the usual process of "writing a grant proposal, submitting it, and then 6 months later getting back three pages of detailed comments. … But we probably got just as many incisive comments and a lot fewer nonincisive comments."

Some participants never warmed to the task, however. "I did not expect an environment in which scientists competed against one another [in real time and often late into the night] for a limited pool of funds," wrote one prominent scientist in an anonymous evaluation submitted at the end of the week. The exercise evoked "Darwinian selection for limited resources in a pleasant natural environment (Airlie House), where the least successful individuals die a slow and agonizing death. … It was one of the most unpleasant weeks of my life."

The prospective winners—no decisions will be final until July—have taken on big challenges within this sprawling field. Ellington and four other scientists hope to create genetically altered polymers, in effect, artificial versions of amino acids and their related genes. Ayers is part of a four-person team that is building a "cyberplasm," a device possessing an integrated system of fuel cells, activators, muscles, and sensors that will move through the water like a lamprey. A third team hopes to produce synthetic taxol, a cancer-fighting drug, in large amounts and at low cost, building on the success of team member Jay Keasling of the Joint BioEnergy Institute at the University of California, Berkeley, with the antimalarial drug artemisinin. There's even a project to address ethical and societal issues, in hopes of avoiding the controversy that has bedeviled the related field of genetically modified crops.

–J.D.M.

*Science*Insider

From the *Science* Policy Blog

News about the impact of the U.S. **stimulus funding package** on researchers, the ongoing **battle against swine flu**, and the impact of **California's financial troubles** on the state's universities were among the headlines on *Science*Insider last week.

The competition for **Grand Opportunities (GO) grants at NIH**, which start at $1 million and use stimulus money, has drawn 2400 letters of intent, in contrast with the 20,000 applications submitted for the smaller Challenge Grants. NIH officials expect **success rates** for the GO grants to be **as high as 10%.** Meanwhile, NIH plans to fund more than 30% of the 1600 scientists who have applied to expand an existing grant. In other NIH news, the agency has announced **a $120 million, 5-year plan** to set up a drug-development service center that will focus on **rare and neglected diseases**.

The U.S. Centers for Disease Control and Prevention (CDC) last week sought to reassure the public that **a vaccine for swine flu** would be ready by late fall, in time to combat a possible comeback by the H1N1 virus. CDC's statement came after a World Health Organization working group estimated that it could be December before authorities are able to start immunizing people.

Last week's resounding defeat of ballot measures aimed at helping California's finances darkens the outlook for **the University of California (UC)**. UC had already instituted hiring and salary freezes and raised student fees by 9.3%. The university now faces a possible $322 million budget reduction, which could lead to further fee increases, larger classes, and pay cuts.

The tough economic climate will force more than **a quarter of medical charities** in the United Kingdom **to cut funding** by anywhere between 10% and 40%, according to a survey released this week by the country's Association of Medical Research Charities.

To keep up with science policy news daily, visit **http://blogs.sciencemag.org/scienceinsider/**.

Published by AAAS

ARCHAEOLOGY

Arsenic and Old Mummies: Poison May Have Spurred First Mummies

About 6800 years ago in the Camarones River valley of northern Chile, a 6-month-old male infant died mysteriously. After death, his head and internal organs were removed and his body cavities packed with animal hides. Someone, perhaps the child's mother or another female relative, modeled a new head and mask of white clay and placed it atop the small torso. Then she painted the mask with black pigment and adorned the head with tufts of human hair. The resulting mummy, created by the Chinchorro people, is among the oldest intentionally created mummies in the world.

Archaeologists have long puzzled over the nearly 200 Chinchorro mummies found to date. At the Society for American Archaeology meetings in Atlanta, Georgia, last month, researchers presented new evidence for a provocative hypothesis about why the Chinchorro began the practice and why their morticians initially focused on young children. They showed that the Chinchorro were being poisoned by arsenic in their water, likely leading to a high rate of miscarriage and child mortality. Such deaths may have helped to spawn a mummification practice in "an emotional response to an environmental contaminant," says anthropologist Bernardo Arriaza of the University of Tarapacá in Arica, Chile.

Mummification is known from more than a dozen ancient societies around the globe, but the Chinchorro practice was different. Other intentional mummies are later in time and generally come from politically and socially complex societies, with the privilege of mummification reserved for adult elites. But the Chinchorro lived in a relatively simple society of fishers and seal and sea lion hunters, and they started out mummifying young children. Eventually, they extended the practice to adults, before abandoning it in about 1700 B.C.E.

After reading about arsenic's toxic effects on human fetuses and infants, Arriaza began examining in 2007 the possibility of arsenic poisoning among the Chinchorro. Arsenic occurs naturally in geological formations in many parts of the world, and as precipitation weathers these strata, it carries the poison into local rivers, often with devastating effects (*Science*, 23 March 2007, p. 1659). This hazard came to public attention in Chile in the 1960s, after the city of Antofagasta started drawing water from a river that turned out to be laced with 860 micrograms of arsenic per liter—86 times higher than the World Health Organization's (WHO's) current provisional guideline. During the peak exposure from 1958 to 1965, infant mortality rates in Antofagasta soared by as much as 24%. From 1958 to 1961, 4% of newborns and 9% of all older infants died in the city. It was "a major public health issue," says José Centeno, a senior research scientist at the U.S. Armed Forces Institute of Pathology in Washington, D.C.

Arriaza suspected that the Chinchorro suffered similarly high infant mortality rates for exactly the same reason. The four earliest Chinchorro mummies—two newborns and two infants between 12 and 24 months of age—came from the Camarones River valley, where today the water tests as high as 1000 micrograms of arsenic per liter. Moreover, a 1996 study of Inca mummies from northern Chile identified arsenic in soft-tissue samples and discerned skin lesions characteristic of arsenic poisoning.

Arriaza collected hair samples from 46 Chinchorro and pre-Inca mummies excavated from 10 sites in northern Chile where the water tested above WHO guidelines for arsenic. He sent the samples to chemist Dulasiri Amarasiriwardena of Hampshire College in Amherst, Massachusetts, for mass-spectrometry testing.

Arsenic values in hair from all 10 sites point to chronic arsenic poisoning, Arriaza reported in his talk. Ten mummies from the Camarones River valley, for example, exhibited a mean value of 37.8 micrograms per gram, well above the 1 to 10 micrograms considered to indicate chronic arsenic poisoning. The two most contaminated individuals were a Chinchorro infant and an adult, each of whom had readings in excess of 219 micrograms. Although some arsenic could have come from washing hair in contaminated water, washing is unlikely to have pushed levels that high, says pathologist Larry Cartmell of the Central Texas Pathology Laboratory in Waco, a specialist in ancient hair analysis: "I believe [Arriaza's] deductions about infant and fetal morbidity are sound."

Arriaza theorizes that grief-stricken Chinchorro parents, who suffered repeated losses of their children, wanted to preserve the infants' bodies and so created mummies they kept in shrinelike areas. (Some mummies' faces reveal repeated paint touchups to cover nicks and dents, suggesting that they were kept aboveground.) Cartmell thinks the idea makes sense, noting that parents today sometimes keep locks of hair from a dead child or preserve an infant's room as though it were a shrine.

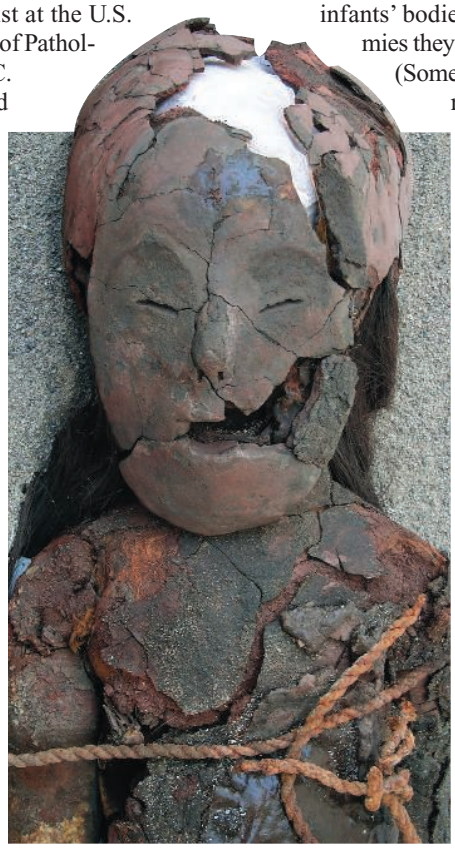

Ancient infant. This mummy from northern Chile, created by the world's oldest mummification process, preserves the body of a child.

CREDIT: B. ARRIAZA/UNIVERSITY OF TARAPACÁ

But the connection between infant deaths and mummification is psychological and therefore hard to prove, says Sonia Guillen, a physical anthropologist at Centro Mallqui-Museo Leymebamba in Lima. "When you can't interview the people, you can't say anything," she says.

All the same, Guillen and others find Arriaza's evidence for arsenic poisoning convincing. Although many researchers may have assumed that environmental contamination became a major problem only for later industrial societies, these findings strongly suggest that earlier societies were at risk, too. "You can't smell arsenic or taste it," says Arriaza. "The Chinchorro had no way of knowing they were being poisoned."

–HEATHER PRINGLE

Heather Pringle is a contributing editor at *Archaeology* magazine.

Published by AAAS

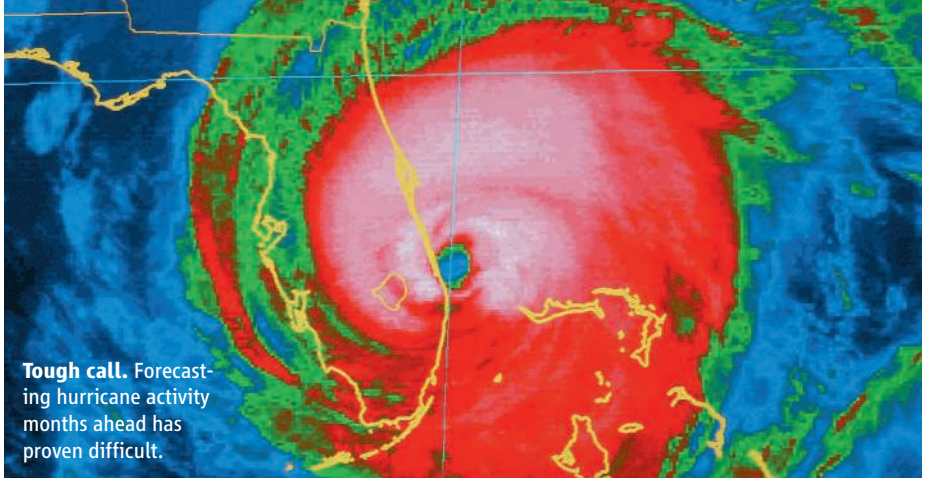

Tough call. Forecasting hurricane activity months ahead has proven difficult.

CREDITS (TOP TO BOTTOM): AP PHOTO; OLEG ABRAMOV

TROPICAL METEOROLOGY

A Cloudy Crystal Ball for the Coming Season's Hurricanes

Every June for 25 years, meteorologist William Gray and associates at Colorado State University (CSU), Fort Collins, have tried to decipher what the coming summer and fall have in store for hurricane country. Now for the first time, the CSU group has graded itself. The researchers' statistical analysis credits their forecasts with a "modest" improvement over the baseline assumption that every season would be normal.

Others concede that the group has shown some measurable skill in forecasting—just not much. The performance of the CSU forecasts has been "not too good" to "pretty bad," says seasonal forecaster Anthony Barnston of Columbia University's International Research Institute for Climate and Society in Palisades, New York. But then, he and colleagues have done their own seasonal hurricane forecasts, and "our skills are lousy also. No one is very good at this."

The trick to forecasting hurricane activity months ahead is to identify conditions that can directly or indirectly influence the number, strength, and duration of storms. To be useful, those "predictors" must also change so slowly that they will still be around months later, during the June-through-November hurricane season. Prominent among the CSU group's predictors has been the tropical Pacific's El Niño.

Gray and CSU colleague Philip Klotzbach reported 13 May in *Geophysical Research Letters* that statistical analyses of forecasts made from 1984 to 2008 "have shown some promise" in forecasting hurricane activity. They compared how far their forecasts departed from reality with how well they would have done by simply assuming that the coming season would be like the average of past intervals ranging from 3 to 50 seasons long.

The CSU forecasts made in early June and especially those made in early August tended to have smaller errors than those made using averages of past seasons, Klotzbach and Gray reported. The forecasts' edge over average-based forecasts was often statistically significant, they found, at least for August forecasts. And using their current set of predictors—the product of 25 years of refinement—to forecast the past 25 seasons in hindsight much improved the forecasts over those made before each season. That bodes well for future forecasts, they say.

Researchers give Gray credit for making the most of the few glimpses of the coming hurricane season that nature provides. "Unquestionably, there is real skill in these forecasts," says Robert Livezey, who is retired from the National Weather Service, where he supervised seasonal forecasting of U.S. climate. The problem, he says, is that "there isn't very much being accomplished" in the early June forecasts. The August results are "a lot better," though still "modest," he adds. For example, CSU August forecasts of the number of tropical storms and hurricanes were off by 2.4 storms from the actual number (typically 9.6 during the past 50 years). Forecasts that assumed every coming season would be typical were off by a bit more: 3.5 storms.

No one is likely to improve much on those results, says Livezey. The CSU group's new forecasting methodology is not nearly as useful as the group claims, he says, due to an error in the group's statistical analysis. Tropical meteorologist Peter Webster of the Georgia Institute of Technology in Atlanta sees a sunnier future elsewhere. "Bill Gray has pointed the way," he says, but "I think we're now doing better with [computer] models." As happened 50 years ago in day-to-day weather forecasting, the job of forecasting the next hurricane season might begin to pass to the machines.

–RICHARD A. KERR

ScienceNOW.org

From *Science*'s Online Daily News Site

Compact Discs Enter the Fifth Dimension. Better clear a shelf in your basement for that high-end Blu-ray DVD player you just bought. Researchers report that they can boost the amount of data stored on a disc 10,000-fold by using gold nanoparticles. If commercialized, the technology could allow a single disc to hold as many as 300 movies or 250,000 songs.
http://tinyurl.com/oh3uex

A Shake May Prevent a Crash. You're driving down the highway late at night, talking on your cell phone and fiddling with the radio. As you begin drifting into the lane on your right, your steering wheel suddenly vibrates, and you swing back to the left, narrowly missing a car you never saw. Such tactile warnings may be more effective than audio or visual cues in preventing collisions, according to a new study.
http://tinyurl.com/oo6as8

Earth's Hellish Era Not So Bad for Life. Four billion years ago, asteroids and comets rained down on our planet with such ferocity that scientists have labeled the era the "Hadean"—literally, hell on Earth. Yet despite these infernal conditions, early life could have survived—and may even have thrived in the warm, wet spots left in the crust by impactors—according to a new study.
http://tinyurl.com/otonso

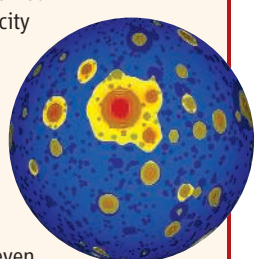

New Clue to Cancer Protection in Down Syndrome. Down syndrome causes mental retardation and a host of health problems. But it also appears to protect people from cancer. Researchers have now found a potential genetic mechanism for this protective effect. The findings might one day lead to cancer-prevention treatments in the general population.
http://tinyurl.com/plox7b

Read the full postings, comments, and more on **sciencenow.sciencemag.org**.

Published by AAAS

WHALE STOCKS

Mystery of the Missing Humpbacks Solved by Soviet Data

In 1991, Victoria University postdoc C. Scott Baker set out to study humpback whales migrating through New Zealand's Cook Strait. Although locals hadn't spotted a humpback for 30 years, Baker knew that the whales, once hunted to the brink of extinction, were recovering elsewhere, even in Australia, and that the Cook Strait had been one of their classic migration routes from the Antarctic to the islands of Oceania. Baker, now a conservation geneticist at Oregon State University's Marine Mammal Institute in Newport, quickly learned that "the locals were right. There weren't any humpbacks. And there should have been." Had there been some environmental change in their breeding or feeding grounds? "It was a puzzle because the Australian and Oceania populations feed in the same [Antarctic] waters," says Baker.

A paper in *Marine Fisheries Review*, made available online last week in advance of its June publication, now solves the mystery: "It was massive illegal hunting by the Soviet Union and other countries," especially of the Oceania humpbacks, says whale biologist Phillip Clapham of the National Marine Mammal Laboratory in Seattle, Washington, lead author of the study and an accompanying commentary. The study concludes that the high number of unreported catches by Soviet whalers of humpbacks in the Southern Ocean decimated this population so severely that it has not yet recovered. These revelations have implications for the management of whales today, for the papers come at a time when the International Whaling Commission (IWC), the primary body for the global conservation and management of whales, is itself at a crossroads, divided between pro- and antiwhaling factions (*Science*, 27 April 2007, p. 532).

"These papers lay out how [IWC] got into this mess," says marine biologist Douglas DeMaster of NOAA Fisheries in Juneau. DeMaster headed the U.S. delegation this year to a series of IWC negotiations designed to reconcile the organization's differences, which have so far failed, according to an IWC report posted online last week. IWC's troubles "all stem from this overharvesting as well as the illegal, unreported, and unregulated hunting," says DeMaster.

From 1947 to 1973, the Soviet Union, as a member of IWC, was allowed to take a certain number of whales of certain species in certain areas. (IWC was created in 1948 to put commercial whaling on a sustainable course.) As required, each Soviet whaling vessel carried biologists to record various data about the harpooned whales.

But instead of the prescribed catch, Clapham and his colleagues report, whalers on Soviet ships such as the *Sovetskaya Ukraina* killed every whale they encountered, regardless of species, age, size, or sex. Marine biologists on the Soviet whaling fleet in the Southern Ocean recorded the correct data, then turned these over to KGB commissars who created a second set of books with false figures for IWC, say the study's authors, who have extensively interviewed four biologists through a translator. "The marine biologists had to sign a KGB statement saying they would never release any of their data," says co-author Robert Brownell Jr., a cetacean biologist with NOAA Fisheries in Pacific Grove, California.

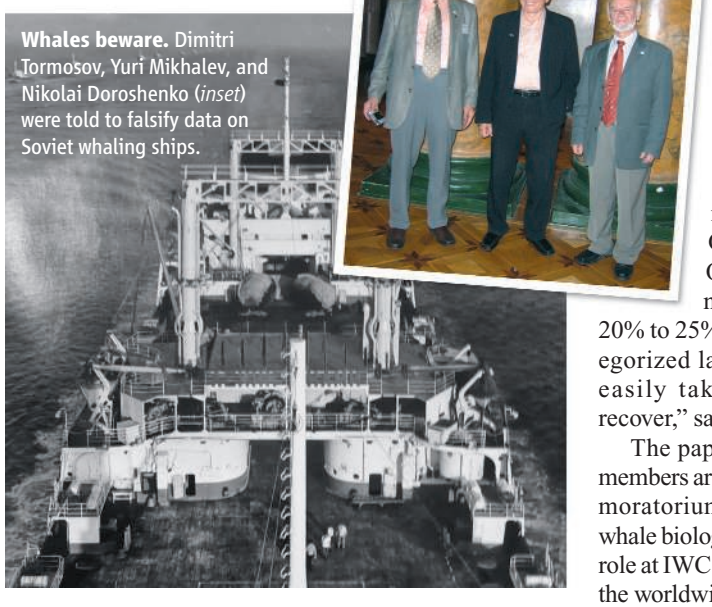

Whales beware. Dimitri Tormosov, Yuri Mikhalev, and Nikolai Doroshenko (*inset*) were told to falsify data on Soviet whaling ships.

All four biologists, however, went to extraordinary lengths to protect their real records for eventual release. One, Dimitri Tormosov, spirited away nearly 60,000 pages, each a record of a killed whale, says Brownell. Tormosov surreptitiously removed each page, one at a time, from his Ministry of Fisheries lab and stashed them in his potato cellar. Another, Yuri Mikhalev, distributed the true records to colleagues in other labs; he complained so loudly about the fake data that he lost his job as a researcher. In 1993, a top Russian scientist admitted the deception, and later, the biologists began turning over their original data to IWC.

In the current paper, Clapham's team combines interviews with the biologists with other records to link the Soviet catch data to specific IWC-management areas in the Southern Hemisphere—thereby solving the mystery of Baker's missing Oceania whales. The study reveals that the Soviets hit this population in the Antarctic waters south of New Zealand particularly hard from 1959 to 1961, killing more than 25,000. Later, they took another 23,000, but they reported only 2710 total to IWC.

Because of earlier whaling, "those humpbacks were already in decline," says Baker, "and the Soviets took the rest. Their whaling cast a very long shadow." Clapham's team says that the Oceania subpopulation today numbers between 3000 and 5000, 20% to 25% of its original size, and was categorized last year as endangered. "It will easily take them another 50 years to recover," says Baker.

The paper is timely because some IWC members are calling for modifying the current moratorium on commercial whaling, says whale biologist Sidney Holt, who played a key role at IWC for 49 years. Two years ago, citing the worldwide recovery of humpbacks, Japan announced that it would begin hunting the humpbacks of the Southern Ocean as part of its scientific whaling, although that plan is now on hold.

IWC, then as now, relies on self-reporting of results and has no enforcement provisions. To Holt, the Soviet catch data "show how essential it must be to put in place a watertight international system to ensure compliance with regulations." But Lars Walløe, a whale scientist at the University of Oslo, Norway, says that "it is quite a different story today." Nowadays, whales are hunted for meat, not oil, and so there "isn't the same incentive for such deception."

The moratorium will be at the heart of discussions next month at the IWC annual meeting in Madeira. Mikhalev plans to attend—a living reminder, says Clapham, that "self-regulation in environmental matters doesn't work." **–VIRGINIA MORELL**

CREDITS: ODESSA ANTARCTIC WHALING FLEET MUSEUM; PHIL CLAPHAM

Published by AAAS

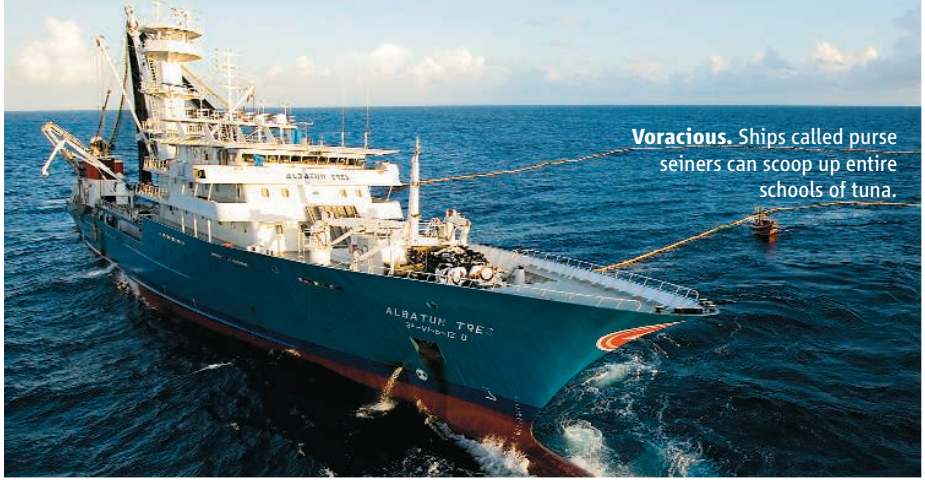

Voracious. Ships called purse seiners can scoop up entire schools of tuna.

CREDIT: © GREENPEACE/PAUL HILTON; SOURCE: GREENPEACE

FISHERIES

Protecting the Last Great Tuna Stocks

Representatives of Western Pacific island nations put the finishing touches last week on a series of bold, new measures aimed at saving the world's last great tuna stocks.

Last May, the group decided to bar fishing in two huge pockets of international waters, creating the largest ever no-fishing zone. Fishing in the rest of the Western Pacific is regulated by the Western and Central Pacific Fisheries Commission, a treaty-based organization that includes 15 island nations and 10 countries that pay them for the right to fish in their so-called Exclusive Economic Zones (EEZs), which stretch 200 nautical miles from land. Meeting last week in Niue, a tiny island nation 4000 kilometers south of Hawaii, the ministers decided to add two smaller pockets of international waters.

The result: four no-take areas totaling 1.2 million square kilometers stretching 7000 km from French Polynesia to Palau. Combined, the no-take zones are more than three times the size of California and dwarf the 360,000-km^2 reserve in the Northwestern Hawaiian Islands, whose waters contain far fewer fish.

"It's a big victory for us, because these pockets were being fished much more intensively than our own waters," says Sylvester Pokajam, managing director of the National Fisheries Authority of Papua New Guinea. "They were also used as refuges by ships that poach in our waters." Phil Kline of Greenpeace USA says the agreement "proves that an international process can actually achieve this" united front.

The measures, which take effect in January, would reduce by 10% the number of fishing days in these EEZs for most of the 225-ship international fleet of purse seiners, says Pokajam. The ships, which use huge nets to take out entire schools of tuna, account for three-quarters of the catch. The new rules also oblige the ships to carry independent observers, restrict the use of floating platforms, called fish-aggregating devices, that disproportionately attract juveniles, and ban throwing dead fish overboard to make room for more valuable fish. All boats, even those that use hooks and lines, will be barred from fishing in the high-seas pockets.

"These are the broadest and most effective measures of any tuna fishery in the world," says James Joseph, a fisheries scientist who for decades managed the commission that regulates the eastern Pacific, and they come none too soon. He says most of the world's tuna stocks are being fished at an unsustainable rate. "Bluefin is a catastrophe, bigeye and yellowfin are in trouble in most places, and so are some albacore," he says. "Only skipjack are still in good shape."

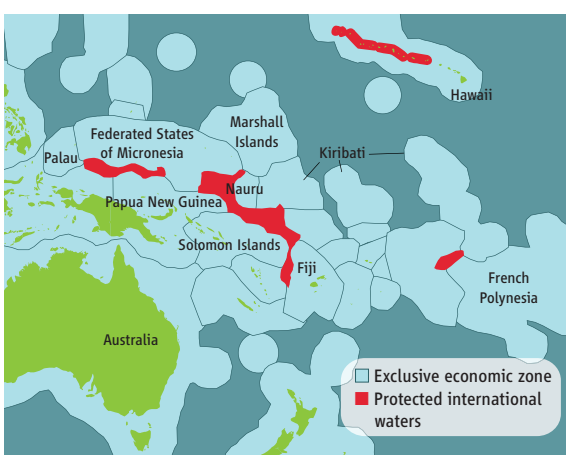

Tuna sanctuary. Four pockets of international waters (red) will be permanently closed to all fishing in January to protect tuna.

The Western Pacific's catch has gone from 500,000 tons a year in 1970 to 2.4 million tons in 2008. That's 60% of the world tuna catch, worth $3.9 billion, with purse seiners accounting for most of the increase. As a result, in the past half-century, the Pacific stocks have shrunk by 50% to 80%, except for skipjack. In the past decade, the fleets that depleted the tuna stocks in the Atlantic and the Eastern Pacific moved in, aggravating the problem. The spike in fishing created a bonus for the region's microstates, which receive an average of 5% of the value of the landed catch. For Kiribati, for example, the windfall provides a third of the government's revenue.

When fisheries scientists warned that these rates were not sustainable, the islands' leaders embraced their advice, including a recommendation for an immediate cut of at least 30% for bigeye and 10% for yellowfin. The fishing nations, including Japan, Taiwan, and South Korea, resisted, and a compromise solution was designed to lower the take by 10% a year over 3 years.

The United States has resisted even that reduction. Under a separate treaty that lumps together access fees and development aid, the U.S. government pays most of the access fees for the 40-ship U.S. fleet. The U.S. has agreed to abide by the new agreement but says that the treaty exempts it from the 10% reduction.

The island nations are not happy. "The United States has expanded its fleet from 11 to 40 ships in the past few years, mostly by allowing Asian ships to take the American flag," says Pokajam. "These ships, which don't even supply the American market, now fish without limits in our waters. The U.S. talks about conservation but behaves differently."

Several fisheries experts warn that the new measures probably aren't sufficient to stop the bigeye's free-fall. "It's a great leap forward, for sure," says Kelvin Passfield of the Pacific Ocean fisheries program of the International Union for Conservation of Nature. "But I'm afraid it's not going to be enough. If you don't cut 30% of the take when you need to, it usually means you'll have to cut 50% later."

Daniel Pauly, a fisheries scientist at the University of British Columbia, Vancouver, says fish species have survived only because some of their ranges have been inaccessible to fishers. "Now that fishing methods are much more effective, we need to create no-take zones so that we don't exploit the whole range of any given species," he explains. "In other words, a natural sustainability mechanism has to be replaced by a deliberate one to avoid species collapse."

–CHRISTOPHER PALA

Christopher Pala is a writer based in Hawaii.

Published by AAAS

Ominous sign. Little brown bats are one of six species in trouble.

CREDIT: CRAIG STIHLER

Biologists Struggle To Solve Bat Deaths

An epidemic has stricken the northeastern United States for 3 years. As it spreads, researchers wonder whether a white fungus is the real killer

CHALKHILL, PENNSYLVANIA—Leaning back against a grimy rock wall, wildlife biologist Greg Turner of the Pennsylvania Game Commission focuses his headlamp on a brown, furry clump of bats hanging in a cramped underground passageway. After a few seconds, he spies what he's looking for: the gleam of a tiny temperature sensor glued to the back of a bat. Gingerly, Turner plucks the hibernating bat with his gloved hands and stashes it in a cloth sample bag.

Turner and two colleagues have spent the past 3 hours scouring this cave for instrumented bats that may provide clues to a pressing mystery. An unknown killer has been wiping out populations of six species of hibernating bats in the northeastern United States in what appears to be the biggest die-off on record. "We're stabbing in the dark in a lot of ways, just trying to understand what's going on," Turner says.

Scrambling out of the cave in the late afternoon, Turner is feeling upbeat. There were no dead or dying bats, and no sign of the telltale white fungus that may or may not be involved in the trouble. Moreover, he and his colleagues retrieved 17 bats with data loggers to reveal more about the hibernation patterns of healthy bats, which could shed light on what's going wrong elsewhere. Euthanized bats and soil samples will be shipped to researchers in other states for analysis.

All told, the crew gathered data for six experiments involving dozens of scientists. Similar missions are under way throughout the eastern United States, as bat researchers on the East Coast have shifted gears from routine bat research in the past 2 years to investigate the malady. So far, there are more questions than answers. Efforts are ramping up farther west as well: Scientists are forming a Midwest Bat Working Group, which met for the first time earlier this month in Indiana to plan and coordinate future bat-research strategies.

The task is urgent. The disappearance of these northeastern hibernating bats could have larger impacts on ecosystems, as these night flyers hunt insects that annoy humans and damage crops. And last October, a group of more than 100 participants from a science strategy meeting concluded that if the problem continues to expand at its current rate, entire species—including the endangered big-eared bat in Virginia and Indiana—could be in jeopardy.

Bleak midwinter

The first sign of trouble came in February 2006, while researchers in New York state were conducting a routine census of bats in four caves some 80 kilometers west of Albany. To their horror, they discovered either a precipitous drop in population or many dead bats in the four caves, located less than 13 kilometers from each other. At Hailes Cave, for example, the number had dropped by 43%, from 15,584 the year before to 6735.

Many bats—both dead and alive—had a whitish fungus ringing their muzzles and dotting their ears and wings. Although fungi on bats are not unusual, there was far more than normal. The dead bats had no obvious diseases, toxins, or parasites. Instead, they lacked enough body fat to get through the winter. Apparently, they had come out of hibernation early and exited caves during daylight, perhaps to search for insects. With nothing to eat, they starved to death.

The situation worsened over the next winter. Bat populations in these four caves fell by 50% to 100%. Even more alarming, researchers were finding emaciated or dead bats in other caves and mines in a widening area. Because the white fungus was seen in all these locations, the researchers dubbed the problem white-nose syndrome.

Last winter, the syndrome continued to spread. By April, it had reached 10 caves and mines in eastern and central Pennsylvania. Several caves in Virginia and West Virginia also showed signs. Many caves visited by bat biologists in these newly affected areas remain free of white-nose, but the syndrome is clearly advancing across an ever-wider front.

Early clues

The same fungus, a new species of the cold-loving genus *Geomyces*, is turning up everywhere. David Blehert of the U.S. Geological

Online
sciencemag.org
Podcast interview about this article.

Published by AAAS

Survey's National Wildlife Health Center in Madison, Wisconsin, identified the fungus in affected bats from multiple sites (*Science*, 9 January, p. 227). He and a dozen coauthors concluded that the fungus is "consistent with properties predicted for a causative agent." But the central question remains: Is the white-nose fungus the primary cause of the deaths or simply an opportunistic infection?

Further tests by Blehert's group may settle the issue. Since last fall, researchers and recreational cavers have been collecting soil samples from more than 200 sites in almost 30 states. If *Geomyces* spp. turns out to be present in unaffected sites distant from the syndrome's epicenter, the fungus may not be the primary pathogen. Blehert expects results by the fall.

Blehert has also conducted trials to see if *Geomyces* spp.—and clinical signs of white-nose syndrome—can be spread among hibernating bats. Using little brown bats (*Myotis lucifugus*) in the lab, the researchers brushed spores onto bats, allowed infected bats to touch unaffected ones, and housed unaffected bats in mesh enclosures near separate enclosures containing infected bats. These experiments wrapped up last month, and it appears that bats can spread the fungus among themselves.

Still, many researchers doubt that the fungus itself is to blame. "Fungal infections don't typically kill animals," explains DeeAnn Reeder of Bucknell University in Lewisburg, Pennsylvania. Instead, she says, fungi tend to be secondary infections that attack an animal already compromised by some other pathogen, such as a virus or bacteria.

To find out more about what could be going wrong, researchers are probing the basics of bat biology. Reeder and her colleagues have put more than 300 temperature data loggers and transmitters on bats in six states. Hibernating bats will arouse and triple their body temperature for a few hours every 12 to 15 days. In bats with white-nose syndrome, however, the arousals seem to be more frequent. One hypothesis is that the bats do this to groom the fungus away or to reactivate their immune systems to fight off an unknown pathogen.

A team led by Marianne Moore of Boston University is testing the latter idea. She and colleagues have been measuring the strength of the immune system in bats at various times during hibernation season, both in torpor and when aroused. They hope to find out if the immune systems of bats with white-nose syndrome have been compromised.

Another question is whether the sick bats lose most of their body fat during hibernation or start out the winter already in trouble. Jonathan Reichard of Boston University measured the body fat of bats during the fall, when they fatten up, and followed them during hibernation. "We're hoping to narrow down when bats are being most affected," he says. Preliminary results suggest that regardless of when white-nose initially attacks the bats, it worsens over time. Even if bats survive hibernation, many either die prematurely in the spring or enter the next hibernation scrawny.

Intriguing clues are also emerging from the digestive system, according to microbiologist H. Kathleen Dannelly of Indiana State University in Terre Haute. Bats eat a lot of chitin, the hard exoskeleton of insects, and in summer they don't digest it. But they seem to do so in winter. Inside the digestive tract are bacteria that produce chitinase, an enzyme that breaks down chitin, and the bats might be extracting energy from the chitin, according to Dannelly.

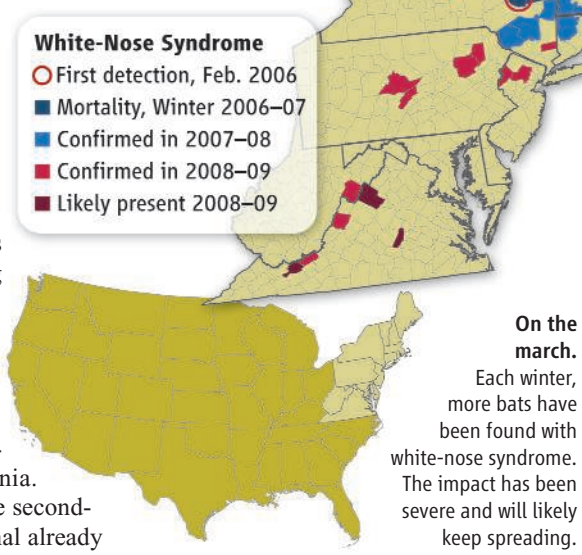

On the march. Each winter, more bats have been found with white-nose syndrome. The impact has been severe and will likely keep spreading.

SOURCE: CAL BUTCHKOSKI/PENNSYLVANIA GAME COMMISSION

Bats with white-nose syndrome seem different. Compared with healthy hibernating bats, 18 affected bats from New York state had far fewer chitinase-producing bacteria. "In fact, in the majority of white-nosed bats, we couldn't isolate any chitinase producers," Dannelly says. Her team has found "several predominant organisms" in the digestive systems of all 18, but she declines to elaborate, as the data are still preliminary. Still, she suspects a pathogen might be compromising the bats' ability to digest chitin, which is possibly their only winter fuel other than fat. This could explain their starvation.

Stopgap measures

As researchers struggle to identify the culprit behind white-nose syndrome, an even larger question looms. What, if anything, can be done to help the bats?

One idea, proposed by Justin Boyles of Indiana State University and Craig Willis of the University of Winnipeg in Canada, is to put heated refuges in caves. They have found that when bats arouse during hibernation, they naturally go to the cave's warm spots in order to conserve energy. Because white-nose syndrome forces them to arouse more frequently, Boyles and Willis hope that heated areas could increase their chances of survival.

In another effort, a partnership of the U.S. Fish and Wildlife Service (FWS), the West Virginia Division of Natural Resources, and the Association of Zoos and Aquariums is considering whether to place several dozen Virginia big-eared bats in captivity. Assuming that white-nose eventually hits this endangered species, the hope is that this captive population might prevent its extinction.

Meanwhile, researchers are taking measures to prevent the accidental spread of pathogens; gear is either new or thoroughly washed and disinfected. And on 26 March, FWS recommended a voluntary moratorium on all recreational caving in any state where white-nose syndrome has been found within or adjacent to its borders. Then, on 24 April, the U.S. Forest Service closed all caves and mines for 1 year in all national forests in the northeastern United States. A similar closure for the southeastern United States is expected before the end of May.

Because bats migrate, experts expect that the syndrome will keep moving west and south in the coming years. As the pathogen moves south, it might not be as damaging, because hibernation is shorter and the bats might make it through the milder winter. As for the prospects of bats in the Northeast, most bat specialists seem pessimistic. "The future does not look good," says Craig Stihler of the West Virginia Division of Natural Resources.

–ROBERT ZIMMERMAN

Robert Zimmerman is a writer in Greenbelt, Maryland.

Poop search. In barnyards and zoos, Ruth Ley seeks out interesting gut microbial communities.

PROFILE: RUTH LEY

Gut Reactions

A young microbial ecologist helps transform medical microbiology into a modern interdisciplinary science

When Ruth Ley arrived at Washington University School of Medicine in St. Louis, Missouri, 5 years ago, she didn't quite know what she was getting into. "As a microbial ecologist working in a medical lab, I was a little lost," Ley recalls. She came to Jeffrey Gordon's lab because it was moving into large-scale studies of organisms inhabiting the human gut, yet she had no background in physiology or human biology. At one point, she says, a colleague in immunology asked her if she knew any biology at all.

But she turned out to be the right person in the right place at the right time. Part of a new generation of microbiologists trained in genomics, ecology, and bioinformatics, she was in a good position to help pull medical microbiology out of a long-standing rut. In that field, most research had focused on the few pathogens that could be grown in the lab and disregarded the rest. "Ecology," says David Relman, a microbiologist at Stanford University in Palo Alto, California, had "been ignored by a large subset of the more medically inclined microbiologists." Into that gap stepped Ley.

During her 4 years in St. Louis, Ley and her colleagues demonstrated that individuals vary in the repertoire of microorganisms they host—and that those variations can affect health and disease. They discovered a link between obesity and the gut flora of mice and humans, and they traced the evolution of gut communities, showing the effects of phylogeny, diet, and other factors on the makeup of those communities. "These were foundational studies," says Martin Blaser, a physician and microbiologist at New York University, and they are helping to shape policy and scientific agendas. "She brought a very useful perspective to a group of workers who weren't thinking about [the gut] as an ecological question," adds Norman Pace, an evolutionary microbial ecologist at the University of Colorado, Boulder.

Now an assistant professor at Cornell University, Ley plans to be digging in cornfields, chasing down bacteria associated with maize roots to try to tease apart how a host's genotype affects the genetic makeup of its microbial partners. That will be yet another change of environment for a scientist who has spent her professional life so far tramping through snow after alpine bacteria, sweating under the hot sun sampling microbial mats in salt ponds, and scooping up feces in the cages of lions, tigers, and bears. "What it comes down to is I'm just interested in what microbes are, and why and what are they doing," Ley explains.

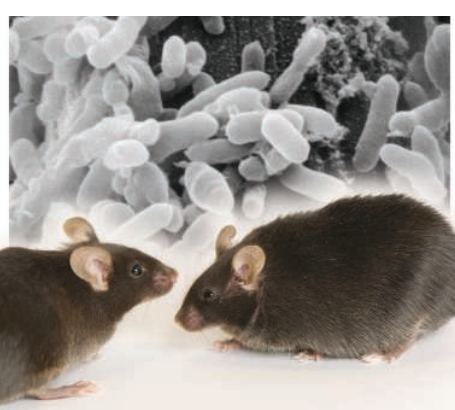

Microbial bias. Fat and lean mice—and people—have different proportions of these *Bacteroides* bacteria (*background*) in their guts.

CREDITS (TOP TO BOTTOM): ROBERT BARKER, CORNELL UNIVERSITY PHOTOGRAPHY; JASON HE, JACKSON LABORATORY

Macro to micro

Ley began her scientific life as a plant community ecologist. For 3 years after graduating from the University of California, Berkeley, she worked in Hawaii for UC Berkeley's Carla D'Antonio, looking at the role of fire in paving the way for grasses to take over dry tropical woodlands on the island of Hawaii. A change in the pattern and timing of wildfires altered the nitrogen content of the soil and resulted in "a tropical woodland that turned itself into an African savanna," Ley says. Her work there sparked her interest in soils, and when she started her graduate program at the University of Colorado, Boulder, in 1995, she moved her field site from the tropics to the Rockies.

At the time, Colorado's water authorities were scratching their heads because snowmelt—the key source of municipal water—was rich in nitrogen, despite the apparent lack of much life on those high, cold peaks. Ley set up remote monitoring stations to measure environmental parameters such as temperature and nitrogen under the snow. The work revealed that the snow provided enough insulation for nitrogen-producing microbes to thrive in the soil. "Just the mass of organisms in those kinds of soils and their activity were much more than predicted," recalls her adviser, Steven Schmidt.

"At the end of my Ph.D., I became interested in what the microbes were," Ley recalls. Metagenomics was the new buzzword among microbiologists, who were using rapid sequencing technologies to decipher the DNA in entire samples of soil or water. By checking the results against databases of microbial genes, researchers

Published by AAAS

can get a handle on the diversity of invisible life the sample contained. Ley teamed up with Pace, newly arrived at the University of Colorado, to apply metagenomics to what they thought would be a fairly simple system: salt flats. She spent 3 years traveling back and forth to Baja California, battling sun and wind scraping samples from 15-centimeter-thick mats growing in meter-deep salt-works ponds. She and her colleagues dug out 15 major groups of novel bacteria.

Microbes matter

The move east to Missouri brought her into contact with yet another ecosystem: the human gut. Gordon was surveying gut communities in mice and humans and wanted to know what determined which bacteria lived where. Was it diet? Host choice? Environmental factors? And were there differences that affected how efficiently an organism processed food? Ley's experience turned out to be a perfect fit. "She comes from the perspective of studying things as a system and how they are interrelated," says Schmidt.

Gordon put Ley in charge of assessing the microbial makeup of the gut of mice carrying mutations that predisposed them to obesity. Ley and Peter Turnbaugh, a graduate student, sequenced the 16*S* ribosomal genes—which are often used to distinguish microbial species—from bacteria inhabiting the gut of fat mice and lean siblings lacking the mutation and compared them with what was in the public databases. They discovered that in lean mice, a group called *Bacteroidetes* predominated, but in their plump peers, the *Firmicutes* held sway; the obese animals had 50% fewer *Bacteroidetes*.

Turnbaugh transplanted microbes from both sets of mice into germ-free lean mice and watched how they grew. The ones that got microbes from obese mice "ate the same amount, had the same initial body weight and body fat, but gained more," Ley says. Gut microbes were contributing to excess girth, they reported in the 21 December 2006 issue of *Nature*, making headlines across the globe.

Once Ley started to get an inkling of the role microbes might play in obesity, she moved into the clinic, where she followed a dozen unrelated obese people on either a low-carbohydrate or a low-fat diet for a year. The exact species makeup varied from person to person, but like the obese mice, the study participants had fewer *Bacteroidetes* and more *Firmicutes* than people of regular girth; as they lost weight, the numbers shifted in favor of the *Bacteroidetes*, Ley and colleagues reported in the same issue of *Nature*. With these studies, "she has opened very important vistas in human metabolism," says Blaser. Adds Jo Handelsman of the University of Wisconsin, Madison, the work "revolutionizes our understanding of [obesity]" and "is a model for determining [the] microbial contribution to other diseases and conditions."

Ley didn't spend all her time in St. Louis working with mice and people. She became a regular visitor to the local zoo, collecting fecal samples from as many different animals as she could. She also got samples from the San Diego Zoo and from a field biologist who provided material from 29 wild animals, for a total of 106 samples from 60 species, including 17 nonhuman primates. She tried to pick a few with diets at odds with those of the rest of the group—such as leaf-eating colobus monkeys to contrast with their omnivore cousins, or vegetarian pandas as the outliers to fellow carnivores. She isolated and sequenced more than 20,000 16*S* ribosomal genes and compared those sequences with the known gut microbiota from humans, rats, cattle, and gorillas.

The flora tended to be species-specific. Pandas from the two zoos had quite similar communities, despite the geographic separation, for example. Diet also seems to have an effect: The herbivore communities tended to be more similar to each other than to communities in carnivores, and the human microbial repertoire fell squarely in line with that of other omnivore primates. "Ruth showed that there are different signatures for different types of diets," says Bryan White, a microbiologist at the University of Illinois, Urbana-Champaign. When she built a family tree to see how the microbial communities were related, the branching pattern mirrored the family trees of the animals providing the samples. The flora of brown bears and polar bears were closely related and distantly related to that of their second cousin the dog, for example. "The ancestral bear microbial community of the gut has been passed along, and you can see it," Ley explains.

Online
sciencemag.org
Read an "In Person" essay by Ruth Ley on dual-career couples at sciencecareers.org.

Genes perspective?

Ley's work has helped drive home the close association between our microbes and ourselves. Studies of the full complement of microbial genes in and on the body—the microbiome—show that although there is quite a bit of variation from person to person, there is a core set of genes that provide essential services. In the gut, for example, those genes help break down food and make it available to the body.

Gordon thinks that because the microbes have evolved certain genes and functions, the host doesn't have to. But Ley wonders whether the reverse is also true. For example, people with high-starch diets have more copies of amylase genes than people who eat more protein have. These amylases break down starches in the gut, a function that might in certain circumstances be done by the microbes themselves. Thus variation in the numbers of copies of these genes "might have a direct impact on the genes in the microbiome or the [microbial] lineages in the gut," she suggests.

Ley plans to first attack these questions using maize stocks of known genotypes and root bacteria associated with them. Such studies should help scientists interpret results from the Human Microbiome Project, a $115 million, 5-year effort funded by the National Institutes of Health that will sequence hundreds of human-associated microbes and conduct surveys of the communities living in various parts of the body. The effort "needs to be more than just a description of parts," Gordon warns. The microbiome is quite dynamic, with selective forces operating on many levels shaping the diversity and functionality of these gut communities.

Widely traveled. Ley's studies have led her from tropical Hawaiian volcanoes to Rocky Mountain peaks to the dry valleys of Antarctica (*top to bottom*) and, ultimately, into the world of gut microbial ecology.

This push means that for microbiome researchers, "all of us are becoming ecologists," says Blaser. And that's where people like Ley come in, he adds. "It's great that we have a card-carrying ecologist to teach us."

–ELIZABETH PENNISI

CREDITS: PHOTODISC/GETTYIMAGES; RUTH LEY

ENVIRONMENTAL RESTORATION

Obama Moves to Revitalize Chesapeake Bay Restoration

With progress stalled for years, EPA takes the reins on cleaning up the largest estuary in the United States. It's not going to be easy

Teeming with crabs and oysters, the Chesapeake Bay was legendary for its biological richness. In the early 17th century, English explorer John Smith described fish so abundant, he tried to catch them in a frying pan. But by the 1960s, those days of plenty were long gone. As sewage and fertilizer ran into the bay, huge algal blooms had erupted from excess nitrogen and phosphorus. Fish and crabs were suffocating in oxygen-poor dead zones.

For more than 25 years, the federal government and six states in the watershed have repeatedly promised to fix the problem—and repeatedly failed. They have poured billions of dollars into the effort, yet few measures of biological health have improved beyond the halfway mark to success. The challenge is daunting, because stresses on the bay continue to increase; population in the 165,000-square-kilometer watershed has doubled since 1950 to nearly 17 million, meaning more wastewater, concentrated animal farms, and nitrogen-rich air pollution. The costs involved in reducing nutrients are enormous, and a patchwork of local governments makes it difficult to restrict or guide development.

Now, advocates see some signs of hope. On 12 May, President Barack Obama directed the Environmental Protection Agency (EPA) to take charge of a new federal effort and to exercise its full authority under the Clean Water Act. The order also calls for better agricultural practices and the development of a strategy to deal with threats from climate change. "We're very happy to have an executive order, for the first time ever," says William Baker, president of the Chesapeake Bay Foundation, an advocacy group in Annapolis. "It's saying, 'Let's get on with this right now.'"

At the same time, the leaders of six states and the District of Columbia announced a plan to institute a series of 2-year deadlines to increase political accountability and clean up the bay by 2025. Some states may have to double their existing efforts to meet that goal. Meanwhile, substantial sums of new money are flowing to restoration efforts, including $891 million from the Recovery and Reinvestment Act for upgrading wastewater treatment plants. EPA is nearing completion of a baywide pollution cap, as well as a clean-air rule for the East Coast that will reduce the amount of nitrogen from power plants. "I'm optimistic that substantial improvements are within reach," says biological oceanographer Donald Boesch of the University of Maryland Center for Environmental Science in Cambridge.

Long road

The first restoration goals were set in 1987 when a state-federal partnership called the Chesapeake Bay Program agreed to reduce nitrogen and phosphorus entering the bay by 40% by the year 2000. The levels fluctuated but did not fall. The amount of chlorophyll a, which indicates algal blooms, rose, and water clarity worsened. Still, there was progress: More water had adequate dissolved oxygen (see charts).

The effort required actions by farmers from Virginia to New York because agriculture is the single largest source of nutrients to the bay, providing 43% of the nitrogen. Financial incentives were provided to plant buffer strips along streams to reduce fertilizer and manure runoff, for example. Sewage treatment plants, which contribute 20% of the nitrogen that ends up in the bay, were upgraded. At the same time, more people moved into the area; during the 1990s, there was about a 41% increase in the amount of pavement and other impervious surfaces that send pulses of nutrient- and sediment-rich storm water to the bay. "The fact that [the Bay Program] pretty much held the line in the face of growth and development is not a minor accomplishment," says Thomas Simpson, a soil scientist who leads Water Stewardship Inc., a nonprofit in Annapolis.

Despite having missed its first goal, in 2000, the Bay Program set another, even more ambitious, target. Officials pledged to reduce nutrients enough by 2010 to restore the bay to its 1950s state of health. They also set a target for reducing excess sediments flowing into the bay, which lower the

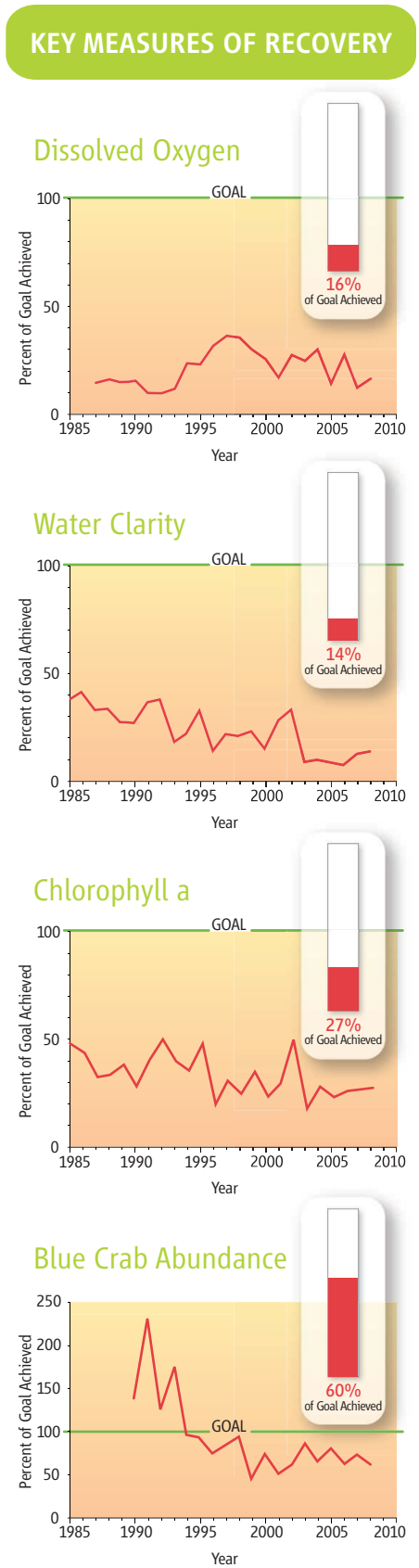

Running in place. Despite many recovery actions, continued development has meant that many indicators of bay health are flat or declining.

CREDITS: ADAPTED FROM BAYSTAT.MARYLAND.GOV

Published by AAAS

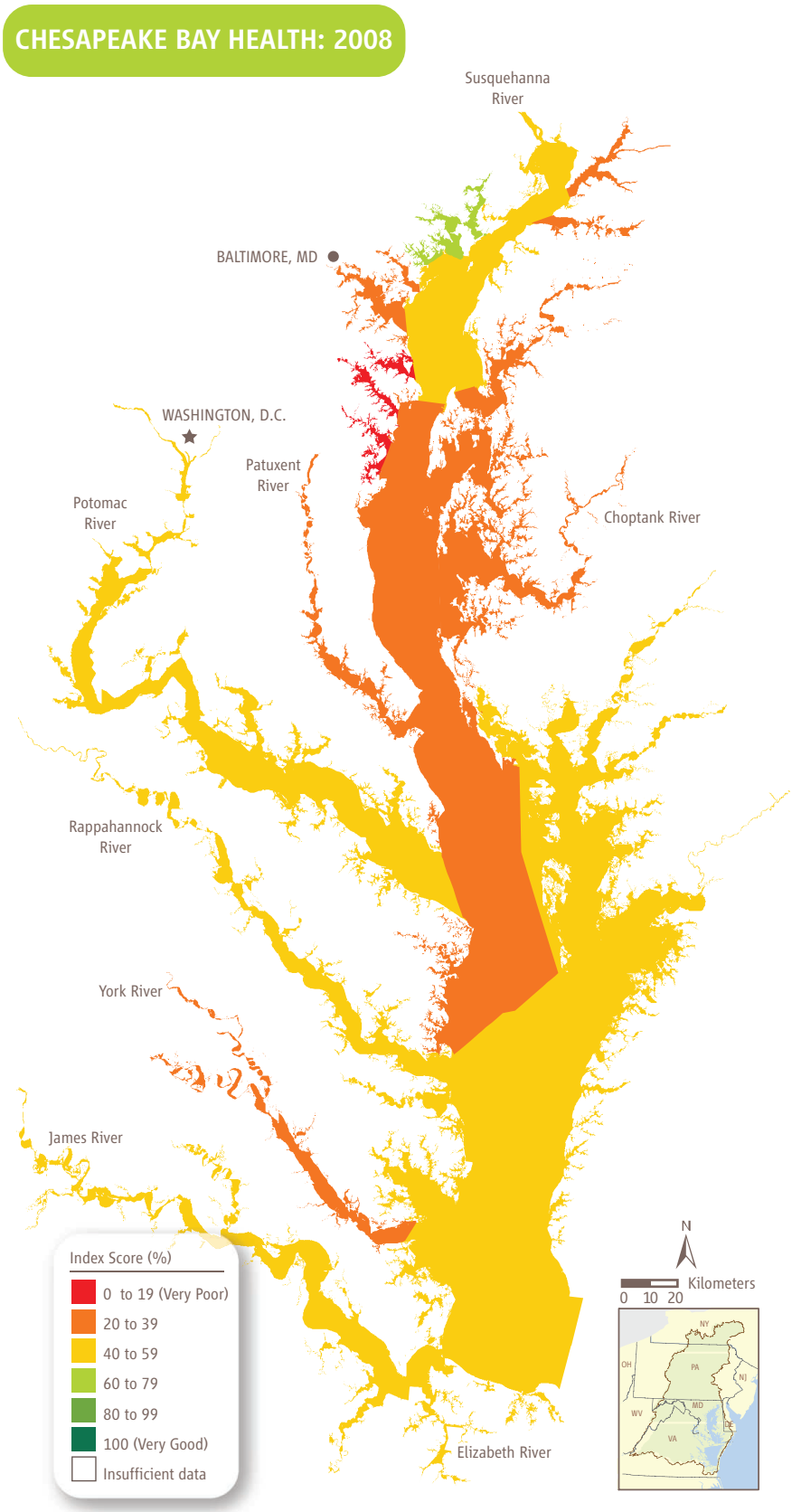

CREDITS: ADAPTED FROM ECO-CHECK.COM

Poor health. This overall index combines the status of aquatic grasses, benthos, and phytoplankton with water quality. It has held roughly stable over the past decade.

clarity of the water, which in turn harms the submerged grasses needed by crabs and young fish. Even so, during this decade, many indicators have been on a downward trend. "I don't think anyone is happy with the progress or performance of the Bay Program," says J. Charles Fox, who is EPA Administrator Lisa Jackson's special assistant on the Chesapeake.

EPA has several options to flex more muscle under its existing authority, which it says it will discuss with the states. The agency could expand its reach over concentrated animal-feeding operations, for example, or give specific conditions for stormwater permits that local governments need for development. "There are plenty of sanctions EPA could apply that would be very attention-getting," says Baker, such as withdrawing certain funding it provides to states if goals aren't met.

But EPA has little clout over an even bigger problem: so-called nonpoint-source pollution, such as fertilizer seeping from farm fields into streams. Right now, farmers are encouraged to use "best management practices," such as planting cover crops that reduce runoff, but few states have requirements, and penalties are minimal. The 2008 Farm Bill provides $188 million over 4 years for the U.S. Department of Agriculture's Chesapeake Bay Watershed Initiative, the largest amount ever—but not nearly enough, says ecologist Carlton Hershner of the Virginia Institute of Marine Sciences in Gloucester Point. The problem is that many of these practices have turned out to be much less effective than they seemed in experimental fields. "We're going to need to do more to get to the same end goal," says Richard Batiuk, associate director of science for the Bay Program.

The Bay Program hopes to encourage more action by providing local governments with more information about their impact on the bay. "If you provide numbers for the entire Eastern Shore of Maryland, no one feels accountable," Batiuk says. But now, improved computer models of the watershed and bay have enough spatial resolution to predict how much nitrogen, phosphorus, and sediment come from small watersheds. EPA is exploring possible enforcement actions to include in its baywide pollution cap, which is due by the end of next year. Adding more teeth to regulations is essential, says Boesch: "I don't know of any cases where these kinds of problems have been addressed simply by voluntary actions and payments."

–ERIK STOKSTAD

Published by AAAS

LETTERS

edited by Jennifer Sills

"Agriculture" Is Not a Dirty Word

AGRICULTURAL SCIENCE IS RIPE FOR A RENAISSANCE. FOR TOO MANY YEARS, THE AGRICULture sciences have been disparaged in the science and education communities, perhaps because agronomy, soil science, plant pathology, and animal science use a problem-solving approach rather than simply seeking knowledge.

When science research funds are handed out—for example, in the federal stimulus bill—agriculture often gets left off the list. I suspect this is because policy-makers and some scientists see "agriculture" as synonymous with "agribusiness," rather than as a purely scientific discipline, and they assume private funding will take care of agriculture-related research needs. Agricultural scientists at land-grant institutions do receive some research dollars from noncompetitive sources, but not all research is funded this way.

Adding insult to injury, the major U.S. science journals don't devote specific sections or editors to agricultural research. Some schools of agriculture have taken the word "agriculture" out of their names, presumably to attract more students in a country where only 2% of the population farms. (It hasn't worked: Enrollment in university agricultural science majors has dropped steadily nationwide since the early 1980s.)

In short, agricultural science has an image problem. Our disciplines are not considered relevant and, more disturbing, we're not seen as a source of solutions to many of the world's most pressing challenges, even though many of those challenges directly relate to agricultural science.

That's unfortunate, particularly in a world where people are starving or eating unsafe food, where climate change will affect every aspect of 21st-century life, and where new kinds of sustainable fuel are needed. The urgency of these global issues—all of them related to the agricultural sciences—amplifies the need for an applied-science approach.

Agricultural scientists can do amazing things when they combine their expertise and have access to the resources they need. Recently, scientists at an international conference in Mexico announced that they have found a wheat variety that is resistant to Ug99—a strain of stem rust that could affect up to 90% of the world's wheat (*1*). Although the scientists have not completely eliminated the threat, it's clearly a breakthrough with enormous implications.

Other recent signs also point to a renewed interest in and respect for agriculture. When the first lady plants a vegetable garden on the White House lawn for the first time in half a century, she's sending a strong message: Food is important. Books about eating a sustainable, healthy diet top our best-seller lists. The National Gardening Association expects a 19% jump in the number of people growing at least some of their own food this year. Clearly, a growing number of Americans are interested in where their food comes from, even on a small scale.

The 2008 Farm Bill creates the National Institute for Food and Agriculture, which will be headed by a distinguished scientist directly appointed by the president. A small thing, perhaps, but it elevates agriculture to a level of prominence along the lines of health and other sciences. The farm bill also increases funding for competitive grants in both basic and applied agricultural research, which will provide opportunities for advanced study.

Enrollment is up 16% since 2005 among college students in the professional associations that specialize in soil and crop sciences and agronomy, which suggests that today's students are interested in learning more about agricultural and environmental issues. Job prospects also are good; the Bureau of Labor Statistics predicts that employment for agricultural and food scientists will be at least average overall and much higher than average in some specialties.

In the long run, does it really matter whether "agricultural scientists" are what we call the people who ensure a safe and plentiful food supply, clean water, and healthy soil? Maybe not, as long as this critical work is funded and accomplished. But as we move into a new era of shared accountability and responsibility, let's keep in mind that agricultural sciences affect us all, and when agricultural science is thriving, our communities likely are thriving, too.

ALLEN S. LEVINE

College of Food, Agricultural, and Natural Resource Sciences, University of Minnesota, St. Paul, MN 55108–6074, USA, and Minnesota Obesity Center, Minneapolis VA Medical Center, Minneapolis, MN 55417, USA. E-mail: aslevine@umn.edu

Reference

1. J. Vidal, " 'Stem rust' fungus threatens global wheat harvest," *Guardian* (19 March 2009); www.guardian.co.uk/ environment/2009/mar/19/ rust-fungus-global-wheat-crops.

Schools Anxiously Await NRC Program Rankings

FACULTY MEMBERS AT U.S. INSTITUTIONS usually have mixed feelings about *U.S. News and World Report*'s graduate school rankings. On one hand, we often criticize its "one size fits all" approach and the importance assigned to different categories. On the other hand, we are keenly aware that the ranking of our school can affect our ability to recruit top graduate students and even faculty. It was thus exciting to hear, in mid-2006, that the National Research Council (NRC) decided to perform its own evaluation of graduate programs, the first in more than a decade (*1*).

In January 2007, I and thousands of my colleagues completed a lengthy questionnaire sent by the NRC. Given that *U.S. News* publishes these rankings on an annual basis, the anticipated NRC release date of December 2007 seemed achievable.

CREDIT: DAVID HANSEN/UNIVERSITY OF MINNESOTA

Published by AAAS

Elucidating microbial consortia
1150

Symbiosis and calcification in corals
1153

Unfortunately, it was not. The release has been postponed again and again, for more than a year. Currently, they do not specify even a tentative release date. Time is an issue, because the rankings are based on attributes that may change over a period of a few years, including funding and publications. The longer the delay between data collection and release of results, the less relevant they become.

The students applying to graduate schools are most affected by this delay. Unfortunately, like fellow students from past years, they will not be able to use the new rankings to choose a school.

ZIV BAR-JOSEPH

School of Computer Science, Carnegie Mellon University, Pittsburgh, PA 15213, USA. E-mail: zivbj@cs.cmu.edu

Reference

1. Research Doctorate Programs, Board on Higher Education and Workforce, Assessment of Research Doctorate Programs (http://sites.nationalacademies.org/pga/Resdoc/index.htm).

Response

WE ARE IN TOTAL AGREEMENT WITH BAR-Joseph in our concern over the length of time that this study has consumed.

The principal product of the study will be the release of a great deal of data covering graduate education in the United States, much of it gathered for the first time, which will be of use to prospective students, the faculty in these programs, and the leadership of institutions of higher education throughout the United States. The data were collected from 93,626 individual faculty members, 222 institutional coordinators providing information about 5009 programs, and many independent private and public sources of information. We are extraordinarily grateful to the participating institutions for the care, time, and work that they have put into this project!

Because data verification is of the utmost importance in a study of this nature, we have taken extraordinary pains to check and to recheck the input information for accuracy and uniformity. An ever-relevant question has been "Did all respondents to a given query address the identical issue?" External checks for consistency and accuracy were made by NRC staff, data were returned to the surveyed institutions several times for verification and correction (with changes recorded for over 400 programs), and queries to independent sources were checked repeatedly. It is of the greatest importance that the differences that we report between different programs be real and not based on either error or misunderstandings. Although the results will never be free of error, we believe that we are now at the end of this process.

The section of the report in which we outline our methodology has been submitted to the rigorous review process of the NRC and should soon be available to interested readers. The release of the full report, with the complete set of data for university graduate programs, should follow not too long thereafter and will be made available to faculty and students well before the beginning of the next academic year. We fully concur that the reported data and analysis should be as current as possible and hope that, working together with the participating universities, a mechanism can be developed to provide updates to the report on a timely and prompt basis.

JEREMIAH P. OSTRIKER[1]* AND CHARLOTTE KUH[2]

[1]Department of Astrophysical Sciences, Princeton University, Princeton, NJ 08544–1001, USA. [2]National Academy of Sciences, Washington, DC 20001, USA.

*To whom correspondence should be addressed. E-mail: ostriker@princeton.edu

Note

1. J.P.O. is the committee chair for the study. C.K. is the study director.

White Wolves Can Stand the Heat

T. M. ANDERSON *ET AL*. REPORT THAT WOLVES of the northwestern forest in North America are dark in comparison to the wolves of the tundra ("Molecular and evolutionary history of melanism in North American gray wolves," Reports, 6 March, p. 1339). Anderson *et al*. suggest in passing that the dark coats might better hide preying wolves in the forest. An alternative adaptive explanation is that in the summer, a black tundra wolf could overheat.

Dive In!

With MISSION® esiRNA genome-wide libraries

SIGMA Life Science

NEW! MISSION esiRNA (Endoribonuclease-prepared siRNA) provides RNAi researchers with a proven, cost-effective, and simple way to perform RNAi screens. MISSION esiRNA are available for genome-wide libraries, custom libraries, and individual genes.

- **Value** – Dive in today with affordable genome-wide libraries
- **Proven** – esiRNA have been successfully used in a variety of published RNAi screens
- **Confidence** – Highly specific and reduced off-target effects
- **Simplify** – Rapid genome-wide primary screens

Dive into screening and leave the rest to us. Visit ***sigma.com/esirna***

Our Innovation, Your Research — Shaping the Future of Life Science

A study by Finch and Western provides evidence of the temperature-related consequences of coat color among pastoralists' cattle in Kenya (*1*). Finch and Western showed experimentally that black Boran Zebu cattle in the sun became hotter than did white cattle and that across Kenya, as heat stress increased, the proportion of dark cattle in herds decreased. They also found that herders report more dark than light cattle dying during droughts at low altitude. Finch and Western related the variation in color to the social system of the Kenyan herders. Some of them divide themselves into clans according to the preferred color of their cattle, and the preference correlates adaptively with the usual heat stress of the clans' home ranges.

ALEXANDER H. HARCOURT

Department of Anthropology, Graduate Group in Ecology, University of California, Davis, CA 95616, USA. E-mail: ahharcourt@ucdavis.edu

Reference

1. V. A. Finch, D. Western, *Ecology* **58**, 1384 (1977).

CORRECTIONS AND CLARIFICATIONS

Perspectives: "Tipping pointedly colder" by L. R. Kump (27 February, p. 1175). In the figure caption, the cooling trajectory was mistakenly referred to as red (it is blue) and the warming trajectory as blue (it is red). In the third paragraph, references 4 and 5 were reversed (reference 4 is to Lear *et al*., 2008; reference 5 is to Katz *et al*.), and in the fifth paragraph, the reference to Lear *et al*. (*5*) should be to reference 3 (Lear *et al*., 2000). In the ninth paragraph, the citation to references (*2*–*4*) should be to references (*2*–*5*).

Perspectives: "Harvesting ocean wave energy" by J. Scruggs and P. Jacob (27 February, p. 1176). For panel A of the figure, the photo credit should have read "Copyright 2007 New York Times Graphics" and the caption should have read "Schematic of a direct-drive point absorber developed at Oregon State University." The rated power of the Ocean Power Technologies array in Oregon is 1.5 MW, rather than 2.0 MW, and the company name for the AWS point absorber is Teamwork Technology BV.

Reports: "Spending money on others promotes happiness" by E. W. Dunn *et al*. (21 March 2008, p. 1687). We recently identified a bug in the statistical package SPSS 14.0 that we used to analyze our data. The bug causes the first line of data to overwrite the sixth line of data (see www.is.stir.ac.uk/itsupport/software/SPSS.php). This bug affected the data set for our longitudinal study ($N = 16$). Primarily because this error decreased the variance in our data set, correcting this error alters the critical statistical test such that the effect of prosocial spending on happiness is reduced from the originally reported effect of $b = 0.81$, $P < 0.02$ to $b = 0.55$, $P < 0.115$ (which falls within the 95% confidence interval for the original parameter estimate). The corrected data set is available from the first author's Web site. The other three studies reported in our paper were unaffected by this bug.

Reports: "Adaptive plasticity in female mate choice dampens sexual selection on male ornaments in the lark bunting" by A. S. Chaine and B. E. Lyon (25 January 2008, p. 459). In the lower right of Fig. 4, $N = 384$, not 87. The statistics reported are correct.

TECHNICAL COMMENT ABSTRACTS

COMMENT ON "A Large Excess in Apparent Solar Oblateness Due to Surface Magnetism"

J. R. Kuhn, M. Emilio, R. Bush

Fivian *et al*. (Reports, 24 October 2008, p. 560) analyzed data from the Reuven Ramaty High-Energy Solar Spectroscopic Imager satellite and reported that the Sun is more oblate than previous measurements have suggested. We argue that their threshold-based analysis yields a biased measure of the solar limb shape geometry.

Full text at www.sciencemag.org/cgi/content/full/324/5931/1143-b

RESPONSE TO COMMENT ON "A Large Excess in Apparent Solar Oblateness Due to Surface Magnetism"

M. D. Fivian, H. S. Hudson, R. P. Lin, H. J. Zahid

Our analysis of satellite data from the Reuven Ramaty High-Energy Spectroscopic Imager revealed a strong correlation with a magnetic proxy, leading to an anomalous increase of the solar oblateness. We modeled this effect to yield an oblateness measurement of an assumed underlying nonmagnetic Sun. Kuhn *et al*. note that this measurement could be confused with a systematic spatial brightness variation. The existing data on this are ambiguous.

Full text at www.sciencemag.org/cgi/content/full/324/5931/1143-c

Letters to the Editor

Letters (~300 words) discuss material published in *Science* in the previous 3 months or issues of general interest. They can be submitted through the Web (www.submit2science.org) or by regular mail (1200 New York Ave., NW, Washington, DC 20005, USA). Letters are not acknowledged upon receipt, nor are authors generally consulted before publication. Whether published in full or in part, letters are subject to editing for clarity and space.

Comment on "A Large Excess in Apparent Solar Oblateness Due to Surface Magnetism"

J. R. Kuhn,[1,2]* M. Emilio,[3] R. Bush[4]

Fivian *et al*. (Reports, 24 October 2008, p. 560) analyzed data from the Reuven Ramaty High-Energy Solar Spectroscopic Imager satellite and reported that the Sun is more oblate than previous measurements have suggested. We argue that their threshold-based analysis yields a biased measure of the solar limb shape geometry.

Space observations can yield precise information on the shape of the Sun, which is an important tool for understanding the solar cycle and the solar interior. Fivian *et al*. (*1*) recently argued that the shape of the Sun could be accurately obtained from optical observations from the Reuven Ramaty High-Energy Solar Spectroscopic Imager (RHESSI) using a technique that locates the edge of the Sun where the limb-darkening function (LDF) reaches a threshold value. Unfortunately, this technique ignores the change in functional form of the LDF at different limb angles. If we describe a solar distortion as a shift in the LDF radially by an amount we label with the function $\beta(\theta)$, then brightness changes can be described by an independent function, say $\alpha(\theta)$, that scales the LDF at each latitude (or limb position angle). Another spacecraft experiment, using observations from the Michaelson Doppler Imager (MDI) onboard the Solar and Heliospheric Observatory, demonstrated (*2*) that the LDF does indeed shift and change shape with solar limb position as $L(r,\theta) = [1 + \alpha(\theta)]\,\overline{L}(r - \beta(\theta))$. In this case, a threshold-only–based limb definition, as in (*1*), mixes the intrinsic solar limb shape and intensity variations. Thus, even a spherical Sun (with $\beta = 0$ identically) that has real brightness variations will exhibit a spurious apparent shape, $\beta'(\theta)$, of the form $\beta'(\theta) = {}^{-\alpha(\theta)}\!/_{\frac{d\ln \overline{L}}{dr}} = 1.5''\alpha(\theta)$. Here, the radial derivative of the logarithm of the average LDF was evaluated near the LDF intensity threshold used in (*1*) to obtain the dimensional constant 1.5 arc seconds.

Fivian *et al*. used extreme ultraviolet observations to obtain a spatial mask for deleting RHESSI data points from the analysis to try to isolate the effects of brightness contamination from their shape determination. Their mask was a proxy for the near-limb magnetic field, just as the limb brightness due to faculae is a well-known proxy for magnetic fields. They found a plateau in their analysis for the solar oblateness after 80% of the brightest pixels were deleted and then hypothesized that this small subset of the data determined the true solar shape. In contrast, the MDI data (*2*) determine both the brightness (α) and limb position (β) with no data masking, so that with these results one can directly compute how the apparent oblateness is biased by a threshold-only limb definition. From the MDI analysis, we can easily identify the bright pixel data and simulate the RHESSI analysis by measuring how the apparent oblateness varies with the severity of the masking. Figure 1 shows the difference between the solar oblateness derived from the full LDF analysis of (*2*) and the RHESSI-style analysis as we mask away successively fainter data until less than 40% of the limb pixels are used. The plot is based on results from solar minimum when there was very little photospheric B-field flux. Still, even after most of the 1997 MDI data were masked (as the RHESSI data were), the brightness-effect oblateness was significantly biased to 0.6 milli–arc sec above the value derived from the full analysis in (*2*). This bias must increase with the degree of solar activity and is likely to be several times larger at the time of the 2004 RHESSI observations.

We have shown that discarding most of a threshold-LDF measurement using a technique that deletes data with diminishing brightness does not recover the true limb shape. Furthermore, the geometric solar oblateness is not described by the plateau in this apparent shape variation. We contend that the Fivian *et al*. RHESSI analysis confuses the Sun's oblateness with brightness contributions and that data masking does not correct this systematic error. In contrast with the Fivian *et al*. results (*1*), earlier satellite observations (*2*) did account for these limb brightness effects.

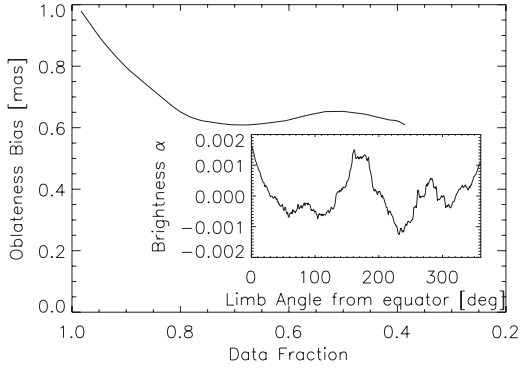

Fig. 1. MDI observations obtained near solar minimum in 1997 were used to derive a threshold-based solar oblateness. The solid curve shows the bias in the true oblateness (*2*) introduced by successively deleting fainter pixels from the analysis. The horizontal axis shows the fraction of bright limb data removed from the calculation, and the plot illustrates how even after 60% of the data are deleted and a plateau in the apparent oblateness is achieved, the derived solar shape remains biased by such a threshold-based limb definition.

[1]Institute for Astronomy, University of Hawaii, Pukalani, Maui, HI 96760, USA. [2]Institute for Astronomy, Eidgenossische Technische Hochschale Zurich, HIT, CH-8093 Zurich, Switzerland. [3]Observatorio Astronomico, Departamento de Geociencias, Universidade Estadual de Ponta Grossa, Parana, Brazil. [4]Stanford University, Stanford, CA 94305, USA.

*To whom correspondence should be addressed. E-mail: kuhn@ifa.hawaii.edu

References and Notes

1. M. D. Fivian, H. S. Hudson, R. P. Lin, H. J. Zahid, *Science* **322**, 560 (2008).
2. J. R. Kuhn, R. I. Bush, P. Scherrer, X. Scheik, *Nature* **392**, 155 (1998).
3. This research was funded by the NASA Solar and Heliospheric Observatory/MDI grant NNX07AK36G to Stanford University and the NASA Solar Dynamics Observatory/Helioseismic Magnetic Imager contract NAS5-02139 to Stanford University and subcontract to the University of Hawaii.

29 December 2008; accepted 30 April 2009
10.1126/science.1170358

Response to Comment on "A Large Excess in Apparent Solar Oblateness Due to Surface Magnetism"

M. D. Fivian,[1]* H. S. Hudson,[1] R. P. Lin,[1,2] H. J. Zahid[1,3]

Our analysis of satellite data from the Reuven Ramaty High-Energy Spectroscopic Imager revealed a strong correlation with a magnetic proxy, leading to an anomalous increase of the solar oblateness. We modeled this effect to yield an oblateness measurement of an assumed underlying nonmagnetic Sun. Kuhn *et al*. note that this measurement could be confused with a systematic spatial brightness variation. The existing data on this are ambiguous.

We thank Kuhn *et al*. (*1*) for their comments, with which we agree in principle but not in detail. Our study (*2*) explicitly recognized the cross talk between the edge location and brightness as they potentially vary around the limb, when using a simple threshold detection as we have done. We quantified this cross talk for the well-known process of gravity darkening ("ellipticity dimming") due to centrifugal effects from the known surface rotation. As we noted, "[t]he RHESSI observations are differential measurements of the radius based on a simple fixed-brightness threshold… This necessarily results in crosstalk between limb position and brightness…Because of this cross talk, it is necessary to make a correction (prolate, 0.03 milli–arc sec) for ellipticity dimming as a result of Von Zeipel's theorem…We make the further strong assumption, discussed in detail in the SOM, that no other global brightness variation presently needs to be considered" (*3*–*5*) [figure 1B in (*2*) and supporting online material for (*2*)].

There is no problem with this assumption unless there is an axisymmetric quadrupole term in limb brightness that is many times larger than that required by Von Zeipel's theorem. Although such a large nonrotational quadrupole term may well exist (*4*, *6*), it is a very difficult measurement and we do not feel that the existing observations have established it well enough to use quantitatively. Our RHESSI data are also extremely suitable for measuring slow variations of solar surface intensity. We have not yet completed a brightness analysis, but our preliminary looks do not show a significant quadrupole intensity variation. The α term in (*1*) also appears not to have a significant axisymmetric quadrupole term and also differs drastically from that observed by Rast *et al*. (*6*). We certainly agree with Kuhn *et al*. (*1*) that a detailed analysis of the photospheric intensity distribution, including the brightness at the extreme limb, is important to carry out and the results will certainly have broad importance in solar and stellar physics. The possible brightness variations include not only the classical limb-darkening function but also several other interesting possibilities associated with interior or surface structures.

The details of the new MDI data analysis cannot be understood in detail from the material presented in (*1*). This difficulty is compounded by the very different instruments and methods; a definitive comparison would require a much more detailed presentation. To correct for the limb brightness variation presented in the inset in figure 1 in (*1*), and to simulate the RHESSI analysis, the identified "bright pixel data" from MDI is used to mask the data to derive an estimated oblateness bias. In the RHESSI analysis, an external and independent data set (EIT 284A) is used to mask magnetic activity. This measure has much greater contrast than the MDI brightness itself, and the "RHESSI-style" analysis method used by Kuhn *et al*. (*1*) cannot sufficiently mask against weak magnetic elements. It therefore tends to overestimate the oblateness. Our masking method uses the asymptotic behavior of the measured oblateness versus data fraction and does not rely on an oblateness measurement at a fixed level of data deletion as stated in (*1*). The asymptotic value is approximately 0.6 milli–arc sec lower than any estimated value at the plateau of the measured oblateness versus data fraction. Also at times of very little photospheric magnetic flux, the images from the Extreme Ultraviolet Telescope (EIT) on the Solar and Heliospheric Observatory (SOHO) (e.g., for 20 March 1997) still show clear structures (especially at the W limb). These are presumably the source of the major peaks in the α profile shown in the inset in figure 1 in (*1*). This sort of low-level activity will certainly perturb the limb signatures but would not have any visibility in the facular magnetic field. Finally, we note that the 0.6 milli–arc sec bias suggested in (*1*) would certainly differ for the different instruments and reduction methods, and it is only speculation to imagine that it would be different between 1997 and 2004.

Our report (*2*) clearly stated how the RHESSI data measure the oblateness of the quiet, presumably nonmagnetic Sun. We acknowledge the possibility of contamination by an axisymmetric quadrupolar brightness variation at the limb. The brightness variation as described by Kuhn *et al*. (*1*) would unfortunately make the RHESSI measurement overestimate the oblateness. Our reported oblateness would then have to be corrected to a still smaller value, in conflict with earlier measurements and theoretical predictions (*5*).

[1]Space Sciences Laboratory, University of California–Berkeley, Berkeley, CA 94720, USA. [2]Physics Department, University of California–Berkeley, Berkeley, CA 94720, USA. [3]Institute for Astronomy, University of Hawaii, Manoa, HI 96822, USA.

*To whom correspondence should be addressed. E-mail: mfivian@ssl.berkeley.edu

References and Notes

1. J. R. Kuhn, M. Emilio, R. Bush, *Science* **324**, 1143 (2009); www.sciencemag.org/cgi/content/full/324/5931/1143-b.
2. M. D. Fivian, H. S. Hudson, R. P. Lin, H. J. Zahid, *Science* **322**, 560 (2008).
3. G. A. Chapman, B. Ziegler, *Sol. Phys.* **168**, 259 (1996).
4. J. R. Kuhn, R. I. Bush, P. Scherrer, X. Scheick, *Nature* **392**, 155 (1998).
5. R. H. Dicke, *Astrophys. J.* **159**, 1 (1970).
6. M. P. Rast, A. Ortiz, R. W. Meisner, *Astrophys. J.* **673**, 1209 (2008).
7. We thank NASA for support under grants NAG5-12878 and NNX07A141G.

27 January 2009; accepted 1 May 2009
10.1126/science.1170433

ANTHROPOLOGY

Debating Reality and Relevance

Troy Duster

During the past decade, the debate about whether to use the concept of race in scientific research and clinical medicine reached such a heated level and took such a polemical turn that it inspired a book with the subtitle *Why Both Sides Are Wrong in the Race Debate* (*1*). Advocates for each of the two warring camps circled the wagons, fired conceptual bullets at their opponents, and often took no prisoners. How did we get to this point, especially in the larger context of the mapping and sequencing of the human genome? Anyone even vaguely familiar with these developments knows the mantra that human DNA is overwhelmingly alike across all cultures, classes, and nationalities—at 99.9% similarity. The surface consensus achieved at the turn of the century generated largely uncontested pronouncements from many of the world's most prominent molecular geneticists that racial taxonomies at the DNA level are or should be dead and buried.

Revisiting Race in a Genomic Age

Barbara A. Koenig, Sandra Soo-Jin Lee, and Sarah S. Richardson, Eds.

Rutgers University Press, New Brunswick, NJ, 2008. 394 pp. $80. ISBN 9780813543231. Paper, $32.95. ISBN 9780813543246. Studies in Medical Anthropology.

However, about this same time the emergence of new fields of clinical application—from pharmacogenomics to nutrigenomics to pharmacotoxicology—began to provide fodder for those who would contest these pronouncements about the end of race. This was also the beginning of an era in which companies making blockbuster drugs, designed for an undifferentiated consumer population, would face costly lawsuits and product recalls when even a small fraction of consumers had adverse drug reactions. Reacting in large measure to such developments, pharmaceutical and biotechnology companies began to reconceive the past strategy of pursuing drugs designed for the general consumer (the one-size-fits-all approach) and substitute a promise of delivering drugs to "specific populations" fine-tuned by DNA analysis. As early as 1999, *Science* published a review article in which the authors proclaimed:

> All pharmacogenetic polymorphisms studied to date differ in frequency among ethnic and racial groups.… The marked racial and ethnic diversity in the frequency of functional polymorphisms in drug- and xenobiotic-metabolizing enzymes dictates that race be considered in studies aimed at discovering whether specific genotypes or phenotypes are associated with disease risk or drug toxicity. (*2*)

The very next year, a congressional mandate directed federal funding agencies to require researchers to address race and ethnicity as categories in their research, in pursuit of a better understanding and mitigation of health disparities. Thus, the early scaffolding of the debate was erected a full decade ago. The intensity of the protagonists would only grow during the ensuing years.

The collection of essays (some previously published) in *Revisiting Race in a Genomic Age* addresses many of the issues surrounding the recent resurgence of race. The volume, edited by Barbara Koenig, Sandra Soo-Jin Lee, and Sarah Richardson, grew out of a project supported by Stanford University's Research Institute for Comparative Studies in Race and Ethnicity. It presents critiques and analyses from a wide range of scholars from different disciplines. Contributors approached the topic using a variety of methods. They include anthropologists doing close-up ethnographic studies of bench science in labs, legal scholars examining intellectual property and patent law, and molecular geneticists working on identifying genetic markers designed to reveal continental ancestral linkages or on polymorphisms linked to alcoholism or asthma in socially designated populations.

To organize this expansive terrain, the book is divided into four sections. The first provides a general history of the concept of race and includes a primer on key concepts in genetics that relate to human taxonomies. One of the most important tools currently deployed to examine human genetic variation is computer software called Structure (*3*). This program permits the researcher to discover patterns or clusters of DNA markers. When an alignment of such clusters overlaps existing categories of race and ethnicity, there arises the siren's seductive call to reinscribe these categories as biologically meaningful. Anthropologist Deborah Bolnick's detailed analysis of the Structure program and its uses, one of the most evocative pieces in the volume, will do much to further illuminate key issues in the debate. Her chapter is especially interesting because the paper most frequently cited for bringing race back into the fields of population and molecular genetics—the Noah Rosenberg, Marcus Feldman, *et al*. article "Genetic structure of human populations" (*4*)—was based on this technology. (In the book's next section, Feldman teams with Richard Lewontin to review recent research in population genetics. They conclude that race is too broad a concept to have medical or clinical utility.) These opening chapters are appropriately foundational, and they will help guide the reader through some of the thicket in the succeeding parts.

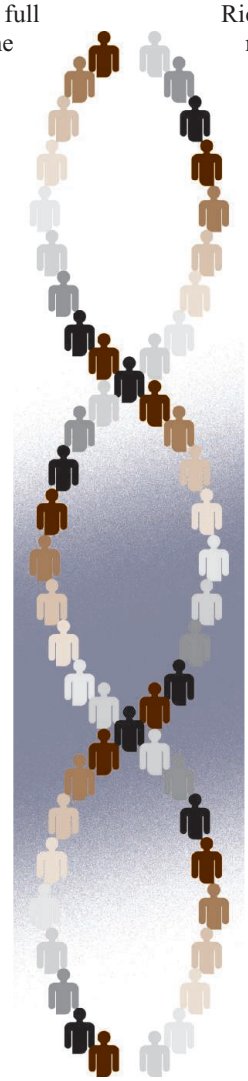

CREDIT: ILLUSTRATION BY ASHLEY HICKS, DESIGN BY TRENT WILLIAMS/COURTESY RUTGERS UNIVERSITY PRESS

The second section deals with substantive matters in contemporary race-based clinical medicine. Here authors engage head-on the matter of drug development for populations categorized by race and ethnicity. Sarah Tate and David Goldstein provide a useful summary of the claims (in peer-reviewed journals) that at least 29 medicines have different efficacy among racial and ethnic groups. Although they are cautious, even skeptical, about attributing these differences primarily to genetics, they wish to leave the door open to further exploration. Other papers highlight the external forces at play shaping the science, such as patent law and marketing decisions. Some authors also follow scientists at work in the laboratory to see how they confront the variable meanings of race in the most determinedly empirical manner, e.g., the framing of the problem under investigation.

The third section displays a

The reviewer is at the Department of Sociology, New York University, New York, NY 10012, USA. E-mail: troy.duster@nyu.edu

range of positions on the meaning and utility of ancestry testing using contemporary molecular genetics. Geneticists Mark Shriver and Rick Kittles demonstrate the effective uses of Y-chromosome and mitochondrial DNA analyses for sex-linked ancestry evaluations. Because of the limits of these two tests, they also argue for the utility of the more-contested technology of ancestry informative markers ("genetic markers that show substantial differences in allele frequency across population groups"). Shriver and Kittles's position is far from polemical in that they readily acknowledge that the meaning of these markers will vary based on the choice, size, and sampling procedure that determine the reference population. Henry Greely provides an overview of the dramatic surge in commercial, direct-to-consumer ancestry testing, and he calls for more transparency in the methods used to determine ancestral origins. This development is of vital interest in certain communities: Kimberly Tallbear documents how Native Americans are dealing (or refusing to deal) with the use of genetics to authenticate tribal membership. Alondra Nelson portrays how African Americans are using these tests to try to find links to specific branches of an African heritage.

There are vigorous proponents for the continued use of race as a proxy for ancestry, some represented in this collection. Yet the full value of *Revisiting Race in a Genomic Age*—and the editors' trenchant analytic summaries—is that the volume substantially raises the level and the terms of the debate. That deserves applause from all sides.

References

1. K. Malik, *Strange Fruit: Why Both Sides Are Wrong in the Race Debate* (One World, Oxford, 2008).
2. W. E. Evans, M. V. Relling, *Science* **286**, 487 (1999).
3. http://pritch.bsd.uchicago.edu/software.html.
4. N. A. Rosenberg *et al.*, *Science* **298**, 2381 (2002).

10.1126/science.1174523

BEHAVIOR

Under the Influence of Hormones

Elizabeth Adkins-Regan

Endocrinology of Social Relationships

Peter T. Ellison and Peter B. Gray, Eds.

Harvard University Press, Cambridge, MA, 2009. 509 pp. $49.95, £36.95, €45. ISBN 9780674031173.

Throughout much of human history, people with no social relationships would not have survived childhood, much less reproduced successfully. It is difficult even to imagine human life completely devoid of family, friends, or romantic interests. Social relationships are an adaptive characterististic of our and many other animal species. These relationships can be cooperative, competitive, or a mixture of both. Humans can even sustain close relationships over long distances, through letters, phone calls, and e-mails.

Understanding the biology of these relationships requires research into both their ultimate causes (evolution and ecology) and their proximate causes (physiology and development). *Endocrinology of Social Relationships* focuses on exciting recent work on endocrine physiology as both a cause and consequence of social interactions. Editors Peter Ellison and Peter Gray (anthropologists at, respectively, Harvard and the University of Nevada, Las Vegas) successfully aim at providing an overview and synthesis of the current state of the field, with an emphasis on—but not restricted to—humans.

Three developments in particular have catalyzed the field. First, more researchers interested in hormones now study systems of social interactions and not just particular acts of social behavior. The difference between a monogamous and a promiscuous mating system lies in how many partners an individual has sex with, not the mechanics of the mating act itself. The relevant research on animals has produced important discoveries about the role of the brain neuropeptides oxytocin and vasopressin in monogamous relationships, discoveries that have captured the interest of human-focused researchers as well. Studies have found that men with one sexual partner have lower testosterone levels than those with multiple or no partners. Second, noninvasive methods for measuring steroid hormones in saliva have made it much easier to collect data through time while subjects are in social contexts such as being defeated in a competitive game, hearing a baby's cry, or entering into a committed romantic relationship. Third, the

The reviewer is at the Department of Psychology, Cornell University, Ithaca, NY 14853–7601, USA. E-mail: er12@cornell.edu

research on humans is no longer being driven primarily by a search for causes of behavioral pathology. Instead, it is inspired by a foundation of concepts and theories of normal behavior taken from evolutionary biology (such as adaptive trade-offs between mating and parental effort), biological anthropology, biological psychology, and social psychology.

The volume is remarkably comprehensive, covering all these disciplinary perspectives and delivering the promised integration of endocrinology with evolution and ecology. It strikes excellent balances between theory and empirical results, nonhuman and human research, what is known and what is not known, and methodological advances and continuing challenges. For example, the chapter "Oxytocin, Vasopressin, and Human Social Behavior" describes findings from fascinating experiments on effects of intranasal administration of these hormones on interpersonal emotions. The authors then offer an illuminative discussion of the difficulties involved in knowing whether these effects are in fact due to actions of these neuropeptides in the brain, the hypothesized target organ.

Another strong point is the consideration several authors give to the psychological processes that mediate effects of hormones on fitness-promoting social relationships in both humans and nonhumans. A hormone like testosterone or oxytocin does not directly determine dominance, affiliation, or paternal behavior. Instead, hormones alter emotional states (such as fear), bias attention (for example, toward sexual stimuli), or change the pleasantness or aversiveness of stimuli (such as infant odors) to alter behavioral probabilities in ways that depend on prior experience. There is an enormous difference between the sophisticated views represented in this book and the oversimplified, popularized human biology in which men are from Mars and driven by testosterone, women are from Venus and driven by estrogen, and a spurt of oxytocin instantly makes new mothers love their babies. Nor is there a heavy emphasis on results of surveys of university undergraduates based on obsolete versions of sexual selection and mate-choice theories. Here, one instead finds the results of clever experiments (e.g., in which testosterone administration decreases tendencies to mimic other people's facial expressions) along with critical information about hunter-gatherer populations. For example, a discussion of lactation and conception in natural-fertility societies (those using no birth control technology) concludes that in the evolutionary past most human female mate choice may have taken place while the women were lactating, a study population largely missing from the human mate choice literature.

How do we know the animal research can shed light on humans? The basic endocrine mechanisms and brain structures have been remarkably conserved in the course of evolution—they are found in all mammals and most other vertebrates—making successful generalization likely. Yet some of the social relationships (such as male-female pair bonds or paternal care of offspring) are not at all universal and instead have a spotty distribution on the evolutionary tree of animals. Even when the distribution is spotty, however, it is still possible that the same mechanisms have been independently co-opted multiple times to support the evolution of those social relationships. Whether they have is an empirical question. Are humans unique in their social relationships? The strongest hint at such a possibility comes in the chapter in which Jane Lancaster and Hillard Kaplan summarize the essential features of the "human adaptive complex," a complex of traits that they see as describing "a very specialized niche." That does not, however, automatically preclude generalization from animal research. The honey bee adaptive complex is very specialized too, yet few would claim that research on other insects is irrelevant to understanding honey bees.

The editors and their authors have produced a definitive and scholarly, yet readable, state-of-the-art presentation of a fascinating and timely topic. This landmark volume is rich in ideas, conclusions, and questions for the future. As the editors point out, we are all being exposed, like it or not, to hormones in the environment and to ads full of claims about the benefits of administering hormones. We need to understand how such hormones might (or might not) be affecting social relationships. Will spraying on some oxytocin make your colleagues like you? Probably not, but reading *Endocrinology of Social Relationships* produced warm feelings about the ability of good science to illuminate the human condition.

10.1126/science.1175165

BROWSINGS

Third Art of Science Exhibition. Andrew Zwicker, Adam Finkelstein, Teresa Riordan, and Elle Starkman, organizers. Friend Center, Princeton University, Princeton, NJ, 2009. Through April 2010. www.princeton.edu/~artofsci/2009/.

Rather than seeking artistic works inspired by science, the organizers invited members of the Princeton University community to submit images captured during the course of their research projects. They received over 200 entries, from undergraduates, faculty, research staff, graduate students, and alumni. The judges selected 48 pieces for their aesthetic value; these are now on display online and in the atrium of the Friend Center. They awarded three cash prizes (apportioned according to the golden mean): third, to alumna Maria Ciocca for *Worm Love*, taken using immunofluorescence microscopy; second, to nanofabrication researchers Pat Watson, Mike Gaevski, Joe Palmer, and Conrad Sylvestre for their scanning electron microscope image *Desert Butte*; and first, to assistant professor of chemical engineering Celeste Nelson for *Baby Squid*, a bright field microphotograph of squid embryos (right). If you visit the Web site by 1 July, your preferences can help determine a "People's Choice" award.

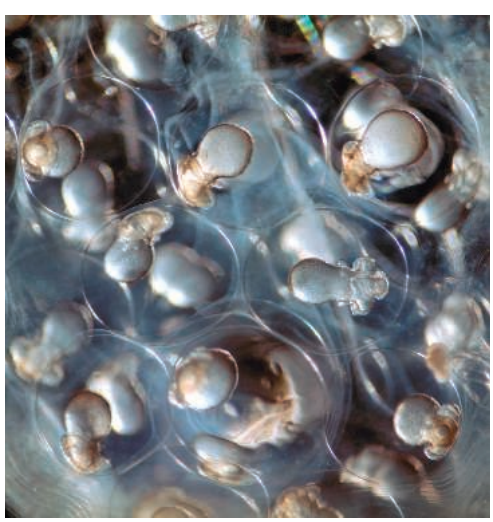

CREDITS: (TOP) OLGALIS/ISTOCK; (BOTTOM) CELESTE NELSON/COURTESY PRINCETON UNIVERSITY

INFRASTRUCTURE

Tenure and the Future of the University

Tenure has been eroded by structural pressures, but remains vital to universities that value creativity.

Dan Clawson

The fundamental rationale for the tenure system has been to promote the long-term development of new ideas and to challenge students' thinking. Proponents argued more than 60 years ago that tenure is needed to provide faculty the freedom to pursue long-term risky research agendas and to challenge conventional wisdom (*1*). Those arguments are still being made today (*2*) and are still valid. However, a 30-year trend toward privatization is creating a pseudo–market environment within public universities that marginalizes the tenure system. A pseudo–market environment is one in which no actual market is possible, but market-like mechanisms (such as benchmarking and rankings based on research dollars, student evaluations, or similar attributes) are used to approximate a market.

Thirty years ago, state and local governments put in $3.99 for every dollar that students and parents paid for higher education; today, states put in $1.76 for every dollar, less than half what they contributed a generation ago (*3*, *4*). This increased pressure on budgets is arguably the most important factor pushing universities to replace long-term, full-time, well-paid faculty with poorly paid, unbenefited, contingent faculty. Core tenure-system faculty—that is, full-time assistant, associate, and full professors—were roughly 55% of all faculty in 1970, 1975, and 1980, but then declined to 41% in 2003; by another data set, tenure-system faculty were 31% of all faculty in 2007. This change in composition took place even as the absolute number of full-time faculty increased from 369,000 in 1970 to 676,000 in 2005 (*5*, *6*).

The move away from tenure has two components—a rise in part-time faculty, especially at community colleges and nonselective institutions, and a rise in full-time non–tenure-track faculty, especially at doctoral degree–granting institutions. The biggest shift is in part-time faculty, who went from 22% of all faculty in 1970 to 49% in 2007 (*5*, *6*). The shift to non–tenure-system faculty has taken place in both private and public institutions and at all levels from research universities to community colleges.

Part-time faculty are most prevalent at community colleges (67% of all faculty) and least common at public doctoral institutions (22%) (*7*). Community colleges often prefer part-time instructors who are themselves practitioners with full-time jobs in the community. At doctoral institutions, full-time non–tenure-track faculty, not part-timers, are the prevalent auxiliary instructors. In the fall of 2003, among newer full-time instructional faculty at doctoral institutions, 32.8% of the male faculty and 47.7% of the female faculty were not on the tenure track (*8*) (see chart, right). More generally, the gender disparities are substantial: Among full-time faculty, women compose 33.9% of tenured and 48.9% of non–tenure-track faculty (*6*). Women also make up 47.9% of part-time faculty (*5*).

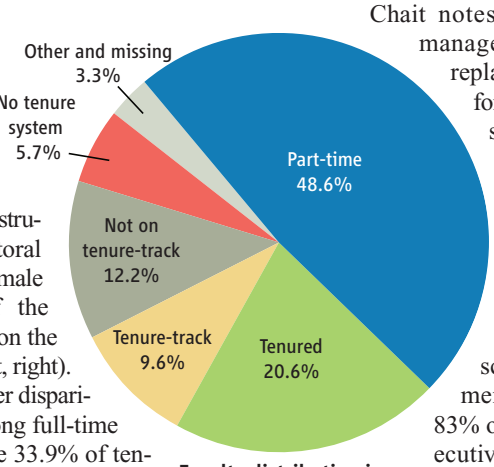

Faculty distribution in higher education (*23*).

Scientific paradigms shift, and student thinking is stimulated, when dissidents take unpopular positions—unpopular not just with the public, but also with administrators and faculty colleagues. People are much more likely to buck the tide if they know their jobs are secure. Cutting costs by cutting tenure means that a smaller proportion of faculty have the structural conditions needed to challenge conventional thinking.

The arguments against tenure are compelling to those who support a world where university "presidents have become CEOs" and "the administration has become management," as described by Richard Chait, professor of higher education at Harvard University (*9*). He was an adviser to Minnesota's Board of Regents in what Chait reports was "widely construed as an initiative to eliminate tenure" (*9*), and he reviews tenure-skeptic arguments as follows:

• "Lifetime job guarantees border on being immoral" according to James Carlin, "a businessman for over 35 years" and the former Chair of the Board of Higher Education of Massachusetts (*10*).

• "Tenure inhibits the strategic reallocation of resources" (*9*).

• "The public perception that tenure protects 'deadwood' is, alas, correct," wrote Donald Kennedy (*11*), former president of Stanford University. "From the perspective of many trustees and administrators," Chait notes, tenure "limits management's capacity to replace marginal performers with demonstrably or potentially better performers" (*9*).

• "The tenure system is inflexible and limits administrators' ability to improve schools and departments" according to 83% of the business executives surveyed (*12*). Trustees believe that tenure creates "an unacceptably potent buffer against centralized initiatives…. Tenure weakens the relative authority of executives (*9*)."

Other arguments against tenure come from non–tenure-system faculty themselves. I have been told by non–tenure-track faculty that their jobs would not exist if many faculty did not think it beneath them to teach writing. Some tenured faculty have, in effect, cooperated in promoting the rise of non–tenure-track faculty, sloughing off those parts of the job (such as advising) that they find least appealing.

The top-down business model of the university presents the need to cut costs as the primary reason to hire part-time and non–tenure-track faculty. This is, however, misplaced: The dramatic increase in tuition and fees is not driven by an increase in the costs of full-time faculty. Since 1970, after adjusting for inflation, real full-time faculty salaries have increased by 5.0%, almost all of that rise due to the aging of the faculty (salaries went down for assistant and associate professors, and went up only 2.8% for

Department of Sociology, University of Massachusetts Amherst, Amherst, MA 01003, USA. E-mail: clawson@sadri.umass.edu

Published by AAAS

full professors, but there are now more full professors). Tuition and fees, however, rose by 125% at public institutions and 253% at private institutions, in real (inflation-adjusted) dollars (*13*). Tenure is not what is driving rising costs.

The shift away from tenure has ramifications for the fundamental social principle on which universities are organized—professionalism. Professionalism operates on the basis of people who develop both expertise and a set of values and commitments (*14*, *15*).

Professionals treat each other as peers and are accorded a considerable degree of self-governance. The idea of professionalism is that professionals cannot be properly evaluated by those from the outside and that professionals can be trusted to evaluate and police themselves, operating not on the basis of self-interest but rather with a vision of some larger good. This is the logic, for example, behind peer review by journals or the practice of faculty making the primary decision of whether or not someone deserves tenure. Professional control, however, gives faculty the leverage to resist efforts to alter the university in response to market logic; for example, at York University, tenured faculty led a campaign to limit online courses (*16*), and at the University of Massachusetts Amherst faculty won a commitment to restoring the number of tenure-system faculty (*17*).

The average tenure of a provost is 5.2 years and of a president 8.5 years (*18*), but many faculty stay at one institution through their entire careers. Just as the business model of recent years focused on short-term profits and stock prices and just as executives made huge bonuses based on illusory success, so too administrators may be concerned with being able to show a short-run accomplishment that will help them get the next job at some other institution, even if their actions undermine the long-run values and strengths of the university.

But I, and other faculty I have discussed this with, believe that a university is not supposed to be a business; viewing it as one shows not hard-headed realism but a failure to understand what gives the university its strength and potential. Tenure-system faculty are a problem to administrators and trustees precisely because tenure-system faculty have an alternative vision of the university and the power to act on that vision.

When administrators respond to trustee and larger societal pressures to cut costs, it typically involves a model in which most faculty engage in "content delivery," not education. If faculty are teaching to the test, delivering a standard curriculum determined from above, with little or no ability to explore alternatives or to respond to student interests, then a de-skilled and vulnerable workforce has important advantages. This may help to explain why tenure is weakest at community colleges and virtually nonexistent at for-profit institutions (*9*, *19*). A market-style model works less well if a university's goals are free speech, creativity, research, and student exploration of alternatives.

Tenure-system faculty produce better outcomes: A study, based on 30,000 student transcripts, found that first-year students were less likely to return for their sophomore year if their large introductory classes were taught by part-time faculty (*20*). A study of community colleges found that students were 4% more likely to transfer to a 4-year institution for each 10% increase in the share of tenured faculty (*21*). Although contingent faculty may be excellent teachers, typically they do not have the continuity and institutional supports that enable them to provide mentoring. If contingent faculty do not have offices, it is hard for them to hold office hours; if they are gone a year later, students have trouble getting letters of recommendation.

Certainly the situation is a complex one, and it would be naïve to say that the current tenure system is perfect in all ways. However, despite the best efforts of administrators and trustees, tenure remains a crucial part of any attempt to have a first-rate college or university.

When faculty have a choice, they strongly prefer jobs in the tenure system; offered hypothetical alternatives, faculty choose the tenured position even if it pays less (*22*). Perhaps paradoxically, for faculty committed to the "knowledge and learning" model, rather than the administrator and trustee "bottom-line" model, the commitment must be not only to increase the proportion of tenure-track faculty, but also to improve conditions for contingent faculty. If non–tenure-system faculty were paid reasonably, received benefits, and had job security, administrators would have less incentive to replace tenure-system faculty with (no longer quite so) contingent faculty. The future evolution of the system may include the emergence of unions or professional associations to provide nontenure faculty a more limited version of the protections offered by tenure. At my own institution, for example, the faculty union presented simultaneous campaigns to win both a net increase of 250 tenure-track faculty and improved conditions and job security for non–tenure-track faculty.

The decision about tenure is also a decision about two visions of a university. A university can be seen as a business with a "product" whose offerings should be driven by student "demand," a business that should rely on contingent faculty combined with highly paid administrators committed to "the bottom line." Alternatively, it can be seen as a center of knowledge where students are educated (not just trained), that should be governed in significant part by tenure-system faculty with a long-term commitment to the institution and to knowledge.

References and Notes

1. American Association of University Professors (AAUP), "1940 Statement of principles on academic freedom and tenure" (AAUP, Washington, DC, 1970); www.aaup.org/AAUP/pubsres/policydocs/contents/1940statement.htm.
2. M. C. Taylor, *New York Times*, 27 April 2009, p. A23; www.nytimes.com/2009/04/27/opinion/27taylor.html.
3. U.S. Bureau of the Census, *Statistical Abstract of the United States: 1981* [Government Printing Office (GPO), Washington, DC, ed. 111, 1980].
4. U.S. Bureau of the Census, *Statistical Abstract of the United States: 2009* (GPO, Washington, DC, ed. 169, 2009); www.census.gov/compendia/statab/cats/education/higher_education_finances_fees_and_staff.html.
5. U.S. Department of Education, *Digest of Education Statistics*, 1972–2007; http://nces.ed.gov/Programs/digest/.
6. National Center for Education Statistics (NCES), *Employees in Postsecondary Institutions* (NCES, Washington, DC, Fall 2007).
7. National Education Association, *Update* **11**(3), 1 (September 2007).
8. NCES, *2004 National Study of Postsecondary Faculty* (NSOPF:04, NCES, Washington, DC, 2006), table 8.
9. R. P. Chait, *The Questions of Tenure* (Harvard Univ. Press, Cambridge, MA, 2002).
10. J. Carlin, *Chron. High. Educ.* **46.11**, A76 (1999).
11. D. Kennedy, *Academic Duty* (Harvard Univ. Press, Cambridge, MA, 1997), p. 131.
12. J. Immerwahr, *Taking Responsibility: Leaders' Expectations of Higher Education* (National Center for Public Policy and Higher Education, San Jose, CA, January 1999).
13. *Digest of Education Statistics 2007* (*5*).
14. E. Freidson, *Professionalism: The Third Logic* (Univ. of Chicago Press, Chicago, 2001).
15. S. Brint, *In an Age of Experts* (Princeton Univ. Press, Princeton, NJ, 1994).
16. D. Noble, *Digital Diploma Mills* (Monthly Review, New York, 2002).
17. D. Clawson, M. Leiblum, *Equity Excell. Educ.* **41**, 12 (2008).
18. J. King, G. G. Gomez, On the *Pathway to the Presidency: Characteristics of Higher Education's Senior Leadership* (American Council on Education, Washington, DC, 2008).
19. D. Kirp, *Shakespeare, Einstein, and the Bottom Line* (Harvard Univ. Press, Cambridge, MA, 2003).
20. M. K. Eagan Jr., A. J. Jaeger, *N. Dir. Teach. Learn.* **2008** (115), 39 (2008).
21. B. Gross, D. Goldhaber, *Community College Transfer and Articulation Policies: Looking Beneath the Surface* (Center on Reinventing Public Higher Education, www.crpe.org, Seattle, WA, 2008).
22. C. T. Clotfelter, in (*9*).
23. The chart is based on data from (*6*).

10.1126/science.1172995

ASTRONOMY

Celebrating the 400th Anniversary of Telescope Astronomy

Since Galileo looked skyward 400 years ago, telescopes have evolved to provide a broader and deeper understanding of the universe.

Giovanni F. Bignami

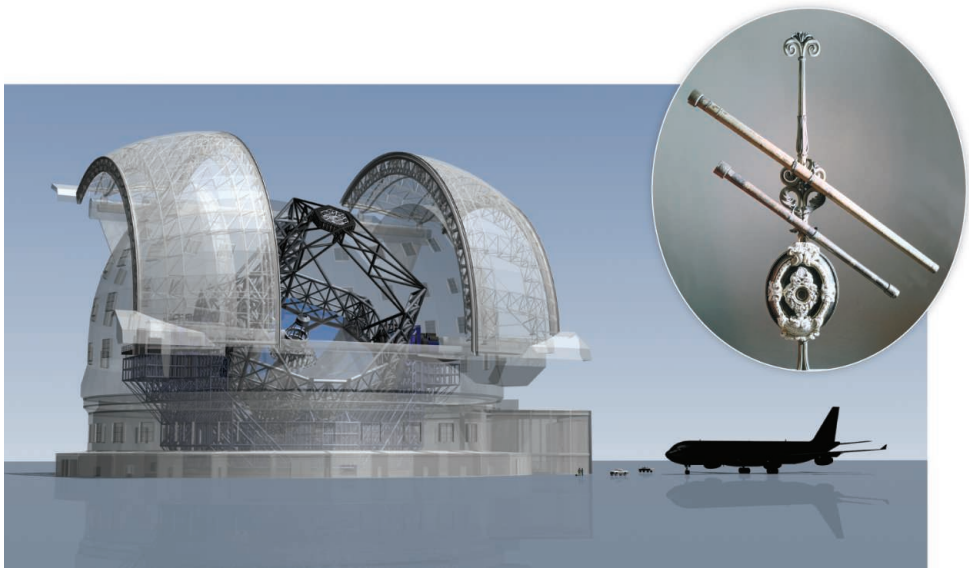

Telescopes past and future. An artist's impression of the European Extremely Large Telescope, planned to have an imaging mirror in excess of 40 m in diameter. The inset shows the telescope used by Galileo to make his astronomical observations of the night skies from 1609 onward.

Science authors laboring under the oppressive yoke of refereeing should think back to the time when Galileo Galilei brought his manuscript to printer Baglioni in Venice at the end of February 1610. The referee for his *Sidereus Nuncius*—a short treatise based on his first observations made through a telescope—was to be the office of the Holy Inquisition. Galileo knew that those referees didn't simply reject what they didn't like: They might invite you in for a few questions. But that time he was in luck. On 1 March, the Venice Council, on advice of the local Inquisitor, gave its consent.

Few know that Galileo (and Baglioni) then took an astonishing risk. Such was his passion for his new telescope that Galileo added observations and comments dated up to 2 March—materials that the Inquisitor could not possibly have seen. But those last few additions are so beautiful. For the first time since 7 January, when Galileo had started observing Jupiter, a "fixed" star had entered the small field of view of his instrument. As he kept pointing to the planet and its twirling satellites, the star appeared to move steadily across, as apparent in his sketches dated 27 February to 2 March. This provided conclusive proof that Jupiter carried these satellites (moons) in its motion against the background sky: a finding that would have definitely risked the Inquisitor's wrath.

By this time, Galileo must have been really busy—finalizing text, checking proofs and figures, a real headache these, especially the famous Moon plates from his earlier 1609 observations. Half-tones had to be hand-etched in wood by one of Baglioni's artists, who had Galileo's beautiful water colors in front of him. Probably hard-pressed, the etcher made a poor job of it. Luckily, however, the originals have survived, revealing the gifted hand of a true son of the Florentine renaissance. They can be admired, along with countless other galileiana, in Florence at the Palazzo Strozzi Exhibition (*1*).

By 13 March 1610, 550 copies of the *Sidereus Nuncius* were ready to document a brave new era, that of astronomy with a telescope. Bigger and better telescopes were soon invented by Isaac Newton (born 1642, the year of Galileo's death), Gian Domenico Cassini (1625 to 1712), and innumerable others to follow, giving mankind an ever-growing universe: from solar system to stars, from stars to our Galaxy, and from there to an expanding universe full of as many galaxies as there are stars in our own, about 100 billion.

In the past 400 years, telescopes have also evolved the capacity to tell us what stars are made of, allowing us to learn that our own bodies (and all we see) have been made by stars. True, the ignition of the first stars in the universe, about 13 billion years ago, has not yet been recorded, but we are working on it. The European Extremely Large Telescope (E-ELT) (*2*), for example, should do the job. With its mirror diameter exceeding 40 m (compare with the 4-cm Galileo lens), the E-ELT will be close to the extreme of what we are currently able to realize and afford for observations at optical wavelengths. But astronomers are also planning a Square Kilometre Array of radio telescopes (*3*), the ultimate challenge in astronomy with radio waves. These large, steerable antenna dishes have detected, for example, radio pulsars, stars that pack the mass of our Sun in a wildly rotating 10-km sphere.

Over the past 40 years, we have been putting telescopes in space for an "astronomy of the invisible" that would have challenged Galileo's comprehension. It's hard to describe as telescopes the Geiger-counter–based contraptions that Riccardo Giacconi and colleagues put in a rocket nose in 1962. Yet, they gave us a glimpse of our first cosmic x-ray sources. Today's state-of-the art orbiting x-ray telescopes have huge photon-focusing optics and will soon log half-a-million x-ray sources in the sky. Among these sources are accreting black holes, objects with exotic physics.

Ten years after x-ray astronomy, gamma-ray astronomy was born. Gamma-ray photons are impossible to focus, so it's much harder to build effective gamma-ray telescopes. Still, mostly thanks to the recently launched Fermi Gamma-ray Space Telescope (*4*), thousands of gamma-ray sources in the sky will be pinpointed. Some of them, such as Geminga-like neutron stars, are only "visible" in the gamma-ray region of the spectrum. So, too, are the 5000 mysterious "gamma-ray bursts." Because these bursts are fantastically energetic, cosmological one-time events, special telescopes have had to be invented.

Even more discoveries have come from telescopes in space: numerous infrared and ultraviolet stars and galaxies, many observed by the Hubble Space Telescope (*5*)—the most productive astronomy machine ever. Yet

Accademia dei Lincei, Palazzo Corsini, Via della Lungara, 10-00165 Roma, and Instituto Universitario di Studi Superiori, 56, Lungo Ticino Sforza, Pavia, 27100 Italy. E-mail: giovanni.bignami@gmail.com

Published by AAAS

another telescope in space imaged the baby universe when it was only 300,000 to 400,000 years old and just twice the size of our Galaxy. At that age, it is visible only at microwave wavelengths, expansion-cooled from Big-Bang temperatures. Those cosmological photons carry, imprinted in their tiny fluctuations, the whole of today's universe.

What telescopes can we expect for the future? Galileo and Newton would go for the unknown. The still truly unknown in the universe is its nonelectromagnetic content—neutrinos and gravitational waves. We know that gravitational waves exist, and we know the theory behind a telescope for catching them, but we've yet to detect them with the likes of the Laser Interferometer Gravitational-Wave Observatory. In contrast, neutrinos have been observed, both from our Sun and from a local supernova, using underground detectors as our telescopes.

Neutrino astronomers are, I believe, on the brink of important discoveries. Some now use Earth as a detector, including its Antarctic ice (the IceCube project) or ocean water (the ANTARES project) (*6*, *7*). It is difficult to imagine a bigger telescope, yet it matches the elusiveness of its target. These telescopes—like the E-ELT, the Square Kilometre Array, and the future space telescopes—are worthy descendants of Galileo's *specillum*, and still look at the same sky.

References

1. Galileo: Images of the Universe from Antiquity to the Telescope, Palazzo Strozzi, Florence, Italy; www.galileofirenze.it.
2. European Extremely Large Telescope; www.eso.org/sci/facilities/eelt.
3. Square Kilometre Array; www.skatelescope.org.
4. Fermi Gamma-ray Space Telescope; www.nasa.gov/mission_pages/GLAST/main/index.html.
5. Hubble Space Telescope; www.nasa.gov/mission_pages/hubble/main/index.html.
6. IceCube Neutrino Observatory; icecube.wisc.edu.
7. Astronomy with a Neutrino Telescope and Abyss Environmental Research; antares.in2p3.fr.

10.1126/science.1172000

MICROBIOLOGY

Getting in Touch with Your Friends

Evolution of complex physical interactions between microbes promotes growth and enables behaviors that neither party can perform alone.

Christopher J. Marx

Microbes use a broad palette of chemical transformations to harvest energy and nutrients, but they do not always accomplish these conversions on their own. Particularly in anaerobic environments, various metabolisms are stimulated by, or depend upon, partnerships (*1*). In this form of interaction—termed syntrophy—one organism typically converts the primary resource to an intermediate that can be used by a partner (which perhaps passes it along to the next, and so on). In other cases, one partner may use a resource and provide a different type of service in return, such as a trace vitamin or motility. Recent studies are beginning to shed light on the mechanisms by which such partners communicate and interact and on how such interactions emerge in the first place.

Recently, a novel interspecies signaling mechanism was found (*2*) between two syntrophic partners present in high-temperature anaerobic sewage digesters: the bacterium *Pelotomaculum thermopropionicum* strain SI and the methanogenic archaeon *Methanothermobacter thermautotrophicus* strain ΔH. *P. thermopropionicum* can ferment propionate to acetate, bicarbonate, and three H_2 molecules, but this conversion is highly endergonic (ΔG° = 76.1 kJ mol^{-1}). Propionate oxidation can proceed if the partial pressure of H_2 is kept low by *M. thermautotrophicus*, which consumes four H_2 molecules for every CH_4 produced (combined ΔG° = –25.6 kJ mol^{-1}). This interaction provides an energy source to *M. thermautotrophicus* while enabling propionate oxidation by *P. thermopropionicum*.

When grown together, these two strains form aggregates that are held together by the flagellum of *P. thermopropionicum* (*3*). The average distance between cells of each species needed to achieve the observed growth rate is just 2 μm (see the figure, panel A). Shimoyama *et al.* (*2*) have uncovered an additional role for flagellum adherence: an interspecies signal that stimulates methanogenesis in *M. thermautotrophicus* (see the figure, panel B). The flagellar tip protein (FliD) from *P. thermopropionicum* induced widespread changes in gene expression in *M. thermautotrophicus*, including transcripts encoding hydrogenases and many of the enzymes of methanogenesis. In *M. thermautotrophicus* monocultures, stimulation by FliD led to a sharp increase in the rate of H_2 use, and hence CH_4 formation. Given that FliD adherence was only found with two methanogens across 21 genera screened, this appears to be a fairly specific, but not unique, characteristic of this pair.

This flagellum-dependent communication system differs from other known interspecies signaling systems (*4*) in that it is not mediated by a small molecule or peptidoglycan, but rather by a protein constituent of a cellular appendage. In this regard, the system resembles within-species recognition, for example, in slime mold (*5*), yeast (*6*), and the bacterium *Proteus mirabilis* (*7*). In these systems, recognition via shared surface loci is relevant for partner recognition and mediates multicellular behaviors such as forming a fruiting body, flocculation, and the formation of swarm boundaries, respectively. It may be that nondiffusible signals such as appendages are preferable for associations in which the partners must be arranged within a few micrometers to function optimally.

Perhaps the most intricate, highly developed microbial consortium thus far identified is the pairing known as "*Chlorochromatium aggregatum*" (*8*). This assemblage contains a single, motile β-proteobacterium (central bacterium) encrusted with a layer of nonmotile photosynthetic green sulfur bacteria (epibionts) (see the figure, panel C). Rather than overcoming thermodynamic constraints, the driving force for this consortium appears to be behavioral: The nonmotile photosynthesizers hitch a ride on their partner to move to their optimal depth in stratified lakes (no O_2, plenty of H_2S, and light of a wavelength matching the absorption maximum of their pigments). The photosynthesizers appear to pay their fare through supplying the central heterotroph with fixed organic carbon. Wanner *et al.* (*8*) have reported evidence for specialized attachment structures at the point of contact of each photosynthesizer with the central cell; furthermore, periplasmic tubules extending from the central bacterium appear to generate a continuous periplasmic space between all partners (see the figure, panel D). Well-developed signaling mechanisms—perhaps mediated by surface structures—probably also underlie this partnership.

From an evolutionary perspective, these sophisticated symbioses illustrate two very different classes of interactions. In *C. aggregatum*, there appears to be reciprocation of two costly

Department of Organismic and Evolutionary Biology, Harvard University, Cambridge, MA 02138, USA. E-mail: cmarx@oeb.harvard.edu

acts: motility in exchange for fixed carbon. Where investing in a partner comes at an expense, natural selection will only favor making this investment if the investing individual disproportionately benefits from its partner relative to genotypes that invest less (*9*). For microbes, there are two ways to disproportionately collect benefits: live in a structured population or recognize your partner (or kin) to bias interactions in your population. The sophisticated coupling of photosynthesizers to a central motile bacterium achieves the structure needed for positive feedback between the reciprocal altruistic acts.

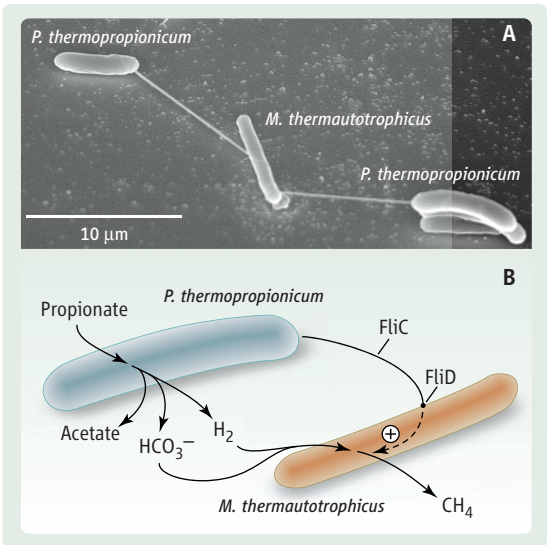

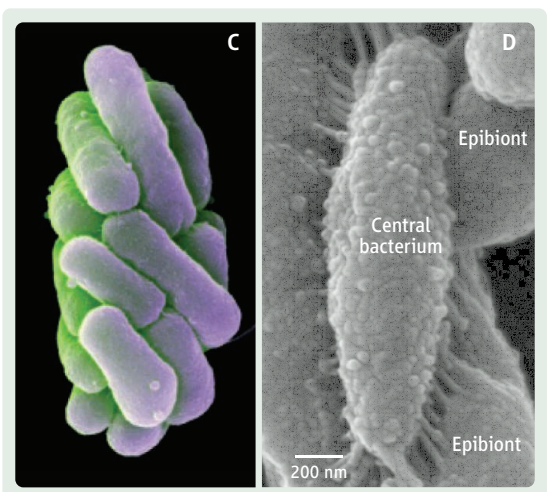

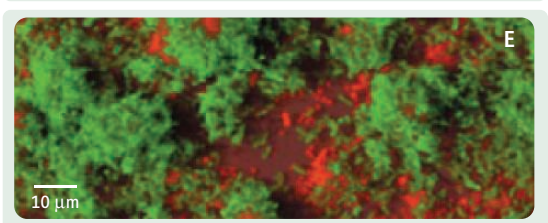

Physical associations in microbial consortia. In a first example of microbial symbiosis, *P. thermopropionicum* flagella adhere to *M. thermautotrophicus* (**A**) to facilitate between-organism H_2 exchange (*3*). Furthermore, the FliD protein at the tip of the *P. thermopropionicum* flagellum stimulates methanogenesis by *M. thermautotrophicus* (**B**). In a second example, nonmotile epibionts completely surround a motile central bacterium in *C. aggregatum* (**C**). Specialized morphologies such as periplasmic tubules connect partners in this system (**D**). Laboratory studies of synthetic consortia have shown how *P. putida* (green) evolves to cover over the *Acinetobacter* sp. strain C6 (red) microcolonies from which they receive metabolites (**E**).

CREDITS: (PANEL A) FROM (*3*). (PANEL B) ADAPTED BY P. HUEY/*SCIENCE*. (PANELS C AND D) FROM (*3*). (PANEL E) FROM (*12*)

In contrast, the between-organism H_2 exchange between *P. thermopropionicum* and *M. thermautotrophicus* is a type of mutualism in which there are, seemingly, no costs to the parties involved. Each party exerts a positive effect on the growth of the other, but doing so appears to be in both organisms' immediate self-interest. Although neither party incurs a cost, this pair uses the same classes of mechanisms outlined above (structure and recognition) to take advantage of the positive feedbacks that emerge from interactions that are both local and selective.

How do microbial associations such as these emerge in the first place? One powerful approach to address this issue has been to take advantage of synthetic consortia in the laboratory. In these experimental populations, new partnerships can emerge through the action of selectively advantageous, naturally arising mutations. With the emergence of low-cost pyrosequencing, the mutations underlying cooperation can now be unraveled fairly easily (*10*).

Thus far, the closest laboratory incarnation to the physically structured metabolic exchanges described above has been the development of a coculture of *Acinetobacter* sp. strain C6 and *Pseudomonas putida* (*11*). In this system, benzyl alcohol is consumed by the first organism, but a portion is excreted as benzoate, which can be used by the second. Although this is a syntrophy, benzoate consumption is not necessary for substrate use, and in fact, growth by *P. putida* suppresses that of *Acinetobacter*, likely due to limiting O_2 supply. Hansen *et al.* (*12*) found that *P. putida* quickly evolves altered lipopolysaccharides that allow it to overgrow its partner in biofilms, leading to greater exploitation of the supplied resource and further suppression of its partner's growth. This observation is in contrast to the prediction that growth in biofilms promotes altruism within a species because yield from substrate—and not just growth rate—contributes to fitness such that efficient use of substrate can be considered cooperative (*13*). Thus far, no laboratory experimental systems have shown the evolution of increased cooperation that came at a cost to the investing individual.

The study of the physiology, ecology, and evolution of synthetic consortia opens the door to many fascinating problems: Do outcomes predicted for mutualist pairs hold when combined into multiway interactions involving layers of cooperation and conflict? What factors influence the emergence of reciprocal specificity for partners? Can metabolic models provide testable predictions of conditions that will permit mutualisms? Will synthetic consortia evolve to stick together and enhance nutrient exchange (while also perhaps helping cheaters stick)?

Beyond these fundamental questions, there are myriad practical applications of engineered communities, such as the recent demonstration that a synthetic consortium based upon formate exchange can be used for H_2 production (*14*). Through a synthesis of knowledge from studies of sophisticated natural interactions, as well as the evolutionary processes that transpire in novel partnerships, microbial consortia can serve as an exciting tool for a synthetic biology in which the assembled parts are not just genes, but organisms and communities.

References

1. B. Schink, *Antonie van Leeuwenhoek* **81**, 257 (2002).
2. T. Shimoyama, S. Kato, S. Ishii, K. Watanabe, *Science* **323,** 1574 (2009).
3. S. Ishii, T. Kosaka, K. Hori, Y. Hotta, K. Watanabe, *Appl. Environ. Microbiol.* **71**, 7838 (2005).
4. E. A. Shank, R. Kolter, *Curr. Opin. Microbiol*. **12**, 205 (2009).
5. J. E. Strassmann, Y. Zhu, D. C. Queller, *Nature* **408**, 965 (2000).
6. S. Smukalla *et al.*, *Cell* **135**, 726 (2008).
7. K. A. Gibbs, M. L. Urbanowski, E. P. Greenberg, *Science* **321**, 256 (2008).
8. G. Wanner, K. Vogl, J. Overmann, *J. Bacteriol.* **190**, 3721 (2008).
9. J. L. Sachs, U. G. Mueller, T. P. Wilcox, J. J. Bull, *Quart. Rev. Biol.* **79**, 135 (2004).
10. G. J. Velicer *et al.*, *Proc. Natl. Acad. Sci. U.S.A.* **103,** 8107 (2006).
11. B. B. Christensen, J. A. Haagensen, A. Heydoryn, S. Molin. *Appl. Environ. Microbiol.* **68**, 2495 (2002).
12. S. K. Hansen, P. B. Rainey, J. A. J. Haagensen, S. Molin, *Nature* **445**, 533 (2007).
13. J.-U. Kreft, *Microbiol.* **150**, 2751 (2004).
14. Z. Waks, P. A. Silver, *Appl. Environ. Microbiol.* **75**, 1867 (2009).

10.1126/science.1173088

GEOPHYSICS

Slabs Do Not Go Gently

High-resolution seismic tomography reveals an active vertical tear in a descending ocean plate off the coast of Japan.

Guust Nolet

In geology textbooks, the fate of the oceanic crust seems straightforward. The ocean floor is created by upwelling of lighter magma at spreading ridges. The magma cools as it moves away from the ridge, forming a stiff layer or "plate" called the oceanic lithosphere. Having increased in density, it then descends back into the mantle in trench regions. Precise seismic tomography studies have revealed that many descending slabs have a more complex evolution and have developed tears, detached from the surface plate, or even broken up into fragments. On page 1173 of this issue, Obayashi *et al*. (*1*) not only show clear tomographic evidence for the development of a vertical tear under southwest Japan, but have also found evidence for ongoing plate rupturing. The authors correlated the images directly with measurements of stress revealed by active seismic sources.

Insights into the descent of oceanic lithosphere come partly from seismic studies, because the descent is accompanied by earthquakes. These earthquakes can originate from regions as deep as 660 km, the bottom of the upper mantle, where the mantle mineral spinel transforms into the denser perovskite structure (see the figure, panel A).

Geosciences Azur, Université de Nice and CNRS, 250 rue A. Einstein, 06560 Sophia Antipolis, France. E-mail: nolet@geoazur.unice.fr

The idea that slabs do not stay intact but rupture as they descend through the upper mantle is not new. It has been used to explain observations in Indonesia (*2*), New Hebrides (*3*), Taiwan (*4*), and the Alps (*5*). Such tears are generally hypothesized to propagate horizontally and detach the slab from the ocean lithosphere that remains at the surface (see the figure, panel B). Slab rupture cannot, however, be distinguished from sharp flexure from the locations of earthquakes alone: High-resolution tomographic reconstructions and data collection networks are needed to address such questions (*6*) and to observe the vertical tear seen by Obayashi *et al*. (see the figure, panel C). The first tentative tomographic indications for a slab rupturing came from investigations in the Mediterranean (*7*, *8*) that took advantage of the dense coverage of the Italian peninsula with seismic stations. A temporary deployment of seismographs on Kamchatka led to the discovery that the westernmost tip of the Aleutian slab has completely disappeared, which implies that a rupture process occurred in the past (*9*).

Sufficiently detailed tomography has only recently come about after dense seismic networks ("superarrays") were implemented that deploy hundreds of stations in the western United States and Japan. Such studies have recently revealed that the Farallon slab under North America is heavily fragmented (see the figure, panel D), with some disconnected blobs of material lodged in the transition zone between the upper and lower mantle and some sinking into the lower mantle (*10*, *11*).

However, the tear observed by Obayashi *et al*. is in the vertical direction. The parts of the slab that sink at the southern Kurile-Japan and Izu-Bonin trenches descend together but meet resistance at the lower mantle interface, where they flatten and rupture apart. The authors locate the gap in these slabs with high precision and show how its expansion continues to generate a small cluster of earthquakes.

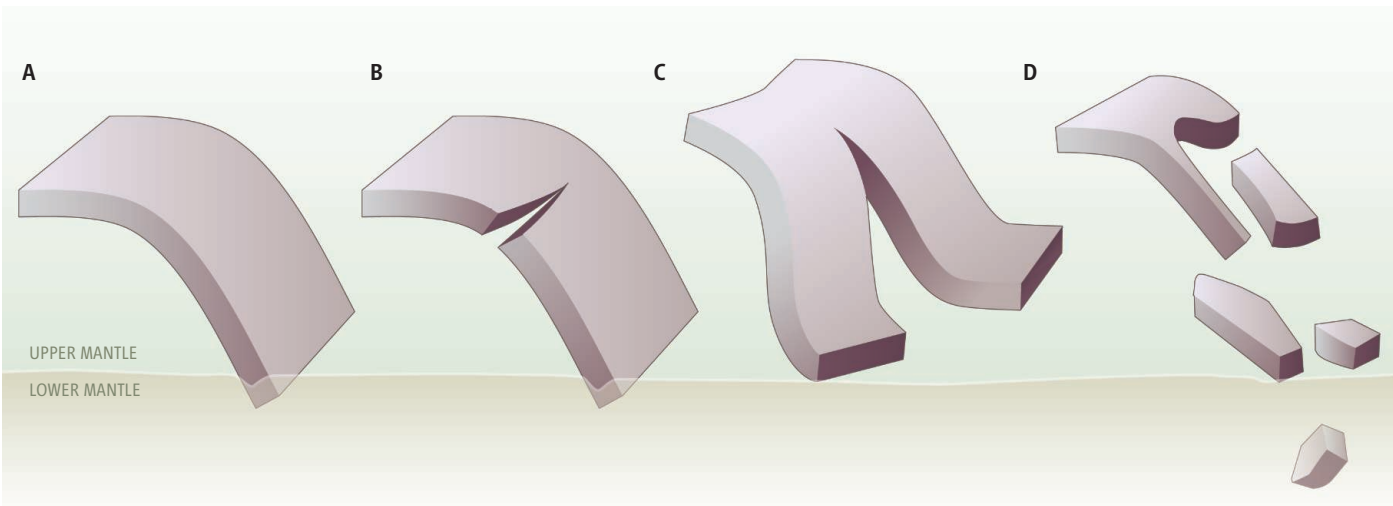

Modes of slab fragmentation. (**A**) An idealized, coherent slab stays intact. (**B**) A horizontal tear is driven by opposing buoyancy at continental collision. (**C**) The vertical tear as observed by Obayashi *et al.*, possibly along a fracture zone, is caused by resistance at 660 km depth. (**D**) Extensive slab fragmentation can occur when both processes shown in (B) and (C) occur.

Their analysis points to the existence of horizontal tensional stress parallel to the slab that is pulling it apart.

The vertical tear observed by Obayashi *et al*. beneath Japan seems to be generated by resistance at the bottom of the upper mantle. This simple explanation is fortuitous, because if the slab is being pulled apart by tensional stresses, these stresses should show up in the source mechanisms of earthquakes located at the tip of the tear. This prediction was successfully tested by the authors. The breakup of the slab beneath Japan is surprising because such old, thick lithosphere is supposedly strong.

A third observation by Obayashi *et al*., that of seismic waves reflecting off the rupture surface, is also surprising because it seems to indicate that this surface is smooth. Old fracture zones may provide the necessary weakness for tearing and would account for the

CREDIT: P. HUEY/SCIENCE

Published by AAAS

highly reflecting, specular nature of the rupture surface. Yet these reflections are unexpected: The geometry of the trenches will lead to compression of the slab before it undergoes tension when flattening at depth. This resulting deformation of the slab—in particular, a thinning before rupturing—is not an ideal condition to create a smoothly reflecting surface. If the reflection interpretation is correct, it would argue against thinning of the plate before rupturing. The tectonic situation is similar to that beneath Kamchatka, so the process seen here may reflect what happened there several million years ago.

The idea of slab tears is attractive because it can explain other related phenomena. A horizontal tear releases the slab from drag forces that hinder its movement. Below the crust, tearing leads to an influx of hot material from the asthenosphere (the region of low viscosity that underlies the lithosphere), which can explain both magmatic events and vertical motions observed at Earth's surface. Especially during continental collisions, when the lighter continental plate is buoyant but the denser oceanic lithosphere tends to sink, opposing forces of gravity provide the tension needed to create a tear (*12*).

The observed fragility of slabs has serious implications for the way the convective process is organized in Earth's deep interior. Seismologists have recognized for some time that only a fraction of descending slabs penetrate the boundary between the upper and lower mantle. The slab is cooler than the surrounding mantle, and because the phase transition requires higher pressure at lower temperature, the slab's conversion into perovskite is delayed; thus, the slab is temporarily buoyant. This buoyancy, combined with a much greater viscosity of the lower mantle (*13*), hampers slab penetration into the lower mantle. Slab fragmentation makes it even more difficult to pile up enough slab mass to overcome the resistance posed by the phase transition and by high viscosity. Detached fragments will need to equilibrate in temperature before changing to the denser phase, further delaying (or perhaps inhibiting) their sinking. The slowing of these processes limits mass flux between the upper and lower mantle and hinders the cooling of Earth's interior.

Further insights into these processes will likely require an increase in the resolving power of global tomography so that small blobs can be observed individually in the lower mantle (if they exist, they are currently blurred into larger structures). The seismic superarrays are a step in this direction but will never cover the oceans. For this, tentative efforts to observe seismic waves using floating sensors are promising (*14*). New tomographic techniques that overcome the resolution limitations of ray theory also need to be fully exploited.

References and Notes

1. M. Obayashi, J. Yoshimitsu, Y. Fukao, *Science* **324**, 1173 (2009).
2. R. McCaffrey, P. Molnar, S. W. Roecker, *J. Geophys. Res.* **90**, 4511 (1985).
3. J.-L. Chatelain, P. Molnar, R. Prévot, B. Isacks, *Geophys. Res. Lett*. **19**, 1507 (1992).
4. S. Lallemand, Y. Font, H. Bijwaard, H. Kao, *Tectonophysics* **335**, 229 (2001).
5. F. von Blanckenburg, J. H. Davies, *Tectonics* **14**, 120 (1995).
6. T. Cahill, B. L. Isacks, *J. Geophys. Res*. **97**, 17503 (1992).
7. W. Spakman, M. J. R. Wortel, N. J. Vlaar, *Geophys. Res. Lett.* **15**, 60 (1988).
8. M. J. R. Wortel, W. Spakman, *Science* **290**, 1910 (2000).
9. V. Levin, N. Shapiro, J. Park, M. Ritzwoller, *Nature* **418**, 763 (2002).
10. S. van der Lee, G. Nolet, *Nature* **386**, 266 (1997).
11. K. Sigloch, N. McQuarrie, G. Nolet, *Nat. Geosci.* **1**, 458 (2008).
12. J. H. Davies, F. von Blanckenburg, *Earth Planet. Sci. Lett*. **129**, 85 (1995).
13. B. H. Hager, *J. Geophys. Res.* **89**, 6003 (1984).
14. F. Simons, G. Nolet, J. Babcock, R. Davis, J. Orcutt, *Eos* **31**, 305 (2006).

15. Supported by the European Research Council. I thank T. Monfret for discussion.

10.1126/science.1174664

PHYSIOLOGY

What Determines Coral Health?

Genomic and cellular studies are revealing the physiological mechanisms of symbiosis and calcification, which are central to coral health.

Virginia M. Weis[1] and Denis Allemand[2]

Corals are to coral reefs as trees are to forests: They form both the trophic and structural foundation of the ecosystem. The trophic anchor arises from the intimate mutualism between corals and their intracellular symbionts—photosynthetic dinoflagellates that fix large quantities of carbon dioxide, making coral reefs among the most productive ecosystems on Earth. The structural anchor comes from the deposition of massive calcium carbonate skeletons that form the reef architecture and serve as habitat for a breathtaking diversity of organisms. Central to the severe global decline of coral reefs (*1*) is the dysfunction and collapse of both symbiosis and calcification in corals due to environmental stressors imposed by climate change. Insights into the physiological mechanisms that underlie healthy as well as stressed corals (*2*) are thus critical for predicting whether—and if so, how—corals will cope with rapid environmental change.

Genomic studies have shown that the genomes of early evolved animals such as corals are unexpectedly complex and remarkably similar to those of vertebrates (*3*). It now seems that complexity is the ancestral condition and that more recently evolved invertebrates, such as worms and flies, have over evolutionary time developed derived simplicity. The complexity in corals is evident in cellular pathways central to both symbiosis (*4*, *5*) and biomineralization (*6*). This information is providing a new foundation for developing testable hypotheses on coral physiology.

How do healthy corals maintain a stable partnership with their symbionts (see the figure, panels A and B), and how does this stability collapse under environmental stress? Similar questions have been posed for years in other better-studied host-pathogen and host-parasite interactions (*7*). Investigations of corals can be modeled on these studies. For example, which interpartner signaling events occur during initial contact between the partners? Does the host mount an innate immune response that is in turn modulated by the invading symbiont? And how does interpartner signaling and regulation change during the dysfunction and collapse of a symbiosis?

Recent studies in corals and anemones have started to address these questions. Initial interpartner lectin-glycan signaling events—so well described in other host-microbe interactions (*8*)—are present in corals during the onset of symbiosis, and a wide array of lectins have now been described in anemones (*9*). It remains to be shown to what extent these events confer interpartner specificity and whether there are other signaling mechanisms. Once inside the host cells, symbionts alter host

[1]Department of Zoology, Oregon State University, Corvallis, OR 97331, USA. E-mail: weisv@science.oregonstate.edu
[2]Departement des sciences de la vie, Université de Nice-Sophia Antipolis, Parc Valrose, 28, avenue Valrose, 06108 Nice Cedex 2, France.

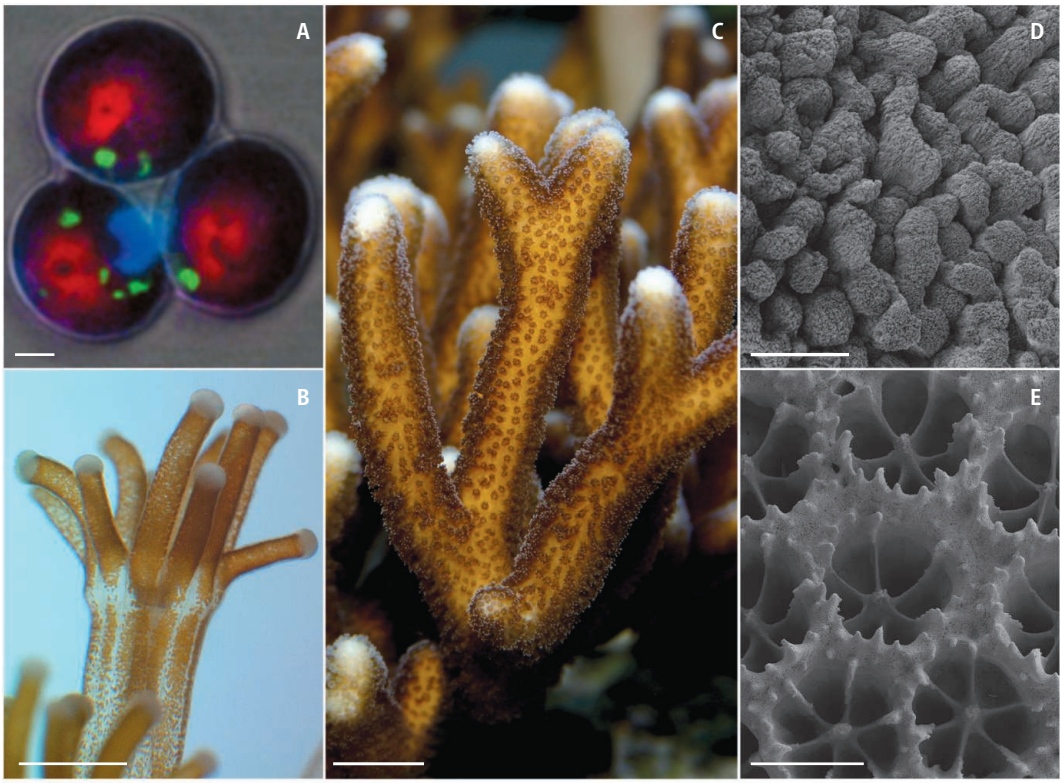

Calcification and symbiosis in the coral *Stylophora pistillata*. (**A**) Confocal micrograph (scale bar 2 μm) of an isolated coral cell with three resident symbionts in red, host mitochondria in green, and cell nucleus in blue. (**B**) Light micrograph (scale bar 0.5 mm) of a single polyp showing brown, spherical symbionts resident within the host. (**C**) A whole coral colony (scale bar 1 cm). Scanning electron micrographs of the skeleton at high [(**D**) scale bar 10 μm] and low [(**E**) scale bar 1 mm] magnifications.

cellular behavior in order to persist—for example, by interrupting host membrane trafficking such that host lysosomes fail to fuse with the vacuoles housing the symbionts (*10*). The same strategy is used by various intracellular parasites of vertebrates to persist within macrophages (*11*). Future cell studies should investigate the dynamics of symbiont invasion of host tissues and the coordination of cell division; genomic and metabolomic studies could provide insight into the types of nutrients moving between partners and the mechanisms of transport and regulation.

Changes to the stability of coral-dinoflagellate symbioses are central to coral bleaching, a phenomenon that results in the loss of symbionts from host tissues (*12*). Bleaching events attributed to global warming are threatening reefs worldwide (*1*). Elevated temperatures, often in concert with high light levels, cause severe oxidative stress in the symbiont that overwhelms its oxygen-handling mechanisms and damages proteins, lipids, and nucleic acids in both partners (*13*).

Bleaching may be a host innate immune response to a compromised symbiont (*14*). Concentrations of the immune effector nitric oxide (*15*) and two pro-apoptotic molecules, p53 and caspase (*16, 17*), are high in heat-stressed animals, suggesting that hosts become intolerant of symbionts and initiate processes to eliminate them. It is not yet clear which cellular events result in the loss of symbionts, but recent studies point to host cell apoptosis and autophagy (*17, 18*), two highly conserved immune mechanisms that are commonly used to eliminate detrimental microbial invaders in vertebrates.

Like symbiosis, calcification is central to coral physiology and health. Corals form the reef structure by biomineralization (see the figure, panels C to E). Biominerals are composite materials consisting of both mineral (calcium carbonate in the case of corals) and organic fractions. Genomic and cellular studies are revealing some pieces of the coral calcification puzzle. Two ion transporters, Ca^{2+}-ATPase (adenosine triphosphatase) and a Ca^{2+} channel, have been identified, and physiological studies suggest the presence of corresponding anion carriers (*19*). The intraskeletal, macromolecular organic matrix is central to the calcification process (*20*). However, whereas about 520 proteins have been identified in the matrix of chicken eggshell (*21*), just one protein has been identified in coral skeleton (*22*), with genomic and proteomic studies suggesting the presence of many others (*20*, *23*).

Regulation of calcification and calcifying cells is controlled by several mechanisms. Calcifying coral tissue expresses carbonic anhydrases, enzymes that interconvert inorganic carbon species critical for calcification (*24*). A homolog to bone morphogenetic protein (BMP), a signaling protein important in the development of mineralizing cells in vertebrates, has been characterized in corals (*6*). Coral BMP localizes to calcifying tissue and binds human BMP-binding proteins, suggesting a common evolutionary origin and function of mineralizing tissue in vertebrates and corals. As in some other mineralizing organisms, calcification in symbiotic corals is enhanced in light, but the physiological basis for this is still debated. Symbiotic dinoflagellates could be providing calcifying host cells with organic precursors for organic matrix synthesis when they are photosynthesizing in the light (*20*).

Calcification by corals is threatened by ocean acidification, caused by the dissolution of atmospheric carbon dioxide into seawater. The resulting decreased pH moves the inorganic carbon balance in seawater away from carbonate, which is required for calcium carbonate deposition. The expected pH decrease by 0.2 units during the next century may decrease calcification rates by up to 50%, as well as promoting skeleton dissolution (*25*).

What causes the extreme sensitivity of corals to decreased pH? The general hypothesis is that a decrease in seawater carbonate concentration is to blame, but this is probably not the whole story, because noncalcifying organisms such as marine worms and fish eggs are also affected by the pH decrease. Another factor may be pH-mediated perturbations in the homeostatic balance within organisms (*26*).

The study of coral physiology has entered an active and exciting era, spurred on by new information from genomic and cellular studies. With the very survival of coral reefs in question, never has the information coming from coral physiology been more important. A deeper understanding of the fundamental physiological mechanisms of symbiosis and calcification will contribute to our ability to predict how and whether corals will be able to adapt to and survive climate change.

References

1. O. Hoegh-Guldberg *et al.*, *Science* **318**, 1737 (2007).
2. V. M. Weis, S. K. Davy, O. Hoegh-Guldberg, M. Rodriguez-Lanetty, J. R. Pringle, *Trends Ecol. Evol.* **23**, 369 (2008).
3. N. H. Putnam *et al.*, *Science* **317**, 86 (2007).
4. M. K. Desalvo *et al.*, *Mol. Ecol.* **17**, 3952 (2008).
5. D. J. Miller *et al.*, *Genome Biol.* **8**, R59 (2007).
6. D. Zoccola *et al.*, *Mar. Biotechnol.* **11**, 260 (2009).
7. D. A. Relman, *Nat. Rev. Microbiol.* **6**, 721 (2008).
8. E. M. Wood-Charlson, L. H. Hollingsworth, D. A. Krupp, V. M. Weis, *Cell. Microbiol.* **8**, 1985 (2006).
9. E. M. Wood-Charlson, V. M. Weis, *Dev. Comp. Immunol.*, 10.1016/j.dci.2009.01.008 (2009).
10. M.-C. Chen *et al.*, *Biochem. Biophys. Res. Commun.* **338**, 1607 (2005).
11. A. O. Amer, M. S. Swanson, *Curr. Opin. Microbiol.* **5**, 56 (2002).
12. A. E. Douglas, *Mar. Pollut. Bull.* **46**, 385 (2003).
13. M. P. Lesser, *Annu. Rev. Physiol.* **68**, 253 (2006).
14. V. M. Weis, *J. Exp. Biol.* **211**, 3059 (2008).
15. S. Perez, V. M. Weis, *J. Exp. Biol.* **209**, 2804 (2006).
16. M. P. Lesser, J. H. Farrell, *Coral Reefs* **23**, 367 (2004).
17. S. Richier *et al.*, *FEBS J.* **273**, 4186 (2006).
18. S. R. Dunn, C. E. Schnitzler, V. M. Weis, *Proc. R. Soc. London B* **274**, 3079 (2007).
19. D. Allemand *et al.*, *C. R. Palevol.* **3**, 453 (2004).
20. S. Tambutté *et al.*, in *Handbook of Biomineralization. The Biology of Biominerals Structure Formation*, E. Baeuerlein, Ed. (Wiley-VCH, Weinheim, Germany, 2007), pp. 243–259.
21. K. Mann, B. Macek, J. Olsen, *Proteomics* **6**, 3801 (2006).
22. I. Fukuda *et al.*, *Biochem. Biophys. Res. Commun.* **304**, 11 (2003).
23. S. Sunagawa *et al.*, *PLoS ONE* **4**, e4865 (2009).
24. A. Moya *et al.*, *J. Biol. Chem.* **283**, 25475 (2008).
25. J. A. Kleypas *et al.*, *NSF-NOAA-USGS* (2006); see www.isse.ucar.edu/florida/.
26. F. Marubini *et al.*, *Coral Reefs* **27**, 491 (2008).

10.1126/science.1172540

CELL BIOLOGY

Sorting Out Diabetes

Altered trafficking of storage vesicles that harbor a glucose transport protein in muscle and fat tissue may contribute to diabetes.

Charisse M. Orme and Jonathan S. Bogan

Early during the development of type 2 diabetes, insulin's ability to stimulate the cellular uptake of glucose from the blood is compromised (*1*). Muscle is the main tissue responsible for this absorption, and insulin enhances glucose movement into muscle cells through the GLUT4 transporter at the cell surface (*2*, *3*). This hallmark action of insulin is conserved in vertebrates, and the molecular machinery by which it occurs is thought to be similar among mammals. On page 1192 of this issue, Vassilopoulos *et al.* (*4*) identify a key protein that mediates insulin action in humans, but not in mice, a distinction with potential implications for understanding glucose metabolism and diabetes pathophysiology.

During fasting, when the concentration of circulating insulin is low, GLUT4 is sequestered from the plasma membrane, restricting glucose entry into the cell. After meals, an increase in insulin concentration triggers the insertion of GLUT4 transporters at the cell surface to facilitate glucose uptake and storage. Like other proteins that cycle to and from the cell surface, GLUT4 is internalized at the plasma membrane (via endocytosis) into endosomal vesicles. Yet unlike most "recycling" proteins, endosomal GLUT4 is targeted to a specific population of small, preformed vesicles that are poised for mobilization to the cell surface in response to insulin (*5*, *6*). These storage vesicles are present selectively in muscle and adipose tissue. Although much progress has been made toward understanding the intracellular insulin signaling pathways that control GLUT4 translocation, the specific membrane trafficking mechanisms involved remain poorly understood.

Vassilopoulos *et al.* focused on the role of CHC22, a constituent (heavy chain) of the clathrin protein complex, in the transport of GLUT4. Clathrin is a major component of a protein coat that surrounds vesicles involved in transporting proteins among the plasma membrane, trans-Golgi network, and endosomal system (*7*). Clathrin deforms membranes, facilitating vesicle formation. In humans, CHC22 is expressed selectively in muscle, but in mice, it is a pseudogene, and therefore not expressed at all. Vassilopoulos *et al.* show that unlike its ubiquitously expressed cousin, CHC17, which functions in endocytosis, CHC22 participates in a

Section of Endocrinology and Metabolism, Department of Internal Medicine, and Department of Cell Biology, Yale University School of Medicine, New Haven, CT 06520–8020, USA. E-mail: jonathan.bogan@yale.edu

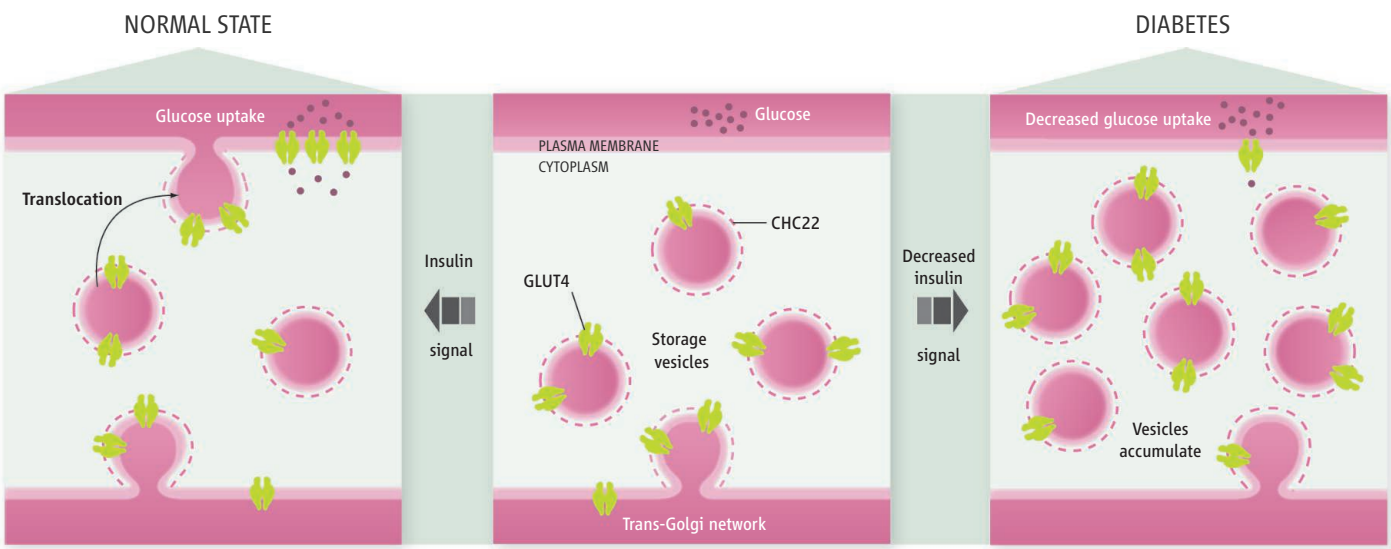

CREDIT: N. KEVITIYAGALA/*SCIENCE*

Transporter sorting. The clathrin protein CHC22 mediates the formation of storage vesicles containing GLUT4 in human muscle cells. In diabetic humans, the storage vesicles accumulate and are not well mobilized to the cell surface by insulin. The vesicles arise from the trans-Golgi network (or possibly from recycling endosomes).

tissue-specific membrane trafficking pathway for GLUT4. Specifically, CHC22 copurifies with proteins important for sorting GLUT4 out of endosomes or the trans-Golgi network and into storage vesicles in human muscle cells. CHC22 colocalizes with GLUT4 in these vesicles, and its depletion results in the apparent loss of these vesicles. Conversely, expression of the human gene encoding CHC22 in mice resulted in abnormal glucose homeostasis. The number of GLUT4 storage vesicles appears to be increased. GLUT4 was poorly mobilized by insulin, as seen in humans with type 2 diabetes (see the figure).

The findings by Vassilopoulos *et al.* highlight the possibility that altered vesicle trafficking may contribute to diabetes pathophysiology, independent of impaired insulin signaling (*8*). CHC22-coated storage vesicles harboring GLUT4 may not be targeted by the insulin signal. In cultured adipocytes, for example, only about two-thirds of GLUT4 storage vesicles are translocated by maximal insulin stimulation (*5*, *9*). Why is the remainder of this pool inaccessible? Is the fraction of GLUT4 that can be translocated reduced in diabetes? Alternatively, GLUT4 may accumulate within storage vesicles because of deficient insulin signaling. Yet in the mice engineered to express human CHC22, activation of Akt, an enzyme that functions in one signaling pathway that affects GLUT4 translocation, was increased. Other signaling pathways have been implicated in both GLUT4 translocation and diabetes pathophysiology, and these may be important to mobilize vesicles formed by CHC22 (*10*–*12*).

Muscle contraction causes translocation of GLUT4 to enhance glucose uptake, similar to insulin, and it will be interesting to learn if the vesicles that are mobilized also have CHC22 coats. CHC22 appears to participate in trafficking GLUT4 storage vesicles in adipose tissue as well as in muscle. An interesting possibility is that GLUT4 storage vesicles shed their clathrin coats in response to insulin. Finally, it will be important to learn if obesity alters the abundance of CHC22 or of associated proteins, in either muscle or adipose tissue, to curtail insulin action.

Most studies on GLUT4 trafficking have used rodent models, in which CHC17 forms the GLUT4 storage vesicles (*13*, *14*), so it's not clear how CHC22 functions differently. For example, why does the diabetes-like phenotype of mice that express CHC22 become apparent with age; would a high-fat diet exacerbate the defect? A detailed analysis of the metabolic phenotype in these mice, possibly by infusions of insulin and a glucose tracer, should provide some answers.

The work of Vassilopoulos *et al.* highlights the differences between humans and mice by providing the first molecular identification of human-specific GLUT4 sorting. The exact role CHC22 may play in human diabetes remains uncertain. However, this work reminds investigators studying diabetes pathogenesis that it is important to think outside the vesicle.

References

1. D. B. Savage, K. F. Petersen, G. I. Shulman, *Physiol. Rev.* **87**, 507 (2007).
2. S. Huang, M. P. Czech, *Cell Metab.* **5**, 237 (2007).
3. M. Larance, G. Ramm, D. E. James, *Mol. Endocrinol.* **22**, 226 (2008).
4. S. Vassilopoulos *et al.*, *Science* **324**, 1192 (2009).
5. B. R. Rubin, J. S. Bogan, *Vitam. Horm.* **80**, 155 (2009).
6. P. F. Pilch, *Acta Physiol. (Oxf.)* **192**, 89 (2008).
7. M. A. Edeling, C. Smith, D. Owen, *Nat. Rev. Mol. Cell Biol.* **7**, 32 (2006).
8. W. T. Garvey *et al.*, *J. Clin. Invest.* **101**, 2377 (1998).
9. R. Govers, A. C. Coster, D. E. James, *Mol. Cell. Biol.* **24**, 6456 (2004).
10. L. Chang, S. H. Chiang, A. R. Saltiel, *Endocrinology* **148**, 27 (2007).
11. K. L. Hoehn *et al.*, *Cell Metab.* **7**, 421 (2008).
12. K. J. Gaulton *et al.*, *Diabetes* **57**, 3136 (2008).
13. D. J. Fazakerley, S. P. Lawrence, V. A. Lizunov, S. W. Cushman, G. D. Holman, *J. Cell Sci.* **122**, 727 (2009).
14. J. Li *et al.*, *J. Cell Biol.* **178**, 453 (2007).

10.1126/science.1174841

CELL BIOLOGY

It's the DNA That Counts

A simple genetic circuit that counts molecular events may be further developed to program complex cell behaviors.

Christina D. Smolke

Natural biological systems have evolved genetic programs that control complex activities through the coordinated processing of signals received from their environments. The engineering of synthetic biological systems to perform programmed information processing and computational functions has remained a challenge. Counters represent one class of information-processing systems and can be used to trigger events in response to a series of detected signals that are integrated and processed over time. Engineered biological counters would enable many applications, such as regulating cell death after a specified number of cell division cycles, controlling cell differentiation in response to temporal cues, noninvasive monitoring of aging, and recording the frequency of environmental events. On page 1199 in this issue, Friedland *et al.* (*1*) report an important step toward the construction of genetically encoded counters.

Counters can be assembled from a variety of simpler functions, such as signal detection and processing (the ability to respond to an input signal), time delay (the ability to integrate signals and trigger events after a delay from the initial detection event), and memory (the ability to remember and track earlier detection events). Genetic circuits that encode these basic operations have been demonstrated, including systems that use both protein-based transcriptional regulators (*2*–*4*) and RNA-based posttranscriptional regulators (*5*–*7*). For example, time delays have been encoded in cascades of transcription (the production of RNA from corresponding DNA) that trigger the production (or repression) of a protein (via translation of the corresponding RNA) upon the detection of an initial signal. This event subsequently activates the production (or repression) of the next protein. A linear sequence of such events, in the form of repeating modules, can be designed in which the last module triggers the production of the desired protein output (*8*, *9*).

Transcriptional cascades introduce delays in triggering the final protein output through the latency associated with expressing each intermediate protein in the series. Such cascading systems exhibit other properties including signal amplification, signal filtering, sensitivity to detecting the signal, and modulation of variation across cell populations (*8*). Other genetic mechanisms for introducing time delays in protein production are based on increasing the time associated with RNA processing steps (*10*).

Memory has been encoded in genetic circuits by means of feedback loops that lock a system in one state following a signal that sets that state. For example, a circuit based on the incorporation of two mutually inhibitory tran-

Department of Bioengineering, Stanford University, Stanford, CA 94305, USA. E-mail: csmolke@stanford.edu

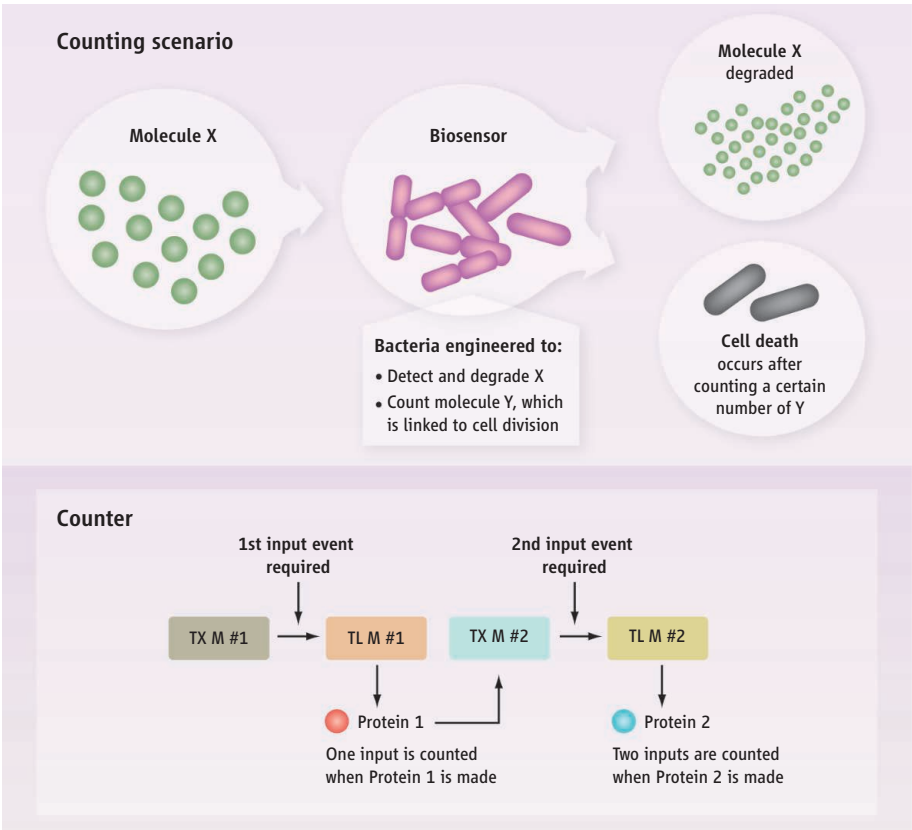

Why count, and how? (**Top**) In the hypothetical counting scenario shown, bacteria can be engineered to sense molecule X and degrade it (such as in bioremediation). At the same time, as a safety mechanism, the bacteria are engineered to count molecule Y, which is associated with cell division. After counting a certain number of molecule Y, the bacteria execute a cell death function. (**Bottom**) An example of a simple genetic counter that counts up to two, based on a conditional transcriptional cascade. The cascade includes transcription modules (TX M) and translation modules (TL M).

scriptional negative-feedback loops acted as a genetic toggle switch, in which transient input signals moved the system between two states (*11*). Each state was associated with the production of a protein that inhibited the system from moving into the other state unless the appropriate input signal was applied. In a different memory circuit, based on an autoregulatory transcriptional positive-feedback loop (*12*), a transient input signal triggered the production of a protein that subsequently activated its own production, such that the system remained in the activated state after removal of the signal.

Early attempts to build heritable memory systems that do not require the sustained production of proteins were based on enzymatic mechanisms that allow the system state to be written directly into the structure of DNA (*13*). To date, these systems have been developed with recombinases, enzymes that can invert, insert, or remove specified DNA sequences and thus dynamically rewrite genetic programs in response to specified signals. For example, a genetic circuit based on two overlapping inversion systems encoded multiple output states depending on the order in which recombinases processed the DNA (*14*).

Friedland *et al.* take important steps to build biological counters by integrating these functional operations. The authors propose two different circuit architectures for encoding counters that trigger the expression of a desired protein following the processing of two or three input signal pulses. Each counter combines a time-delay operation (triggered by the initial detection event—setting the "1" state) with conditional regulation linked to the immediate detection of subsequent signals (allowing the counting of additional detection events "2" and "3"). In one system, the time delay is encoded through a transcriptional cascade operation. Conditional regulation is achieved through an RNA molecule that is expressed only when the input signal is present. The expression of this RNA is under the control of a protein-based transcriptional regulator and is required for the expression of the protein output from the transcriptional cascade modules. Because of the delay associated with protein accumulation from each transcription module and difference in decay rates between the protein and RNA components, the RNA regulator decays before a sufficient amount of the protein output from the previous module has accumulated to trigger activation of the next module. This resets the conditional regulation operation and allows counting of input pulses (see the figure).

In their second system, the time-delay operation is encoded within a heritable memory cascade. Each memory module encodes a protein that flips a segment of DNA within that module to turn off its own expression and primes the next module to be activated by the input signal by correctly orienting a protein-based transcriptional regulatory element. The time required for each memory module to prime the next module is longer than the signal pulse length such that counting is achieved. By incorporating memory modules, this second architecture allows signals to be integrated over longer time frames, as the priming of the module is "hard-coded" into the DNA. In addition, this architecture could allow identical or different input signals to be counted via the choice of each module's conditional regulatory element.

Friedland *et al.* provide examples from which to build more sophisticated counters. An important next step will be to develop circuits that can report on intermediate states, in addition to the final state. Another critical counter property will require the development of circuits that allow counters to distinguish between continuous and transient signals. Given the broad applications of counters that operate inside living cells, the continued development of next-generation genetically encoded counters will be of critical importance to synthetic biology (*15*).

References

1. A. E. Friedland *et al.*, *Science* **324**, 1199 (2009).
2. C. C. Guet, M. B. Elowitz, W. Hsing, S. Leibler, *Nature* **296**, 1466 (2002).
3. J. C. Anderson, C. A. Voigt, A. P. Arkin, *Mol. Syst. Biol.* **3,** 133 (2007).
4. R. S. Cox III, M. G. Surette, M. B. Elowitz, *Mol. Syst. Biol.* **3**, 145 (2007).
5. F. J. Isaacs *et al.*, *Nat. Biotechnol.* **22**, 841 (2004).
6. M. N. Win, C. D. Smolke, *Science* **322**, 456 (2008).
7. M. N. Win, J. C. Liang, C. D. Smolke, *Chem. Biol.* **16**, 298 (2009).
8. S. Hooshangi, S. Thiberge, R. Weiss, *Proc. Natl. Acad. Sci. U.S.A.* **102**, 3581 (2005).
9. W. Weber, B. P. Kramer, M. Fussenegger, *Biotechnol. Bioeng.* **98,** 894 (2007).
10. I. A. Swinburne *et al.*, *Genes Dev.* **22**, 2342 (2008).
11. T. S. Gardner, C. R. Cantor, J. J. Collins, *Nature* **403**, 339 (2000).
12. C. M. Ajo-Franklin *et al.*, *Genes Dev.* **21**, 2271 (2007).
13. T. S. Ham, S. K. Lee, J. D. Keasling, A. P. Arkin, *Biotechnol. Bioeng.* **94**, 1 (2006).
14. T. S. Ham *et al. PLoS One* **3**, e2815 (2008).
15. D. Endy, *Nature* **438**, 449 (2005).

10.1126/science.1174843

SCIENCE POLICY

Though New Funding Fuels Hope, S&T Leaders See Challenges Ahead

A historic transition in Washington, D.C., has brought strong political support and new funding for research, but it also creates new responsibilities for scientists, engineers, and educators to take action on critical issues and to communicate the value of their work to the public, science leaders said at the AAAS Forum on Science & Technology Policy.

President Barack Obama's commitment to increased research and development funding could renew the American innovation culture, yielding progress on climate and energy, public health, science education, and other fields, they said. John P. Holdren, assistant to the president for science and technology, acknowledged that achieving Obama's goals "is going to be hard" given the economic crisis, but he said that the effort is critical to global prosperity.

"Without energy there is no economy; without climate, there is no environment; and without economy and environment, there's no well-being," Holdren said during an address that opened the Forum. "So we had better figure out how to get this right."

Other speakers warned that pressures to cut the federal deficit could put R&D budget gains at risk by 2011, and they urged scientists and engineers to undertake a sustained effort to build public support. "You have to help us help the public understand that science is about creating jobs … and improving the quality of life," said U.S. Representative Bart Gordon (D–Tennessee), who chairs the House Committee on Science and Technology.

The 34th annual AAAS Forum drew more than 600 leaders from U.S. and foreign governments, businesses, research centers, and universities to Washington on 30 April and 1 May. The Forum, organized by AAAS Science and Policy Programs, is the largest and most important annual science and technology policy conference in the United States.

Sessions focused on a range of issues, including the governance of emerging technologies; the links between climate change, energy sources, and public health; and the future of science journalism. MIT President Susan Hockfield described a revolution driven by the convergence of life sciences with physical and engineering sciences. In the annual William D. Carey Lecture, eminent American scientist and adviser Richard L. Garwin detailed the increasing importance of computer modeling and simulation in addressing health and energy issues. And top S&T officials from Canada, Japan, and the U.K. discussed innovation policy in their nations.

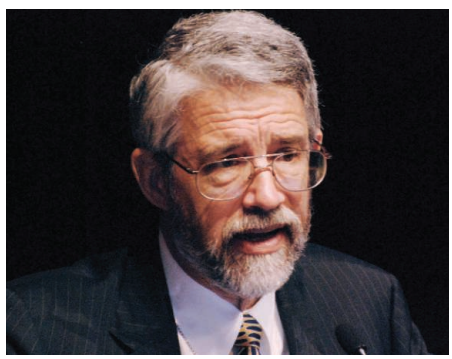

The challenge. White House science adviser John P. Holdren said that energy, the environment, and the economy are inseparable.

The research agenda. U.S. Energy Secretary Steven Chu described efforts to achieve paradigm-shifting energy breakthroughs.

But almost every session included some discussion of policy and funding under the Obama administration.

Just days before the Forum, Obama announced that he would seek to push total U.S. R&D spending to 3% of gross domestic product, up from the current 2.66%. Al Teich, head of Science and Policy Programs at AAAS, said that total federal R&D spending for 2009, including funding from the economic stimulus plan, would hit $172 billion—"a huge increase" over 2008. Much is destined for research outside the defense realm—in public health, climate, and energy.

Holdren, who served as the 2006 AAAS president, said that Obama will move to increase the energy efficiency of buildings, cars, and manufacturing. Next-generation nuclear energy also is of interest.

"We are still living in a world that's about 80% dependent on fossil fuels—[in] the United States, more than 85% dependent," Holdren said. "That's not going to change overnight, so we can't just say we're going to go immediately, all the way, to unconventional renewables. We have no way to do that. We have to fix in various ways the conventional options that we're using, as well."

He added, "You'll see the alternative energy supplies coming in somewhat more slowly, but ultimately growing to a very large level."

In a separate address to the Forum, Energy Secretary Steven Chu said that "energy frontier research grant centers" are being established by the Department of Energy. He also pointed to the 2-year, $400 million start-up budget for high-risk, high-reward initiatives under the Advanced Research Projects Agency-Energy, or ARPA-E.

Gordon envisioned ARPA-E as a lean, nimble agency that would identify a challenge, recruit a team of top research talent, and then press for "transformational" breakthroughs. "There's going to be things coming out of ARPA-E that we can't imagine now," he said.

U.S. Representative Brian Baird, a Washington state Democrat and a Ph.D. psychologist, urged that policy-makers not overlook social sciences for tools to address climate and energy issues.

Changing consumer behavior is "the single most immediate thing we can do" to reduce energy consumption, said Baird, who chairs a House subcommittee on energy and environment. In fact, he said, U.S. energy consumption could be reduced as much as 20%—in a matter of months—by measures such as carpooling, using less air conditioning, and installing efficient appliances.

Advancing these ambitious new S&T initiatives is going to require the commitment of scientists and engineers nationwide, speakers told the Forum. Chu said that hundreds of scientists and engineers would be needed to help review a surge of applications for new projects funded under the economic stimulus package. And from the Capitol to the grassroots, they said, researchers need to reach out and build a bond of common purpose with the public.

Visit www.aaas.org/spp/rd/forum for presentations and podcasts from the Forum.

—Ginger Pinholster and Earl Lane contributed to this report

Published by AAAS

SCIENCE DIPLOMACY

China, U.S. Plan Projects In S&T Ethics Education

SAN DIEGO, CALIFORNIA—A panel of influential science scholars and educators from China and the United States said that they would explore a range of cooperative projects in ethics education following a workshop organized by the China Association for Science and Technology (CAST) and AAAS.

After 3 days of presentations and discussions, Chinese and U.S. delegates identified several possible joint projects: Surveys on misconduct; exchanges on training ethics educators; a collection of case studies; and perhaps even a practical guidebook on ethics in science.

Li Jinghai, vice president of the Chinese Academy of Sciences and vice-chair of CAST's Commission on Ethics and Rights of Scientists and Engineers, said in a keynote address that scientists have an ethical obligation to make the innovation system more efficient so that it benefits more people. "We have a duty to minimize the negative effects and maximize the positive effects [of scientific research]," Li said.

AAAS Chief Executive Officer Alan I. Leshner stressed that building trust is crucial for U.S. and Chinese researchers because of their position as global leaders in addressing health, energy, climate, and other challenges. "We won't be taken seriously if we don't have credibility," said Leshner, who also serves as executive publisher of *Science*. "And our credibility depends on our ability to behave at the highest level ethically."

The workshop, which opened on 27 April and was hosted by the University of California-San Diego (UCSD) and the Reuben H. Fleet Science Center, was the latest engagement in the deepening relationship between the science and engineering communities in China and the United States. It was the outgrowth of a September 2007 trip to Beijing by Leshner and a AAAS-organized delegation for a workshop on research integrity. In other meetings during that visit, AAAS and Chinese science and engineering leaders agreed to joint publishing and education projects and pledged to seek additional collaboration.

In San Diego, nine Chinese science and education leaders, including several high-ranking CAST representatives and one university president, held detailed and candid talks with 14 U.S. colleagues, including some of the nation's leading scholars on science ethics and research integrity.

They quickly established common ground: While the roots of China's ethical practices date 2500 years to Confucius, and while science ethics in the United States have evolved over 200 years, both have found that misconduct has a host of causes, from lack of understanding to competition and fear of failure.

Melissa Anderson, director of the Post-Secondary Education Research Institute at the University of Minnesota, reported that her research found that an estimated 24% of mid-career U.S. scientists per year engaged in questionable use of funds, with nearly as many cutting corners in their research practices.

Wang Chunfa, the director-general of CAST's Department of Policy Studies and Publicity, cited a survey of 30,000 Chinese researchers in which 40% described misconduct as "very common"; over half reported that they had never been educated about research ethics.

Though focus on U.S. ethics education has intensified since the 1970s, the rate of misconduct has not appreciably changed, said workshop co-organizer Michael Kalichman, director of the UCSD Research Ethics Program. The key question, then, is how to create an environment where researchers routinely discuss and evaluate ethical issues—and know how to respond to misconduct.

Tianjin University President Gong Ke described an ambitious 4-year ethics course recently introduced for undergraduates at his institution, one of China's largest multidisciplinary engineering universities. But Chinese and U.S. educators agreed that the commitment varies widely in schools and disciplines.

A new steering committee comprised of experts from the two countries is being considered to guide future collaborations. The committee would develop joint projects such as collections of case studies and best practices in both countries, possibly assembled into a guidebook that could be used in education.

Commitment to integrity. Tianjin University President Gong Ke described an ambitious 4-year ethics course for undergraduates.

SCIENCE & SECURITY

Experts Say Technology Can Enforce Test Ban Treaty

Technological advances have made it possible to zero in on small nuclear explosions around the globe, and experts at a AAAS briefing said that could persuade the United States to ratify a treaty banning nuclear tests.

When the Comprehensive Test Ban Treaty (CTBT) was last considered by the U.S. Senate in 1999, some lawmakers feared that nations could evade the treaty's detection network with small test explosions.

"While the United States raised legitimate concerns … about the ability to detect small nuclear tests around the world, we now have much more sensitive technology to allay those apprehensions," said Ola Dahlman, an expert with the Preparatory Commission of the CTBT.

The administration of President Barack Obama may urge the Senate to reconsider the treaty's ratification, "bringing the U.S. on board into the CTBT regime by 2010, or after the next (mid-term) elections," David Hafemeister, a visiting fellow at the Arms Control Association, said at the AAAS briefing.

Innovations in underground, underwater, and atmospheric vibration detection now make it possible to pinpoint explosions as small as 0.01 kiloton in certain parts of the world. Dahlman said that improved atmospheric detection of noble gases such as xenon—"an earmark of a nuclear explosion"—was key to confirming a nuclear test in the Democratic People's Republic of Korea in October 2006.

The 8 April briefing was cosponsored by the AAAS Center for Science, Technology, and Security Policy and the Center for Media and Security. Benn Tannenbaum, associate program director at the AAAS center, said that the political debate over the test ban treaty has evolved along with the treaty's technical aspects.

Obama "has made it clear on several occasions that the treaty is in the interest of the United States and the world," said Tannenbaum. "And part of the president's case to Congress is going to be based on science and our ability to verify that nations will not be able to test without the world knowing."

--Benjamin Somers and Becky Ham

Published by AAAS

The Computation of Social Behavior

Timothy E. J. Behrens,* Laurence T. Hunt,* Matthew F. S. Rushworth*

Neuroscientists are beginning to advance explanations of social behavior in terms of underlying brain mechanisms. Two distinct networks of brain regions have come to the fore. The first involves brain regions that are concerned with learning about reward and reinforcement. These same reward-related brain areas also mediate preferences that are social in nature even when no direct reward is expected. The second network focuses on regions active when a person must make estimates of another person's intentions. However, it has been difficult to determine the precise roles of individual brain regions within these networks or how activities in the two networks relate to one another. Some recent studies of reward-guided behavior have described brain activity in terms of formal mathematical models; these models can be extended to describe mechanisms that underlie complex social exchange. Such a mathematical formalism defines explicit mechanistic hypotheses about internal computations underlying regional brain activity, provides a framework in which to relate different types of activity and understand their contributions to behavior, and prescribes strategies for performing experiments under strong control.

Social cognitive neuroscience attempts to identify and describe the brain areas and mechanisms that mediate social life. It is a field with a strange status. On the one hand, the proliferation of papers and conferences on the neural mechanisms of social cognition attest to a widespread excitement: Techniques for brain imaging now make it possible to investigate the biological basis of aspects of behavior that seem the most intrinsically human. On the other hand is the unusual skepticism with which such findings are sometimes greeted. Ultimately, behind this skepticism lies a concern that there may be something fundamental missing from our understanding of the neural mechanisms of social cognition that we take for granted when we study the neural mechanisms of other perceptual, cognitive, and motor processes.

If the most frequently studied aspects of social cognition are distinctively human, then is social cognitive neuroscience hampered by an absence of comparative models in other species? Like other perceptual, cognitive, and motor processes, does social cognition have a firm neuroanatomical basis? If so, can we understand its importance in terms of interconnections and interactions between brain areas? Does the complexity of social interactions prevent the investigation of neural mechanisms under controlled conditions? Are social cognitive neuroscientists therefore forced to rely on the fallacy of "reverse inference," misusing neural findings in an attempt to dissect cognitive processes (*1*)? Perhaps most important, is it feasible to describe the neural computations necessary to support social cognition in a way that allows precise and falsifiable predictions of our data in a framework that can be related across different studies? We contend that it is increasingly possible to understand social cognition in the context of an understanding of brain anatomy in human and other species, as well as in mathematical descriptions of behavior recorded in well-controlled experiments.

Clearly there are reasons for thinking that social cognition is an important brain function. According to the data gathered by advocates of the social brain hypothesis, the number and complexity of social interactions that an individual is likely to experience is a major determinant of interspecies differences in forebrain size, both generally in mammals and birds and, more specifically, when we focus on primates or even exclusively on hominoids (*2*). That social cognition should have such an impact is unsurprising when we consider the importance that social interactions have for individual survival and evolutionary fitness (*3*, *4*).

Several distinct approaches have been adopted when attempting to account for the brain basis of social cognition. One suggests that some brain areas have a uniquely social function (see below). Another approach, however, argues that an aggregation of simple, nonsocial processes will account for complex social behavior. Reward-guided behavior is known to depend on brain structures such as the orbitofrontal cortex (OFC) and amygdala (Fig. 1A). It is suggested that these structures might underlie the value associated with a particular person, just as they underlie values assigned to nonsocial stimuli (*5*). Other areas associated with reward and reinforcement, such as the ventral striatum and anterior cingulate cortex sulcus (ACCs), might also be expected to play a role. Some advocates of the social brain hypothesis appear to endorse such a view by arguing that social complexity is correlated with widespread differences in basic neuroanatomical features (such as brain size) rather than with changes limited to small, specialized brain regions.

Combining Formal Behavioral Models with Neurophysiological Data

It is clear that placing behavior in a social context does have a measurable effect on activity in brain regions associated with reward. For example, activity in ventral striatum that increases in receipt of monetary rewards also increases when subjects receive positive appraisals by their peers (Fig. 2A) (*6*).

In the domain of reward-guided behavior, our understanding of such signals has been transformed by recent attempts to provide an underlying mathematical formalism. Mathematical models that predict behavior bring a number of key advantages. Such models have different internal parameters that relate to different precise computations. By designing situations in which these model parameters fluctuate independently through trials, scientists can ask specific questions about neural activity (Fig. 1B) (*7*). These questions relate not to differences between different tasks but to the internal computations necessary to support a single task. In two different trials the stimuli and task might be identical, establishing strong control, but internal computations may differ (e.g., as a result of different previous experiences). Mathematical models make predictions of these internal computations that can be tested in neural data. By relating different parameters together in formal equations, they also predict precisely the effect that differences in neural activity should cause in behavior. In doing so, they obviate the possibility of reverse inference. Hypotheses in such studies are about not only brain regions, but also computational mechanisms.

A key example of this approach comes from reward-sensitive activity in midbrain dopamine neurons, which project to the ventral striatum. Dopaminergic activity does not, however, simply differentiate rewarded from unrewarded events. Rather, it codes a quantitative prediction of expected reward (derived from past experiences) and the quantitative deviation in observed reward from this prediction (*8*). This reward prediction error signal is an essential component of theoretical models of reinforcement learning (RL).

At their most simple, RL algorithms state that expectations of future reward (V_{t+1}) should be a function of current expectations (V_t) and their discrepancy from the actual outcome that is experienced—the prediction error (δ_t). More specifically, future expectations should be updated by the product of the prediction error and the learning rate (α_t) (*9*):

$$V_{t+1} = V_t + \alpha_t \delta_t \quad (1)$$

Many recent studies have used situations in which such parameters (V_t, α_t, δ_t, and other more complex ones) fluctuate independently from trial to trial and have simultaneously recorded neural activity electrophysiologically or with brain-imaging

Oxford Centre for Functional MRI of the Brain (FMRIB Centre), John Radcliffe Hospital, Oxford OX3 9DU, UK, and Department of Experimental Psychology, University of Oxford, Oxford OX1 3UD, UK.

*To whom correspondence should be addressed. E-mail: behrens@fmrib.ox.ac.uk (T.E.J.B.); lhunt@fmrib.ox.ac.uk (L.T.H.); matthew.rushworth@psy.ox.ac.uk (M.F.S.R.)

techniques. Trial-to-trial fluctuations in activity in particular cells or brain regions have been found to correlate with different model parameters, demonstrating dissociations and specializations in functional processing [for reviews, see (*10*, *11*)]. Despite addressing particular aspects of computation, these studies work in common or related mathematical frameworks. This mathematical framework therefore also serves as a conceptual framework for understanding the relationships between neural signals observed in different studies (*12*).

This approach is clearly well suited to modeling social interactions where an important aim is to obtain a reinforcer (usually money). In a two-person investment game, an investor is given money that he or she can choose to keep or invest with a trustee, with whom its value will triple. The trustee then decides how much money to return to the investor. Both players must consider their own actions and those of the opponent. Functional magnetic resonance imaging (fMRI) signal in the striatum of the trustee predicts the likelihood of the trustee to reciprocate investment (*13*). In early rounds of the game, this signal appears only after the investor has revealed his or her investment. In later rounds, however, when the trustee has experience of previous investments, the signal shifts to a period before the investment has been made (Fig. 2B). This temporal shift is reminiscent of the shift in dopaminergic prediction error activity from the time of a reward to the time of its predictive conditioned stimulus (*8*). Notably, although the implication of this time shift is that subjects make a neural prediction of opponent play, the striatal signal itself is predictive of the subject's own actions—whether to reciprocate a trusting investment.

Reward and Social Preferences

In social decision-making tasks, most people do not simply consider their own individual best interest. Instead, humans naturally perceive certain actions as rewarding or aversive because of their effect on other individuals. These "other-regarding" preferences can still be formalized within a framework in which people seek to maximize their expected benefit or utility by including terms that describe an aversion to inequality (β) (*14*). For example, if an event has outcome values V_i and V_j for players i and j, an inequality averse player i might only extract utility $U_i = V_i - \beta(V_i - V_j)$ from the event. In other words, it is argued, actors perceive the outcomes of interpersonal interactions from within a frame of reference that is tied to their own personal outcome, but the well-being of others impinges on the utility of this outcome. It is indeed the case that other-regarding preferences elicit neural responses that mirror those to standard rewarding or aversive situations (*14*). For example, acts of altruism thought to be personally rewarding elicit striatal activity, whether in the context of making charitable donations (*15*) or of punishing unfair players (Fig. 2, C and D) (*16*, *17*).

Other-regarding preferences thus serve to modify the value of a subject's own actions to account for his or her effect on other people. Like those of the trustee in the investment game (*13*) and the subjects under peer review (*6*), signals in the altruists' striatums are thus modified by social context, but still ultimately reflect the value of the social situation to the subject. It is unclear, therefore, whether such signals reflect the initial social cognitive events that lead to such a valuation or the consequent impact of social processing on valuation and behavior.

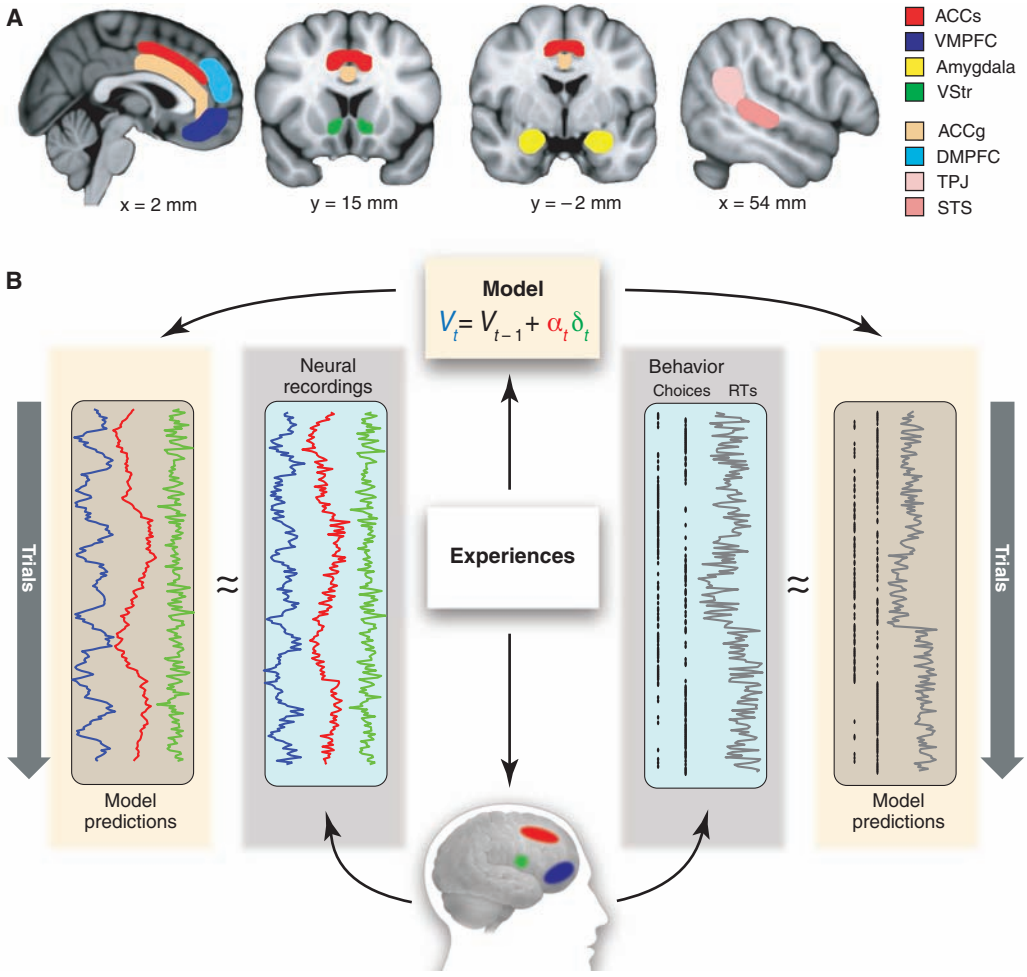

Fig. 1. (**A**) The functional neuroanatomy of social behavior. Primary colors denote brain regions activated by reward and valuation, frequently identified in studies of social interaction within the frame of reference of the subject's own actions: anterior cingulate cortex sulcus (ACCs), ventromedial prefrontal cortex (VMPFC), amygdala, and ventral striatum (VStr). Pastels denote brain regions activated by considering the intentions of another individual: anterior cingulate cortex gyrus (ACCg), dorsomedial prefrontal cortex (DMPFC), temporoparietal junction (TPJ), and superior temporal sulcus (STS). (**B**) Schematic of an approach that combines mathematical models of behavior with neural recordings. The model contains parameters that represent specific computations underlying behavior. As the subject/model undergoes different experiences, these parameters will fluctuate. The fluctuation in these parameters is used to find neural correlates of the specific underlying computations. Separately, the same parameter fluctuations come together to predict changes in behavior.

Functional Specializations for Social Behavior

It has been suggested that some brain regions (Fig. 1A) are involved only in social processing (*18*, *19*). The specificity of such areas' roles has been debated, and it is these areas' functions that have seemed particularly recalcitrant to formal description. A dorsomedial prefrontal region in the vicinity of the paracingulate sulcus is perhaps the most studied of these regions. This region is active during "theory of mind" (ToM) games played against other individuals, but not played against computers (*18*, *19*). Just what contribution the paracingulate region makes to the performance of such games has been harder to ascertain, but some distinct proposals have been made. Some accounts argue that its activation is a consequence of the joint attention that occurs between two individuals in ToM games (*19*). Other accounts ascribe the paracingulate cortex, or frequently co-activated

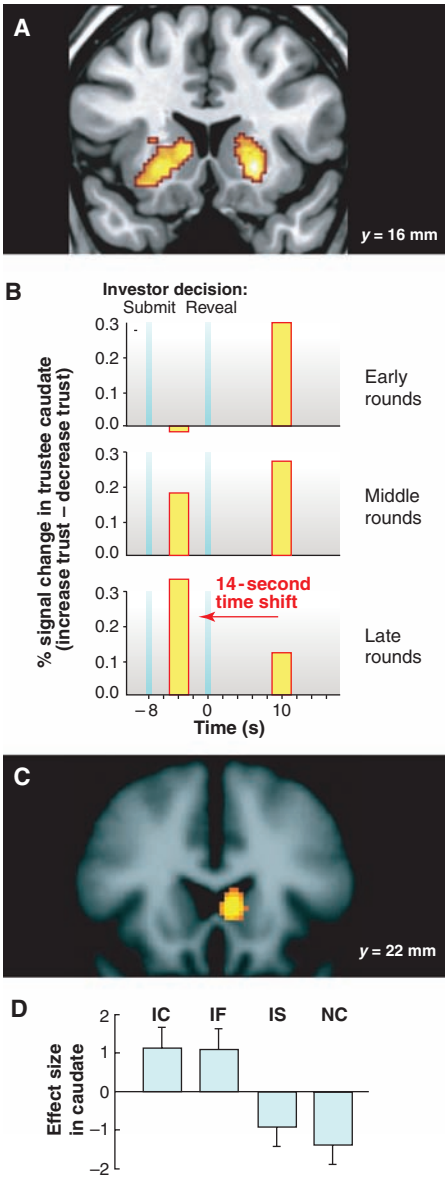

Fig. 2. Reward- and value-related striatal activity during social interactions parallels striatal activity in nonsocial tasks. (**A**) In the same subjects, a region of the caudate nucleus is activated by monetary rewards in a lottery task and is also activated by positive social appraisals. [Reprinted from *Neuron* (*6*) with permission from Elsevier] (**B**) In a reciprocal investment game, activity in the caudate nucleus of the trustee is greater on trials where the trustee's trust increases rather than decreases. In early rounds this signal is seen after the investor decision is revealed, but in later rounds the signal shifts to a time point before revelation, which suggests that the trustee builds a model of the investor's likely actions (*13*). (**C** and **D**) Altruistic punishment of unfair partner behavior in an economic exchange activates the punisher's caudate nucleus (C) in conditions where the punishment costs the partner money [IC and IF in (D)] but not in conditions where the punishment is symbolic (IS) or randomly selected (NC) (*16*).

regions such as the posterior superior temporal sulcus (STS) and temporoparietal junction (TPJ), with roles in metacognition—thinking about the intentions of another person (*18*–*20*). Although it is certainly the case that one's own simple motor intentions do not activate the same regions (*21*, *22*), it has been argued that it is difficult to test with precision the function that is accomplished by these regions, because of the complex set of different mental and neural processes that may be recruited in ToM situations. However, computational approaches (see below) have recently been used to generate quantitative predictions about how activity should change in these brain areas when subjects estimate, and revise their estimations of, another's intentions.

A distinct strand of research has emphasized the importance of parts of the cingulate cortex for social processing. fMRI studies have showed signal increases in two divisions of the cingulate cortex, one in the posterior cingulate cortex adjacent to retrosplenial areas (*19*, *22*) and one in the anterior cingulate cortex gyrus (ACCg) (*23*), when people are engaged in processes that are prerequisite for social cognition, such as the consideration of intentions or emotions. Again, accounts of such activity patterns may be sharpened by computational models that make quantitative predictions about the value of social information to an experimental participant.

Frames of Reference in Social Decision Making

It initially appears difficult to reconcile the emphasis on RL and on brain areas such as the striatum with the quite distinct brain areas revealed by investigations of ToM. It becomes less surprising when one remembers that social preference studies purposively avoid iterative game settings precisely because they want to avoid confounding a social preference for another's payoff with beliefs about another's intentions.

One potential consilience of ToM and reinforcement-based approaches comes from considering the different frames of reference they use in interrogating the data. As discussed above, social preference and game theory tasks often investigate signals in the frame of reference of the subjects' own actions or rewards. In ToM tasks, the analysis identifies areas that are more active when another individual's intentions must be decoded. Evidence for this idea comes from a study that combines an investigation of brain activity in an action observation task and subjective reports of a key social preference: altruism (*24*). Unlike the effects of altruistic behavior on the striatum (*15*), when the frame of reference adopted is not one of value or reward but rather one of intention, it is fMRI activity in a ToM region—the STS—that predicts a subject's altruistic tendencies (*24*).

It is important to recognize the quite distinct frame of reference that is adopted in these different approaches to social decision-making. Very recently, computational accounts have been extended to describe not just how value representations are learned during interpersonal interactions, but also the way in which representations of others' intentions evolve in such settings.

Social Computations

There is evidence that predictions in the frame of reference of an opponent exist at the level of single neurons. In a matching-pennies game, a trial is rewarded if the subject makes the same choice as an opponent. When monkeys played against a computer opponent, neurons were found whose activity was dependent on the monkeys' histories of choices and rewards (*25*, *26*). Intriguingly, however, some neural responses were also dependent on current and previous choices of the computer opponent (*26*), enabling a prediction of the computer's next play. Important questions remain. First, it is unclear whether the monkeys believed they were interacting with an intentional agent, and hence whether activity would occur similarly in social interactions. Second, although it is clear that such neurons are encountered in the dorsolateral prefrontal cortex, little is known about their wider distribution, and recordings have not been made in ToM-related brain areas. Nonetheless, by explicitly decoupling monkey behavior, opponent behavior, and predicted or experienced rewards, this experiment demonstrated separable neuronal activity in all three frames of reference.

Such a decoupling has also been used by two recent human fMRI studies that scanned the whole brain and aimed to dissociate two sorts of neural computations: those associated with predicting the behavior of another individual, and those that determine the effect of these predictions on outcome valuation and hence behavior (*27*, *28*). These studies test whether key concepts that underlie RL may generalize to the domains of social reputation learning (*27*) and mentalizing (*28*). In both studies, subjects were asked to play a game that required them to track and predict the behavior of other individuals (confederates) to optimize their own behavior. Formal computational models, based on principles from RL, were built that tracked this information probabilistically, which allowed for fMRI data to be interrogated for correlates of these models' parameters. In both cases, the use of formal mathematical modeling ensured that key computational variables relating to confederate behavior would fluctuate trial-by-trial, and that these variables would be decoupled from variables relating to reward processing. In both cases, because the mathematical models contained separate parameters relating to expectations of reward and confederate behavior, activity could be assessed separately in each frame of reference. Furthermore, despite considerable differences in the two tasks, the common mathematical framework allows neural signals in the two studies to be compared directly.

Prediction Errors on Confederate Behavior

In one case (*27*), subjects played a game that required them to learn in parallel about the likely

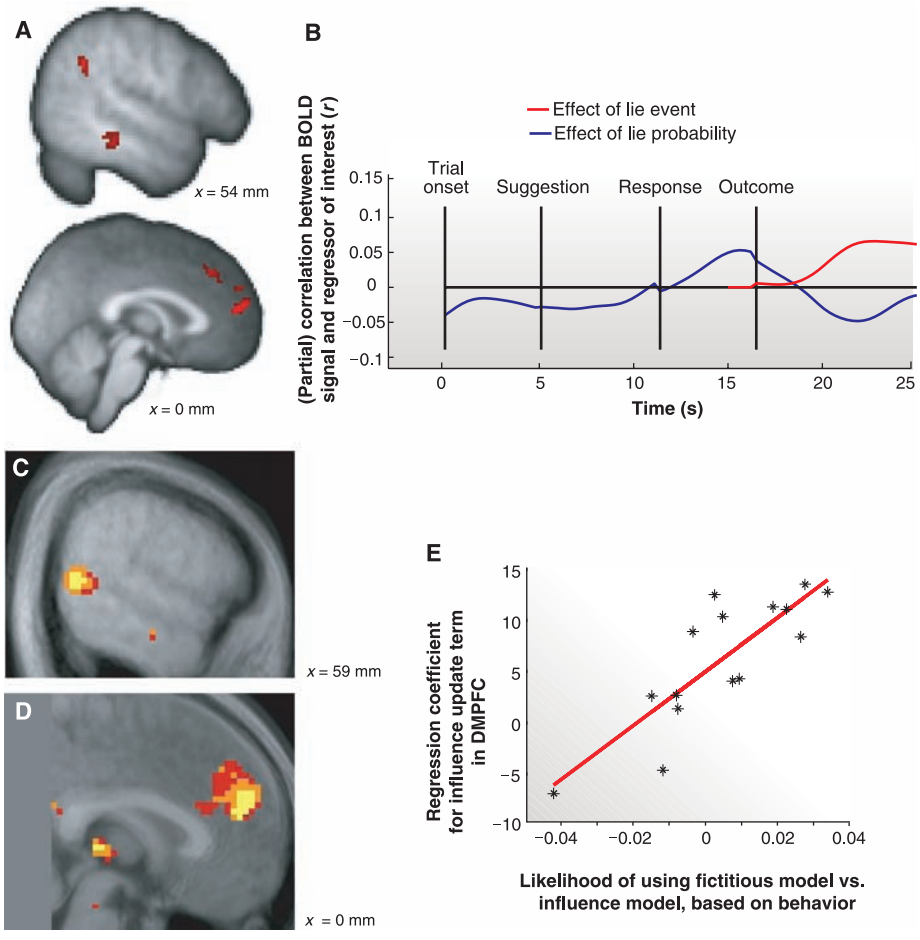

Fig. 3. Prediction errors on the intentions of a social partner's behavior activate theory of mind regions. (**A**) The STS/TPJ, middle temporal gyrus, and DMPFC all correlate with prediction error (Δ_t) on the probability of a confederate lie during a social reputation–building task. (**B**) Time course of activity shows all three components of a prediction error signal: positive correlate of lie probability before revelation of partner behavior ("outcome"), negative correlate of lie probability after, and positive correlate of lie event after. [Adapted by permission from Macmillan Publishers Ltd., *Nature* (*27*), copyright 2008] (**C**) During a "work-or-shirk" game, the STS signals the influence update of the subject's current action on the likely future behavior of the other player. (**D** and **E**) In the DMPFC (D), this signal correlates with the likelihood that the subject was using this "influence" model versus a simpler, "fictitious learning" model (E) (*28*). [Copyright 2008, National Academy of Sciences, U.S.A.]

location of a reward, and about the motives of a confederate advising them on their next choice. After each outcome, subjects were assumed to update the probability of a reward on a choice option (for example, the green rather than the blue card) using RL mechanisms outlined above: $V_{t+1} = V_t + \alpha_t\delta_t$. The same outcome, however, enabled subjects to independently update a running estimate of the probability of unfaithful confederate advice: $L_{t+1} = L_t + \beta_t\Delta_t$, where L_t represents the probability the confederate will lie at the current trial, and Δ_t and β_t represent a prediction error and learning rate on this probability, respectively. Two regions formerly isolated by ToM studies—paracingulate and STS/TPJ—performed a computational role that was directly analogous to dopaminergic activity in the reward domain. Activity first correlated with the probability that the confederate would lie. Subsequently, when the outcome was revealed, activity correlated with the quantitative and signed prediction error on confederate behavior (Fig. 3, A and B). Unlike in the dopaminergic system, the predictions and prediction errors at stake did not concern the scalar value of actions; instead, they concerned the truth of communicative intentions.

In another case (*28*), subjects played a repetitive Inspector game in which workers decide whether to work or shirk at each trial and Inspectors decide whether or not to inspect. Social interactions in such a game are complex. The worker should only work if he or she believes the inspector will inspect. The inspector should only embark on costly inspections if the worker is likely to shirk. In such a task, it is possible for subjects not only to track the intentions of an opponent [as was optimal in (*26*)], but also to try to second-guess the influence of their own actions on opponent behavior. This influence is also amenable to prediction error learning. Here the prediction error represents a deviation in subjects' own behavior (Q) from what they believe the opponent is predicting they will do (q^{**}):

$$\Delta_t = (Q_t - q_t^{**}) \quad (2)$$

fMRI correlates of such a prediction error are observed in the STS (Fig. 3C), not before the subject chooses, but when players witness the other's choice and must update their predictions of future opponent plays. In a paracingulate region, similar activations are witnessed, but predominantly in subjects where a reliance on this influence can be measured in their behavior (Fig. 3, D and E).

Parallel Processing of Reward and Intentional Reference Frames in the Cingulate Cortex

Evidence that key computational parameters, such as prediction errors, can be found in the social domain invites immediate parallels to be drawn between mechanisms underlying social and nonsocial behaviors. Such comparisons may serve to clarify functional dissociations between anatomical regions. For example, several quite distinct strands of evidence suggest an anatomical subdivision within the ACC between social and nonsocial behavior. Social tasks tend to activate the more ventral ACCg (Fig. 1B), whereas reward-guided behavior tends to activate a more dorsal region in the ACCs (Fig. 1A). Such a dissociation may depend on the connection patterns of these regions. In the monkey the ACCs is strongly interconnected with premotor and motor cortex, whereas the ACCg is connected with brain regions concerned with the processing of emotion, facial expression, and biological motion such as the hypothalamus and STS (*29*). Recent studies reveal similar gradients of connectivity across the human cingulate cortex (*23*) (Fig. 4A). Functionally, both the human and macaque ACCs appear to play a role in determining the value of new pieces of information for guiding future behavior (*10*, *30*–*32*). There is evidence suggesting a similar role for the ACCg in the social behavior of both species (*33*, *34*). For instance, healthy male macaques will forego food rewards to view images of certain high-status conspecifics (*35*). Lesions of the ACCg, but not the ACCs, diminish the value assigned to such social information in comparison to food rewards (*33*) (Fig. 4B). Finally, manipulations of human behavior also implicate the ACCg in social cognition. In human subjects, nasal administration of the neuropeptide oxytocin increases the trust that subjects place in confederates in social games (*36*). In early rounds of these games, the ACCg signal is normally greater than in a nonsocial decision-making task; under oxytocin, however, this increased signal disappears (*34*).

This evidence suggests not only that a functional dissociation exists between the ACCg and

ACCs for social and nonsocial behavior, but also that the two regions might play a similar role in the two domains. However, the evidence remains circumstantial, as it was gathered using several different approaches in very different experimental situations. Using formal computational models, however, it was possible to compare directly the computations performed in these two ACC subregions, in the same group of subjects performing the same task (*27*).

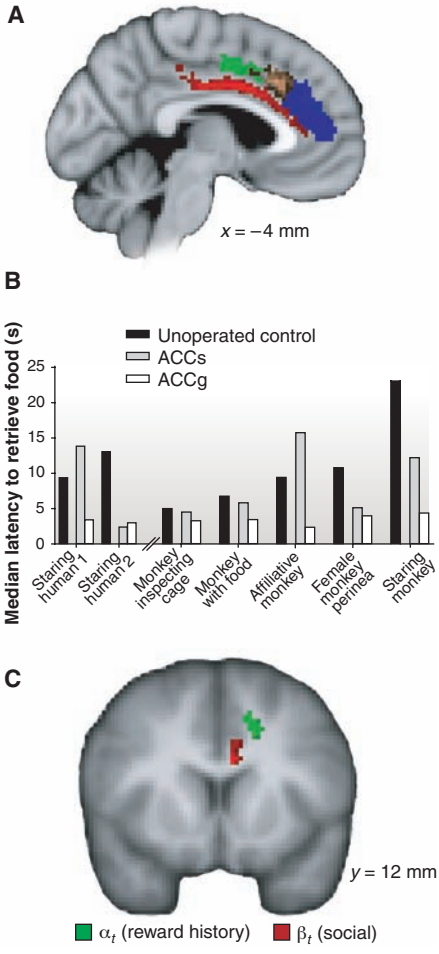

Fig. 4. Converging evidence from anatomy, lesion studies, and computational modeling of fMRI data for a dorsoventral dissociation in ACC. (**A**) Parcellation of cingulate cortex reveals a cluster in ACCg, and three in ACCs, with distinct connectivity patterns to other brain regions (*23*). (**B**) Monkeys are presented simultaneously with food and socially salient stimuli. In control monkeys, the most salient social stimuli (abscissa) induce the longest delays (ordinate) before the food is taken. This effect is abolished in monkeys with lesions to the ACCg but not to the ACCs (*33*). (**C**) Parallel learning rates in a reinforcement learning model for social and reward-based information are signaled in the ACCg and ACCs, respectively; the ACCg signal correlates with degree to which subjects use social information in the task, whereas the ACCs signal correlates with degree to which subjects use reward information. [Adapted by permission from Macmillan Publishers Ltd., *Nature* (*27*), copyright 2008]

During probabilistic learning, the value of a new piece of information can be defined formally. It dictates the instantaneous learning rate (α_t) (Eq. 1) that is used to weigh the current prediction error. In the parallel learning situation used in (*27*), independent fluctuations in the two learning rates for reward-guided (α_t) and social (β_t) learning could be seen in the fMRI data. As previously demonstrated (*30*), the reward-guided learning rate predicted fMRI fluctuations in the ACCs, particularly in individuals who would be more influenced by reward information. However, the ACCg signal reflected the social learning rate, particularly in individuals whose behavior was likely to be guided by confederate advice. The ACCs and ACCg therefore encoded the exact same computational parameter (the instantaneous learning rate) at the exact same time, but in two distinct frames of reference (Fig. 4C).

Notably, computational models of confederate behavior can also make predictions in the more traditional frame of reference—one's own actions. When analyzed in this frame of reference (*27*, *28*), activations closely matched those found in nonsocial studies (*10*, *11*). At the time of feedback, both studies identified a reward prediction error (δ_t in Eq. 1) of the subject's chosen action in the ventral striatum. At the time of action selection, a correlate of the expected value of the subject's chosen action (V_t in Eq. 1) was found by both studies in a ventromedial portion of the prefrontal cortex. Furthermore, despite being analyzed in the frame of reference of reward, in both studies these signals were best explained by models that accounted for the influence of confederate play on the subject's valuations.

Conclusions

There has been an unacknowledged tension between different neural accounts of social behavior. Some have focused on a number of brain regions with a general role in reinforcement processing (*5*). Other accounts have emphasized the importance of a circumscribed circuit concerned with the representations of other's beliefs and intentions (*18*, *19*). It is clear that it is necessary to draw on both traditions. RL-based approaches in conjunction with paradigms drawn from game theory have begun to describe the computations performed by reinforcement-related brain regions, such as the ventral striatum, during the course of social interaction as one person attempts to predict the behavior of another. These models focus on predictions and prediction errors that are tied to the frame of reference of the actor and consider the scalar value that the actor expects from the interaction. Increasingly, however, a similar formalism is being translated to the modeling of beliefs and the joint relationships between one's own actions and intentions and those of another person. Rather than focusing just on scalar value, the emphasis is on predictions about the truth of intentions or the truth of the relationship between an actor and another person. By considering such complex behaviors and signals in a formal fashion (*37*), relationships can be established between signals seen in different experimental situations. It is hoped that these formal relationships will reflect mechanistic properties of neural activity that will generalize across many kinds of social interactions.

References and Notes

1. R. A. Poldrack, *Trends Cognit. Sci.* **10**, 59 (2006).
2. R. I. Dunbar, S. Shultz, *Science* **317**, 1344 (2007).
3. K. E. Holekamp, S. T. Sakai, B. L. Lundrigan, *Philos. Trans. R. Soc. London Ser. B* **362**, 523 (2007).
4. J. B. Silk, *Science* **317**, 1347 (2007).
5. E. T. Rolls, *The Brain and Emotion* (Oxford Univ. Press, Oxford, 1999).
6. K. Izuma, D. N. Saito, N. Sadato, *Neuron* **58**, 284 (2008).
7. G. Corrado, K. Doya, *J. Neurosci.* **27**, 8178 (2007).
8. W. Schultz, P. Dayan, P. R. Montague, *Science* **275**, 1593 (1997).
9. R. A. Rescorla, A. R. Wagner, in *Classical Conditioning II: Current Research and Theory*, A. H. Black, W. F. Prokasy, Eds. (Appleton-Century-Crofts, New York, 1972), pp. 64–99.
10. M. F. Rushworth, T. E. Behrens, *Nat. Neurosci.* **11**, 389 (2008).
11. M. L. Platt, S. A. Huettel, *Nat. Neurosci.* **11**, 398 (2008).
12. N. D. Daw, K. Doya, *Curr. Opin. Neurobiol.* **16**, 199 (2006).
13. B. King-Casas *et al.*, *Science* **308**, 78 (2005).
14. E. Fehr, C. F. Camerer, *Trends Cognit. Sci.* **11**, 419 (2007).
15. J. Moll *et al.*, *Proc. Natl. Acad. Sci. U.S.A.* **103**, 15623 (2006).
16. D. J. de Quervain *et al.*, *Science* **305**, 1254 (2004).
17. T. Singer *et al.*, *Nature* **439**, 466 (2006).
18. D. M. Amodio, C. D. Frith, *Nat. Rev. Neurosci.* **7**, 268 (2006).
19. R. Saxe, *Curr. Opin. Neurobiol.* **16**, 235 (2006).
20. F. Castelli, C. Frith, F. Happe, U. Frith, *Brain* **125**, 1839 (2002).
21. N. Ramnani, R. C. Miall, *Nat. Neurosci.* **7**, 85 (2004).
22. H. E. den Ouden, U. Frith, C. Frith, S. J. Blakemore, *Neuroimage* **28**, 787 (2005).
23. M. Beckmann, H. Johansen-Berg, M. F. Rushworth, *J. Neurosci.* **29**, 1175 (2009).
24. D. Tankersley, C. J. Stowe, S. A. Huettel, *Nat. Neurosci.* **10**, 150 (2007).
25. D. J. Barraclough, M. L. Conroy, D. Lee, *Nat. Neurosci.* **7**, 404 (2004).
26. H. Seo, D. Lee, *Philos. Trans. R. Soc. London Ser. B* **363**, 3845 (2008).
27. T. E. Behrens, L. T. Hunt, M. W. Woolrich, M. F. Rushworth, *Nature* **456**, 245 (2008).
28. A. N. Hampton, P. Bossaerts, J. P. O'Doherty, *Proc. Natl. Acad. Sci. U.S.A.* **105**, 6741 (2008).
29. G. W. Van Hoesen, R. J. Morecraft, B. A. Vogt, in *Neurobiology of Cingulate Cortex and Limbic Thalamus*, B. A. Vogt, M. Gabriel, Eds. (Birkhäuser, Boston, 1993).
30. T. E. Behrens, M. W. Woolrich, M. E. Walton, M. F. Rushworth, *Nat. Neurosci.* **10**, 1214 (2007).
31. M. Matsumoto, K. Matsumoto, H. Abe, K. Tanaka, *Nat. Neurosci.* **10**, 647 (2007).
32. S. W. Kennerley, M. E. Walton, T. E. Behrens, M. J. Buckley, M. F. Rushworth, *Nat. Neurosci.* **9**, 940 (2006).
33. P. H. Rudebeck, M. J. Buckley, M. E. Walton, M. F. Rushworth, *Science* **313**, 1310 (2006).
34. T. Baumgartner, M. Heinrichs, A. Vonlanthen, U. Fischbacher, E. Fehr, *Neuron* **58**, 639 (2008).
35. R. O. Deaner, A. V. Khera, M. L. Platt, *Curr. Biol.* **15**, 543 (2005).
36. M. Kosfeld, M. Heinrichs, P. J. Zak, U. Fischbacher, E. Fehr, *Nature* **435**, 673 (2005).
37. W. Yoshida, R. J. Dolan, K. J. Friston, *PLoS Comput. Biol.* **4**, e1000254 (2008).

38. Supported by the UK Medical Research Council (T.E.J.B., M.F.S.R.) and the Wellcome Trust (L.T.H.).

10.1126/science.1169694

Entropic Evidence for Linguistic Structure in the Indus Script

Rajesh P. N. Rao,[1]* Nisha Yadav,[2,3] Mayank N. Vahia,[2,3] Hrishikesh Joglekar,[4] R. Adhikari,[5] Iravatham Mahadevan[6]

The Indus civilization flourished ~2600 to 1900 before the common era in what is now eastern Pakistan and northwestern India (*1*). No historical information exists about the civilization, but archaeologists have uncovered samples of their writing on stamp seals, sealings, amulets, and small tablets. The script on these objects remains undeciphered, despite a number of attempts and claimed decipherments (*2*). A recent article (*3*) questioned the assumption that the script encoded language, suggesting instead that it might have been a nonlinguistic symbol system akin to the Vinča inscriptions of southeastern Europe and Near Eastern emblem systems. We compared the statistical structure of sequences of signs in the Indus script with those from a representative group of linguistic and nonlinguistic systems.

Two major types of nonlinguistic systems are those that do not exhibit much sequential structure (type 1 systems) and those that follow rigid sequential order (type 2 systems). For example, the sequential order of signs in Vinča inscriptions appears to have been unimportant (*4*). On the other hand, the sequences of deity signs in Near Eastern inscriptions found on boundary stones (*kudurrus*) typically follow a rigid order that is thought to reflect the hierarchical ordering of the deities (*5*).

Linguistic systems tend to fall somewhere between these two extremes: The tokens of a language (such as characters or words) do not follow each other randomly nor are they juxtaposed in a rigid order. There is typically some amount of flexibility in the ordering of tokens to compose words or sentences. One way of quantifying this flexibility is to use conditional entropy (*6*), which measures the amount of randomness in the choice of a token given a preceding token (*7*).

We computed the conditional entropies of five types of known natural linguistic systems (Sumerian logo-syllabic system, Old Tamil alpha-syllabic system, Rig Vedic Sanskrit alpha-syllabic system, English words, and English characters), four types of nonlinguistic systems (two artificial control data sets representing type 1 and type 2 nonlinguistic systems as described above, human DNA sequences, and bacterial protein sequences), and an artificially created linguistic system (the computer programming language Fortran). We compared these conditional entropies with the conditional entropy of Indus inscriptions from a well-known concordance of Indus texts (*8*).

We found that the conditional entropy of Indus inscriptions closely matches those of linguistic systems and remains far from nonlinguistic systems throughout the entire range of token set sizes (Fig. 1A) (*7*). The conditional entropy of Indus inscriptions is substantially below those of the two biological nonlinguistic systems (DNA and protein) and above that of the computer programming language (Fig. 1B). Moreover, this conditional entropy appears to be most similar to those of Sumerian (a logo-syllabic script roughly contemporaneous with the Indus script) and Old Tamil (an alpha-syllabic script) and falls between those for English words and for English characters. These observations are consistent with previous suggestions [e.g., (*9*)], made on the basis of the total number of Indus signs, that the Indus script may be logo-syllabic. The similarity in conditional entropy to Old Tamil, a Dravidian language, is especially interesting in light of the fact that many of the prominent decipherment efforts to date (*9*–*11*) have converged upon a proto-Dravidian hypothesis for the Indus script.

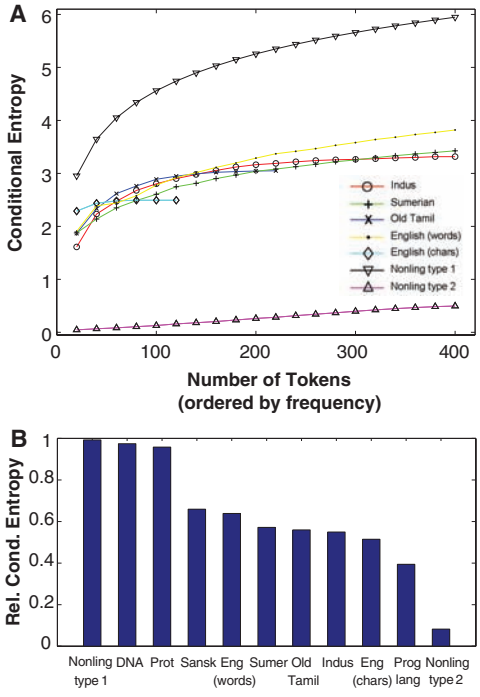

Fig. 1. Conditional entropy of Indus inscriptions compared to linguistic and nonlinguistic systems. (**A**) The conditional entropy (in units of nats) is plotted as a function of the number of tokens (signs, characters, or words) ordered according to their frequency in the texts used in this analysis (*7*). (**B**) Relative conditional entropy (conditional entropy relative to a uniformly random sequence with the same number of tokens) for linguistic and nonlinguistic systems. Prot indicates protein sequences; Sansk, Sanskrit; Eng, English; Sumer, Sumerian; and Prog lang, programming language. Besides the systems in (A), this plot includes two biological nonlinguistic systems (a human DNA sequence and bacterial protein sequences), as well as Rig Vedic Sanskrit and a computer program in the programming language Fortran (*7*).

Given the prior evidence for syntactic structure in the Indus script (*9*, *12*), our results increase the probability that the script represents language, complementing other arguments that have been made explicitly (*13*, *14*) or implicitly (*15*, *16*) in favor of the linguistic hypothesis.

References and Notes

1. A. Lawler, *Science* **320**, 1276 (2008).
2. G. L. Possehl, *Indus Age: The Writing System* (Univ. of Pennsylvania Press, Philadelphia, 1996).
3. S. Farmer, R. Sproat, M. Witzel, *Electron. J. Vedic Stud.* **11**, 19 (2004).
4. S. M. M. Winn, in *The Life of Symbols*, M. L. Foster and L. J. Botscharow, Eds. (Westview, Boulder, CO, 1990) pp. 263–283.
5. J. A. Black, A. Green, *Gods, Demons and Symbols of Ancient Mesopotamia* (British Museum Press, London, 1992).
6. C. E. Shannon, *Bell Syst. Tech. J.* **27**, 379 (1948).
7. Materials and methods are available on *Science* Online.
8. I. Mahadevan, *The Indus Script: Texts, Concordance and Tables* (Archaeological Survey of India, New Delhi, 1977).
9. A. Parpola, *Deciphering the Indus Script* (Cambridge Univ. Press, Cambridge, 1994).
10. I. Mahadevan, *J. Tamil Stud.* **2**, 157 (1970).
11. Y. V. Knorozov, M. F. Albedil, B. Y. Volchok, *Proto-Indica: 1979, Report on the Investigations of the Proto-Indian Texts* (Nauka Publishing House, Moscow, 1981).
12. K. Koskenniemi, *Stud. Orient.* **50**, 125 (1981).
13. A. Parpola, *Trans. Int. Conf. Eastern Stud.* **50**, 28 (2005).
14. A. Parpola, in *Airavati: Felicitation Volume in Honor of Iravatham Mahadevan* (Varalaaru.com, Chennai, India, 2008), pp. 111–131.
15. N. Yadav, M. N. Vahia, I. Mahadevan, H. Joglekar, *Int. J. Dravidian Linguist.* **37**, 39 (2008).
16. N. Yadav, M. N. Vahia, I. Mahadevan, H. Joglekar, *Int. J. Dravidian Linguist.* **37**, 53 (2008).
17. This work was supported by the Packard Foundation, the Sir Jamsetji Tata Trust, and the University of Washington. We thank T. Sejnowski, M. Shapiro, and B. Wells for their comments and suggestions.

Supporting Online Material

www.sciencemag.org/cgi/content/full/1170391/DC1
Materials and Methods
Fig. S1
Table S1
References

30 December 2008; accepted 14 April 2009
Published online 23 April 2009;
10.1126/science.1170391
Include this information when citing this paper.

[1]Department of Computer Science and Engineering, University of Washington, Seattle, WA 98195, USA. [2]Department of Astronomy and Astrophysics, Tata Institute of Fundamental Research, Mumbai 400005, India. [3]Centre for Excellence in Basic Sciences, Mumbai 400098, India. [4]14, Dhus Wadi, Laxminiketan, Thakurdwar, Mumbai 400002, India. [5]The Institute of Mathematical Sciences, Chennai 600113, India. [6]Indus Research Centre, Roja Muthiah Research Library, Chennai 600113, India.

*To whom correspondence should be addressed. E-mail: rao@cs.washington.edu

Magnetic Field Sensing Beyond the Standard Quantum Limit Using 10-Spin NOON States

Jonathan A. Jones,[1] Steven D. Karlen,[2] Joseph Fitzsimons,[2,3] Arzhang Ardavan,[1] Simon C. Benjamin,[2,4] G. Andrew D. Briggs,[2] John J. L. Morton[1,2]*

Quantum entangled states can be very delicate and easily perturbed by their external environment. This sensitivity can be harnessed in measurement technology to create a quantum sensor with a capability of outperforming conventional devices at a fundamental level. We compared the magnetic field sensitivity of a classical (unentangled) system with that of a 10-qubit entangled state, realized by nuclei in a highly symmetric molecule. We observed a 9.4-fold quantum enhancement in the sensitivity to an applied field for the entangled system and show that this spin-based approach can scale favorably as compared with approaches in which qubit loss is prevalent. This result demonstrates a method for practical quantum field sensing technology.

The concept of entanglement, in which coherent quantum states become inextricably correlated (*1*), has evolved from one of the most startling and controversial outcomes of quantum mechanics to become the enabling principle of emerging technologies such as quantum computation (*2*) and quantum sensors (*3*, *4*). The use of entangled particles in measurement permits the transcendence of the standard quantum limit in sensitivity, which scales as $\sqrt{N}$ for N particles, to the Heisenberg limit, which scales as N. This approach has been applied to optical interferometry by using entangled photons (*5*) and by using up to six trapped ions for the measurement of magnetic fields and improvements in atomic clocks (*6*–*8*). Spin-squeezing has been investigated as an alternative mode of entanglement generation and has been proposed for sensitive phase detection (*9*) and demonstrated with four $^{9}Be^{+}$ ions (*10*).

A single spin will precess in the presence of a magnetic field. In the rotating frame used to describe magnetic resonance, this precession occurs at a rate governed by the detuning δ of the magnetic field from resonance (expressed in frequency units), so that the state $|0\rangle + |1\rangle$ evolves as $|0\rangle + e^{i\delta t}|1\rangle$ (for clarity, normalization constants are omitted throughout). This principle forms the basis of several kinds of magnetic field sensor, in which the externally applied field δ is detected as a phase shift. States possessing many-qubit entanglement can acquire phase at a greater rate and thus offer an enhanced sensitivity to the applied field.

The requirements for constructing the resource of a large number of entangled spins are less severe than those for a complete nuclear magnetic resonance (NMR) quantum computer (*11*–*13*). Indeed, rather than striving toward individual addressability of each constituent nuclear spin, global addressing is advantageous in quickly and efficiently growing the state. For example, we considered a star topology with one central spin, A, and N peripheral B spins, which cannot be separately addressed (Fig. 1A).

The B spins cannot be distinguished by means of any NMR observable, and their behavior is well-described by number states, such as those used to describe photon occupation in one of two modes. Many-body entanglement in such states has been referred to as the NOON state (*14*–*16*), and has received much attention for its ability to offer quantum-enhanced sensitivity in optical interferometry. We define the spin-NOON state as $|\psi_{NOON}\rangle = |N_{\downarrow}, 0_{\uparrow}\rangle + |0_{\downarrow}, N_{\uparrow}\rangle$, a superposition of the N spins being all down and all up [this has also been described as a "Schrödinger cat" state, being the superposition of the two most distinct states (*17*)]. Such a spin-NOON state will acquire phase $e^{iN\delta t}$, thus showing an N-fold increase in the phase accrued for a given δ and hence a greater sensitivity to the applied field.

Through single spin-flips, the spin-NOON state may be transformed to "many, some + some, many," or MSSM states. For example, the state $|01000\rangle + |10111\rangle$ is one of the five possible $|\psi_{4114}\rangle$ states. It is convenient to classify these states by the difference in the Hamming weight of the two elements of the superposition, or its lopsidedness l (that is, $|\psi_{pqqp}\rangle$ has $l = |p - q|$). In the general case, spins A and B have different sensitivities to the applied field, and so the enhancement in magnetic field sensitivity of the

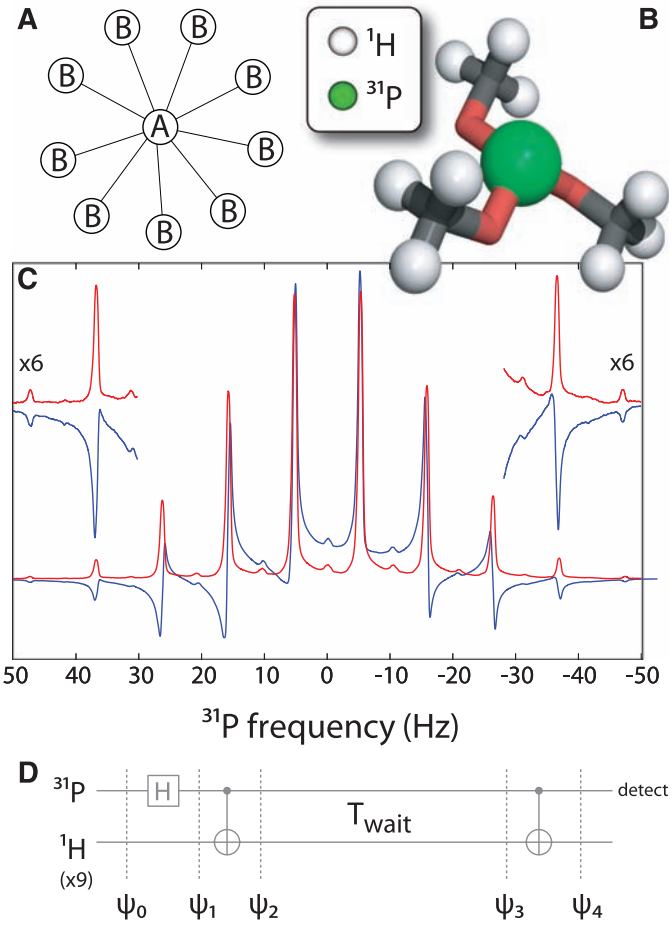

Fig. 1. Ten-spin NOON states are created by using nuclear spins in the TMP molecule. (**A**) Topology of the spin qubits used to generate the spin-NOON state. (**B**) The TMP molecule consists of a central ^{31}P nuclear spin surrounded by nine identical ^{1}H spins. (**C**) The initial ^{31}P NMR spectrum of TMP (red). Nuclear spin-NOON and MSSM states are generated and allowed to evolve for some short time under the influence of an off-resonance magnetic field. After mapping these entangled states back to the ^{31}P, the resulting spectrum (blue) shows how the phase shift acquired increases with the lopsidedness of the state. Low-intensity peaks between pairs of NMR lines arise from coupling to impurities. (**D**) Spin-NOON states are generated by first applying a Hadamard gate to the ^{31}P followed by a C-NOT on the nine equivalent ^{1}H.

[1]Centre for Advanced Electron Spin Resonance (CAESR), Clarendon Laboratory, Oxford University, Oxford OX1 3PU, UK. [2]Department of Materials, Oxford University, Oxford OX1 3PH, UK. [3]Institute of Quantum Computing, University of Waterloo, Waterloo, ON, N2L 3G1, Canada. [4]Centre for Quantum Technologies, National University of Singapore, 3 Science Drive 2, 117543 Singapore.

*To whom correspondence should be addressed. E-mail: john.morton@materials.ox.ac.uk

total system depends on a weighted form of l, which we call l_γ, which includes the relative gyromagnetic ratios of the A and B spins. Analogous ideas have been explored in the context of optical Fock states (*18*).

A molecule with a suitable star topology is trimethyl phosphite (TMP) (Fig. 1B), comprising one central ^{31}P spin and nine identical surrounding ^{1}H spins (the intervening O and C nuclei are mostly spin-zero and may be neglected). The NMR spectrum of ^{31}P is shown in Fig. 1C (red curve) (*19*). Coupling to the local ^{1}H spins shifts the resonance frequency of the ^{31}P by some amount depending on the total magnetization of the ^{1}H. Within the pseudo-pure state model (*11*–*13*), the lines in the ^{31}P NMR spectrum can thus be assigned to the following ^{1}H states: $|9, 0\rangle$, $\rho_{8,1}$, $\rho_{7,2}$, ..., $\rho_{1,8}$, $|0, 9\rangle$. Any experimentally accessible "many, some" (MS) state is an equal mixture of the relevant pure states $|M, S\rangle_i$, where i runs over the indistinguishable permutations of $|M, S\rangle$. We describe MS states in terms of the density matrix $\rho_{M,S} = \sum_i |M,S\rangle_i \langle M,S|_i$.

Given the gyromagnetic ratios of ^{1}H and ^{31}P (42.577 and 17.251 MHz/T, respectively), one would predict a ~23-fold enhancement in phase sensitivity of the 10-spin NOON state over a single ^{31}P nucleus, or a factor of ~9.4 enhancement over the single ^{1}H nucleus, which is most commonly used in present sensors.

We now describe the steps required to generate the spin-NOON state and then map the accumulated phase back onto the A spin (Fig. 1D). The A spin (^{31}P) in the star topology is distinguishable, and its state is therefore given separately in the spin basis. All the spins start in a ground state: $\Psi_0 = |0\rangle_A |000 \ldots 0\rangle_B = |0\rangle |N, 0\rangle$. A Hadamard gate is applied to A, followed by a controlled NOT (C-NOT) gate applied to the B spins, controlled by the state of A, yielding $\Psi_2 = |0\rangle |N, 0\rangle + |1\rangle |0, N\rangle$: an $(N+1)$–spin NOON state with the relevant lopsidedness $l_\gamma = (N\gamma_B + \gamma_A)/\gamma_B$. After some period T_{wait}, $\Psi_3 = |0\rangle |N, 0\rangle + e^{(il_\gamma \delta T_{wait})} |1\rangle |0, N\rangle$. A second identical C-NOT is applied to the B spin in order to map the total phase acquired onto A: $\Psi_4 = (|0\rangle + e^{(il_\gamma \delta T_{wait})} |1\rangle) |N, 0\rangle$, which is directly detected. A similar C-NOT method has been used to create a (1 + 3)–spin entangled state for the purposes of enhanced spin detection (*20*).

Rather than relying on pseudo–pure-state preparation, we can select to observe the evolution of one of the 10 NMR lines and thus effectively post-select the signature of a particular initial state, which is analogous to the way in which post-selection has been employed in linear optics experiments on NOON states (*5*). By applying the entangling operation described above and observing the line corresponding to the original B (^{1}H) state $|9, 0\rangle$, we can identify the 10-spin NOON state $|0\rangle |9, 0\rangle + |1\rangle |0, 9\rangle$ and discern its behavior in the presence of a magnetic field detuning δ.

Figure 1C (blue curve) shows a measurement of ^{31}P obtained after the pulse sequence described above and shown in Fig. 1D. The free evolution time T_{wait} was set to 400 μs so that given the magnetic field detuning (~3.13 μT), a phase shift of ~0.107π would be experienced by a single ^{1}H spin. Observing the left-most line (~48 Hz) is equivalent to post-selecting the $|0\rangle |9, 0\rangle$ initial state and thus the 10-spin NOON state with $l_\gamma = 9.4$, which has instead acquired a ~π phase shift during the free-evolution period.

An advantage of the mixed initial state of the ^{1}H nuclei is that it allows us to simultaneously probe the evolution of all MSSM states for this spin system ($l_\gamma = |9.4 - 2m|$, where $1 \le m \le 9$). For example, the line at ~37 Hz corresponds to the $\rho_{8,1}$ initial state of the B spins, which under the operations applied will yield the MSSM state ρ_{8118} with $l_\gamma = 7.4$, where we define

$$\rho_{MSSM} = \sum_i (|0\rangle|M, S\rangle_i + |1\rangle|S, M\rangle_i) \otimes (\langle 0|\langle M, S|_i + \langle 1|\langle S, M|_i) \quad (1)$$

Each element of the ρ_{8118} mixture acquires phase at the same rate, and a phase shift of ~0.79π was observed (*21*). The phase acquired is less than for the ($l_\gamma = 9.4$) state, but the signal-to-noise is greater. Where spin polarization is weak, one of the intermediate MSSM states with $l < (N+1)$ can yield the optimum sensitivity to magnetic field offset. Moreover, an analysis of the differential phase acquired by successive lines (obtained from a single experiment) can provide more than the single bit of information yielded by one NOON state resource (*22*).

To explore the evolution of the many-body entangled states in more detail, we varied the evolution time T_{wait}. As T_{wait} increases, the signal from each line undergoes oscillations whose frequency varies with l_γ. The Fourier transform with respect to T_{wait} was measured for the 10 different lines in the ^{31}P NMR spectrum (Fig. 2). The frequency, which corresponds to a sensitivity to the magnetic field detuning, increases as one moves to the outer lines of the spectrum, corresponding to MSSM states with larger l, to a maximum for the spin-NOON states at the ends. The linewidth similarly increases slightly because of an enhanced decoherence of the states with larger l; however, this increase is sublinear (*23*), and so when the precession frequency is used to extract an estimate of magnetic field detuning, the uncertainty falls as states with larger l are used (Fig. 2B).

Our $|\psi_{NOON}\rangle$ is a simple Schrödinger cat state of size $N = 10$ particles. A state of the form ρ_{MSSM} is more complex, but we may say that it is

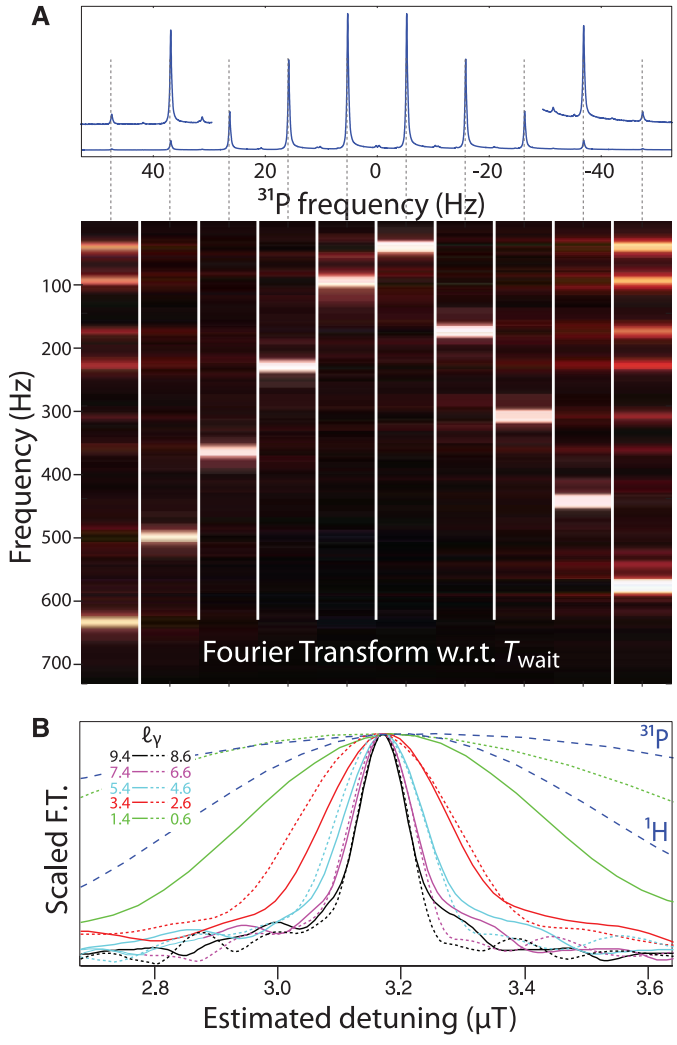

Fig. 2. Nuclear spin-NOON states demonstrate an entanglement-enhanced sensitivity to an external magnetic field. (**A**) The Fourier transform of the evolution of each of the 10 NMR lines with respect to T_{wait} (Fig. 1D) shows an increasing frequency proportional to the increasing lopsidedness l_γ of the entangled state produced. The intensity has been normalized by using the intensities of the initial spectrum; the residual asymmetry in intensities is an artifact of static field inhomogeneity. The ^{31}P NMR spectrum of the TMP molecule is shown above for reference. (**B**) The Fourier transform peak allows an estimate of the effective magnetic detuning from resonance of the ^{1}H spins, which improves with the use of higher-l states. Solid and dashed lines represent NMR lines to the left and right of center, respectively. Experimental traces that use the unentangled ^{31}P or ^{1}H spins are shown for comparison. All peaks are scaled to unit intensity.

equivalent to a canonical Schrödinger cat state that decoheres at the same rate (*24*, *25*). Then, despite being a mixture, ρ_{MSSM} is nevertheless classified as a Schrödinger cat state of full-sized N within the local decoherence model of (*24*) (because neither the bit flips nor the mixing inherent in ρ_{MSSM} alter the rate at which locally independent phases accumulate). If instead we have global decoherence sources, then the effective Schrödinger cat size will correspond to the lopsidedness $|M - S|$ for precisely the reasons of field sensitivity described above.

It is worth contrasting the practical utility of the NOON state approach in two scenarios: in which qubit loss is dominant (such as in optical implementations), and in which phase decoherence is dominant (such as in NMR). Losing even a single photon from a NOON state prevents the phase build up from being measured. Other useful photonic states may have greater inherent robustness (*18*), but such states have yet to be realized experimentally. As the number of photons in the NOON state is increased, the probability of obtaining a successful measurement decreases exponentially. The sensitivity of the NOON state scales only linearly with its size, so the decreasing probability of success rapidly removes any advantage gained through the use of entanglement. For a fixed probability of photon loss ε, this imposes a fundamental limit, corresponding to the minimum of the dashed curves in Fig. 3. The optimum size of an optical NOON state scales as $-\log(1-\varepsilon)^{-1}$, beyond which the use of larger entangled states is detrimental to sensitivity. This practical limitation has motivated the development of alternative methods for optical phase sensing in which neither NOON states, nor indeed entangled states of any kind, are employed (*22*).

Molecular spin-NOON states do not suffer loss in the same manner as optical systems, and the dominant source of error becomes dephasing noise caused by unaccounted-for fields experienced by individual spins. The effect of such noise versus increasing system size can be characterized by using an appropriate measurement strategy. In a noise-free system, the rate at which phase ϕ is acquired by the spin-NOON state would correspond directly to the field strength to be detected. We wish to minimize the variance in this quantity (*16*) so that

$$\Delta^2\left(\frac{\partial\phi}{\partial t}\right) = \frac{\Delta^2\phi}{t^2} = \frac{1}{N^2t^2} \qquad (2)$$

Given a fixed time T_{tot} to perform the sensor operation, one could make M separate measurements each of exposure time $T_E = T_{tot}/M - T_G$, where T_G is the gating and measurement time. This strategy will minimize the effects of finite local noise, provided that $T_G \ll T_E$. The variance on the mean of M individual measurements is

$$\Delta^2\delta = \frac{1}{M}\left(\frac{1}{N^2T_E^2} + \frac{1}{N^2}\sum_{i=1}^{N}\Delta^2h_i\right) \approx \frac{1}{T_{tot}}\left(\frac{1}{N^2T_E} + \frac{T_E}{N}\Delta^2h\right) \qquad (3)$$

where h_i is the phase contribution to spin i from local fields. For any nonzero Δ^2h, minimizing this quantity will yield $T_E \propto N^{-1/2}$, resulting in $\Delta^2\phi \propto N^{-3/2}$. The sensitivity of the system thus limits to $N^{3/4}$. Provided that the measurements can be made on a short time scale as compared with the decoherence time of the spin-NOON state ($\propto N^{-1/2}$), creating larger entangled states will produce greater sensitivity.

In addition to demonstrating how an enhanced sensitivity to magnetic fields can be achieved by using entanglement in nuclear spins, this work represents progress toward the realization of "spin amplification" schemes, which use a bath of B spins to measure the state of A for the purposes of single-spin detection (*20*). Analogous to the way in which photon loss poses a limitation to the extent of the resource (photon number), which can be called up for entanglement-enhanced measurement, a weak thermal polarization restricts the effectiveness of this demonstration for practical magnetometry. Fortunately, the approach described here is readily applicable to electron spins, which can offer a high degree of polarization at experimentally accessible magnetic fields and temperatures. Furthermore, dynamic nuclear polarization, which is already employed in several methods for magnetic field sensing by using nuclear spins (*26*) or algorithmic cooling (*27*, *28*), could be applied here to yield improvements over currently achievable sensitivity.

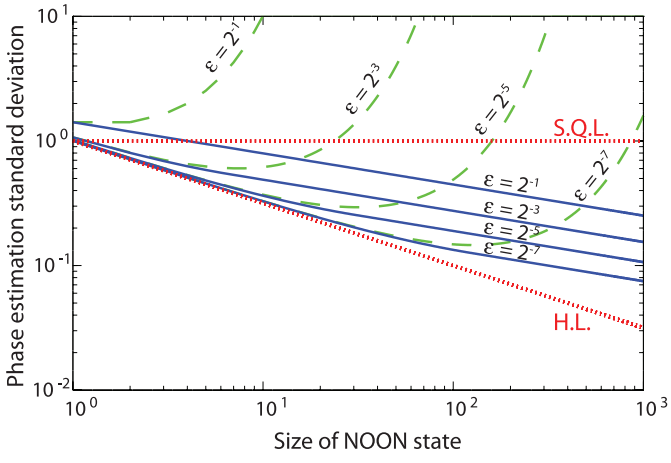

Fig. 3. Spin-NOON states exhibit an enhanced robustness to noise as compared with optical NOON states. Shown is a comparison of the effect of noise on the SD of phase estimates for spin-NOON (blue solid curves) and optical NOON states (green dashed curves) for a range of error probabilities. For photonic systems, the dominant source of error is taken to be photon loss, which is assumed to occur with probability ε. For spin-NOON states, the dominant source of error is taken to be a set of random normally distributed magnetic fields that lead to the complete dephasing of disentangled spins with probability ε over the time scale of the measurement. The upper and lower dotted lines indicate the standard quantum limit and the Heisenberg limit, respectively. The contribution is plotted per spin/photon, rather than per NOON state, in order to allow a direct comparison of states of varying size.

References and Notes

1. E. Schrödinger, *Proc. Camb. Philos. Soc.* **31**, 555 (1935).
2. D. Deutsch, *Philos. Trans. R. Soc. London Ser. A* **400**, 97 (1985).
3. B. Yurke, *Phys. Rev. Lett.* **56**, 1515 (1986).
4. V. Giovannetti, S. Lloyd, L. Maccone, *Science* **306**, 1330 (2004).
5. T. Nagata, R. Okamoto, J. L. O'Brien, K. Sasaki, S. Takeuchi, *Science* **316**, 726 (2007).
6. V. Meyer *et al.*, *Phys. Rev. Lett.* **86**, 5870 (2001).
7. C. F. Roos, M. Chwalla, K. Kim, M. Riebe, R. Blatt, *Nature* **443**, 316 (2006).
8. D. Leibfried, M. Barrett, T. Schaetz, J. Britton, *Science* **304**, 1476 (2004).
9. D. Wineland, J. Bollinger, W. Itano, D. Heinzen, *Phys. Rev. A* **50**, 67 (1994).
10. C. Sackett *et al.*, *Nature* **404**, 256 (2000).
11. D. G. Cory, M. D. Price, T. F. Havel, *Physica D* **120**, 82 (1998).
12. N. A. Gershenfeld, I. L. Chuang, *Science* **275**, 350 (1997).
13. J. A. Jones, *Prog. Nucl. Magn. Reson. Spectrosc.* **38**, 325 (2001).
14. B. C. Sanders, *Phys. Rev. A* **40**, 2417 (1989).
15. A. N. Boto *et al.*, *Phys. Rev. Lett.* **85**, 2733 (2000).
16. H. Lee, P. Kok, J. Dowling, *J. Mod. Opt.* **49**, 2325 (2002).
17. E. Knill, R. Laflamme, R. Martinez, C. H. Tseng, *Nature* **404**, 368 (2000).
18. S. D. Huver, C. F. Wildfeuer, J. P. Dowling, *Phys. Rev. A* **78**, 063828 (2008).
19. Materials and methods are available as supporting material on *Science* Online.
20. P. Cappellaro *et al.*, *Phys. Rev. Lett.* **94**, 020502 (2005).
21. All states of the form ρ_{MSSM} (defined in Eq. 1) contain one full ebit of entanglement as described in more detail in (*19*).
22. B. L. Higgins, D. W. Berry, S. D. Bartlett, H. M. Wiseman, G. J. Pryde, *Nature* **450**, 393 (2007).
23. H. G. Krojanski, D. Suter, *Phys. Rev. Lett.* **93**, 090501 (2004).
24. W. Dür, C. Simon, J. I. Cirac, *Phys. Rev. Lett.* **89**, 210402 (2002).
25. The second approach of (*24*), based on distillation, does not immediately generalize from their pure states to our mixed states: Under the constraint of single-qubit operations one cannot "produce—with unit probability—n-party [Greenberger-Horne-Zeilinger] states" for $n > 1$.
26. N. Kernevez, H. Glénat, *IEEE Trans. Magn.* **27**, 5402 (1991).
27. J. Baugh, O. Moussa, C. A. Ryan, A. Nayak, R. Laflamme, *Nature* **438**, 470 (2005).
28. C. A. Ryan, O. Moussa, J. Baugh, R. Laflamme, *Phys. Rev. Lett.* **100**, 140501 (2008).

29. We thank P. Kok for helpful discussions. This research is supported by the Engineering and Physical Sciences Research Council through the Quantum Information Processing Interdisciplinary Research Collaboration (www.qipirc.org) (GR/S82176/01) and CAESR (EP/D048559/1). J.F. is supported by Merton College, Oxford. G.A.D.B. is supported by the EPSRC (GR/S15808/01). J.J.L.M. acknowledges St. John's College, Oxford. J.J.L.M., S.C.B., and A.A. acknowledge support from the Royal Society.

Supporting Online Material

www.sciencemag.org/cgi/content/full/1170730/DC1
Materials and Methods
SOM Text
References

9 January 2009; accepted 25 March 2009
Published online 23 April 2009;
10.1126/science.1170730
Include this information when citing this paper.

Two-Quantum 2D FT Electronic Spectroscopy of Biexcitons in GaAs Quantum Wells

Katherine W. Stone,[1] Kenan Gundogdu,[1] Daniel B. Turner,[1] Xiaoqin Li,[2] Steven T. Cundiff,[3] Keith A. Nelson[1]*

The motions of electrons in solids may be highly correlated by strong, long-range Coulomb interactions. Correlated electron-hole pairs (excitons) are accessed spectroscopically through their allowed single-quantum transitions, but higher-order correlations that may strongly influence electronic and optical properties have been far more elusive to study. Here we report direct observation of bound exciton pairs (biexcitons) that provide incisive signatures of four-body correlations among electrons and holes in gallium arsenide (GaAs) quantum wells. Four distinct, mutually coherent, ultrashort optical pulses were used to create coherent exciton states, transform these successively into coherent biexciton states and then new radiative exciton states, and finally to read out the radiated signals, yielding biexciton binding energies through a technique closely analogous to multiple-quantum two-dimensional Fourier transform (2D FT) nuclear magnetic resonance spectroscopy. A measured variation of the biexciton dephasing rate indicated still higher-order correlations.

Electron correlations play a predominant role in nearly all forms of matter, influencing the distinctive macroscopic properties of superconductors and giant magnetoresistance materials, the collective modes of high-density plasmas, and the orbital structure and energetics of atoms and molecules. Many-body electron correlations strongly influence the electronic and optical properties of confined systems such as semiconductor quantum wells (QWs) and quantum dots at excited-state densities (~10^{10} excitations/cm^2 in QWs or >1 excitation in single quantum dots) that are reached routinely in applications and experimental studies. Even under conditions of mild irradiation by sunlight, multiple-electron correlations may play important roles in natural photosynthetic antenna complexes, which appear to have evolved rapid relaxation pathways to avert damage under highly energized conditions (*1*), and in semiconductor quantum dots, in which there is hope of extracting extra energy from above-bandgap light absorption through multiple-exciton states (*2*).

Semiconductor QWs are ideally suited for the study of many-electron correlations because of their reduced dimensionality and the fact that the interacting carriers can be generated optically at precisely specified times and densities. Femtosecond laser spectroscopy has been used extensively to study strongly correlated, bound electron-hole pairs (quasiparticles called excitons) in QWs by directly observing exciton coherences induced by ultrashort optical fields and by measuring the dynamics of coherence loss (dephasing) and exciton population lifetimes (*3*). Higher-order correlations were revealed indirectly through measured changes in exciton properties as a function of excitation density, described phenomenologically as local-field effects (*4*, *5*), excitation-induced dephasing (*6*), and excitation-induced energy shifts (*7*). Demanding first-principles calculations that include the full complement of electron-electron interactions and correlations were also performed to understand these correlations (*8*).

The clearest experimental signature of higher-order correlations would be direct observation of the coherences and dynamics of biexcitons [four-particle (or two-quasiparticle) correlations] and higher-order correlated motions. The biexciton is a distinct bound state whose wavefunction is the symmetric combination of the two constituent exciton wavefunctions. The coherent behavior of biexcitons is particularly interesting because they play a key role in coherent control schemes (*9*), quantum information processing (*10*), the manipulation of exciton spin coherences (*11*), and electromagnetically induced transparency in semiconductors (*12*). Biexciton–ground-state coherences generally do not radiate because the corresponding two-quantum transitions are formally forbidden. The exciton-biexciton absorption band that appears at high exciton density can reveal biexciton energetics and some dephasing information (though not that of the biexciton–ground-state two-quantum coherence) if it can be isolated spectrally; that is, if the biexciton binding energy is larger than the low-temperature exciton linewidth (~1 meV). Otherwise, as in the gallium arsenide (GaAs) prototype system, it appears as no more than a shoulder on the much stronger ground-state–exciton absorption band. Measurements in the time domain (*13*, *14*) are just as convolved as in the frequency domain, because coherent signals from both the exciton and biexciton decay because of dephasing within a few picoseconds.

High-order nuclear spin coherences have been isolated through multiple-quantum two-dimensional Fourier transform nuclear magnetic resonance (2D FT NMR) spectroscopy (*15*). As shown in fig. S3 and the supporting online material (SOM) text, dipolar interactions between nearby spins (coherently precessing at frequency ω_s) lead to modulations of the local magnetic field at twice the precession frequency and to corresponding two-quantum signals that appear at frequency $2\omega_s$ along one of the dimensions of multiple-pulse 2D FT NMR spectra. Signals at such frequencies arise only from interacting spins and are isolated spectrally from one-quantum signals at ω_s (*16*). Two-quantum NMR spectra have been used to elucidate the structures of large molecules whose 1D spectra were too crowded with overlapping peaks to allow unambiguous interpretation. Multiple-quantum NMR techniques also permit examination of correlations between spins on different molecules in a liquid mixture, providing information about liquid-state structure and dynamics (*17*, *18*).

In contrast to the NMR case, in which well-understood multiple-quantum spin coherences are exploited to simplify complicated spectra, multiple-quantum optical coherences are of strong interest in their own right because they provide access to spectroscopically "dark" states whose characterization may reveal much about poorly understood high-order correlations in condensed matter systems (*19*). Some of the origins of many-body correlations in semiconductors and the multiple-quantum signals that arise from them in coherent nonlinear spectroscopy measurements are illustrated in fig. S3 and discussed in the SOM text. Two successive optical fields, labeled $\mathbf{E_A}$ and $\mathbf{E_B}$ in Fig. 1, induce coherent responses at the exciton frequency ω_e; and as in the case of spins, interactions between excitons lead to coherences at twice the exciton frequency, $2\omega_e$. These interaction-induced coherences, due to local-field effects and excitation-induced dephasing and energy shifts as mentioned above, can be explained by a two-level model of exciton dynamics in which interactions have been added phenomenologically (SOM text). Unlike pairs of coupled nuclear spins, the two-quantum exciton coherences involve four particles that can adopt new time-averaged locations, forming a biexciton state whose energy $E_b = \hbar\omega_b = 2\,\varepsilon_e - \varepsilon_B$ is minimized at a value lower than twice the exciton energy by a binding energy ε_B. This is reflected directly in the biexciton coherence oscillation frequency $\omega_b = 2\omega_e - \varepsilon_B/\hbar$. The two-quantum interaction-induced and biexciton coherences launched by the first two fields do not radiate, but a third field, $\mathbf{E_C}$, can induce a radiative one-quantum coherence whose amplitude and phase depend on the phase of the third field relative to the phase of the two-quantum coherence that it encounters. The equivalent of rotating frame

[1]Department of Chemistry, Massachusetts Institute of Technology, Cambridge, MA 02139-4307, USA. [2]Department of Physics, University of Texas at Austin, Austin, TX 78712-0264, USA. [3]JILA, University of Colorado, Boulder, and National Institute of Standards and Technology, Boulder, CO 80309-0440, USA.

*To whom correspondence should be addressed. E-mail: kanelson@mit.edu

detection in NMR (SOM text) can be executed if the phase of a selected carrier frequency component, ω_0, contained within the spectral bandwidth of the pulses and distinct from the exciton frequency ω_e, can be held equal in all the fields while varying the relative pulse delays. In that case, the phase evolution of the complex signal field $\mathbf{E_S}(\omega)$, measured as a function of the time delay τ_2 between the first two pulses and the third, will be slowed to the difference frequency $\omega_e - \omega_0$.

At optical frequencies, the emitted signal field $\mathbf{E_S}$ can be determined through its interferometric superposition with a reference field, $\mathbf{E_R}$. A convenient strategy (*20*) is to send the superposed fields into a spectrometer (spectral interferometry) to directly determine the signal field amplitude and phase as a function of emission frequency, ω. This circumvents the need to scan the reference field time delay to determine the $\mathbf{E_S}(\omega)$. After Fourier transformation with respect to τ_2, the results will show distinct two-quantum features that appear along the ω_2 axis at frequencies $2\omega_e$ and ω_b and along the ω axis at the one-quantum emission frequency ω_e.

This scenario shows how two-quantum signals could be observed through an optical analog to two-quantum 2D FT NMR; that is, two-quantum 2D FT optical spectroscopy (2D FT OPT). However, this analog faces many experimental challenges not found in magnetic resonance. In NMR, the radiofrequency (rf) wavelengths exceed the sample dimensions, and the sample is surrounded by the coils that deliver the fields and measure the responses. Therefore, the rf field frequencies and polarizations are important, but their propagation directions are not. In contrast, in optical measurements the sample is large compared to the wavelength, and the fields are delivered to the sample and radiated from it in the form of coherent light beams with well-defined propagation directions (wavevectors). This difference presents both opportunities and challenges.

The key opportunities lie in the use of the noncollinear BOXCARS four-wave mixing (FWM) beam geometry, shown in Fig. 1, and the specification of the pulse time-ordering to isolate the emitted signal field as a coherent beam in a well-defined direction with wavevector $\mathbf{k_S}$ =

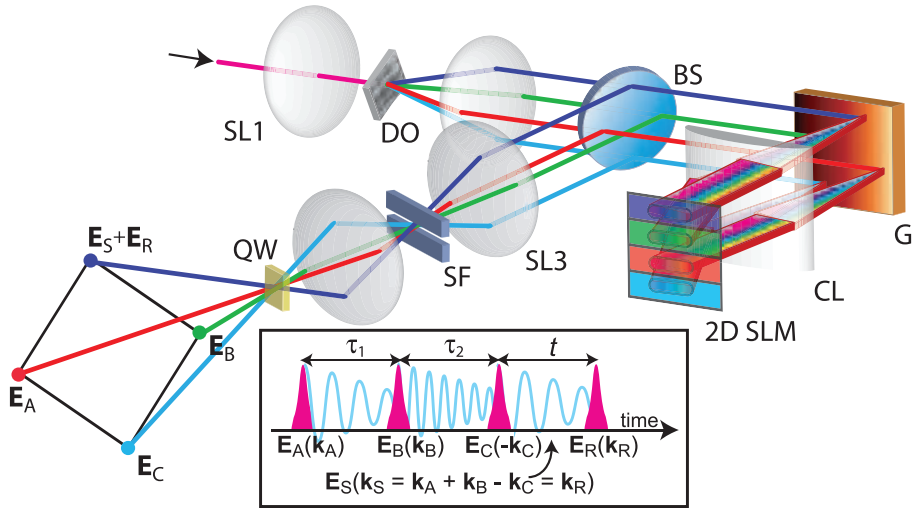

Fig. 1. Fully coherent electronic 2D FT OPT using a spatiotemporal pulse shaper. The laser output is focused by a spherical lens (SL1) into a diffractive optic (DO) whose square-lattice grating pattern produces four first-order diffracted beams that pass through a beam splitter (BS) and into the pulse shaper consisting of a grating (G), cylindrical lens (CL), and 2D liquid crystal SLM. The frequency components of the four beams are dispersed horizontally across four distinct regions of the SLM, where their amplitudes and phases are controlled through diffraction as described in the SOM text and fig. S1 (*33*). The frequency components are recombined at the grating, yielding the four fully phase-coherent, temporally shaped fields $\mathbf{E_A}$, $\mathbf{E_B}$, $\mathbf{E_C}$, and $\mathbf{E_R}$. The fields are reflected by the beam splitter and focused (SL3) through a spatial filter (SF) and then into the QW sample, which consists of 10 layers of 10-nm-thick GaAs separated by 10-nm-thick barriers of $Al_{0.3}Ga_{0.7}As$, and is held at a temperature of 10 K. The signal emerges from the sample in the wavevector-matching direction, collinear with $\mathbf{E_R}$, and the superposed fields are directed into a spectrometer (not shown). The figure shows every optical element in the setup before the sample except for wave plates and a neutral density filter used to reduce the reference beam power by 10^{-3} compared to the others. (**Inset**) Schematic illustration of the pulse sequence used to measure biexciton coherences. The first pulse, $\mathbf{E_A}$, excites exciton coherences that oscillate during τ_1. The second pulse, $\mathbf{E_B}$, converts the exciton coherences to biexciton coherences, which oscillate during τ_2. A third-order polarization in the sample is induced by the third pulse, $\mathbf{E_C}$, and the signal field $\mathbf{E_S}(\tau_1, \tau_2, t)$ is radiated during the emission time t. The 2D FT signal $\mathbf{E_S}(\tau_1 = 0, \omega_2, \omega)$ reveals the coherent emission frequency along the ω coordinate and the two-quantum coherence along the ω_2 coordinate. The 2D surfaces presented in this work show the magnitudes of the complex signal fields $\mathbf{E_S}(\omega_2, \omega)$.

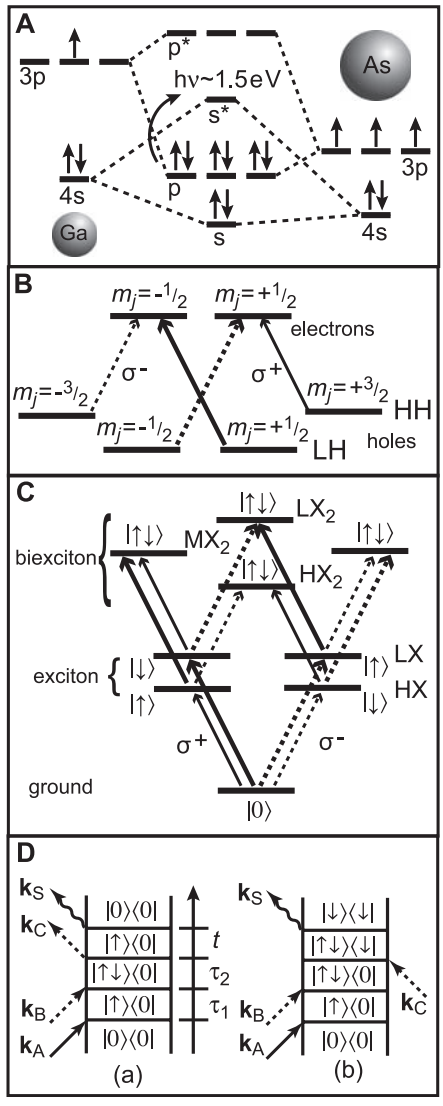

Fig. 2. (**A**) Semiconductor energy-level diagram in the electron and hole representation shows the origins of different exciton states based on the underlying atomic orbital and spin states. (**B**) Expanded view of *p* and *s** states from which excitons are formed. The excited electron is in an *s*-type state with orbital, spin, and total quantum numbers $L = 0$, $S = [1/2]$, $J = L + S = [1/2]$, with degenerate spin sublevels $m_j = \pm[1/2]$. The hole is in a *p*-type state with $L = 1$, $S = [1/2]$, $J = [3/2]$, or $J = [1/2]$ (higher energy, not shown). The $J = [3/2]$ level has spin sublevels $m_j = \pm[3/2]$ and $\pm[1/2]$ whose energies are split by quantum confinement, labeled heavy-hole (HH) and light-hole (LH) because of their effective masses of 0.51 m_e and 0.082 m_e, respectively (the electronic state has effective mass 0.063 m_e). (**C**) Energy-level diagram in the quasiparticle representation illustrating the polarization selection rules for excitons (HX and LX) and biexcitons (HX_2, MX_2, and LX_2). Thin arrows represent HX absorption and thick arrows represent LX absorption. Solid arrows represent right-circularly polarized (σ^+) light; dashed arrows represent left-circularly polarized light (σ^-). (**D**) Relevant Feynman pathways involving HX_2 coherences for cross-circular excitation. Incoming arrows indicate absorption; outgoing arrows indicate emission.

$\mathbf{k_R} = \mathbf{k_A} + \mathbf{k_B} - \mathbf{k_C}$. Many classes of one-quantum measurements have been conducted with this geometry. For example, time-coincident fields $\mathbf{E_A}$ and $\mathbf{E_C}$ produce an excited-state population in a transient grating pattern (with wavevector $\mathbf{k_A} - \mathbf{k_C}$), which yields a coherently scattered signal field $\mathbf{E_S}$ if probed by field $\mathbf{E_B}$ (incident at the phase-matching angle for diffraction) within the excited-state lifetime. Alternatively, field $\mathbf{E_C}$ can arrive first to generate an electronic coherence. A transient population grating forms upon the arrival of field $\mathbf{E_A}$, and field $\mathbf{E_B}$ generates a new coherence whose phase evolution is in reverse of the first, resulting in rephasing of different frequency components (that may originate from within a single inhomogeneously broadened transition or from distinct transitions) to generate a photon echo signal, $\mathbf{E_S}$, that is free of inhomogeneous dephasing. If two distinct transitions interact, then the signal field components at each frequency will be modulated at the other frequency. Interferometric measurement and subsequent Fourier transformation of the signal field yield a one-quantum 2D spectrum that shows diagonal peaks due to each individual rephased coherence and off-diagonal cross-peaks that reveal the interacting coherences. One-quantum 2D FT OPT measurements have revealed key insights into coupled chromophores in photosynthetic antenna systems (*21*) and semiconductor QWs (*22*). Unlike one-quantum 2D FT OPT measurements using collinear phase-controlled pulses (*23*), in which only the absorptive part of the signal is detected, it is through isolation and detection of the full signal field that the full optical analog to 2D FT NMR is realized (*24*).

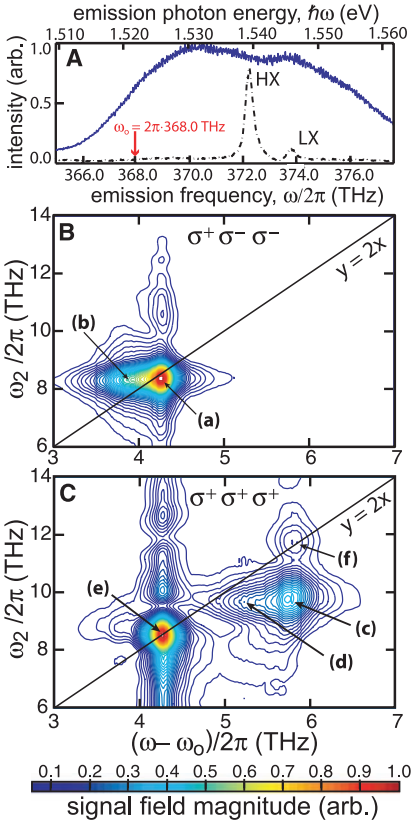

Fig. 3. (**A**) GaAs QW exciton emission spectrum (black dotted trace) with peaks at 372.2 and 373.8 THz from HX and LX, respectively. The reference field $\mathbf{E_R}$ was blocked. The laser pulse spectrum (blue solid trace) is shown with the selected carrier frequency ω_0 indicated by the red arrow. arb., arbitrary units. (**B**) 2D FT OPT spectral magnitude for cross-circularly polarized excitation pulses. The excitation density was 7×10^{10} carriers/cm^2 per well and the pulse energy was 12 pJ per excitation field. The HX_2 biexciton coherence (*a*) is observed directly. The exciton-biexciton coherence that radiated during the emission time is observed as a shoulder (*b*) on the HX emission. (**C**) 2D spectrum for co-circular excitation with the same excitation density as in (B). The MX_2 mixed biexciton coherence peak (*c*) is observed directly and exhibits a red-shifted emission line shape (*d*) due to an exciton-biexciton coherence. The feature *e* at exactly twice the HX frequency in ω_2 and the feature *f* at exactly twice the LX frequency are induced through exciton-exciton interactions described in the SOM text and fig. S3. The contour lines are plotted at 2% intervals. The unlabeled spectral features in (B) and (C) at frequencies higher than those from the discussed two-quantum signals originate from free electron-hole continuum states, not from exciton states.

In terms of the photon echo and transient grating measurements described above, our measurements in which $\mathbf{E_A}$ and $\mathbf{E_B}$ arrive first at the sample should not yield any signal at all. Unlike the previous cases, a population grating (with difference wavevector $\mathbf{k_A} - \mathbf{k_B}$) formed by the first two fields does not give rise to coherent scattering of the third field, $\mathbf{E_C}$, in the signal direction. However, generation of a two-quantum coherence at the sum wavevector $\mathbf{k_A} + \mathbf{k_B}$ followed by a transition induced by field $\mathbf{E_C}$ to a one-quantum coherence at wavevector $\mathbf{k_A} + \mathbf{k_B} - \mathbf{k_C}$ does yield coherent emission in the signal direction. This could only result from a nonlinear response due to interactions between excitons generated by the first two fields, as described above. Thus, the BOXCARS geometry with proper time-ordering of the fields isolates two-quantum signals and eliminates the stronger one-quantum signals.

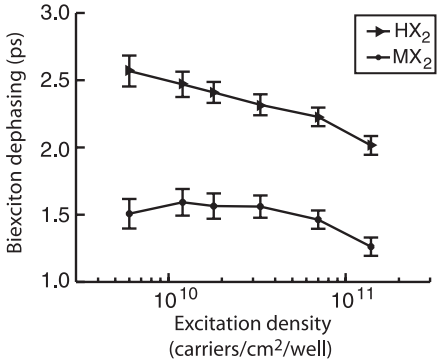

Fig. 4. Dependence of the HX_2 and MX_2 biexciton dephasing times on excitation density in the 10^9 to 10^{11} carriers/cm^2 per well range. The dephasing times of the biexciton coherences decrease as the coherently generated excitation density increases, revealing excitation-induced dephasing of biexcitons similar to that of excitons but due to higher-order (exciton-biexciton) interactions. Error bars represent 95% confidence intervals.

Two-quantum signals were first observed in measurements with just two incident beams, with fields $\mathbf{E_A}$ and $\mathbf{E_B}$ combined. In addition to the expected photon echo signal that was observed when $\mathbf{E_C}$ arrived at the sample first, a signal appeared at "negative" delay times; that is, when the combined $\mathbf{E_A}$ and $\mathbf{E_B}$ fields were incident at the sample first (*25*). The many-body origin of this signal was quickly recognized. However, in this 1D measurement of signal intensity versus $\mathbf{E_C}$ delay time, the various two-quantum contributions were mixed. In addition, the inability to independently control the polarizations of fields $\mathbf{E_A}$ and $\mathbf{E_B}$ imposed severe limitations on two-quantum signal selectivity, as we will see below. The present observations are distinct from those associated with one-quantum exciton-biexciton coherences observed in earlier one-quantum 2D FT OPT measurements as partially resolved shoulders on the excitonic peaks (*22*, *26*). Our measurements not only track the two-quantum signal phase evolutions at optical frequencies but also correlate them to optical one-quantum coherences, unlike previous frequency-domain FWM experiments on single quantum dots (*27*) and time-integrated FWM experiments on QWs (*28*, *29*). Our experiments separate the two-quantum coherences that arise from multi-exciton interactions, allowing the phenomena to be studied even when their signatures cannot be separated spectrally.

The main experimental challenge presented by wavevector definition in the optical regime lies in the difficulty of producing multiple beams of light with pulses whose optical phases are specified and maintained even when the pulses are variably delayed in time-resolved measurements. None of the one-quantum measurements described above required all four optical fields to be phase-coherent, because after the first two field interactions, the system had electronic excited-state population but no optical-frequency coherent superposition between the ground and excited states. The first two fields needed to be phase-related, and the third field and the reference field needed to be as well, but no well-defined phase relationship was needed between the two pulse pairs. Even this partial phase stability among the four fields presents challenges, and only a handful of research groups worldwide have conducted optical 2D FT OPT measurements of this sort with reflective or diffractive beam-splitting optics in order to produce the pulse pairs, and with two interferometers to measure the required phase relationships, which change each time one of the pulse delays is varied. In contrast,

a larger community has studied coupled vibrational transitions through the infrared (IR) analog, 2D FTIR, because it is easier to maintain the phase relationships at the longer IR wavelengths. Although two-quantum 2D FTIR of molecular vibrational overtones has been demonstrated (*30*, *31*), a comparable measurement in the visible region is far more demanding.

Recently, we showed that full phase coherence among all the fields could be accomplished through spatiotemporal pulse shaping, in which the optical fields of multiple beams of light are specified (*32*). The pulse shaper (Fig. 1 and fig. S1) controls the timing and optical phases of all pulses in each beam, so that coherent multiple-field excitation of a sample and interferometric readout of the emitted signal field are possible. The phase of a selected reference frequency, ω_0, can be kept constant among all the fields, permitting rotating frame detection of the signal (SOM text and fig. S2). In the present work, we exploited these capabilities to conduct two-quantum 2D FT OPT measurements (*33*), which revealed biexciton coherences and their dynamics in GaAs QWs.

The origin and energy-level diagram of the different exciton states, labeled heavy-hole exciton (HX), light-hole exciton (LX), and biexciton (X_2) states in GaAs QWs are shown in Fig. 2, A to C. The optical selection rules for the two excitons differ with respect to circular polarization of the light (*34*). Because biexcitons are formed by the correlations of opposite-spin excitons, cross-circular polarization of fields $\mathbf{E_A}$ and $\mathbf{E_B}$ will excite pure HX_2 and LX_2 biexciton coherences, whereas co-circular polarization will excite mixed (MX_2) biexciton coherences. The sample response of primary interest is illustrated by the double-sided Feynman diagram in Fig. 2D(a), in which the sequence of coherences and the fields that induce them are shown. For instance, the HX_2 biexciton coherence was observed when the first circularly polarized resonant field $\mathbf{E_A}$ produced an HX–ground-state coherence, with wavevector $\mathbf{k_A}$, that evolved during τ_1, and the second oppositely circularly polarized field $\mathbf{E_B}$ converted the coherence to a two-quantum HX_2–ground-state coherence, with wavevector $\mathbf{k_A} + \mathbf{k_B}$, that underwent coherent oscillations during τ_2. A third circularly polarized field, $\mathbf{E_C}$, regenerated an HX–ground-state coherence with wavevector $\mathbf{k_A} + \mathbf{k_B} - \mathbf{k_C}$, which during time t radiated the signal field $\mathbf{E_S}$ that was overlapped spatially with the oppositely circularly polarized reference field $\mathbf{E_R}$ and whose amplitude and phase were determined through spectral interferometry, as described above. Another signal contribution expected from biexciton–ground-state coherences induced by the first two fields is indicated in Fig. 2D(b). In this case, the third field generated a new exciton coherence from the ground state. Signal was radiated through an exciton-biexciton (HX-HX_2) coherence whose frequency ω_{eb} is expected to be red-shifted from the exciton coherence frequency ω_e because of the biexciton binding energy, $\omega_{eb} = \omega_e - \varepsilon_B^{eb}/\hbar$, where we have superscripted the binding energy for reasons that will become evident.

The interaction-induced two-quantum coherences at frequency $2\omega_e$ (with no binding energy) cannot be described by standard double-sided Feynman diagrams, because the diagrams indicate distinct states and optical transitions among them but do not explicitly indicate interactions or correlations among states. A recently developed formalism has been advanced to include many-body correlations in QWs (*35*, *36*). These signals are discussed in more detail in the SOM text.

The emission spectrum measured in the phase-matched direction with time-coincident excitation fields is plotted in Fig. 3A with the excitation laser spectrum. The HX and LX exciton transition frequencies are 372.2 and 373.8 THz (1.539 and 1.546 eV), respectively. The 2D surface obtained with cross-circular excitation (Fig. 3B) shows the HX_2 biexciton coherence. (The LX_2 biexciton feature is too weak to be seen here because the LX transition dipole is one-third that of the HX.) Detection by spectral interferometry gives the signal field as a function of the absolute emission frequency, so we have subtracted the carrier frequency (368.00 ± 0.04 THz) to represent both frequency axes in the rotating frame. The HX_2 peak (*a*) appears at the HX emission frequency along the ω axis (4.270 ± 0.003 THz higher than the carrier frequency), but at 8.32 ± 0.01 THz along the ω_2 axis. This ω_2 value is less than twice the HX frequency, yielding a biexciton binding energy of $\varepsilon_B = 0.9 \pm 0.2$ meV (*37*). The exciton-biexciton coherence (*b*) appears as a shoulder of the biexciton peak red-shifted slightly in emission frequency ω. A two-Lorentzian least-squares fit to peaks *a* and *b* as functions of ω gives ω_e and ω_{eb}, respectively. The difference yields a biexciton binding energy of $\varepsilon_B^{eb} = 1.5 \pm 0.1$ meV. The binding energy obtained in this manner is in closer agreement with previously observed values (*38*–*40*) that also were obtained from exciton-biexciton coherences. The values ε_B and ε_B^{eb} differ because they are derived from different correlation terms. A simple definition of the binding energy is the energy difference between uncorrelated and correlated four-particle states, which corresponds to ε_B. However, the value ε_B^{eb} depends on the exciton-biexciton transition, which weights subsets of the correlated two-particle (exciton) and four-particle (biexciton) states that may not reflect the precise energies of either relative to the ground state.

The linewidth of a Lorentzian least-squares fit to peak *a* along ω_2 yields an HX_2 biexciton dephasing time of 2.23 ± 0.07 ps. Figure 4 shows a previously undiscovered dependence of the biexciton dephasing time on the excitation density. The observed excitation-induced biexciton dephasing effects can be ascribed to six-particle correlations (interactions between biexcitons and excitons). Biexciton interactions with free electrons and holes should be negligible because the excitation pulses are detuned from the free carrier absorption band. Correlations of this order have been observed in previous nonlinear spectroscopy measurements (*41*), but only in a highly convolved manner without isolation of their distinct effects. The biexciton binding energy was found to be essentially independent of excitation density in the present study.

Measurements conducted at the same excitation density with co-circularly polarized excitation are shown in Fig. 3C with features denoted *c* to *f*. The MX_2 mixed biexciton ground-state coherence (*c*), which represents correlations between the HX and LX excitons, is observed directly. Its position on ω_2 is 9.72 ± 0.02 THz, indicating a mixed biexciton binding energy of 1.42 ± 0.41 meV. This is larger than the HX_2 binding energy, consistent with the expectation that the binding energy should increase with decreasing electron-hole effective mass ratio (*42*) because the LX has a larger effective mass in the unconfined dimension of the QW. The MX_2 dephasing time is 1.46 ± 0.07 ps and, like the HX_2, it decreases with increasing excitation density (Fig. 4). A red-shifted exciton-biexciton emission (*d*) appears, analogous to *b* in Fig. 3B, but it is not sufficiently distinct to yield an accurate frequency or binding energy.

The mixed biexcitons are found to emit only at the LX frequency, although emission at the HX frequency is also expected. This discrepancy is likely due to interference with emission at the same frequency (*43*) from feature *e*, centered at 8.57 ± 0.02 THz (twice the HX frequency) in ω_2, which is solely the result of interaction-induced correlations that cannot be described in terms of double-sided Feynman diagrams, as discussed earlier. There is also a weak interaction-induced coherence (*f*) at twice the LX transition frequency. Deconvolved two-quantum coherence transients for the HX_2, MX_2, and HX interaction-induced effects can be extracted from Fig. 3 through Fourier filtering (fig. S4). In contrast to conventional FWM experiments (fig. S5), the phase sensitivity and spectral separation of two-quantum 2D FT OPT provide a clear picture of the higher-order Coulomb correlations involved.

The two-quantum 2D FT OPT measurements presented here represent a decisive step in the isolation and elaboration of many-body interactions in the prototype GaAs system that cannot be treated using a mean-field approximation. Comprehensive analysis of the real and imaginary parts of the complex spectra will provide further guidance for first-principles calculations of the correlated electronic responses. In quantum dots, observation of multiple-quantum coherences and populations from biexcitons and higher-lying states will have additional importance in laser gain, solar energy conversion, and other applications. Our present results demonstrate the ability of fully coherent multidimensional optical spectroscopy to access "dark" states using multiple-photon transitions and the simplicity of the spatiotemporal pulse shaping approach for the execution of otherwise daunting measurements. The same apparatus

and measurements can be used for feedback-directed quantum control over the coherences.

References and Notes

1. D. Abramavicius, D. V. Voronine, S. Mukamel, *Proc. Natl. Acad. Sci. U.S.A.* **105**, 8525 (2008).
2. V. I. Rupasov, V. I. Klimov, *Phys. Rev. B* **76**, 125321 (2007).
3. J. Shah, *Ultrafast Spectroscopy of Semiconductors and Semiconductor Nanostructures* (Springer, Berlin, 1999).
4. M. Wegener, D. S. Chemla, S. Schmitt-Rink, W. Schafer, *Phys. Rev. A* **42**, 5675 (1990).
5. R. W. Boyd, *Nonlinear Optics* (Academic Press, San Diego, CA, ed. 2, 2003).
6. H. Wang *et al.*, *Phys. Rev. Lett.* **71**, 1261 (1993).
7. J. M. Shacklette, S. T. Cundiff, *Phys. Rev. B* **66**, 045309 (2002).
8. H. Haug, S. W. Koch, *Quantum Theory of the Optical and Electronic Properties of Semiconductors* (World Scientific Publishing, New York, ed. 4, 2004).
9. T. Voss, I. Ruckman, J. Gutowski, V. M. Axt, T. Kuhn, *Phys. Rev. B* **73**, 115311 (2006).
10. X. Li *et al.*, *Science* **301**, 809 (2003).
11. P. Gilliot *et al.*, *Phys. Rev. B* **75**, 125209 (2007).
12. M. C. Phillips *et al.*, *Phys. Rev. Lett.* **91**, 183602 (2003).
13. E. J. Mayer *et al.*, *Phys. Rev. B* **50**, 14730 (1994).
14. A. L. Smirl, M. J. Stevens, X. Chen, O. Buccafusca, *Phys. Rev. B* **60**, 8267 (1999).
15. M. Munowitz, A. Pines, *Science* **233**, 525 (1986).
16. R. R. Ernst, G. Bodenhausen, A. Wokaun, *Principles of Nuclear Magnetic Resonance in One and Two Dimensions* (Oxford Univ. Press, New York, 1990).
17. W. Richter, W. S. Warren, *Concepts Magn. Reson.* **12**, 396 (2000).
18. G. Galiana, R. T. Branca, E. R. Jenista, W. S. Warren, *Science* **322**, 421 (2008).
19. V. Chernyak, W. M. Zhang, S. Mukamel, *J. Chem. Phys.* **109**, 9587 (1998).
20. L. Lepetit, G. Cheriaux, M. Joffre, *J. Opt. Soc. Am. B* **12**, 2467 (1995).
21. T. Brixner *et al.*, *Nature* **434**, 625 (2005).
22. T. Zhang *et al.*, *Proc. Natl. Acad. Sci. U.S.A.* **104**, 14227 (2007).
23. P. Tian, D. Keusters, Y. Suzaki, W. S. Warren, *Science* **300**, 1553 (2003).
24. D. M. Jonas, *Science* **300**, 1515 (2003).
25. K. Leo *et al.*, *Phys. Rev. Lett.* **65**, 1340 (1990).
26. L. Yang, I. V. Schweigert, S. T. Cundiff, S. Mukamel, *Phys. Rev. B* **75**, 125302 (2007).
27. G. Chen *et al.*, *Phys. Rev. Lett.* **88**, 117901 (2002).
28. K. B. Ferrio, D. G. Steel, *Phys. Rev. B* **54**, R5231 (1996).
29. T. Saiki, M. Kuwata-Gonokami, T. Matsusue, H. Sakaki, *Phys. Rev. B* **49**, 7817 (1994).
30. E. C. Fulmer, P. Mukherjee, A. T. Krummel, M. T. Zanni, *J. Chem. Phys.* **120**, 8067 (2004).
31. S. Sul, D. Karaiskaj, Y. Jiang, N.-H. Ge, *J. Phys. Chem. B* **110**, 19891 (2006).
32. J. C. Vaughan, T. Hornung, K. W. Stone, K. A. Nelson, *J. Phys. Chem. A* **111**, 4873 (2007).
33. Materials and methods are available as supporting material on *Science* Online.
34. P. Y. Yu, M. Cardona, *Fundamentals of Semiconductors: Physics and Materials Properties* (Springer-Verlag Telos, Berlin, ed. 2, 1999).
35. L. Yang, S. Mukamel, *Phys. Rev. Lett.* **100**, 057402 (2008).
36. T. Meier, P. Thomas, S. W. Koch, *Coherent Semiconductor Optics—From Basic Concepts to Nanostructure Applications* (Springer, Berlin, 2007).
37. The uncertainty in the binding energy includes the 95% confidence interval for the Lorentzian least-squares fitting parameters and the uncertainty in the frequency resolution of the scanned coordinate, which is related to the spectral dispersion over one pixel of the 2D spatial light modulator (SLM).
38. K.-H. Pantke, D. Oberhauser, V. G. Lyssenko, J. M. Hvam, G. Weimann, *Phys. Rev. B* **47**, 2413 (1993).
39. H. Wang, J. Shah, T. C. Damen, L. N. Pfeiffer, *Solid State Commun.* **91**, 869 (1994).
40. D. Birkedal, J. Singh, V. G. Lyssenko, J. Erland, J. M. Hvam, *Phys. Rev. Lett.* **76**, 672 (1996).
41. D. S. Chemla, J. Shah, *Nature* **411**, 549 (2001).
42. T. Meier, S. W. Koch, M. Phillips, H. Wang, *Phys. Rev. B* **62**, 12605 (2000).
43. L. Yang, S. Mukamel, *Phys. Rev. B* **77**, 075335 (2008).

44. This work was supported in part by NSF grant CHE-0616939. The authors thank M. Kira for helpful discussions. D.T. thanks the National Defense Science and Engineering Graduate Fellowship Program for financial support. X.L. acknowledges support from the Army Research Office and the Welch Foundation. A patent application for the optical setup presented here is currently being filed.

Supporting Online Material

www.sciencemag.org/cgi/content/full/324/5931/1169/DC1
Materials and Methods
SOM Text
Figs. S1 to S5
References

29 December 2008; accepted 24 March 2009
10.1126/science.1170274

Tearing of Stagnant Slab

Masayuki Obayashi,* Junko Yoshimitsu, Yoshio Fukao

Subducted slabs of oceanic lithosphere below the western Pacific tend to be stagnant in the transition zone with poorly known mechanical properties. Typical examples are the Izu-Bonin and Japan slabs that meet each other to form a cusplike junction beneath southwest Japan. Here, we show that these two slabs are torn apart at their junction when they bend to flatten over the 660-kilometer discontinuity, as is expected from a simple geometric argument. We present three lines of evidence for this ongoing slab tear.

Among the slabs subducted from the Kurile, Japan, Izu-Bonin, and Mariana arcs, the northern Kurile and Mariana slabs penetrate the 660-km seismic discontinuity into the lower mantle down to depths of ~900 km (*1*). Here, the shape of the penetrated slab is bloblike, suggesting that the slab was strongly deformed as it penetrated the lower mantle. On the other hand, the southern Kurile, Japan, and Izu-Bonin slabs bend sharply and flatten over the 660-km discontinuity. Their shape remains slablike, implying that the slab behaves as a thin elastic plate undergoing deformation only by bending or tearing, not by internal shearing (*2*). Here, we show that slab tearing occurs as a consequence of slab flattening.

The idea is schematically illustrated in Fig. 1, which shows the Japan and the Izu-Bonin slabs meeting to form a cusplike junction. Bending of the two slabs to the horizontal requires a separation of their horizontal parts with a gap in between (Fig. 1A). The resultant stress concentration at the tip of the slab gap allows back-propagation of the slab gap to shallower depths along the junction (Fig. 1B). We present three lines of evidence to show this slab gap. The first is the absence of both deep seismicity and slab-related velocity anomalies in a place corresponding to the slab gap [arrow (a)]. The second is the occurrence of lateral tension–type earthquakes near the tip of the slab gap [arrow (b)]. The third is the finding of a near vertical plane that may correspond to a side wall of the slab gap [arrow (c)].

We obtained a three-dimensional *P* wave velocity model for the whole mantle by inverting ~50,000 *P* wave arrival times, manually picked records from seismic networks deployed in the central to western Pacific region (*3*–*6*); ~15,000 *PP-P* differential travel times obtained through waveform correlation (*7*); and ~7.4 million first-arrival times from the bulletins of the International Seismological Centre. The fast *P* wave speed anomalies near Japan (Fig. 2) reveal laterally continuous subducting slabs along the Kurile, Japan, and Izu-Bonin arcs to depths of 300 km (Fig. 2A). The Japan and Izu-Bonin slab images are, however, disconnected from each other at their junction (~35°N) just below 300 km (Fig. 2B), indicating a slab gap. This gap is more noticeable than our previous model (*8*) and is also observed in the *S* wave speed model of (*9*). The gap persists to

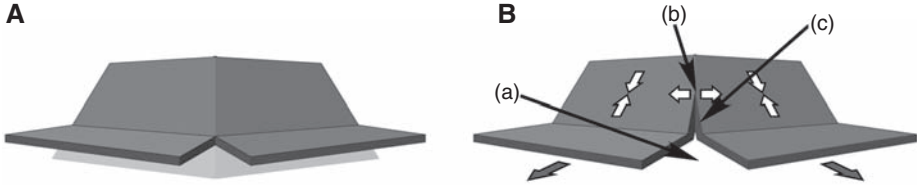

Fig. 1. (**A**) Schematic explaining how slab bending to the horizontal causes slab tearing at the slab–slab junction. Dipping slabs without horizontal bending are shown in a light gray for reference. (**B**) Schematic illustration for the Japan and Izu-Bonin slabs at their junction. The white arrows indicate the dominant principal stress in the slab inferred from the focal mechanisms. The gray arrows show the approximate direction of motion of each segment of the stagnant slab. The resultant direction of the two gray arrows should coincide with the direction of the motion of the Pacific plate.

Institute for Research on Earth Evolution, Japan Agency for Marine-Earth Science and Technology, 2-15 Natsushima-cho, Yokosuka 237-0061, Japan.

*To whom correspondence should be addressed. E-mail: obayashi@jamstec.go.jp

depths of more than 600 km and westward to the Yellow Sea across the Korean peninsula.

As shown in Fig. 2A, many slab earthquakes around 35°N have occurred at depths shallower than ~300 km, whereas deeper activity is sparse and practically nonexistent below 410 km (*10*). The depth of the deepest earthquakes along the Japan–Izu-Bonin arcs is the shallowest near this junction and becomes deeper (≥550 km) both to the north and south (*11*, *12*). A small cluster of hypocenters is seen within the slab gap at depths of 350 to 410 km (Fig. 2C). Focal mechanisms for the clustered events (*13*) are different from the typical down-dip compression mechanisms for neighboring events (*14*). Instead, they have lateral-tension axes parallel to the strike of the slab (Fig. 3). These events have been interpreted as hinge-faulting that may be responsible for the small but abrupt change in the strike and dip of the deep seismic zone across the arc–arc junction (*14*, *15*).

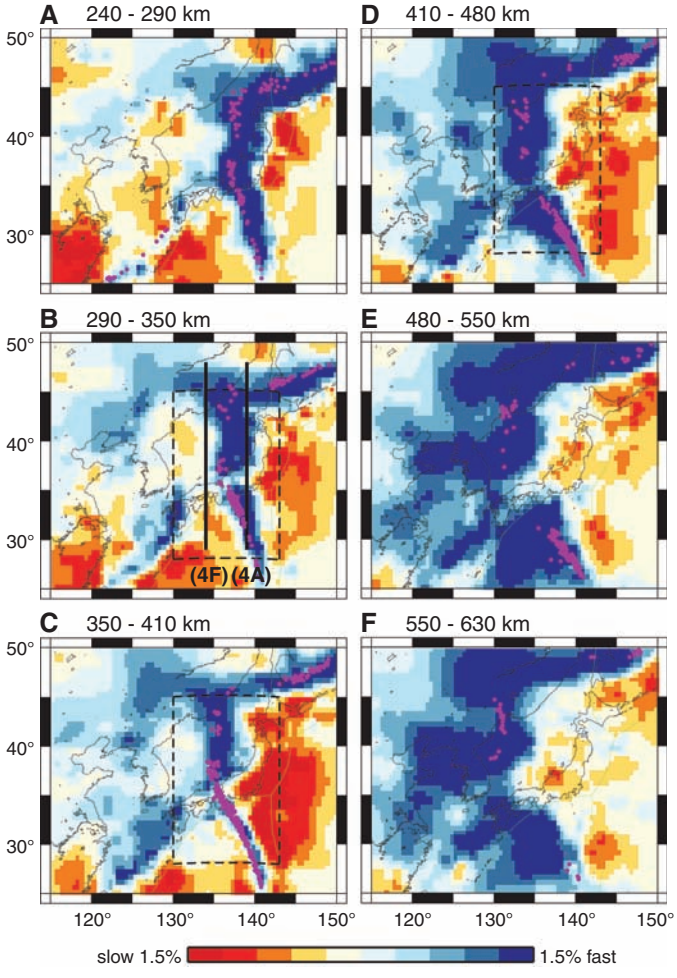

Fig. 2. (**A** to **F**) *P* wave speed anomalies around the Japan and Izu-Bonin slab junction at successive layers from depths of 240 to 630 km. Fast and slow anomalies are indicated by blue and red colors, respectively. The dots indicate earthquakes with magnitude (m_b) of ≥4.0 from 1964 to 2004 in the depth range of each layer. The regions bound by broken lines are magnified in Fig. 3. The cross section profiles for Fig. 4, A and F, are indicated by thick lines.

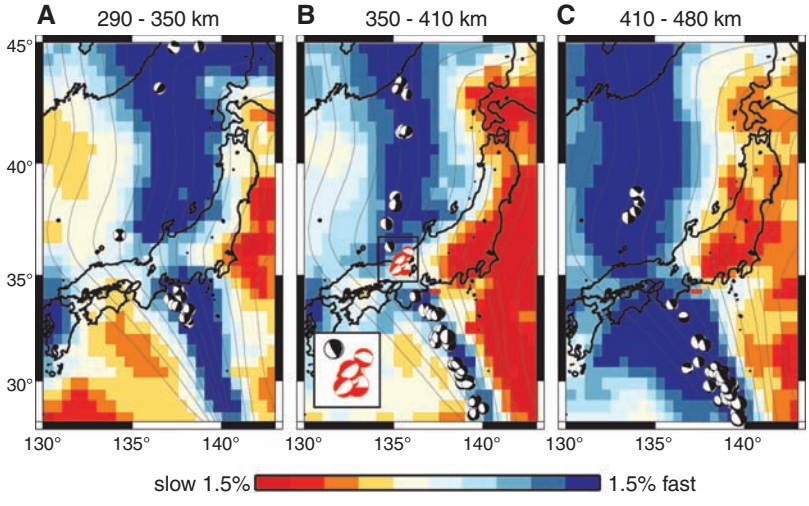

Fig. 3. (**A** to **C**) Magnified images of the regions bounded by broken lines in Fig. 2, B to D, respectively, with focal mechanisms of the Harvard centroid moment tensor catalogs. Mechanisms with lateral tension are shown in red, and other mechanisms with dominant down-dip compression are shown in black. The focal mechanisms in the square region are enlarged in the white box. The red bar indicates the location of the *S*-to-*P* conversion plane obtained from analysis of the *X* phase.

Tearing at the junction creates the southern-edge surfaces of the Japan slab and the northern-edge surface of the Izu-Bonin slab with a slab gap in between. We observed an unknown phase (*X* phase) between the *P* and *S* arrivals for the 398-km-depth earthquake of 2003 on the Hi-net (*16*) seismograms only in central Japan (figs. S4 and S6). The *X* phase arrives about 20 s after the direct *P* wave with an apparent velocity that is slightly higher than that of the direct *P* wave. It has a predominantly vertical amplitude as large as that of the direct *P* wave. These characteristics indicate that the *X* phase is an *S*-to-*P* converted phase. We grid-searched for the conversion interface that meets these characteristics, assuming that it is a flat plane at which conversion takes place so as to satisfy Snell's law [supporting online material (SOM) text]. The obtained *S*-to-*P* conversion plane has its center at 137.3°E, 34.3°N, and 380 km depth and extends over a depth range of ~70 km and a length of ~50 km along the strike. The strike is almost east-west and the dip angle is ~80°, both different from those of the Izu-Bonin slab, which strikes almost north-south and dips at ~45°. The conversion plane projected onto the tomographic map of Fig. 3, B and C (red line), delineates, in our interpretation, the northern edge of the Izu-Bonin slab. Cross sections of *P* wave speed anomalies from 134°E to 139°E show that to the west of 136°E (Fig. 4, D to F), the Izu-Bonin slab is clearly separated from the Japan slab with a slab gap in between. To the east of 138°E (Fig. 4, A and B), the Izu-Bonin slab continues without a gap to the Japan slab. Figure 4C shows the 137°E-parallel cross section, onto which the conversion plane is projected (red line). This projection delineates the northern edge of the Izu-Bonin slab, which is separated from the southern edge of the Japan slab at depths of >300 km but continues to the latter at shallower depths. The well-developed cut surface at the northern edge of the Izu-Bonin slab and the occurrence of lateral tension–type earthquakes in the southernmost part of the Japan slab suggests that slab-tearing here is a process laterally asymmetric with respect to the junction. Slab-related *S*-to-*P* converted phases so far reported near Japan have been attributed to the upper surface of the slab beneath Japan (*17*–*20*).

Deep slab gaps have been observed in various regions (*21*–*23*). Most of them are associated with detachment of a deeper part of the slab from

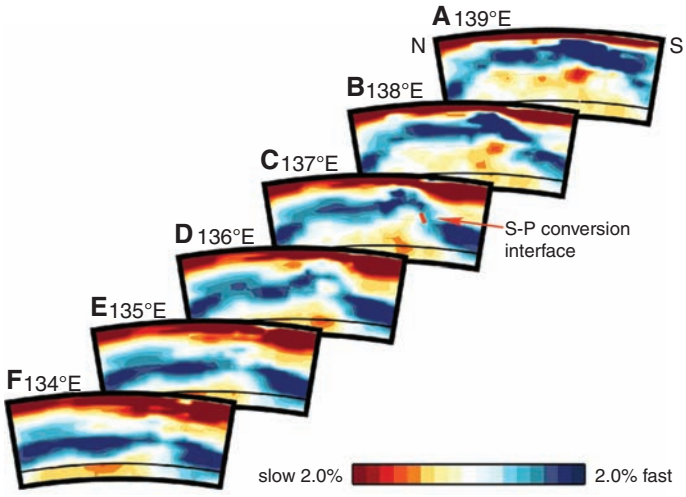

Fig. 4. (**A** to **F**) Cross sections of the *P* wave speed anomalies along meridians from 134°E to 139°E at one-degree intervals. The depth range is from the surface to 800 km. A red line segment in (C) indicates the *S*-to-*P* conversion plane. The profiles for (A) and (F) are shown in Fig. 1B.

the shallower part. In the southern Mariana, differential slab dip between two adjacent segments has been detected and attributed to slab tear (*24*). We for the first time report the slab tear and consequent slab gap associated with slab stagnation.

The process of slab tearing should reflect the subduction history of the Pacific plate. Paleogeographic reconstruction models indicate that the Izu-Bonin trench migrated eastward with a clockwise rotation between the mid-Eocene and late Miocene, leading to the eastward migration of the junction of the Izu-Bonin and Japan trenches (*25*–*27*). This migration of the trench–trench junction implies an eastward migration of the tip of the slab gap, which should have been synchronous with the westward advance of the leading edge of the flattened part of the Izu-Bonin slab. Thus, the slab gap has extended over time both to the west and to the east.

References and Notes

1. Y. Fukao, S. Widiyantoro, M. Obayashi, *Rev. Geophys.* **39**, 291 (2001).
2. K. Yamaoka, Y. Fukao, M. Kumazawa, *Rev. Geophys.* **24**, 27 (1986).
3. Y. Fukao *et al.*, in *Workshop Report of OHP/ION Joint Symposium, Long-Term Observations in the Oceans* (Earthquake Research Institute, Univ. of Tokyo, 2001), pp. 13–29.
4. M. Ishida, S. Maruyama, D. Suetsugu, S. Matsuzaka, T. Eguchi, *Earth Planets Space* **51**, 1 (1999).
5. T. Ohtaki, JISNET Group, *Eos. Trans. Am. Geophys. Un.* **79**, *Western Pacific Geophysics Meet. Suppl.*, W80 (1998).
6. R. van der Hilst, B. Kennett, D. Christie, J. Grant, *Eos. Trans. Am. Geophys. Un.* **75**, 177 (1994).
7. M. Obayashi, D. Suetsugu, Y. Fukao, *Geophys J. Int.*, **157**, 1152 (1994).
8. M. Obayashi, H. Sugioka, J. Yoshimitsu, Y. Fukao, *Earth Planet. Sci. Lett.* **243**, 149 (2006).
9. M. S. Miller, B. L. N. Kennett, V. G. Toy, *J. Geophys. Res.* **111**, 10.1029/2005JB003705 (2006).
10. E. R. Engdahl, R. D. van der Hilst, R. P. Buland, *Bull. Seismol. Soc. Am.* **88**, 722 (1998).
11. S. H. Kirby, S. Stein, E. A. Okal, D. C. Rubie, *Rev. Geophys.* **34**, 261 (1996).
12. J. C. Castle, K. C. Creager, *Earth Planets Space* **50**, 977 (1998).
13. B. Isacks, P. Molnar, *Rev. Geophys. Space Phys.* **9**, 103 (1971).
14. G. V. Burbach, C. Frohlich, *Rev. Geophys.* **24**, 833 (1986).
15. A. M. Dziewonski, T. A. Chou, J. H. Woodhouse, *J. Geophys. Res.* **86**, 2825 (1981).
16. Y. Okada *et al.*, *Earth Planets Space* **56**, 15 (2004).
17. S. Hori, *Tectonophysics* **176**, 355 (1990).
18. T. Matsuzawa, T. Kono, A. Hasegawa, A. Takagi, *Tectonophysics* **181**, 123 (1990).
19. M. Nakamura, M. Ando, T. Ohkura, *Phys. Earth Planet. Inter.* **106**, 63 (1998).
20. S. Ohmi, S. Hori, *Geophys. J. Int.* **141**, 136 (2000).
21. M. J. R. Wortel, W. Spakman, *Science* **290**, 1910 (2000).
22. E. Hafkenscheid, M. J. R. Wortel, W. Spakman, *J. Geophys. Res.* **111**, 10.1029/2005JB003791 (2006).
23. K. Sigloch, N. McQuarrie, G. Nolet, *Nat. Geosci.* **1**, 458 (2008).
24. M. S. Miller, A. Gorbatov, B. L. N. Kennett, *Geochem. Geophys. Geosyst.* **7**, 10.1029/2005GC001110 (2006).
25. R. van der Hilst, T. Seno, *Earth Planet. Sci. Lett.* **120**, 395 (1993).
26. T. Seno, S. A. Stein, A. E. Gripp, C. R. Demets, *J. Geophys. Res.* **98**, 17941 (1993).
27. R. Hall, *J. Asian Earth Sci.* **20**, 353 (2002).

28. We thank the National Research Institute for Earth Science and Disaster Prevention for providing Japan-Indonesia Seismic Network, South Pacific Broadband Seismic Network, and Hi-net data. We are grateful to B. L. N. Kennett for use of SKIPPY data and to Incorporated Research Institutions for Seismology for use of their broadband network data. This study was supported by Grants-in-Aid for Science Research in the Priority Areas of "Stagnant Slab: A New Keyword for Mantle Dynamics" (16075208).

Supporting Online Material

www.sciencemag.org/cgi/content/full/324/5931/1173/DC1
SOM Text
Figs. S1 to S8
References

18 February 2009; accepted 23 April 2009
10.1126/science.1172496

Assessment of Undiscovered Oil and Gas in the Arctic

Donald L. Gautier,[1]* Kenneth J. Bird,[1] Ronald R. Charpentier,[2] Arthur Grantz,[3] David W. Houseknecht,[4] Timothy R. Klett,[2] Thomas E. Moore,[1] Janet K. Pitman,[2] Christopher J. Schenk,[2] John H. Schuenemeyer,[5] Kai Sørensen,[6] Marilyn E. Tennyson,[2] Zenon C. Valin,[1] Craig J. Wandrey[2]

Among the greatest uncertainties in future energy supply and a subject of considerable environmental concern is the amount of oil and gas yet to be found in the Arctic. By using a probabilistic geology-based methodology, the United States Geological Survey has assessed the area north of the Arctic Circle and concluded that about 30% of the world's undiscovered gas and 13% of the world's undiscovered oil may be found there, mostly offshore under less than 500 meters of water. Undiscovered natural gas is three times more abundant than oil in the Arctic and is largely concentrated in Russia. Oil resources, although important to the interests of Arctic countries, are probably not sufficient to substantially shift the current geographic pattern of world oil production.

Among the greatest uncertainties concerning future energy supply is the volume of oil and gas remaining to be found in high northern latitudes. The potential for resource development is of increasing concern to the Arctic nations, to petroleum companies, and to all concerned about the region's fragile environments. These concerns have been heightened by the recent retreat of polar ice, which is changing ecosystems and improving the prospect of easier petroleum exploration and development. For better or worse, limited exploration opportunities elsewhere in the world combined with technological advances make the Arctic increasingly attractive for development. To provide a perspective on the oil and gas resource potential of the region, the U.S. Geological Survey (USGS) completed a geologically based assessment of the Arctic, the Circum-Arctic Resource Appraisal (CARA), which exists entirely in the public domain.

Of the 6% of Earth's surface encompassed by the Arctic Circle, one-third is above sea level and another third is in continental shelves beneath less than 500 m of water. The remainder consists of deep ocean basins historically covered by sea ice. Many onshore areas have already been explored; by 2007, more than 400 oil and gas fields, containing 40 billion barrels of oil (BBO), 1136 trillion cubic feet (TCF) of natural gas, and 8 billion barrels of natural gas liquids had been developed

[1]U.S. Geological Survey, 345 Middlefield Road, Menlo Park, CA 94025, USA. [2]U.S. Geological Survey, Box 25046 Federal Center, Denver, CO 80225, USA. [3]930 Van Auken Circle, Palo Alto, CA 94303, USA. [4]U.S. Geological Survey, 12201 Sunrise Valley Drive, Reston, VA 20192, USA. [5]Southwest Statistical Consulting, 960 Sligo Street, Cortez, CO 81321, USA. [6]Geological Survey of Denmark and Greenland, Øster Voldgade 10, DK-1350 Copenhagen K Denmark.

*To whom correspondence should be addressed. E-mail: gautier@usgs.gov

north of the Arctic Circle, mostly in the West Siberian Basin of Russia and on the North Slope of Alaska (*1*).

Deep oceanic basins have relatively low petroleum potential, but the Arctic continental shelves constitute one of the world's largest remaining prospective areas. Until now, remoteness and technical difficulty, coupled with abundant low-cost petroleum, have ensured that little exploration occurred offshore. Even where offshore wells have been drilled, in the Mackenzie Delta, the Barents Sea, the Sverdrup Basin, and offshore Alaska, most resulting discoveries remain undeveloped.

The CARA only considered accumulations with recoverable hydrocarbon volumes larger than 50 million barrels of oil or 300 billion cubic feet of gas (50 million barrels of oil equivalent, 50 MMBOE) (*2*). Smaller accumulations were excluded as were nonconventional resources such as coal bed methane, gas hydrates, oil shales, and heavy oil and tar sands. Geological risk was explicitly assessed, but technological and economic risks were not. Resources were assumed to be recoverable even in the presence of sea ice or oceanic water depths. Initial results are presented without reference to costs of exploration and development.

Petroleum is overwhelmingly associated with sedimentary rocks. Therefore, a new map was assembled to delineate the Arctic sedimentary successions by age, thickness, and structural and tectonic setting (*3*). The map provided the basis for defining assessment units (AUs), which are mappable volumes of sedimentary rocks that share similar geological properties. The CARA defined 69 AUs (*4*), each containing more than 3 km of sedimentary strata, the probable minimum thickness necessary to bury petroleum source rocks sufficiently to generate significant petroleum. Areas outside the 69 AUs were interpreted to have low petroleum potential.

Geologic information about each AU was compiled from published literature and from data made available by cooperating organizations, including the Bundesanstalt für Geowissenschaften und Rohstoffe, the Geological Survey of Canada, the Geological Survey of Denmark and Greenland, the Norwegian Petroleum Directorate, and the U.S. Minerals Management Service. Many active industry petroleum geologists also generously shared concepts and data. Although many organizations and individuals contributed to the geological analysis, the numerical assessments are the sole responsibility of the USGS.

The study relied on a probabilistic methodology of geological analysis and analog modeling (*2*). Burial history-fluid evolution models were prepared with use of standard modeling software such as PetroMod (http://www.petromod.com/) and BasinMod (www.platte.com/). On the basis of the presence and maturity of source rock, migration pathways, reservoir, and trap and seal, geologists postulated the presence of petroleum systems for review by the CARA team. Analogs were derived from a world database of 246 AUs previously defined for the USGS World Petroleum Assessment 2000 (*5*). The 246 AUs, which account for

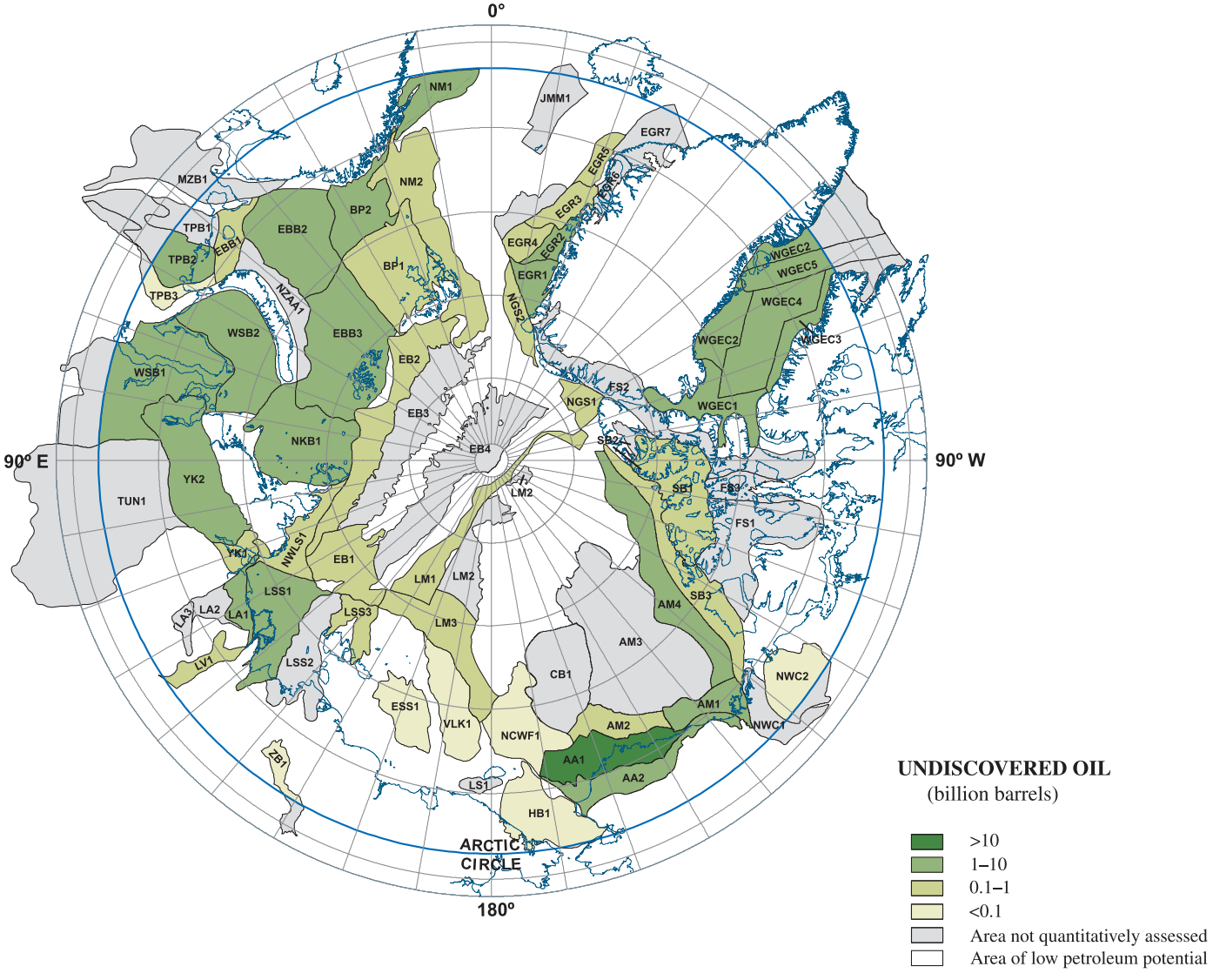

Fig. 1. Map showing the AUs of the CARA is color-coded for mean estimated undiscovered oil. Only areas north of the Arctic Circle are included in the estimates. AU labels are the same as in table S1. Black lines indicate AU boundaries.

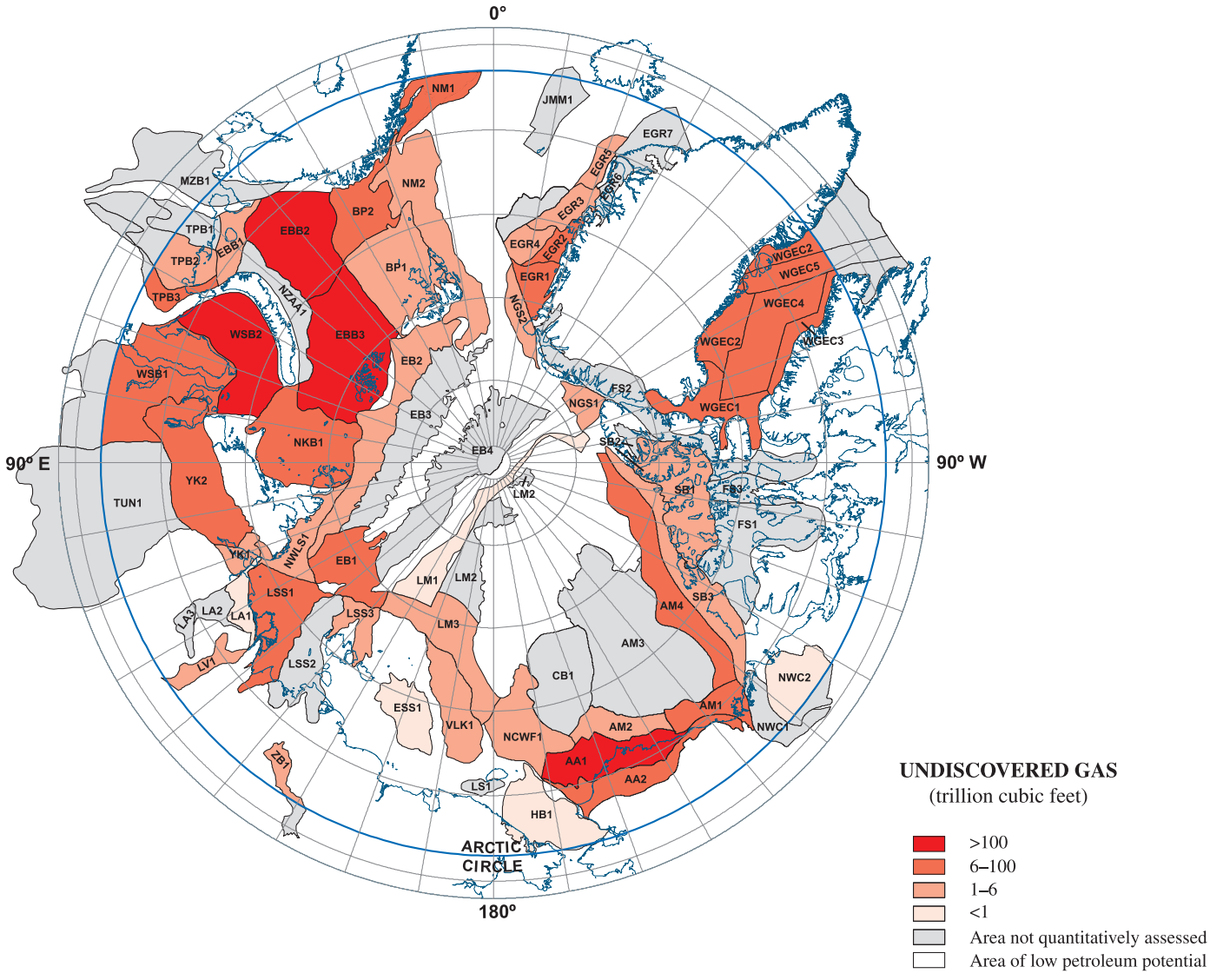

Fig. 2. Map showing the AUs of the CARA is color-coded for mean estimated undiscovered gas. Only areas north of the Arctic Circle are included in the estimates. AU labels are the same as in table S1. Black lines indicate AU boundaries.

more than 95% of known oil and gas outside the United States, were classified according to geologic parameters such as age of source rocks, structural style, and tectonic setting (*6*). With use of data from IHS Incorporated (*1*), we identified oil and gas fields in each of the 246 AUs and used them to compile global distributions for field sizes, field densities (fields per 1000 km^2), and other parameters.

The CARA team analyzed each Arctic AU to determine the geologic properties most likely to control the sizes and numbers of undiscovered petroleum accumulations. Families of AUs from the analog database with similar geologic properties were identified. For example, the assessment units of northeastern Greenland exhibit the geologic features of rift-sag basins and rifted passive continental margins. Accordingly, for the assessment of northeastern Greenland, groups of analogs were selected from the world's population of rift-sag basins and rifted passive margins. In most cases, field data from these populations of analogs provided numerical information for the assessment.

The marginal (unconditional) probability that at least one undiscovered accumulation greater than minimum size (>50 MMBOE) exists within the AU was assessed on the basis of three geologic elements: charge, including source rocks and thermal maturity; rocks, including reservoirs, traps, and seals; and timing, including the relative ages of migration and trap formation, as well as preservation.

The marginal probability of each AU was calibrated against a ranked list of all other CARA AUs. Only CARA AUs with known accumulations were assigned a probability of 1; AUs with <0.1 probability were not quantitatively assessed (table S1). Worldwide, 50 to 60% of similarly defined AUs contain at least one accumulation >50 MMBOE (*7*). However, the resulting mean of assessed AU probabilities in this study is about 41%, significantly less than the global average. This difference reflects the geologic judgment of the CARA team that the petroleum potential of the Arctic differs somewhat from the global population of petroleum basins.

Given the presence of at least one accumulation, three conditional distributions were assessed for each AU: the numbers of undiscovered accumulations, the size frequency of undiscovered accumulations, and the likelihood of oil versus gas in each accumulation. The three conditional distributions were combined in a Monte Carlo simulation of 50,000 trials. Forty-nine of the 69 AUs were quantitatively assessed. Quantitative results of the CARA are listed in table S1 and illustrated in Figs. 1 and 2.

Individual AU assessments were statistically aggregated into Circum-Arctic totals, taking into account partial correlations between AUs with geologic similarities (*2*, *8*). The CARA results suggest there is a high probability (>95% chance) that more than 44 BBO, a one in two chance (50%) that more than 83 BBO, and a 1 in 20 chance (5%) that as much as 157 BBO could be added to proved

reserves from new oil discoveries north of the Arctic Circle. Correlation increases the spread in estimated aggregate volume compared with an assumption of geologic independence. A perfect positive correlation, although geologically unreasonable, would yield the widest spread of aggregate volumes. If perfect positive correlation among all AUs were assumed, the estimated volume of undiscovered oil would range from about 22 BBO to about 256 BBO.

The mean estimate is more than double the amount of oil that has previously been found in the Arctic. For comparison, at the end of 2007, world proved reserves of oil, excluding Canadian oil sands, stood at about 1238 BBO and consumption was about 30 BBO per year (*9*). On the basis of the USGS World Petroleum Assessment 2000 (*5*) adjusted for discoveries since 1996, the Arctic may contain about 13% of the mean estimated global undiscovered oil resource of about 618 BBO. Assuming reserves in existing fields will increase by an additional 400 BBO, undiscovered oil in the Arctic may account for almost 4% of the world's remaining conventionally recoverable oil resources.

All 49 assessed AUs were estimated to contain undiscovered oil, but 60% of the resource is concentrated in just six of them. The Alaska Platform stands out (Fig. 3), with more than 31% of mean undiscovered Arctic oil (27.9 BBO). Other important AUs include the Canning-Mackenzie (6.4 BBO), North Barents Basin (5.3 BBO), Yenisey-Khatanga (5.3 BBO), Northwest Greenland Rifted Margin (4.9 BBO), and two AUs on the northeast Greenland Shelf: South Danmarkshavn Basin (4.4 BBO) and the North Danmarkshavn Salt Basin (3.3 BBO). The Alaska Platform is already a well-known petroleum-producing area; new discoveries there could maintain the flow of Alaskan oil for many years to come. Oil discoveries in the other areas could change the economic landscape and way of life of local inhabitants. However, the estimated resource is probably not sufficient to shift the world oil balance. Moreover, the estimated oil resources, if found, would not come into production at once but rather be added to reserves and produced incrementally.

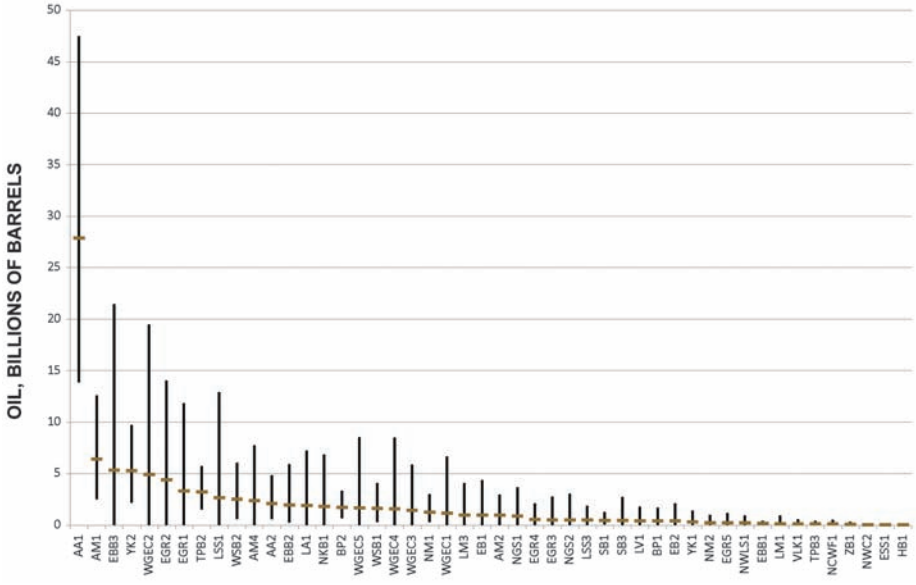

Fig. 3. Estimated undiscovered oil resources, in BBO, north of the Arctic Circle in AUs of the CARA. Vertical lines indicate the range of estimated oil resources from a 5% probability (fifth fractile) to a 95% probability (95th fractile). Horizontal lines correspond to mean estimated oil volumes.

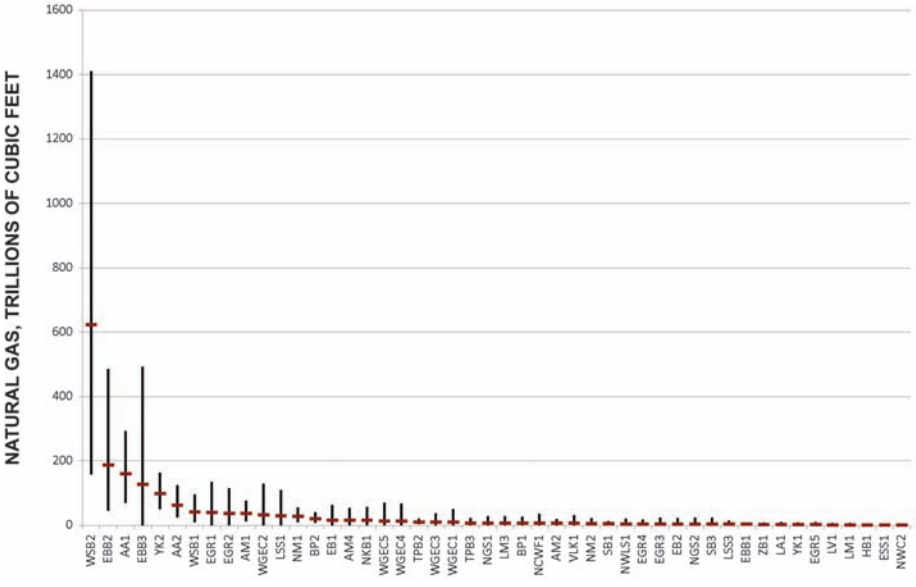

Fig. 4. Estimated undiscovered natural gas resources, in TCF, north of the Arctic Circle in AUs of the CARA. Vertical lines indicate the range of estimated natural gas resources from a 5% probability (fifth fractile) to a 95% probability (95th fractile). Horizontal lines correspond to mean estimated natural gas volumes.

On an energy-equivalent basis, we estimate that the Arctic contains more than three times as much undiscovered gas as oil. The estimated largest undiscovered gas accumulation is almost eight times the estimated size of the largest undiscovered oil accumulation (22.5 BBOE versus 2.9 BBO) and therefore more likely to be developed (table S1). The aggregated results suggest there is a high probability (>95% chance) that more than 770 TCF of gas occurs north of the Arctic Circle, a one in two chance (50%) that more than 1547 TCF may be found, and a 1 in 20 chance (5%) that as much as 2990 TCF could be added to proved reserves from new discoveries. For comparison, current world gas consumption is almost 110 TCF per year. The median estimate of undiscovered gas is a volume larger than the volume of total gas so far discovered in the Arctic and represents about 30% of global undiscovered conventional gas.

Two-thirds of the undiscovered gas is in just four AUs (Figs. 2 and 4): South Kara Sea (607 TCF), South Barents Basin (184 TCF), North Barents Basin (117 TCF), and the Alaska Platform (122 TCF). The South Kara Sea, the offshore part of the northern West Siberian Basin, contains almost 39% of the undiscovered gas and is the most prospective hydrocarbon province in the Arctic. Although substantial amounts of gas may be found in Alaska, Canada, and Greenland, the undiscovered gas resource is concentrated in Russian territory, and its development would reinforce the preeminent strategic resource position of that country.

It is important to note that these estimates do not include technological or economic risks, so a substantial fraction of the estimated undiscovered resources might never be produced. Development will depend on market conditions, technological innovation, and the sizes of undiscovered accumulations. Moreover, these first estimates are, in many cases, based on very scant geological information, and our understanding of Arctic resources will certainly change as more data become available.

References and Notes

1. IHS Incorporated, *International Petroleum Exploration and Production Database* (IHS Incorporated, Englewood, CO, 2007).

2. Materials and methods are available as supporting material on *Science* Online.
3. A. Grantz, R. A. Scott, S. S. Drachev, T. E. Moore, "Maps showing the sedimentary successions of the Arctic Region (58°-64° to 90° N) that may be prospective for hydrocarbons," American Association of Petroleum Geologists GIS-UDRIL Open-File Spatial Library, 2009, http://gisudril.aapg.org/gisdemo/.
4. U.S. Geological Survey, "Circum-Arctic Resource Appraisal (north of the Arctic Circle) assessment units GIS data," 2009, http://energy.usgs.gov/arctic/.
5. USGS World Assessment Team, "U.S. Geological Survey world petroleum assessment 2000: Description and results," USGS Digital Data Series DDS60, 2000, http://pubs.usgs.gov/dds/dds-060/.
6. R. R. Charpentier, T. R. Klett, E. D. Attanasi, "Database for assessment of assessment unit-scale analogs (exclusive of the United States)," U.S. Geological Survey Open-File Report 2007-1404, 2008, http://pubs.usgs.gov/of/2007/1404/.
7. R. R. Charpentier, paper presented at the 2008 American Association of Petroleum Geologists Annual Convention and Exhibition, San Antonio, TX, 22 April 2008.
8. J. H. Schuenemeyer, "Procedures for aggregation used in the Circum-Arctic Resource Appraisal," U.S. Geological Survey Open File Report, in press.
9. British Petroleum (BP) Public Limited Company, "BP statistical review of world energy 2008," London, 2008, http://www.bp.com/statisticalreview.
10. We thank P.I. McLabe and R.S. Bishop for their comments on an earlier version of the manuscript.

Supporting Online Material

www.sciencemag.org/cgi/content/full/324/5931/1175/DC1
Materials and Methods
Table S1

8 December 2008; accepted 16 March 2009
10.1126/science.1169467

Volcanism, Mass Extinction, and Carbon Isotope Fluctuations in the Middle Permian of China

Paul B. Wignall,[1]* Yadong Sun,[2] David P. G. Bond,[1] Gareth Izon,[3] Robert J. Newton,[1] Stéphanie Védrine,[1] Mike Widdowson,[3] Jason R. Ali,[4] Xulong Lai,[2] Haishui Jiang,[2] Helen Cope,[5] Simon H. Bottrell[1]

The 260-million-year-old Emeishan volcanic province of southwest China overlies and is interbedded with Middle Permian carbonates that contain a record of the Guadalupian mass extinction. Sections in the region thus provide an opportunity to directly monitor the relative timing of extinction and volcanism within the same locations. These show that the onset of volcanism was marked by both large phreatomagmatic eruptions and extinctions amongst fusulinacean foraminifers and calcareous algae. The temporal coincidence of these two phenomena supports the idea of a cause-and-effect relationship. The crisis predates the onset of a major negative carbon isotope excursion that points to subsequent severe disturbance of the ocean-atmosphere carbon cycle.

The temporal link between mass extinction events and large igneous province volcanism is one of the most intriguing relationships in Earth's history, with the end-Permian extinction–Siberian Traps association being the most celebrated (*1*, *2*), but the causal link is far from resolved. A major problem is that the site of volcanism can rarely be directly correlated with the marine extinction record (*3*), and so comparison can only be achieved with the use of geochronological bio- and chemostratigraphic correlation techniques, with their inherent timing inaccuracies. To clarify some of these relations, we have studied the Emeishan flood basalt province in southwest China, where Middle Permian platform limestones pass up into a volcanic pile with interbedded limestones. These record both a marine extinction record and a major C isotope excursion. Thus, we were able to document multiple phenomena associated with the Middle Permian mass extinction within the same geological sections.

Middle Permian (Guadalupian) platform carbonate rocks of the Maokou Formation are widespread throughout south China. In western Guizhou, southern Sichuan, and Yunnan Provinces they pass laterally into the flows of the Emeishan large igneous province (Fig. 1). The original size of the province is difficult to estimate because much has been eroded (scattered outcrops of contemporaneous volcanic rocks are found up to 300 km from the main sections, Fig. 1), but its main outcrops cover 2.5×10^5 km^2 in southwest China; the original volume was probably substantially less than 1×10^6 km^3 (*4*). Despite their relatively small size, the coincidental timing of the Emeishan eruptions with the Guadalupian mass extinction has led to suggestions that they may be implicated in this environmental calamity (*2*, *5*).

Sections from both within the volcanic province and around its margins record a prolonged phase of stable carbonate platform deposition before its termination by abrupt base-level changes. To the north of the province, in northern Sichuan, the Maokou limestones are capped by a karstic surface dated by conodont studies to

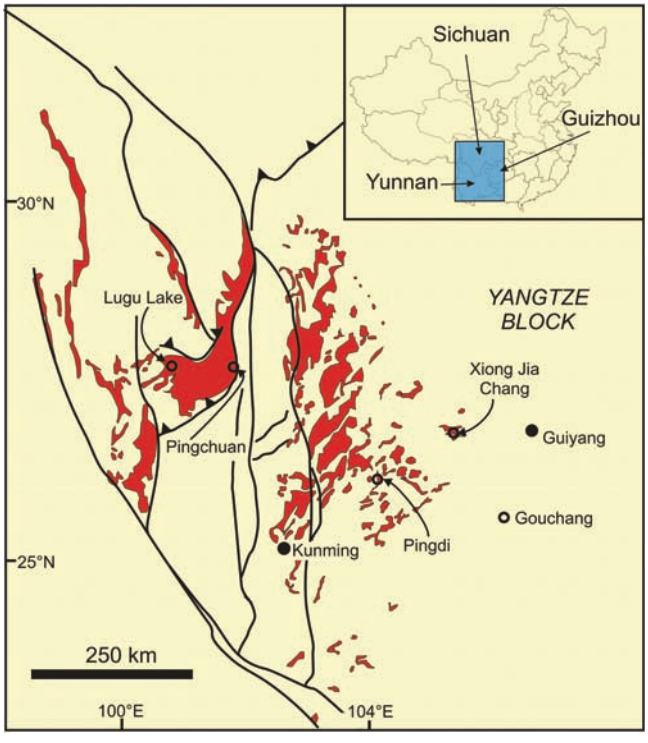

Fig. 1. Outcrop map (red) of the Emeishan large igneous province in southwest China (*4*).

[1]School of Earth and Environment, University of Leeds, Leeds LS2 9JT, UK. [2]Faculty of Earth Sciences, China University of Geosciences, Wuhan, Hubei 430074, China. [3]Department of Earth and Environmental Science, The Open University, Milton Keynes MK7 6AA, UK. [4]Department of Earth Sciences, Pokfulam Road, University of Hong Kong. [5]Department of Bioengineering, University of Strathclyde, Wolfson Building, 106 Rottenrow, Glasgow G4 0NW, UK.

*To whom correspondence should be addressed. E-mail: p.wignall@see.leeds.ac.uk

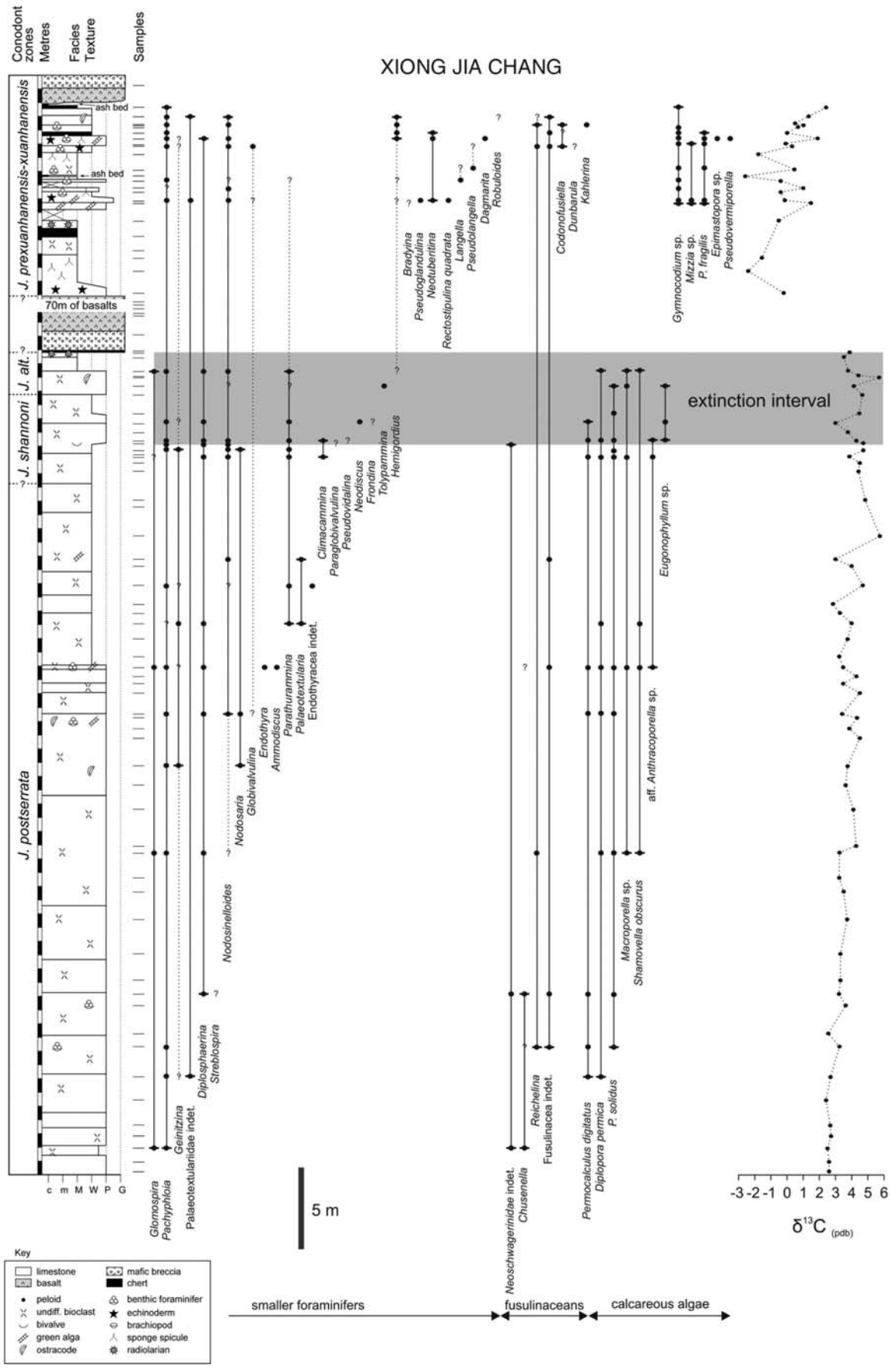

Fig. 2. Xiong Jia Chang section (26.5°N, 105.7°E), 40 km west of Zhijin, western Guizhou Province, showing the transition from Maokou Formation carbonates to volcanics at the base of the Emeishan province. Range charts for foraminifers and calcareous algae show the extinction to occur immediately below the first eruptive unit. These phenomena also coincide with a sharp negative carbon isotope excursion.

an interval within the early Capitanian Stage (*6*). In contrast, within the outcrop area of the igneous province, shallow-water carbonate rocks persisted longer but were abruptly drowned, whereupon deep-water radiolarian-spiculite chert became established. Conodont biostratigraphic control at the Xiong Jia Chang section, in western Guizhou (Fig. 2) and other sections (*7*), shows that the deepening occurred around the beginning of the *Jinogondolella altudaensis* zone in the mid-Capitanian. The brief phase of deep-water chert deposition was terminated by

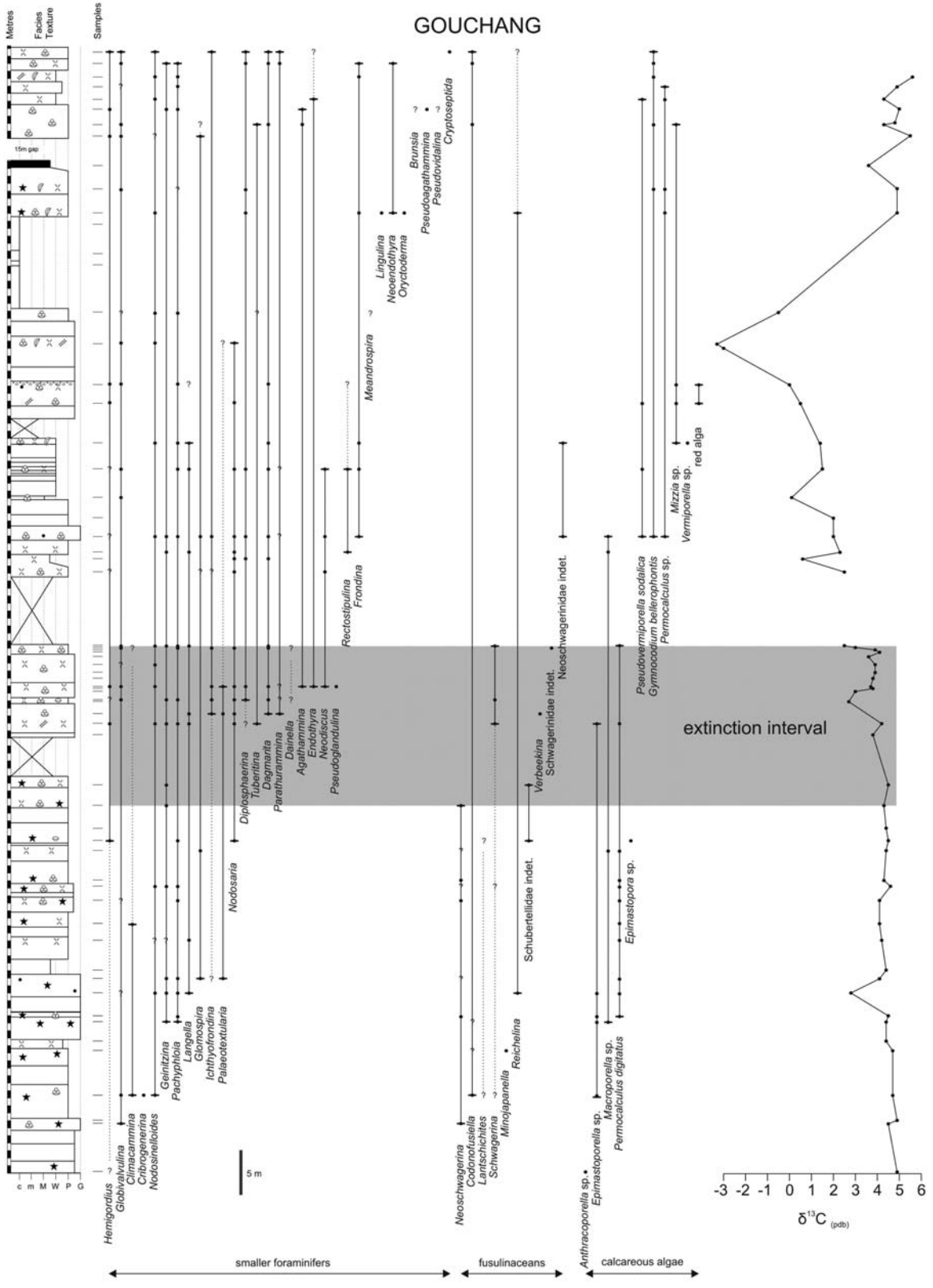

Fig. 3. Gouchang section, near Ziyun, central Guizhou, developed 50 km east of the eastern margin of the Emeishan province, showing the coincidence of the mass extinction level seen in range truncations of schwagerinids and calcareous algae. The post-extinction neoschwagerinids are fragmented and abraded specimens interpreted to be reworked from pre-extinction strata, but they may suggest that the interval of extinction is longer than depicted. A major negative shift of $\delta^{13}C$ isotope values (analyzed in whole-rock carbonate) is seen to occur after the extinction. Several gaps in this otherwise continuous road section may reflect the presence of shale and/or volcanic ash levels.

the onset of Emeishan volcanism. At Xiong Jia Chang, the basal volcanic rocks consist of a 70-m-thick composite unit comprising aphyric basalt and interbedded mafic volcaniclastic rocks. The latter are dominated by vesicular basalt clasts, many of which display chilled or glassy margins, which testify to an explosive style of mafic volcanism. Some clasts show a fiammé texture, typical of terrestrial emplacement, whereas others are dominated by palagonite-rimmed clasts, indicating subaqueous emplacement (*8*). Lithoclasts of platform carbonate, spiculite, and isolated marine fossils are also common (*8*), indicating that seafloor erosion accompanied emplacement. Such violent phreatomagmatic-style volcanism is typical of much of the early to mid-stages of Emeishan volcanism (*9*).

The initial phase of volcanism was followed by the reestablishment of diverse carbonate facies. Thus, at Xiong Jia Chang, the lowest volcanic pile is overlain by deep-water chert, with euxinic framboid populations (*10*); this unit is then abruptly succeeded by carbonate beds belonging to the *J. prexuanhanensis/J. xuanhanensis* assemblage zone, with a shallow-water microbiota (Fig. 2). Intertrappean limestone developments at other sections include *Tubiphytes* sponge reefs up to 30 m thick (*11*) and steep slope facies with allodapic limestones (*12*). The volcanic interregnum was terminated by the return of spectacular pyroclastic-phreatomagmatic volcanism and the deposition of individual mafic volcaniclastic beds approaching 200 m in thickness (*11*).

Fossil range data show that the collapse of carbonate platform deposition, shortly before the onset of eruptions, coincides with the disappearance of a shallow-water marine biota dominated by foraminifers and calcareous algae. Similar platform facies reappear above the basal volcanic pile, but many of the lost taxa do not (Fig. 2): The species-level composition of the calcareous algae shows complete turnover. The foraminifers also show extinctions, with the loss of the distinctive keriotheca-walled Schwagerinidae and Neoschwagerinidae and their replacement with assemblages consisting of small, long-ranging lagenides, the miliolinid *Hemigordius*, and small fusulinaceans (*Codonofusiella* and *Reichelina*).

This mid-Capitanian age for the mass extinction is substantially earlier than previous estimates (*13*, *14*). C isotope data (*15*) from Xiong Jia Chang reveal a 5 to 6 per mil (‰) negative shift above the lowest volcanic bed (Fig. 2). This big excursion postdates the extinction interval, which is within a phase of stable values around the *J. shannoni/J. altudaensis* zonal boundary. Similar faunal turnover is seen in the carbonate platform sections at Gouchang (Fig. 1), approximately 50 km east of the Emeishan volcanic margin, and here too it coincides with stable $\delta^{13}C$ values below a major negative excursion (Fig. 3). A similar large-amplitude negative excursion was reported from the mid-Capitanian in northern Sichuan Province, to the north of the Emeishan volcanic province (*6*). This excursion is now seen to be widespread (sites are up to 1000 km apart) and from several types of depositional environment (*16*), which suggests that it is a global signal. A further large negative excursion has been reported at the end of the Capitanian Stage (*17*), indicating that the post-extinction interval was marked by several large fluctuations.

The close temporal link between the onset of eruptions and extinction suggests a cause-and-effect scenario. Cooling and acid rain (caused by SO_2 effusion and sulfate aerosol formation) and consequent environmental deterioration are candidates for this link (*18*, *19*). The dominance of pyroclastic volcanism (rather than more quiescent-style flood basalt eruptions) in the initial eruptive stages of the Emeishan province and the large scale of the flows (30 to 200 m thick) suggest that such effects are likely to have been severe. The subsequent negative shift of C isotope values is too large to be attributed to relatively heavy volcanic CO_2 ($\delta^{13}C = -5‰$), but it may record the release of much lighter thermogenic C from the site of volcanism (*20*). This was in the aftermath of the biotic crisis, but the high diversity of the post-extinction biota suggests that the light C flux is not linked to any prolongation of the environmental stress that caused the extinction.

Our study of the volcano-sedimentary record of southwest China reveals that the Middle Permian marine crisis precisely coincided with the onset of Emeishan volcanism. This provides evidence for a potential link between mass extinction and the eruption of this igneous province, although the absolute time scale for the event is not yet known. The subsequent negative $\delta^{13}C$ excursion implies that the C cycle was destabilized for some time after the extinctions, perhaps by C release from thermogenic sources.

References and Notes

1. V. Courtillot, *Evolutionary Catastrophes: The Science of Mass Extinctions* (Cambridge Univ. Press, Cambridge, 1999).
2. P. B. Wignall, *Earth Sci. Rev.* **53**, 1 (2001).
3. G. Keller, T. Adatte, S. Gardin, A. Bartolini, S. Bajpai, *Earth Planet. Sci. Lett.* **268**, 293 (2008).
4. J. R. Ali, G. M. Thompson, X.-Y. Song, Y.-L. Wang, *Lithos* **79**, 475 (2005).
5. M.-F. Zhou *et al.*, *Earth Planet. Sci. Lett.* **196**, 113 (2002).
6. X.-L. Lai *et al.*, *Palaeogeogr. Palaeoclimatol. Palaeoecol.* **269**, 78 (2008).
7. Composite sections around Pingdi, on the Guizhou-Yunnan border, show the development of Maokou Formation platform carbonates overlain by deeper-water radiolarian cherts and slumped carbonates, with a conodont fauna spanning the *J. shannoni/J. altudaensis* zones. These are overlain by the lowest flood basalts of the Emeishan volcanic pile.
8. See supporting material on *Science* Online.
9. I. Ukstins Peate, S. E. Bryan, *Nat. Geosci.* **1**, 625 (2008).
10. Pyrite framboid populations from deep-water cherts in the basal *J. prexuanhanensis/J. xuanhanensis* assemblage zone at Xiong Jia Chang are dominated by framboids with a mean diameter of less than 7 μm, a characteristic of populations formed in anoxic bottom water (*21*).
11. A section on the eastern access road to Lugu Lake (27°41.711′N, 100°58.788′E) in northern Yunnan shows the lower Emeishan volcanic pile to be dominated by thick, mafic volcaniclastic flows. These are overlain by a 30-m-thick *Tubiphytes* sponge-cement reef, a further mafic volcaniclastic unit approaching 200 m thick, another limestone approximately 20 m thick, and finally a continuous section of basalt lavas, in excess of 1 km thick. These contain flows showing well-developed pillows.
12. The Pingchuan section (27°40.779′N, 101°53.104′E), a roadside section developed immediately to the east of the small town of Pingchuan (southern Sichuan), shows the main succession of Emeishan flood basalts to be underlain by alternations of clast-supported breccia beds (containing clasts of Maokou limestone, basalt, and dacite) and laminated cherty micrites yielding goniatites.
13. Y.-G. Jin *et al.*, *Episodes* **29**, 253 (2006).
14. K. Kaiho *et al.*, *Palaeogeogr. Palaeoclimatol. Palaeoecol.* **223**, 172 (2005).
15. Carbonate-C isotopes were measured at the stable isotope laboratory at the University of Leeds on CO_2 generated by the addition of anhydrous phosphoric acid to around 20 mg of powdered whole rock in a vacuum (*22*). Values are corrected with standard methods (*23*) and reported relative to the Vienna Pee Dee belemnite (VPDB) standard. The analytical precision for this analysis, based on replicate analyses of an in-house strontium carbonate standard, is estimated at 0.1‰.
16. The negative $\delta^{13}C$ excursion at Xiong Jia Chang (analyzed in whole-rock carbonate) occurs within a section showing abrupt deepening from platform carbonate to deep-water, calcareous chert deposition associated with the development of the Zhijin Basin, a north-south rift structure developed immediately before volcanism (*24*). The excursion at Gouchang occurs within a shallow-water platform carbonate succession. A potential third example of the excursion is seen in the upper part of unit 2 of the Maokou Formation at the Chaotian section in northern Sichuan, where it occurs within lagoonal carbonates on the southern margin of the North Yangtze Basin (*6*).
17. W. Wang, C.-Q. Cao, Y. Wang, *Earth Planet. Sci. Lett.* **220**, 57 (2004).
18. S. Self, M. Widdowson, T. Thordarson, A. E. Jay, *Earth Planet. Sci. Lett.* **248**, 517 (2006).
19. S. Self, S. Blake, K. Sharma, M. Widdowson, S. Sephton, *Science* **319**, 1654 (2008).
20. G. J. Retallack, A. H. Jahren, *J. Geol.* **116**, 1 (2008).
21. P. B. Wignall, R. Newton, *Am. J. Sci.* **298**, 537 (1998).
22. J. M. McCrea, *J. Chem. Phys.* **18**, 849 (1950).
23. H. Craig, *Geochim. Cosmochim. Acta* **12**, 133 (1957).
24. B. He, Y.-G. Xu, Y.-M. Wang, Z.-Y. Luo, *J. Geol.* **114**, 117 (2006).

25. We thank for funding the Natural Environment Research Council (grant no. NE/D011558/1), Natural Science Foundation of China (grants nos. 40872002, 406210022, and 40232025), Chinese State Administration of Foreign Experts Affairs (grant B08030), and Hong Kong Research Grant Council (grant no. HKU700204).

Supporting Online Material

www.sciencemag.org/cgi/content/full/324/5931/1179/DC1
Fig. S1

6 February 2009; accepted 26 March 2009
10.1126/science.1171956

Implications of Limiting CO_2 Concentrations for Land Use and Energy

Marshall Wise, Katherine Calvin, Allison Thomson, Leon Clarke, Benjamin Bond-Lamberty, Ronald Sands,* Steven J. Smith, Anthony Janetos, James Edmonds†

Limiting atmospheric carbon dioxide (CO_2) concentrations to low levels requires strategies to manage anthropogenic carbon emissions from terrestrial systems as well as fossil fuel and industrial sources. We explore the implications of fully integrating terrestrial systems and the energy system into a comprehensive mitigation regime that limits atmospheric CO_2 concentrations. We find that this comprehensive approach lowers the cost of meeting environmental goals but also carries with it profound implications for agriculture: Unmanaged ecosystems and forests expand, and food crop and livestock prices rise. Finally, we find that future improvement in food crop productivity directly affects land-use change emissions, making the technology for growing crops potentially important for limiting atmospheric CO_2 concentrations.

There is increasing concern over the connection between fossil and industrial emissions and terrestrial ecosystem emissions, and the implications of this interaction for climate change mitigation strategies. Several research studies (*1*–*8*) have shown that the outcome of imposing a mitigation regime that only values carbon from energy and industrial sources creates incentives to increase bioenergy. As the use of bioenergy increases, land uses shift from food and fiber crops, forests, and unmanaged ecosystems to dedicated biomass crops. This in turn increases terrestrial carbon emissions globally—a perverse result of curbing energy and industrial emissions.

Terrestrial systems hold ~2000 Pg C in soils and aboveground biomass (*9*), and a long history of research has highlighted the benefits of slowing or reversing carbon emissions that occur with land-use change. Because the total carbon emissions budget for 2005 to 2100 would have to be kept below ~500 Pg C to keep the atmospheric CO_2 concentration from exceeding 450 parts per million (ppm) (*8*, *10*), terrestrial emissions must be limited, in addition to energy and industrial emissions.

Numerous integrated analyses have examined the implication of limiting the concentration of atmospheric CO_2 with prescribed land use and land-use change assumptions. This literature is summarized by the Intergovernmental Panel on Climate Change (IPCC) (*11*). Here, we examine

Pacific Northwest National Laboratory, Joint Global Change Research Institute at the University of Maryland–College Park, 5825 University Research Court, Suite 3500, College Park, MD 20740, USA.

*Present address: Economic Research Service, U.S. Department of Agriculture, 1800 M Street NW, Washington, DC 20036, USA.

†To whom correspondence should be addressed. E-mail: jae@pnl.gov

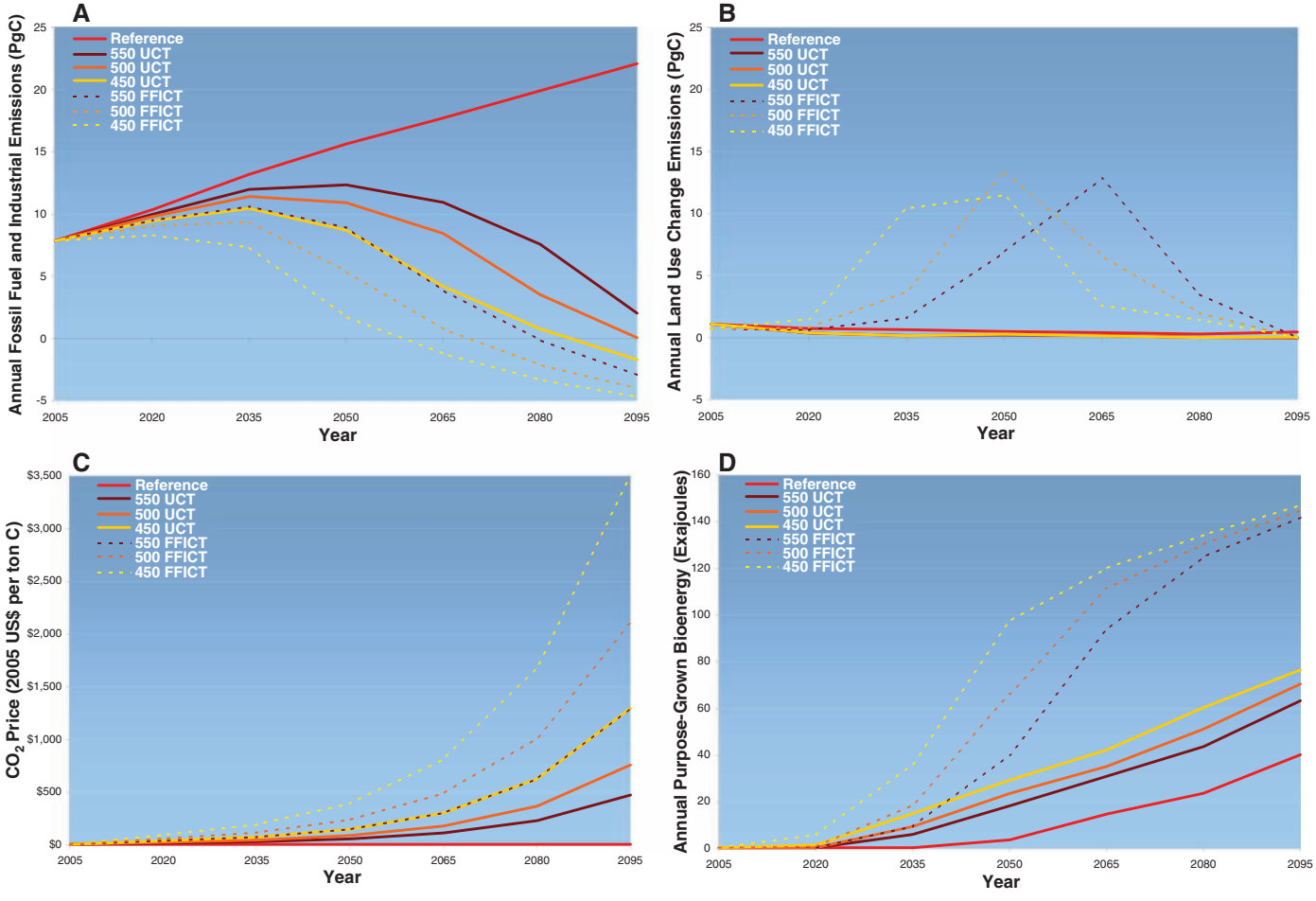

Fig. 1. A comparison of three alternative CO_2 concentration targets under UCT pathways that limit fossil fuel, industrial, and terrestrial carbon emissions with a common carbon tax on emissions to the corresponding FFICT scenarios in which only fossil fuel and industrial emissions are controlled to achieve the same CO_2 concentration. (**A**) Fossil fuel and industrial carbon emissions under these pathways. (**B**) Corresponding carbon emissions from land-use changes. (**C**) Carbon taxes associated with these CO_2 concentration targets and pathways. (**D**) Global quantity of purpose-grown biomass energy in each of these scenarios.

the implications for land use and land-use change from limiting atmospheric CO_2 concentrations in an analysis that endogenously integrates land use with demands in both the agriculture and energy systems.

The results from this integrated assessment study show that if terrestrial carbon emissions are valued equally with carbon emissions from energy and industrial systems in a regime designed to limit atmospheric CO_2 concentrations, there are wide-ranging differences from the case where only carbon emissions from energy and industrial systems are valued. Deforestation is replaced by afforestation, crop prices rise, purpose-grown bioenergy becomes an important agricultural product, and people shift away from consumption of beef and other carbon-intensive protein sources. Further, the total cost of limiting atmospheric CO_2 concentrations is reduced, relative to an alternative regime that prices only fossil fuel and industrial carbon emissions, which implies that lower atmospheric CO_2 concentrations are achievable for any commitment of society's resources, a result consistent with other studies (*12*–*14*) that have examined the potential role of afforestation in limiting CO_2 concentrations. We also find that for any given atmospheric CO_2 limitation goal, the reduction in the cost relative to an alternative regime that prices only fossil fuel and industrial carbon emissions becomes more pronounced as the concentration limit is lowered. We further find that the assumed rate of improvement in crop productivity has a strong influence on land-use change emissions and, correspondingly, on the cost of mitigating climate change.

We employ the Joint Global Change Research Institute's MiniCAM integrated assessment model (*15*–*20*) to explore the implication of limiting atmospheric CO_2 concentrations at levels ranging from 450 ppm to 550 ppm. MiniCAM is a dynamic recursive model of energy, economy, agriculture, land use, and land cover that fully integrates the energy and agriculture systems with economic equilibrium in energy and agriculture markets. Our analysis employs the MiniCAM scenario documented in (*8*) but with an updated, fully integrated terrestrial ecosystem component as described in (*15*, *16*). This MiniCAM scenario assumes a growing population, an increasing standard of living, and the improvement of technology over time. Available energy technology options include CO_2 capture and storage (CCS); hydrogen production and use; nuclear energy; wind, solar, and geothermal power; improved end-use energy technologies in the building, industry, and transportation sectors; and bioenergy. We consider bioenergy production from biological waste streams and next-generation bioenergy from cellulosic (purpose-grown) bioenergy crops. In our reference scenario, we assume that the productivity of land-based products is subject to change over time based on future estimates of crop productivity change up to 2030 (*21*) and then converges to 0.25% per year thereafter (*15*). Land use is determined endogenously in MiniCAM by market forces (*15*, *22*). We also consider fossil fuel, industrial, and land-use change emissions in response to policy intervention modeled as a carbon tax. The distribution of terrestrial carbon reservoirs and their rates of change are computed endogenously in MiniCAM. Emissions limitation scenarios treat bioenergy as carbon neutral in the energy system. We assume that bioenergy can be used in a wide range of applications, including liquefaction to create fuels for transport. We also consider options to gasify bioenergy and use it in conjunction with CCS to make electricity. Market forces are assumed to determine the highest value applications.

We limit the concentration of atmospheric CO_2 by imposing a global carbon tax on anthropogenic carbon emissions (*23*). We consider two canonical tax regimes: (i) a Universal Carbon Tax regime (UCT) in which all carbon emissions in all sectors—including emissions from land-use change—and all regions of the world have

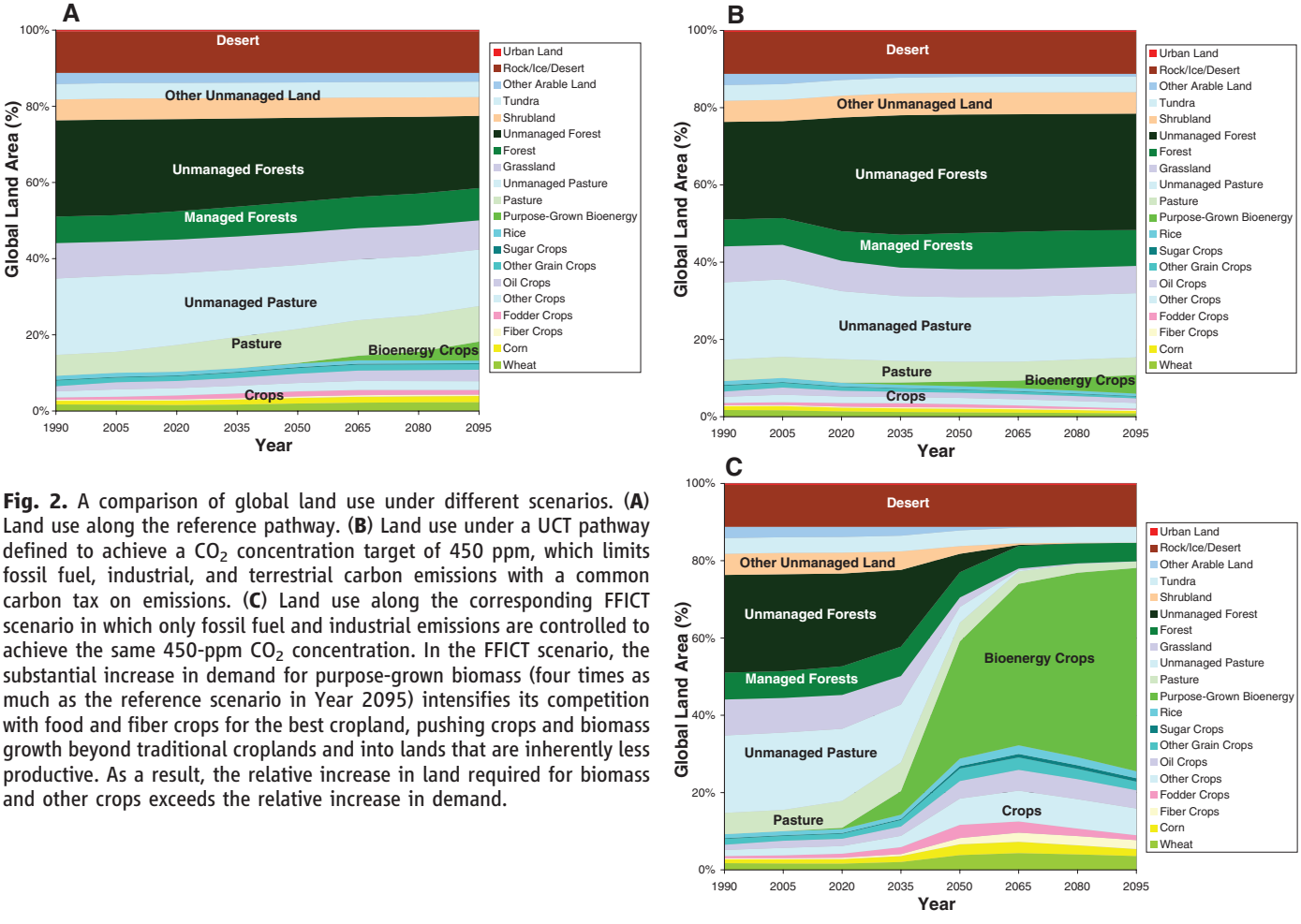

Fig. 2. A comparison of global land use under different scenarios. (**A**) Land use along the reference pathway. (**B**) Land use under a UCT pathway defined to achieve a CO_2 concentration target of 450 ppm, which limits fossil fuel, industrial, and terrestrial carbon emissions with a common carbon tax on emissions. (**C**) Land use along the corresponding FFICT scenario in which only fossil fuel and industrial emissions are controlled to achieve the same 450-ppm CO_2 concentration. In the FFICT scenario, the substantial increase in demand for purpose-grown biomass (four times as much as the reference scenario in Year 2095) intensifies its competition with food and fiber crops for the best cropland, pushing crops and biomass growth beyond traditional croplands and into lands that are inherently less productive. As a result, the relative increase in land required for biomass and other crops exceeds the relative increase in demand.

the same value at any point in time, and (ii) a Fossil Fuel and Industrial Emissions Carbon Tax regime (FFICT) in which the carbon tax is applied to fossil fuel and industrial emissions but not to terrestrial carbon emissions. In both cases, the carbon tax rises over time so as to limit atmospheric CO_2 concentrations to a prescribed level.

Whether the carbon tax is applied as a UCT or a FFICT has important implications for the source of emissions and for land-use patterns. Placing an increasingly stringent tax on only the fossil fuel and industrial carbon emissions without placing any corresponding tax on terrestrial carbon (i.e., the FFICT regime) causes land-use change emissions to increase to a peak greater than 10 Pg C per year, as lands are converted to meet the growing demands for purpose-grown bioenergy crops in a growing but decarbonizing energy system (Fig. 1). This is the same effect observed by earlier studies, including (*1*, *3*). The increased demand for bioenergy crops pushes land requirements beyond traditional croplands and into lands that are increasingly less productive, requiring increasing quantities of land to grow each successive unit of agricultural product. The result is that in the FFICT regimes virtually all land that is not required for growing food and forest products is used for growing bioenergy (Fig. 2).

Such grand-scale deforestation is hard to imagine in reality, because it is hard to imagine that society would find this result acceptable. Nevertheless, this admittedly extreme case stands in sharp contrast to the UCT regime in which land-use change emissions face the same carbon tax as fossil fuel and industrial emissions. The application of a carbon tax to terrestrial carbon emissions sends an increasingly strong price signal that expands forested land while land dedicated to bioenergy crop production is limited (Fig. 2) (*24*), although bioenergy remains an important technology in the overall mitigation portfolio. The difference in cumulative land-use change emissions between the FFICT and UCT regimes, from 2005 through 2100, ranges from >300 Pg C (550-ppm limit) to >400 Pg C (450-ppm limit).

For any given concentration limit, the proportion of emissions from fossil fuel and industrial sources and land-use change is affected by the tax regime. The UCT regime results in a higher proportion of emissions from fossil fuel and industrial sources, with a correspondingly lower proportion of emissions from land-use change (*25*). Equivalently, at any given carbon price, carbon emissions are lower when terrestrial carbon is valued.

Applying a carbon tax to all carbon emissions (the UCT regime) reduces economic impacts relative to the FFICT approach. At all atmospheric CO_2 concentration limits, we find that the resulting carbon tax under the UCT regime was less than half that of the carbon tax resulting from the FFICT regime. This reduction in economic impacts flows naturally from economic principles. The UCT regime covers all emissions sources rather than a subset of emissions sources and thus is economically more efficient.

We also note that crop (including food and fiber) prices rise in the UCT regime as a consequence of the economic impact from valuing terrestrial carbon, even in the absence of purpose-grown bioenergy crops. This follows directly from limitations on land availability and the expanded use of land in the form of managed forests and unmanaged ecosystems in the UCT scenarios. The crop price increase is highest for the most carbon-intensive agricultural activities, and the crop price effect becomes more pronounced for stricter concentration limits. Changing agricultural prices flowing from the UCT also drive changes in dietary composition, reducing emphasis on beef and other carbon-intensive protein sources, which in turn frees up land for bioenergy and other crop production.

By comparing results to scenarios in which no purpose-grown bioenergy crops are allowed, Fig. 3 decomposes the effects of valuing carbon on crop prices, using corn prices as representative. The figure shows that there is virtually no discernible effect on corn prices in the reference scenario when purpose-grown bioenergy crops are removed from the analysis. However, when CO_2 concentration is limited (to 500 ppm here, for example), both valuing terrestrial carbon and allowing purpose-grown bioenergy exert upward pressure on crop prices.

Finally, terrestrial carbon emissions are sensitive to crop productivity growth assumptions. As a sensitivity experiment, we held crop productivity constant at 2005 levels. Land-use change carbon emissions in a scenario where no climate policy was imposed were more than 70 Pg C higher over the 21st century because greater amounts of land were necessary to produce the same amount of food. In the "frozen productivity" scenario, crop land expansion dramatically encroaches on forested lands, releasing the carbon stored in forest vegetation and soils. The difference in land-use change emissions in 2050 is larger than one "wedge" (*26*), defined as approximately 1 Pg C per year in 2050. Improved crop productivity thus has the potential to reduce anthropogenic carbon emissions at a magnitude similar to the energy technologies identified by other studies (*26*, *27*).

Limiting atmospheric CO_2 concentrations through a comprehensive approach that fully incorporates both terrestrial emissions and fossil and industrial emissions carries with it profound implications for forests, crop and livestock prices, diet, the global energy system, and the cost of meeting environmental goals. However, in this study we have not examined the implications for non-CO_2 emissions, which are a major component of terrestrial system emissions. These interactions are important, as was shown by (*6*, *28*). Another limitation of this study is water, which we have not explicitly modeled.

Most of the world's fossil fuel and industrial carbon emissions today carry no value, explicit or implicit. Considerable research has investigated alternative mechanisms for pricing fossil fuel and industrial carbon, both explicitly through taxes or cap-and-trade regimes and implicitly through regulatory frameworks. Less attention has been placed on developing methods of associating carbon values with terrestrial systems, at least in part because they are less straightforward than those dealing with fossil fuel carbon emissions and because the cost of implementing emissions mitigation policies in terrestrial systems would probably be higher than in the energy system. The development of methods for conveying carbon values to land-use decision-makers could substantially improve the environmental effectiveness of global carbon emissions limitation systems. Improved land-use management and improved agricultural practices could reduce upward pressure on crop prices and the cost of emissions mitigation. However, the allocation of scarce land resources to competing ends will remain a major challenge for the 21st century.

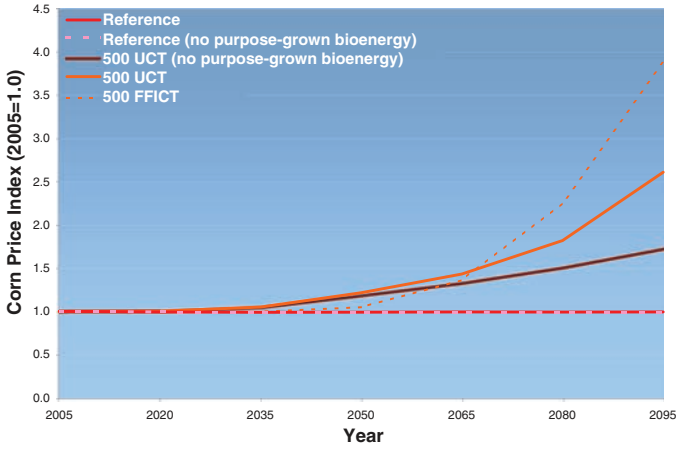

Fig. 3. The price of corn associated with a reference pathway; a pathway defined to achieve a UCT CO_2 concentration target of 500 ppm in 2095, which limits fossil fuel, industrial, and terrestrial carbon emissions with a common carbon tax on emissions; and a comparison to the corresponding FFICT scenario in which only fossil fuel and industrial emissions are controlled to achieve the same CO_2 concentration. To isolate the impact of bioenergy on the price, a second reference pathway and a second UCT-derived 500-ppm 2095 CO_2 concentration target pathway are constructed under the assumption that no purpose-grown bioenergy is available.

References and Notes

1. J. A. Edmonds *et al.*, in *Greenhouse Gas Control Technologies*, J. Gale, Y. Kaya, Eds. (Pergamon, Amsterdam, 2003), pp. 1427–1432.
2. J. Fargione *et al.*, *Science* **319**, 1235 (2008).
3. T. Searchinger *et al.*, *Science* **319**, 1238 (2008).
4. M. R. Schmer *et al.*, *Proc. Natl. Acad. Sci. U.S.A.* **105**, 464 (2008).
5. K. T. Gillingham, S. J. Smith, R. D. Sands, *Mitig. Adapt. Strategies Glob. Change* **13**, 675 (2008).
6. P. J. Crutzen, A. R. Mosier, K. A. Smith, W. Winiwarter, *Atmos. Chem. Phys.* **8**, 389 (2008).
7. A. Gurgel, J. M. Reilly, S. Paltsev, *J. Agric. Food Ind. Org.* **5** (no. 2), article 9 (2007); www.bepress.com/jafio/vol5/iss2.
8. L. Clarke *et al.*, *CCSP Synthesis and Assessment Product 2.1, Part A: Scenarios of Greenhouse Gas Emissions and Atmospheric Concentrations* (U.S. Government Printing Office, Washington, DC, 2007).
9. IPCC, *Climate Change 2007: The Physical Science Basis. Working Group I Contribution to the Fourth Assessment Report of the Intergovernmental Panel on Climate Change*, S. Solomon *et al.*, Eds. (Cambridge Univ. Press, Cambridge, 2007), fig. 7.3, chap. 7, p. 515.
10. About 800 Pg C can be emitted if the atmospheric CO_2 concentrations are held below 550 ppm.
11. IPCC, *Climate Change 2007: Mitigation of Climate Change. Contribution of Working Group III to the Fourth Assessment Report of the Intergovernmental Panel on Climate Change*, B. Metz, O. R. Davidson, P. R. Bosch, R. Dave, L. A. Meyer, Eds. (Cambridge University Press, Cambridge, 2007), chap. 3.
12. S. Rose *et al.*, *Land in Climate Stabilization Modeling: Initial Observations, Stanford Energy Modeling Forum*, EMF21, Land Modeling Subgroup; www.stanford.edu/group/EMF/projects/EMF21/EMF21FinalReport.pdf (2008).
13. M. Tavoni, B. Sohngen, V. Bosetti, *Energy Policy* **35**, 5346 (2007).
14. D. Rokityanskiy *et al.*, *Technol. Forecast. Soc. Change* **74**, 1057 (2007).
15. M. Wise *et al.*, The Implications of Limiting CO_2 Concentrations for Agriculture, Land-use Change Emissions, and Bioenergy (Tech. Rep. PNNL-18341; available at www.pnl.gov/gtsp/publications/2009/200902_co2_landuse.pdf) (2009).
16. Materials and methods are available as supporting material on *Science* Online.
17. S. H. Kim, J. A. Edmonds, J. Lurz, S. J. Smith, M. A. Wise, *The Energy Journal*, Special Issue: Hybrid Modeling of Energy-Environment Policies: Reconciling Bottom-up and Top-down, Special Issue No. 2, 63 (2006).
18. L. Clarke *et al.*, *Model Documentation for the MiniCAM Climate Change Science Program Stabilization Scenarios: CCSP Product 2.1a* (PNNL Tech. Rep. PNNL-16735, 2007).
19. A. Brenkert, S. Smith, H. Kim, H. Pitcher, *Model Documentation for the MiniCAM. Pacific Northwest National Laboratory* (PNNL Tech. Rep. PNNL-14337, 2003).
20. J. Edmonds, J. Reilly, *Global Energy: Assessing the Future* (Oxford Univ. Press, New York, 1985).
21. J. Bruinsma, *World Agriculture: Towards 2015/2030: An FAO Perspective* (available at www.fao.org/docrep/005/y4252e/y4252e00.HTM) (2003).
22. R. D. Sands, M. Leimbach, *Clim. Change* **56**, 185 (2003).
23. The carbon tax serves in the model as a means to place an economic value on carbon. The same mitigation actions could be achieved through a variety of policy mechanisms, including cap-and-trade approaches. The carbon tax approach is used here because of its simplicity and explanatory value, but the results would hold under different approaches that place a value, implicit or explicit, on carbon.
24. Our analysis finds that bioenergy derived from biological waste streams (e.g., agriculture and forestry residues) is potentially of comparable magnitude to purpose-grown bioenergy production in the UCT policy regimes.
25. Negative net annual global FFI carbon emissions observed in Fig. 1 for the 450-ppm atmospheric CO_2 concentration limit are the result of employing bioenergy for power production in conjunction with CCS.
26. S. Pacala, R. Socolow, *Science* **305**, 968 (2004).
27. M. I. Hoffert *et al.*, *Science* **298**, 981 (2002).
28. P. L. Lucas, D. P. van Vuuren, J. G. J. Olivier, M. G. J. den Elzen, *Environ. Sci. Policy* **10**, 85 (2007).

29. The authors are grateful to the U.S. Department of Energy's Office of Science and to the Electric Power Research Institute for financial support for the research the results of which are reported here. The authors also thank E. Malone for helpful comments on an earlier draft. Of course, the opinions expressed here are the authors' alone.

Supporting Online Material

www.sciencemag.org/cgi/content/full/324/5931/1183/DC1
Materials and Methods
SOM Text
Figs. S1 and S2
Table S1
References

13 November 2008; accepted 23 March 2009
10.1126/science.1168475

Penultimate Deglacial Sea-Level Timing from Uranium/Thorium Dating of Tahitian Corals

Alex L. Thomas,[1]* Gideon M. Henderson,[1] Pierre Deschamps,[2] Yusuke Yokoyama,[3,4,5] Andrew J. Mason,[1] Edouard Bard,[2] Bruno Hamelin,[2] Nicolas Durand,[2] Gilbert Camoin[2]

The timing of sea-level change provides important constraints on the mechanisms driving Earth's climate between glacial and interglacial states. Fossil corals constrain the timing of past sea level by their suitability for dating and their growth position close to sea level. The coral-derived age for the last deglaciation is consistent with climate change forced by Northern Hemisphere summer insolation (NHI), but the timing of the penultimate deglaciation is more controversial. We found, by means of uranium/thorium dating of fossil corals, that sea level during the penultimate deglaciation had risen to ~85 meters below the present sea level by 137,000 years ago, and that it fluctuated on a millennial time scale during deglaciation. This indicates that the penultimate deglaciation occurred earlier with respect to NHI than the last deglacial, beginning when NHI was at a minimum.

Fossil corals are a valuable archive of past sea level, but the density of coral data is biased toward sea-level highstands because of the inaccessibility of fossil corals that grew during lower sea level and are now further submerged. Reconstruction of lower sea levels has relied on dredging and submersible sampling, occasional fortuitous finds in uplifted terraces (*1*, *2*), and the challenging approach of coral-reef drilling. Such drilling, while technically demanding and expensive, has yielded valuable records of sea-level change for the last deglacial (*3*, *4*) and more limited constraints on the onset of the last interglacial (*5*).

To target deeper and earlier portions of the sea-level curve, Integrated Ocean Drilling Program (IODP) Expedition 310 (known as the "Tahiti Sea Level" expedition) drilled submerged reefs in seawaters ranging from 41.7 to 117.5 m (*6*). The island of Tahiti Nui (French Polynesia) is located in the southern tropical Pacific and is distant from locations of glacial ice sheets. Sea-level change at Tahiti during deglaciation is therefore dominated by the addition of meltwater to the oceans rather than by the effects of ice mass redistribution and isostacy. Steady subsidence of 0.25 m per 1000 years (*4*), resulting from the load of the island on the underlying oceanic plate coupled with a location distant from ice loading, makes Tahiti an ideal site to reconstruct past sea levels. Material from before the Last Glacial Maximum was recovered at each of the three locations where Tahiti drilling was performed (Faaa, Maraa, and Tiarei) (*6*) (fig. S1) and seven separate cores have yielded pre-LGM corals suitable for U/Th dating from 113 to 147 m below sea level (mbsl).

Corals were screened for secondary calcite and aragonite by x-ray diffraction (XRD) and thin-section petrography. Of the 25 pre-LGM corals analyzed for U-Th isotopes (*7*), 12 had values of $(^{234}U/^{238}U)_i$ ($^{234}U/^{238}U$ ratios corrected for decay since deposition) between 137 and 151 per mil (‰), which we take as a reasonable range on the basis of known variability of past seawater $^{234}U/^{238}U$ ratios during the glacial-interglacial cycle (*5*, *8*). These 12 are considered pristine and are discussed further here; replicate measurements that differ significantly have been excluded from discussion (but are illustrated in Fig. 1B as small circles).

Corals of marine isotope stage 3 (MIS 3) age, after a correction for subsidence [0.25 m per 1000 years (*4*)], occur at 105 to 130 mbsl with ages

[1]Department of Earth Sciences, Oxford University, Parks Road, Oxford OX1 3PR, UK. [2]CEREGE (UMR 6635), Aix-Marseille Université, CNRS, IRD, Collège de France, Europole de l'Arbois, BP80, 13545 Aix-en-Provence, France. [3]Ocean Research Institute, University of Tokyo, Tokyo 164-8639, Japan. [4]Department of Earth and Planetary Sciences, Graduate School of Science, University of Tokyo, Tokyo 113-0033, Japan. [5]Institute for Research on Earth Evolution, Japan Agency for Marine-Earth Science and Technology, Yokosuka 237-0061, Japan.

*To whom correspondence should be addressed. E-mail: alext@earth.ox.ac.uk

of 29,600 to 33,000 years ago (29.6 to 33.0 ka) and are considered to be in situ (table S1 and fig. S2). They have $(^{234}U/^{238}U)_i$ values that agree closely with one another, and there is no indication of alteration. These new coral data, once corrected for subsidence, are at substantially greater depth (by ~30 to 40 m) than corals of similar age from the Huon Peninsula (*9*, *10*)—corrected for uplift—and are also at a similarly greater depth with respect to $\delta^{18}O$-based reconstructions of sea level from the Red Sea (*11*, *12*) (Fig. 1A). This difference is too large to be accounted for by variability of the non-eustatic component of relative sea level (RSL) at far-field sites (distant from ice sheets), or error in the subsidence/uplift rates.

The most plausible explanation for the discrepancy between the new Tahitian coral data and sea-level reconstructions from the Red Sea and Huon Peninsula is that they grew in deeper water. The MIS 3 corals are part of an assemblage (encrusting *Montipora* and foliaceous *Pachyseris*, thinly encrusted by coralline algae, with the absence of infilling muds) suggesting a deeper forereef subfacies and indicative of paleo–water depths greater than 20 m (*13*). Such paleodepths are consistent with sea level remaining at ~80 mbsl until at least 29.6 ka, in agreement with records from the Huon Peninsula (*9*, *10*) and Red Sea (*11*, *12*).

Subsidence-corrected depths of two MIS 6 corals (310-M0009D-25R-2W-41,49 and 310-M0009D-25R-2W-52,55) are at 109 mbsl (Fig. 1B). The abundance of tabular *Acropora* and massive *Porites*, coupled with the presence of thick algal crusts on the upper surfaces of corals and their incorporation in a coarse sandy matrix, suggests a facies similar to "robust-branching coral" (*13*) and indicates a probable depth of 0 to 6 m for these samples. These samples therefore provide the first coral-based estimate of sea level during the fully glacial portion of MIS 6. From 153.4 (±0.5) to 152.7 (±0.7) ka, RSL at Tahiti was <109 mbsl and likely within 6 m of this (i.e., in the range 103 to 109 m). Glacial isostatic adjustment modeling has indicated that, at the LGM, RSL at Tahiti was 6 (±6) m lower than the purely eustatic ice volume equivalent sea level (ESL) (*14*). If ice loadings during MIS 6 and at the LGM were broadly similar, as seems a reasonable approximation, a similar discrepancy would have occurred and ESL would be 97 to 103 mbsl at 153 ka. It is likely that sea level fell slightly further after 153 ka toward the penultimate glacial maximum as suggested by $\delta^{18}O$ (*15*) (Fig. 1B).

Two corals are from early in the penultimate deglacial. Replicate analyses of coral 310-M0019A-29R-1W-0,4 are in agreement: 136.9 (±0.9) and 137.8 (±0.4) ka. As with the MIS 3 and MIS 6 samples, this coral has no calcite, no aragonite overgrowths, and no signs of visible alteration. The two analyses have $(^{234}U/^{238}U)_i$ values within error (2 standard deviations) of one another and within the expected seawater range. The age of this coral indicates that RSL must have risen to <85 mbsl by 137 ka. Another coral (310-M0019A-27R-1W-62,83) has a similar uplift-corrected depth but younger replicate ages of 133.1, 133.2, and 134.0 ka (Fig. 1B). This may reflect drowning of the reef after 137 ka, with accretion unable to keep up with rising sea level across the deglaciation. Alternatively, sea level may have risen to an early highstand shortly after 137 ka and then fallen back to within 20 m of the

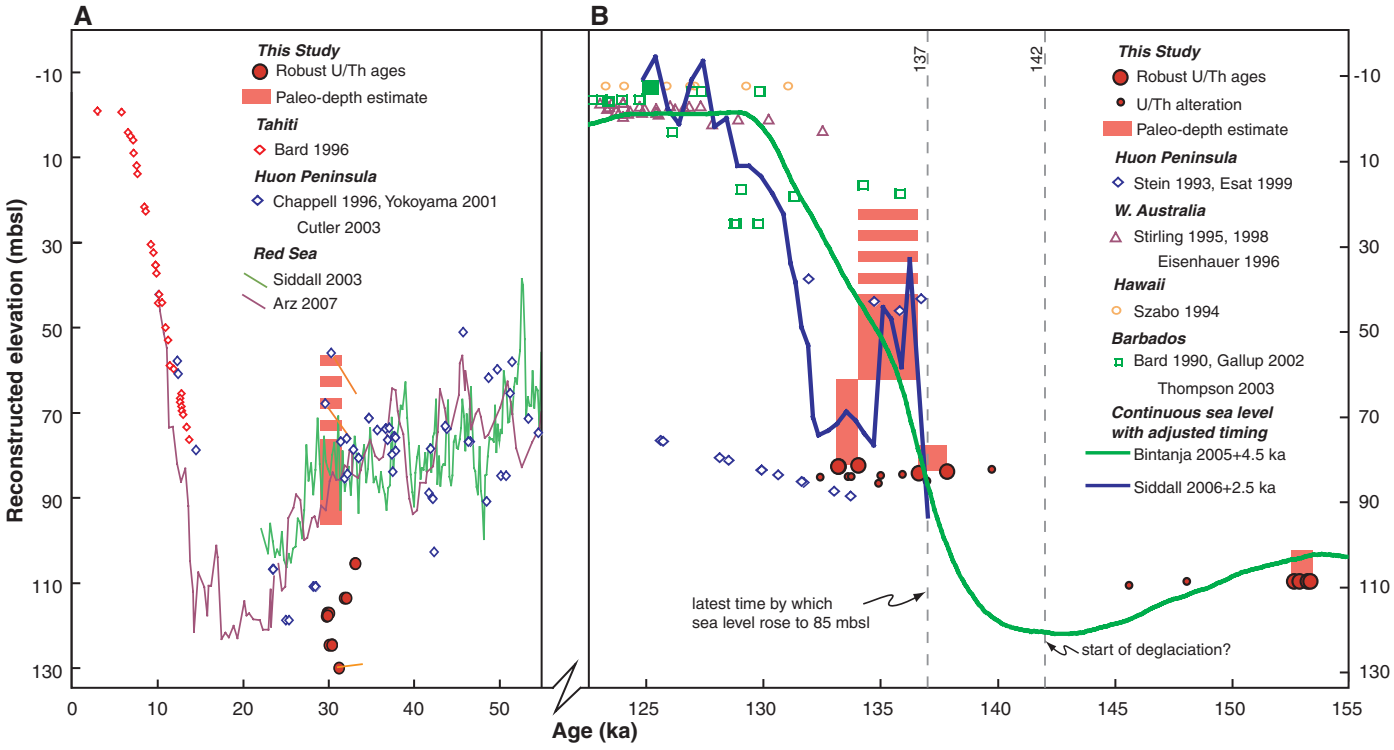

Fig. 1. Sea-level plot for MIS 3, the penultimate deglaciation, and MIS 6. (**A**) Age versus subsidence-corrected depth plot, showing in situ samples measured in this study as solid red circles. Paleo–water depth estimate of greater than 20 m is illustrated with a red bar; the dashed continuation illustrates the possibility that water depth may have been even greater. Subsidence rate used is 0.25 m per 1000 years for consistency with the previous coral record from Tahiti (*4*). Shown for comparison are ages versus reconstructed depth for corals from the Huon Peninsula [blue diamonds (*9*, *10*, *30*)]. Subsidence/uplift rates are illustrated for both Tahiti and a section of the Huon Peninsula by orange lines. Sea-level reconstructions from the Red Sea are shown in green (*11*) and purple (*12*). The deglacial coral sea-level record from Tahiti (*4*) is shown in red diamonds. (**B**) Subsidence/uplift-corrected coral elevations versus age, for the penultimate deglaciation. New data from this study are reported as solid red circles; small circles are corals that are interpreted to have undergone some alteration, whereas large circles are considered to have robust chronology. Red boxes represent paleodepth estimates based on fossil assemblages and lithologies (*13*); the dashed continuation illustrates the large possible depth range of these facies. Existing coral data (*1*, *2*, *5*, *31*–*35*) are shown as open symbols. A coral from Bard *et al.* (*5*) is shown (green-filled square), from which the timing of MIS 5e in Lisiecki and Raymo (*18*) is constrained. Two proposed sea-level curves are shown for the deglacial: The green line is a sea-level reconstruction based on an ice sheet model and high-latitude air temperature (*15*), but with the chronology adjusted to be 4500 years older on the basis of Tahiti coral data; the blue line is a RSL reconstruction from the Red Sea (*16*) with the chronology adjusted +2500 years. The gray dashed vertical lines are timing constraints of the deglaciation for the suggested start (142 ka) and the time by which sea level must have risen above 85 mbsl at Tahiti (137 ka).

310-M0019A-27R-1W-62,83 sample by 133 ka. Such a millennial-scale sea-level fluctuation has been suggested previously on the basis of Huon Peninsula corals (*2*) and Red Sea $\delta^{18}O$ (*16*). This interpretation is supported by the lithology and fossil assemblage of the M00019A cores. Sample 310-M0019A-29R-1W-0,4 is from a unit containing a coralgal framework dominated by *Acropora*, suggestive of shallow water depth, whereas 310-M0019A-27R-1W-62,83 is from a framework of massive *Porites* indicating a water depth from 0 to 25 m (*13*) (fig. S3). Although no U/Th ages were successful in the core section between these two dated samples, this section contains a coralgal framework of encrusting *Porites* that suggests development in deeper water during an early sea-level highstand. This sedimentological evidence suggests a reversal of sea level during the penultimate deglacial, in agreement with earlier studies (*2*, *16*). The magnitude of this early highstand—about two-thirds of the total deglaciation—makes it substantially larger than millennial-scale variability such as that seen during MIS 3 (*17*).

The Tahiti coral data alone indicate that global ice volume must have reduced markedly between 153 and 137 ka. A more detailed reconstruction

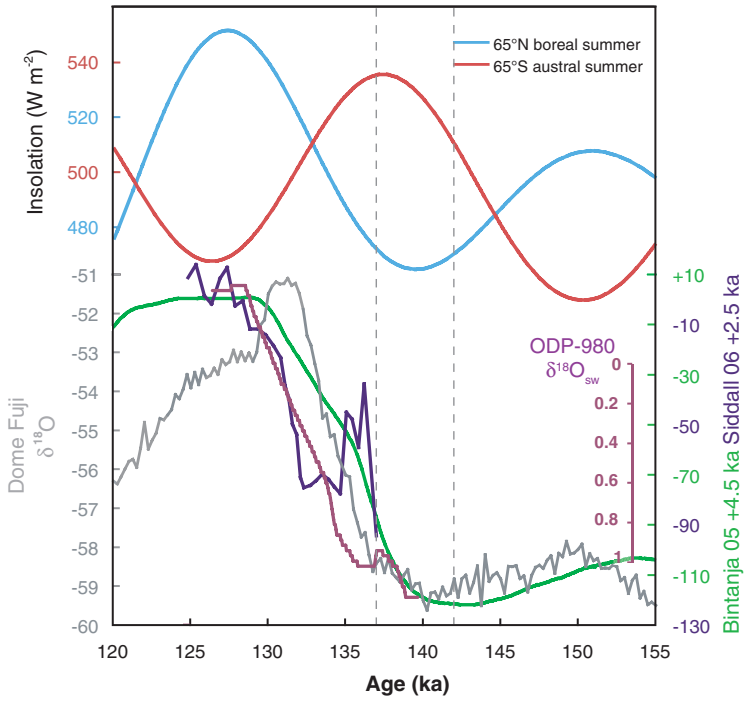

Fig. 2. The timing of the penultimate deglacial, illustrated with the data of Bintanja *et al*. (*15*) (in green), with the chronology adjusted (+4500 years) to match new coral data of this study (Fig. 1B), and the Red Sea record of Siddall *et al*. (*16*) (in dark blue), adjusted by +2500 years. The Dome Fuji ice core $\delta^{18}O$ (*23*) and North Atlantic bottom water $\delta^{18}O$ (*22*) records are shown for comparison in gray and purple, respectively. Local summer insolation is shown for 65°N (light blue) and 65°S (red) (*36*). The gray dashed vertical lines are the timing constraints of the deglaciation from Fig. 1B. Note that deglaciation must start when NHI is at or close to a minimum.

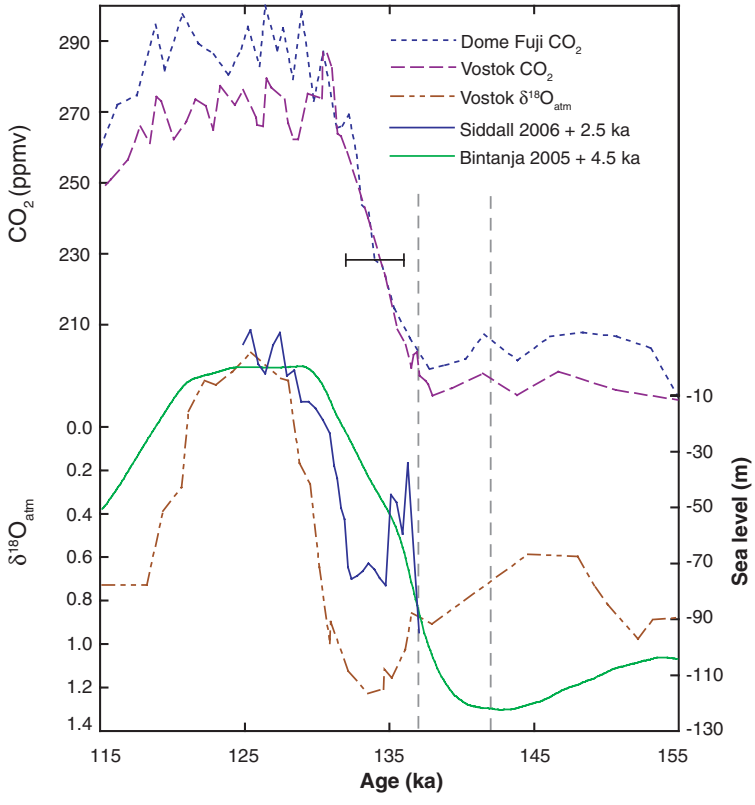

Fig. 3. Timing of the increase of atmospheric CO_2 and decrease of atmospheric $\delta^{18}O$ compared to sea-level rise across the penultimate deglaciation. Sea-level rise is illustrated by the curves of Bintanja *et al*. (*15*) and Siddall *et al*. (*16*), adjusted to fit the new coral constraints on this study (Fig. 1B). The timing of CO_2 rise is based on the Dome Fuji record, on the time scale of Kawamura *et al*. (*23*). The uncertainty of this time scale, shown by the horizontal bar, is ±2000 years at 134 ka (*23*). The Vostok CO_2 time series is aligned to this Dome Fuji record to provide the timing of atmospheric $\delta^{18}O$ (involving a shift of 1600 years at the midpoint of the deglaciation relative to the Vostok glaciological time scale, GT4) (*37*). Note the clear lag between sea level and atmospheric $\delta^{18}O$. The gray dashed vertical lines are the timing constraints of the deglaciation from Fig. 1B.

of the deglaciation may be constructed by combining continuous sea-level curves with the chronological constraints from the coral data. When comparing different localities it is important to consider that there may be regional differences in RSL, and between RSL and ESL, that strictly indicate deglaciation. RSL at far-field sites such as Tahiti provides a reasonable approximation of ESL, although the isostatic component is important at the start and end of deglaciations. RSL at Tahiti is expected to be lower by 0 to 15 m during the early deglacial and higher than ESL by 1.5 to 3.5 m during the early interglacial highstand (*14*). Tahiti RSL during the early deglacial may therefore lag ESL slightly.

To assess the magnitude and duration of the penultimate deglacial sea-level change, we used the sea-level reconstruction of Bintanja *et al*. (*15*) (based on modeling of the ice volume component of deep-sea benthic $\delta^{18}O$) and draped this over our far-field coral data (Fig. 1B), maintaining the duration of the deglaciation and altering only the timing. The original time scale of the Bintanja *et al*. record is based on the Lisiecki and Raymo (*18*) time scale, so comparison of our timing of the deglaciation also provides some assessment of the error in that time scale. The Bintanja *et al*. reconstruction uses a 3000-year mean of the input data, so any millennial-scale structure to the deglaciation is not represented. For consideration of millennial-scale variability, we compared the coral data to modeled sea level from $\delta^{18}O$ of planktonic foraminifera from the Red Sea (*16*), although that record does not extend to the glacial maximum.

Adjusting the Bintanja *et al*. time scale to be consistent with Tahiti corals requires a shift to ages that are 4500 years older. This suggests that the midpoint (the time by which sea level rose to half of the total glacial-interglacial rise) of the penultimate deglaciation occurred at ~136 ka, consistent with the previous assessment from some highstand corals (*1*, *19*) and from U/Th dating of Bahamas sediments (*20*). Our data also require the early deglacial portion of the Red Sea sea-level curve (*16*), which has a chronology based on the highstand age in an "open-system" coral compilation of Thompson and Goldstein (*21*), to be ~2500 years earlier. The timing presented here is also slightly earlier than the North Atlantic benthic $\delta^{18}O$ change placed on a chronology based on correlation of ice-rafted debris events with weak Asian monsoon intervals, precisely dated in Chinese speleothems (Fig. 2) (*22*).

The sea-level rise at the penultimate deglacial can also be compared with the accompanying rise in atmospheric CO_2 on the independent chronology of Kawamura *et al*. (*23*) for the Dome Fuji ice core record based on matching N_2/O_2 variations to local insolation at the ice core site (Fig. 3). This comparison indicates no resolvable difference in timing between sea level and CO_2. This is in disagreement with a sea-level lag of 4000 years previously inferred with the use of ice-core atmospheric $\delta^{18}O$ as a lagged response to sea-level change (*24*). This discrepancy suggests that atmospheric $\delta^{18}O$ is not a reliable indicator of sea level, and that the 1‰ shift seen at the deglaciation (although of similar size to that occurring in seawater during deglaciation) is controlled by changes in the Dole effect across the deglacial (*25*). The apparent synchroneity of sea level and CO_2 change at this deglacial [and the slight sea-level lag during the last deglaciation (*3*, *23*)] means that mechanisms involving sea-level changes as drivers of CO_2 change are no longer falsified by timing constraints, as had previously been suggested (*24*).

Determining the start of sea-level rise is useful to elucidate the cause of the deglaciation, but is harder to define than the midpoint of deglaciation. The coral age at 137 ka constrains the start of the deglaciation to be at least that old. A more gradual start to the penultimate deglaciation, as is suggested by the Bintanja *et al*. curve, would place the onset of ice sheet collapse at ~142 ka (Fig. 1B).

Early orbitally tuned chronologies (*26*, *27*) followed the suggestion of Milankovitch (*28*) and assumed that the rate of ice sheet collapse should be greatest when Northern Hemisphere summer insolation (NHI) was at a maximum because of enhanced summer melting. Depending on the precise month used to define the peak of summer, this suggests a maximum of melting rate close to 129 ka. Tahiti corals indicate that sea level was clearly rising before this at the penultimate deglacial, indicating that orbitally tuned chronologies (*26*) may be incorrect by up to 7000 years. It is clear that the phasing of the penultimate deglacial was very different from that of the last deglacial, and that tuning approaches assuming a constant phasing are inappropriate if millennial-scale accuracy is required.

Melting of the penultimate deglaciation started during a minimum of NHI (Fig. 2). This requires the climate system to be unusually poised for deglaciation if it were driven by NHI, with the subsequent rise in NHI being responsible for pacing the rate of melting throughout the deglaciation (somewhat at odds with the millennial variability seen during the deglaciation). It is interesting that the initiation of both this and the last deglaciation occurred during Southern Hemisphere summer insolation maxima, albeit with slightly different phasing, suggesting a possible role for the Southern Hemisphere. The different phasing of this deglaciation relative to the last one, however, indicates a more complex relationship between insolation and deglaciation, perhaps involving a stochastic response to insolation (*29*) or control by more than a single season and latitude. Any mechanism proposed to link insolation to orbital–time scale climate change must be tested against the difference in phasing of the two most recent deglaciations, as constrained by U-Th dating of corals.

References and Notes

1. C. D. Gallup, H. Cheng, F. W. Taylor, R. L. Edwards, *Science* **295**, 310 (2002).
2. T. M. Esat, M. T. McCulloch, J. Chappell, B. Pillans, A. Omura, *Science* **283**, 197 (1999).
3. R. G. Fairbanks, *Nature* **342**, 637 (1989).
4. E. Bard *et al*., *Nature* **382**, 241 (1996).
5. C. H. Stirling, T. M. Esat, K. Lambeck, M. T. McCulloch, *Earth Planet. Sci. Lett.* **160**, 745 (1998).
6. G. F. Camoin, Y. Iryu, D. B. McInroy, Expedition 310 Scientists, *Proc. IODP, 310, Tahiti Sea Level* (IODP Management International, Washington, DC, 2007).
7. See supporting material on *Science* Online.
8. T. M. Esat, Y. Yokoyama, *Geochim. Cosmochim. Acta* **70**, 4140 (2006).
9. K. B. Cutler *et al*., *Earth Planet. Sci. Lett.* **206**, 253 (2003).
10. Y. Yokoyama, T. M. Esat, K. Lambeck, *Earth Planet. Sci. Lett.* **193**, 579 (2001).
11. M. Siddall *et al*., *Nature* **423**, 853 (2003).
12. H. W. Arz, F. Lamy, A. Ganopolski, N. Nowaczyk, J. Patzold, *Quat. Sci. Rev.* **26**, 312 (2007).
13. L. F. Montaggioni, *Earth Sci. Rev.* **71**, 1 (2005).
14. G. A. Milne, J. X. Mitrovica, *Quat. Sci. Rev.* **27**, 2292 (2008).
15. R. Bintanja, R. S. W. van de Wal, J. Oerlemans, *Nature* **437**, 125 (2005).
16. M. Siddall, E. Bard, E. J. Rohling, C. Hemleben, *Geology* **34**, 817 (2006).
17. M. Siddall, E. J. Rohling, W. G. Thompson, C. Waelbroeck, *Rev. Geophys.* **46**, RG4003 (2008).
18. L. E. Lisiecki, M. E. Raymo, *Paleoceanography* **20**, PA1003 (2005).
19. D. R. Muhs, K. R. Simmons, B. Steinke, *Quat. Sci. Rev.* **21**, 1355 (2002).
20. G. M. Henderson, N. C. Slowey, *Nature* **404**, 61 (2000).
21. W. G. Thompson, S. L. Goldstein, *Quat. Sci. Rev.* **25**, 3207 (2006).
22. H. Cheng *et al*., *Geology* **34**, 217 (2006).
23. K. Kawamura *et al*., *Nature* **448**, 912 (2007).
24. W. S. Broecker, G. M. Henderson, *Paleoceanography* **13**, 352 (1998).
25. M. Bender, T. Sowers, L. Labeyrie, *Global Biogeochem. Cycles* **8**, 363 (1994).
26. J. Imbrie, A. McIntyre, A. C. Mix, in *Climate and Geosciences, A Challenge for Science and Society in the 21st Century*, A. Berger, S. H. Schneider, J.-C. Duplessy, Eds. (Reidel, Hingham, MA, 1984), pp. 121–164.
27. D. G. Martinson *et al*., *Quat. Res.* **27**, 1 (1987).
28. M. Milankovitch, in *Handbuch der Klimatologie*, W. Köppen, R. Geiger, Eds. (Bornträger, Berlin, 1930), Band 1, Teil A, pp. 1–176.
29. C. Wunsch, *Quat. Sci. Rev.* **23**, 1001 (2004).
30. J. Chappell *et al*., *Earth Planet. Sci. Lett.* **141**, 227 (1996).
31. C. H. Stirling *et al*., *Earth Planet. Sci. Lett.* **135**, 115 (1995).
32. A. Eisenhauer *et al*., *Geol. Rundsch.* **85**, 606 (1996).
33. B. J. Szabo *et al*., *Science* **266**, 93 (1994).
34. W. G. Thompson *et al*., *Earth Planet. Sci. Lett.* **210**, 365 (2003).
35. E. Bard, B. Hamelin, R. G. Fairbanks, *Nature* **346**, 456 (1990).
36. J. Laskar *et al*., *Astron. Astrophys.* **428**, 261 (2004).
37. J. R. Petit *et al*., *Nature* **399**, 429 (1999).

38. Supported by UK Natural Environment Research Council grant NE/D001250/1 and the Gary Comer Abrupt Climate Change Fellowship (A.L.T.). We thank the Expedition 310 scientists for the use of samples and data provided by the IODP, and R. Pearce and R. Williams at the National Oceanography Center Southampton for their assistance with XRD measurements.

Supporting Online Material

www.sciencemag.org/cgi/content/full/1168754/DC1
Materials and Methods
Figs. S1 to S3
Table S1
References

19 November 2008; accepted 30 March 2009
Published online 23 April 2009;
10.1126/science.1168754
Include this information when citing this paper.

Topographical and Temporal Diversity of the Human Skin Microbiome

Elizabeth A. Grice,[1] Heidi H. Kong,[2] Sean Conlan,[1] Clayton B. Deming,[1] Joie Davis,[3] Alice C. Young,[4] NISC Comparative Sequencing Program,[4]* Gerard G. Bouffard,[4,5] Robert W. Blakesley,[4,5] Patrick R. Murray,[6] Eric D. Green,[4,5] Maria L. Turner,[2] Julia A. Segre[1]†

Human skin is a large, heterogeneous organ that protects the body from pathogens while sustaining microorganisms that influence human health and disease. Our analysis of 16*S* ribosomal RNA gene sequences obtained from 20 distinct skin sites of healthy humans revealed that physiologically comparable sites harbor similar bacterial communities. The complexity and stability of the microbial community are dependent on the specific characteristics of the skin site. This topographical and temporal survey provides a baseline for studies that examine the role of bacterial communities in disease states and the microbial interdependencies required to maintain healthy skin.

The skin is a critical interface between the human body and its external environment, preventing loss of moisture and barring entry of pathogenic organisms (*1*). The skin is also an ecosystem, harboring microbial communities that live in a range of physiologically and topographically distinct niches (*2*). For example, hairy, moist underarms lie a short distance from smooth dry forearms, but these two niches are likely as ecologically dissimilar as rainforests are to deserts. Traditional culture-based characterizations of the skin microbiota are biased toward species that readily grow under standard laboratory conditions, such as *Staphylococci* spp. However, molecular approaches have revealed a greater diversity of skin microbiota within and between distinct topographical regions (*3*–*5*), underscoring the need to systematically survey multiple skin sites with the use of more contemporary genomic techniques.

Characterizing the microbiota that inhabit specific sites may provide insight into the delicate balance between skin health and disease. Certain dermatological disorders manifest at stereotypical skin sites [e.g., psoriasis on the outer elbow and atopic dermatitis (eczema) on the inner bend of the elbow]. Moreover, antibiotic exposure, modified hygienic practices, and lifestyle changes have the potential to alter the skin microbiome selectively and may underlie the increased incidence of human disorders such as atopic dermatitis. Understanding naturally occurring symbiotic microbial communities will provide insight into the conditions that favor the emergence of antibiotic-resistant organisms [e.g., the highly pathogenic strain of methicillin-resistant *S. aureus*, which acquired genes that promote growth on skin from the symbiont *S. epidermidis* (*6*)].

We characterized the topographical and temporal diversity of the human skin microbiome with the use of 16*S* rRNA gene phylotyping, and generated 112,283 near-full-length bacterial 16*S* gene sequences from samples of 20 diverse skin sites on each of 10 healthy humans (*7*) (fig. S1 and table S1). Nineteen bacterial phyla were detected, but most sequences were assigned to four phyla: Actinobacteria (51.8%), Firmicutes (24.4%), Proteobacteria (16.5%), and Bacteroidetes (6.3%). Of the 205 identified genera represented by at least five sequences, three were associated with more than 62% of the sequences: *Corynebacteria* (22.8%; Actinobacteria), *Propionibacteria* (23.0%; Actinobacteria), and *Staphylococci* (16.8%; Firmicutes). At the species level, we observed greater diversity than revealed by culture-based methods (*2*).

We selected skin sites that are not only representative of distinct niches but also characteristically affected by dermatologic disorders where microbes have been implicated in disease pathogenesis. We compared the relative abundance of major bacterial groups, as defined by the Ribosomal Database Project taxonomy (*8*), relative to three microenvironment types: (i) sebaceous [glabella (between the eyebrows), alar crease (beside the nostril), external auditory canal (inside the ear), occiput (back of the scalp), manubrium (upper chest), and back]; (ii) moist [nare (inside the nostril), axillary vault (armpit), antecubital fossa (inner elbow), interdigital web space (between the middle and ring fingers), inguinal crease (side of the groin), gluteal crease (topmost part of the fold between the buttocks), popliteal fossa (behind the knee), plantar heel (bottom of the heel), and umbilicus (navel)]; and (iii) dry [volar forearm (inside of the mid-forearm), hypothenar palm (palm of the hand proximal to the little finger), and buttock] (Fig. 1 and table S2). *Propionibacteria* species and *Staphylococci* species predominated in sebaceous sites (Fig. 1A). *Corynebacteria* species predominated in moist sites, although *Staphylococci* species were also represented (Fig. 1B). A mixed population of bacteria resided in dry sites, with a greater prevalence of β-Proteobacteria and Flavobacteriales (Fig. 1C). These observations were all significant ($P < 0.05$, one-tailed *t* test).

The taxonomic diversity, evenness, and richness of each site's microbiome were assessed using ecological diversity statistics (*7*). To perform these analyses, we clustered sequences into species-level operational taxonomic units (OTUs) of 99% sequence similarity by the furthest-neighbor method, using the DOTUR (Distance-based OTU and Richness) program (*9*). The richest site, or the site with the greatest number of OTUs, was the volar forearm with 44 median OTUs; the least rich site was the retroauricular crease with 15 median OTUs (fig. S3A). Taxonomic evenness, or the relative distribution of sequences among the OTUs, was assessed by the Shannon Equitability Index. The most even site was the popliteal fossa, followed by plantar heel and antecubital fossa; the least even sites were back, retroauricular crease, and toe web space (fig. S3B). The Shannon Diversity Index accounts for both richness and evenness of OTUs and largely mirrors the evenness findings of our data set (Fig. 2). In general, sebaceous sites were less diverse, less even, and less rich than moist and dry sites ($P < 0.05$, one-tailed *t* test).

To assess interpersonal variation, we used two OTU-based measurements: (i) community membership, a measure of shared OTUs, and (ii) community structure, which accounts for relative OTU abundance in addition to community membership. By these measures, the degree of interpersonal variation depended on skin site (table S5). The least similar sites were interdigital web spaces, toe webs, axillae, and umbilici. The most similar sites were alar creases, nares, and backs. We analyzed three paired symmetric sites (left and right antecubital fossae, axillae, and volar forearms) to assess intrapersonal variation. Subjects were more similar to themselves than to others (fig. S4 and table S3). A similar analysis of sampling techniques showed that swabbing was a suitable surrogate for scraping as a method for sample collection to assess microbial diversity (fig. S5 and table S4).

Microbes are predicted to play a role in the pathophysiology of many common dermatoses with predilection for specific skin sites (e.g., atopic dermatitis, psoriasis, acne, seborrheic dermatitis). Atopic dermatitis preferentially involves the antecubital and popliteal fossae, sites that were highly diverse, even, and rich relative to other sites (Fig. 2 and fig. S3). These sites also harbored similar ranges of organisms, but community membership was better preserved than community structure (table S6A). Psoriasis also occurs at stereotypical sites: umbilici, gluteal creases, occiputs, elbows, and knees (*10*). We did not identify common characteristics between

[1]Genetics and Molecular Biology Branch, National Human Genome Research Institute, Bethesda, MD 20892, USA. [2]Dermatology Branch, Center for Cancer Research, National Cancer Institute, Bethesda, MD 20892, USA. [3]Office of Translational Research, National Human Genome Research Institute, Bethesda, MD 20892, USA. [4]NIH Intramural Sequencing Center, National Human Genome Research Institute, Bethesda, MD 20892, USA. [5]Genome Technology Branch, National Human Genome Research Institute, Bethesda, MD 20892, USA. [6]Clinical Microbiology Laboratory, Department of Laboratory Medicine, National Institutes of Health Clinical Center, Bethesda, MD 20892, USA.

*See supporting online material for names of group members.
†To whom correspondence should be addressed. E-mail: jsegre@nhgri.nih.gov

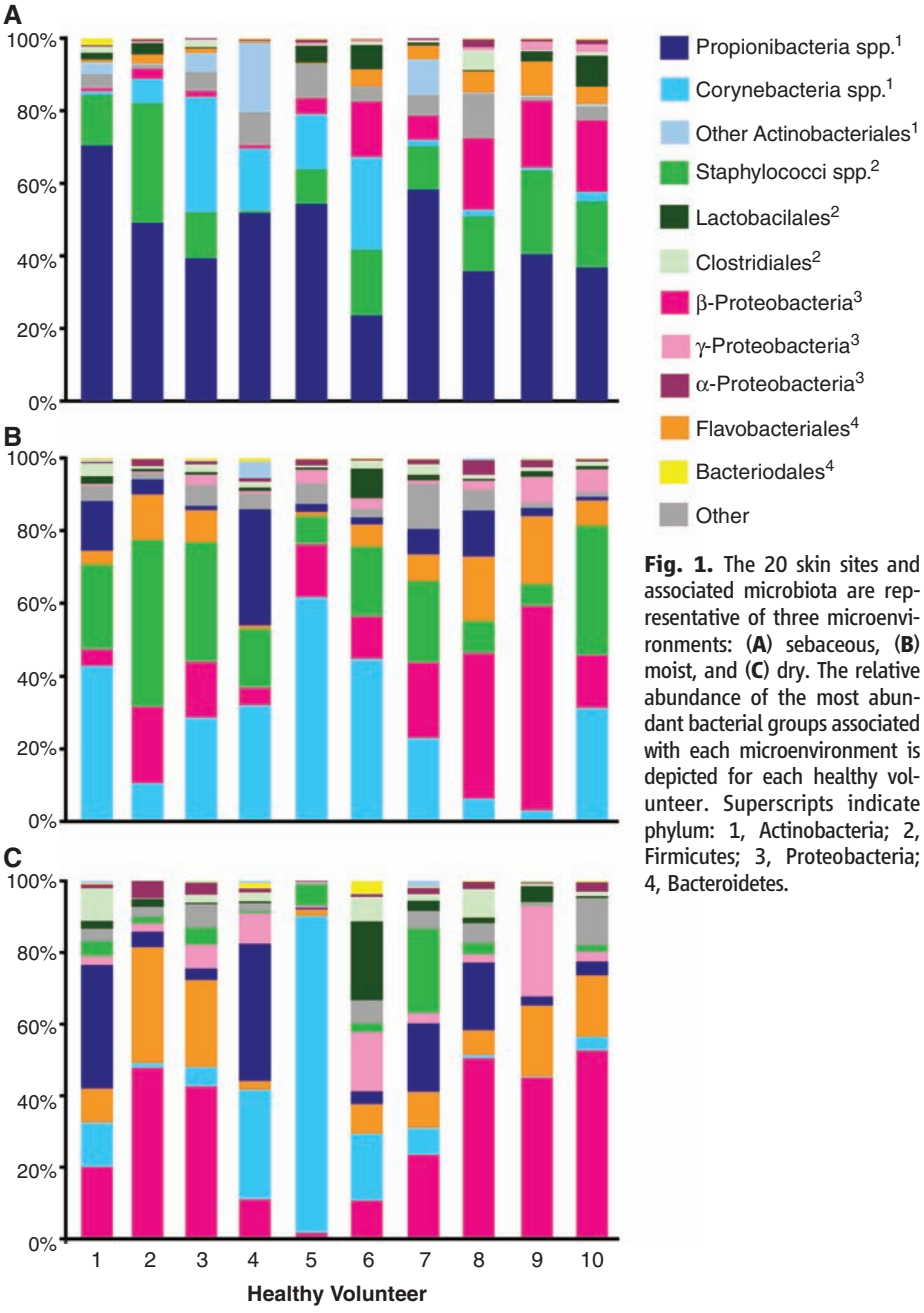

Fig. 1. The 20 skin sites and associated microbiota are representative of three microenvironments: (**A**) sebaceous, (**B**) moist, and (**C**) dry. The relative abundance of the most abundant bacterial groups associated with each microenvironment is depicted for each healthy volunteer. Superscripts indicate phylum: 1, Actinobacteria; 2, Firmicutes; 3, Proteobacteria; 4, Bacteroidetes.

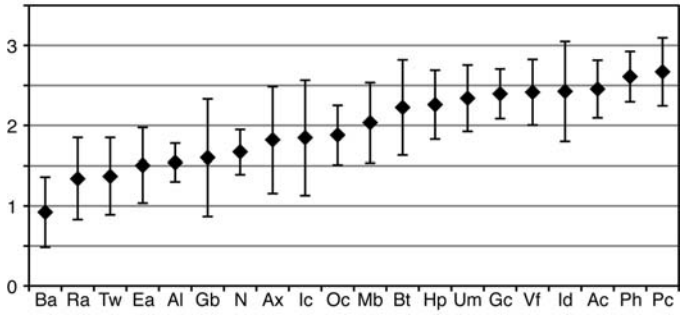

Fig. 2. Median diversity of sites as measured by the Shannon Diversity Index. Error bars represent median absolute deviation. See fig. S1 for key to site codes displayed on the *x* axis.

bacterial communities at psoriasis-associated sites (table S6B).

Because of increasing public health concerns regarding methicillin-resistant *S. aureus* infections, we included the anterior nares in our survey. A measurable proportion of the population harbors *S. aureus* here, and this constitutes a risk factor for the development of localized skin, soft tissue, and systemic infections (*10*). The unique microenvironment of the anterior nares consists of moist, hair-bearing, keratinized epithelia contiguous with both noncornified nasal mucosa and drier keratinized skin surfaces. When comparing community structure and membership, we found that microbes in the nares most closely resemble those collected from the contiguous alar crease (table S6C).

To characterize the temporal variation of the 20 skin sites, we collected follow-up samples 4 to 6 months after the initial visit from 5 of the 10 healthy volunteers. The most consistent sites with respect to community membership and structure were the external auditory canal, inguinal crease, alar crease, and nare, whereas we found appreciable variation on the second sampling of the popliteal fossa, volar forearm, and buttock (Fig. 3 and table S7), which suggests that longitudinal stability of the skin microbiome was site-dependent. Overall, four of the five resampled volunteers were significantly more like themselves over time than they were like other volunteers ($P < 0.005$, two-tailed *t* test) (Fig. 3 and table S7).

The recently launched Human Microbiome Project aims to characterize the human microbiota and its role in health and disease (*11*). The study reported here contributes to the broad goals of this project and may have implications for the future treatment of skin disorders. We have gained insights into the normal skin bacterial variation (intrapersonal, interpersonal, temporal, topographical), which can be used as a reference to calculate the statistical power required to carry out disease-related studies. Although multiple factors, including local skin anatomy, lipid content, pH, sweat, and sebum secretion, have long been recognized as contributing to certain skin disorders, we have shown that these factors correlate with the predominant microbiota. For example, the sebaceous glands of the face, scalp, chest, and back produce large amounts of oily sebum and are the sites where the lipophilic anaerobe *Propionibacterium acnes* predominates.

The effectiveness of antimicrobial agents in the management of some common skin disorders supports a role for microbes in pathophysiology. Elucidation of the baseline skin microbiome is a step toward testing the therapeutic potential of manipulating the microbiome in skin disorders. Indeed, an initial study of psoriasis (*12*) and an animal model of ichthyosis (*13*) describe selective microbial shifts associated with skin diseases. Targeted therapies to maintain healthy skin might require not only inhibiting the growth of pathogenic bacteria, but also promoting the growth of symbiotic bacteria.

References and Notes

1. J. A. Segre, *J. Clin. Invest.* **116**, 1150 (2006).
2. M. Marples, *The Ecology of the Human Skin* (Bannerstone, Springfield, IL, 1965).
3. N. Fierer, M. Hamady, C. L. Lauber, R. Knight, *Proc. Natl. Acad. Sci. U.S.A.* **105**, 17994 (2008).
4. Z. Gao, C. H. Tseng, Z. Pei, M. J. Blaser, *Proc. Natl. Acad. Sci. U.S.A.* **104**, 2927 (2007).
5. E. A. Grice *et al.*, *Genome Res.* **18**, 1043 (2008).

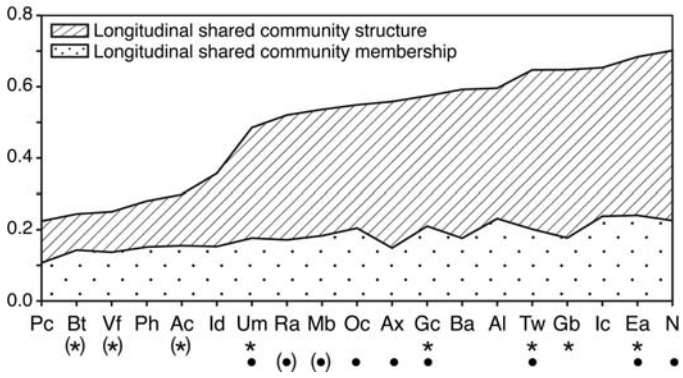

Fig. 3. Longitudinal stability of the skin microbiome. A higher number corresponds to greater shared community membership or structure over time. Sites with an asterisk below the site code retained significant community membership over time; those with a bullet retained significant community structure over time, as compared to interpersonal variation at the same site ($P \leq 0.05$). Parentheses around asterisks or bullets indicate that significance was achieved for that site when the outlier (volunteer 2) was removed from the analysis. See fig. S1 for key to site codes.

6. B. A. Diep *et al.*, *Lancet* **367**, 731 (2006).
7. See supporting material on *Science* Online.
8. J. R. Cole *et al.*, *Nucleic Acids Res.* **35**, D169 (2007).
9. P. D. Schloss, J. Handelsman, *Appl. Environ. Microbiol.* **71**, 1501 (2005).
10. M. P. Schon, W. H. Boehncke, *N. Engl. J. Med.* **352**, 1899 (2005).
11. NIH Human Microbiome Project (http://nihroadmap.nih.gov/hmp).
12. Z. Gao, C. H. Tseng, B. E. Strober, Z. Pei, M. J. Blaser, *PLoS One* **3**, e2719 (2008).
13. T. C. Scharschmidt *et al.*, *J. Invest. Dermatol.* (2009).

14. We thank the volunteers who participated in this study; E. Bassett for assistance with sample collection; members of the Segre laboratory for their underlying contributions; M. Udey, N. Salafsky, and E. Lander for critical reading of the manuscript; and J. Fekecs and D. Leja for graphical assistance. Supported by a NIGMS Pharmacology Research Associate Training Fellowship (E.A.G.) and by the NHGRI and NCI Center for Cancer Research Intramural Research Programs. All sequences are deposited under NCBI Genome Project 30125, GenBank accession numbers GQ000001 to GQ116391.

Supporting Online Material

www.sciencemag.org/cgi/content/full/324/5931/1190/DC1
Materials and Methods
Figs. S1 to S6
Tables S1 to S7
References

2 February 2009; accepted 17 April 2009
10.1126/science.1171700

A Role for the CHC22 Clathrin Heavy-Chain Isoform in Human Glucose Metabolism

Stéphane Vassilopoulos,[1,2,3,4]* Christopher Esk,[1,2,3,4]* Sachiko Hoshino,[1,2,3,4]*† Birgit H. Funke,[5]‡ Chih-Ying Chen,[1,2,3,4] Alex M. Plocik,[5]§ Woodring E. Wright,[6] Raju Kucherlapati,[5,7] Frances M. Brodsky[1,2,3,4]||

Intracellular trafficking of the glucose transporter GLUT4 from storage compartments to the plasma membrane is triggered in muscle and fat during the body's response to insulin. Clathrin is involved in intracellular trafficking, and in humans, the clathrin heavy-chain isoform CHC22 is highly expressed in skeletal muscle. We found a role for CHC22 in the formation of insulin-responsive GLUT4 compartments in human muscle and adipocytes. CHC22 also associated with expanded GLUT4 compartments in muscle from type 2 diabetic patients. Tissue-specific introduction of CHC22 in mice, which have only a pseudogene for this protein, caused aberrant localization of GLUT4 transport pathway components in their muscle, as well as features of diabetes. Thus, CHC22-dependent membrane trafficking constitutes a species-restricted pathway in human muscle and fat with potential implications for type 2 diabetes.

Insulin signaling in skeletal muscle and fat stimulates export of the GLUT4 glucose transporter from intracellular storage compartments to the plasma membrane (PM) to clear glucose from the bloodstream (*1*–*4*). GLUT4 membrane trafficking is disrupted in some forms of human type 2 diabetes leading to increased intracellular sequestration (*5*, *6*). Clathrin forms a protein coat on intracellular membrane vesicles and facilitates selective transport of proteins during membrane trafficking. There are two isoforms of clathrin heavy chain in humans, each named for the encoding human chromosome. The CHC22 isoform is highly expressed in skeletal muscle relative to other tissues, suggesting a potential role in GLUT4 transport (*7*). The more uniformly expressed CHC17 isoform participates in endocytosis and lysosome biogenesis in all cells and some aspects of GLUT4 transport (*3*, *4*, *8*, *9*). The two clathrin isoforms have distinct intracellular distributions and biochemical properties (*10*, *11*), and there is evolutionary conservation of sequence differences between isoforms in the vertebrate lineage. However, the gene encoding CHC22 is a pseudogene in mice (*12*).

To investigate the hypothesized role for CHC22 in human GLUT4 transport and whether it is distinct from that of CHC17, both clathrins and markers of the GLUT4 storage compartment (GSC) were localized in skeletal muscle (Fig. 1). Using new antibodies against GLUT4 and CHC22, we were able to extend earlier inconclusive analyses (*11*, *13*), and we found higher colocalization between CHC22 and GLUT4 than between CHC17 and GLUT4 (Fig. 1, A and B). Adaptor proteins link clathrin to membranes and to vesicle cargo (*14*), which includes vesicle-associated membrane proteins (VAMPs) involved in vesicle fusion (*15*), as well as transporters and receptors. The two clathrins showed differential binding to adaptors and cargo involved in GLUT4 transport when immunoisolated from solubilized muscle membrane preparations (Fig. 1, C and D). CHC22 bound the adaptor protein GGA2 [Golgi-associated, gamma adaptin ear-containing, adenosine diphosphate ribosylation factor (ARF)–binding protein 2], which is implicated in targeting intracellular GLUT4 to the GSC (*16*), and also bound VAMP2, which mediates fusion of GLUT4-containing vesicles with the PM (*17*). Association of these proteins with CHC17 was barely detectable in muscle, which clearly coprecipitated VAMP3 and the PM adaptor protein complex AP2, neither of which associated with CHC22. Lack of CHC22 interaction with AP2 was observed in earlier studies that showed no function for CHC22 in endocytosis (*10*). The adaptor protein complex AP1, which is implicated in intracellular GLUT4 targeting to the GSC (*18*) and also in CHC17 function in the

[1]Department of Bioengineering and Therapeutic Sciences, School of Pharmacy, University of California, San Francisco (UCSF), San Francisco, CA 94143, USA. [2]Department of Pharmaceutical Chemistry, School of Pharmacy, UCSF, San Francisco, CA 94143, USA. [3]Department of Microbiology and Immunology, School of Medicine, UCSF, San Francisco, CA 94143, USA. [4]The George Williams Hooper Foundation, School of Medicine, UCSF, San Francisco, CA 94143, USA. [5]Department of Medicine, Harvard Medical School, Boston, MA 02115, USA. [6]Department of Cell Biology, University of Texas Southwestern Medical Center, Dallas, TX 75390, USA. [7]Department of Genetics, Harvard Medical School, Boston, MA 02115, USA.

*These three authors contributed equally to the work described in this manuscript.
†Present address: Department of Neurology, Institute of Clinical Medicine, University of Tsukuba, 1-1-1 Tennoudai, Tsukuba 305-8575, Japan.
‡Present address: Partners Center for Personalized Genetic Medicine, Harvard Medical School, Cambridge, MA 02139, USA.
§Present address: Program in Biological Sciences, University of California, San Francisco, CA 94143, USA.
||To whom correspondence should be addressed. E-mail: frances.brodsky@ucsf.edu

trans-Golgi network (TGN) (*14*), was associated with both clathrins, as was GLUT4. Protein interactions and localization of each clathrin were supported by immunofluorescence, which also revealed colocalization of CHC22 with the insulin-regulated amino peptidase (IRAP), another marker of the GSC (*19*) (fig. S1, A to D).

In muscle sections from three type 2 diabetic patients, CHC22 was associated with GLUT4 compartments that were expanded compared with nondiabetic samples (Fig. 1, E to G, and fig. S2, A and B). Colocalization between GLUT4 and CHC22 was increased in the muscle of diabetic patients to a greater extent than that observed between CHC17 and GLUT4. Thus, CHC22 associates with GLUT4 and trafficking components involved in intracellular biogenesis and function of the GSC. In contrast, CHC17 clathrin associates with the AP2 adaptor that mediates endocytic GLUT4 traffic (*9*).

A role for CHC22 in GSC formation was assessed in the human myoblast cell line LHCNM2 (*20*) and also in primary human adipocytes, representing the two tissues that form an insulin-responsive GSC. As observed for myoblast differentiation (*10*), CHC22 levels increased during adipocyte differentiation (fig. S3A). Colocal-

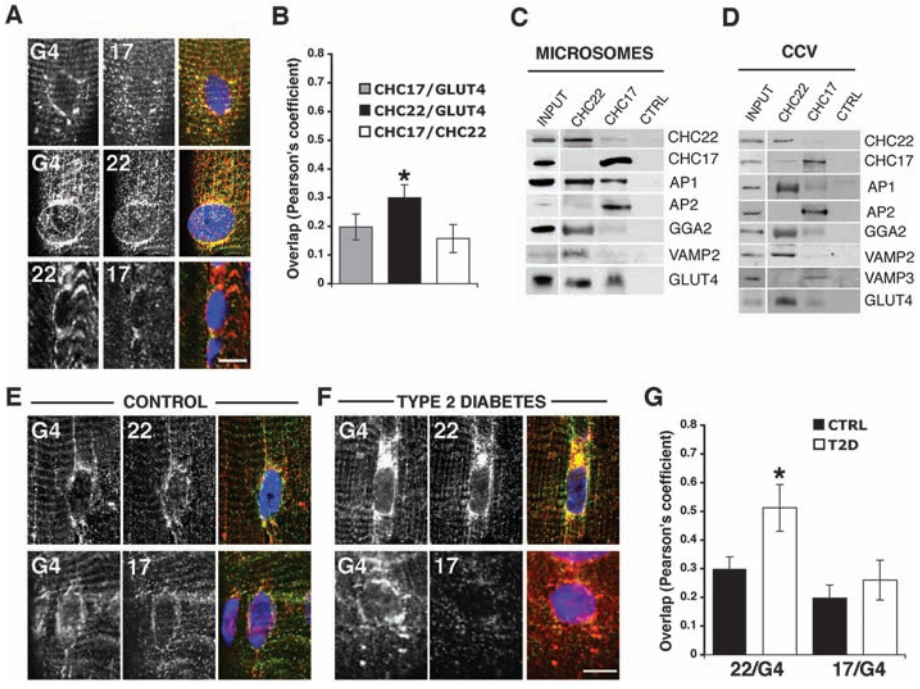

Fig. 1. Association of CHC22 with components of the GLUT4 transport pathway. (**A**) GLUT4 (G4, red) and CHC17 (17, green) or CHC22 (22, green) in human skeletal muscle (top two rows). CHC22 (red) and CHC17 (green) are shown in the bottom row. (**B**) Overlap between red and green illustrated in (A) (n = 5 to 10 images per condition). (**C**) Immunoblot of proteins associated with CHC22, CHC17, or isotype-matched control (CTRL) immunoprecipitates from human muscle microsomes and 1 to 5% microsome input. (**D**) Immunoblot of proteins associated with CHC22, CHC17, or CTRL immunoprecipitates from muscle clathrin-coated vesicles (CCV) and 10% CCV input. (**E**) GLUT4 and CHC22 or CHC17 in skeletal muscle from a control healthy subject. (**F**) GLUT4 and CHC22 or CHC17 in skeletal muscle from patient 1 with type 2 diabetes (T2D) (patient and control details given in fig. S2B). (**G**) Overlap between red and green labeling, as illustrated in (E) and (F) (n = 5 to 10). (A, E, and F) Each row shows individual antibody labeling (grayscale) and the merge (color). Yellow indicates colocalization. Scale bars, 10 μm. Asterisks in (B) and (G) indicate statistical significance ($P < 0.05$) (*13*). Error bars indicate ±SD.

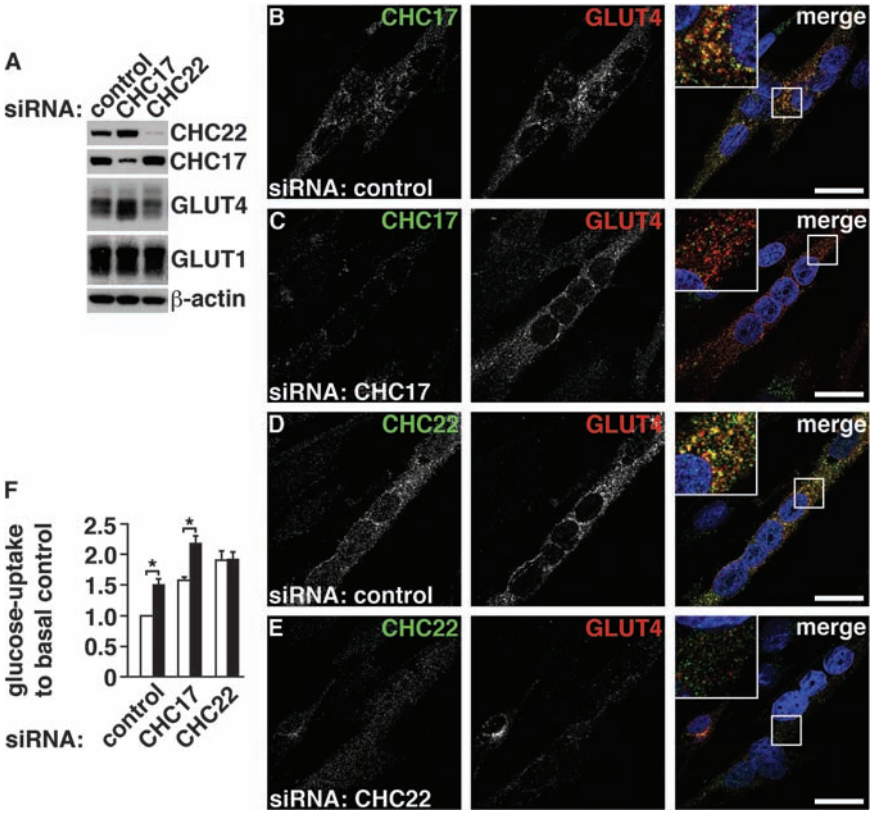

Fig. 2. CHC22 expression in cultured human myotubes and function in GSC formation. (**A**) Differentiated LHCNM2 skeletal muscle cells were treated with siRNA targeting proteins (indicated at the top) and cell lysates immunoblotted for proteins (indicated at the right). Protein levels were reduced by 88.1 ± 4.2% for CHC22 and by 79.8 ± 4% for CHC17 (n = 5) compared with control siRNA-treated cells. (**B** to **E**) CHC17 or CHC22 (green) and GLUT4 (red) in differentiated LHCNM2 skeletal muscle cells treated with control siRNA [(B) and (D)] or siRNA targeting CHC17 (C) or CHC22 (E). DNA staining (4′,6′-diamidino-2-phenylindole, blue) identifies differentiated, multinucleated myotubes. The boxed region in the merged images is magnified in the insets. Scale bars, 20 μm. (**F**) Glucose uptake in differentiated LHCNM2 skeletal muscle cells treated with siRNA against indicated targets. White bars, ratio of basal glucose uptake to basal glucose uptake of control culture; black bars, ratio of glucose uptake after insulin stimulation to basal uptake of control culture. Asterisks indicate statistical significance (n = 5, $P < 0.01$). Error bars indicate ±SEM.

ization of GLUT4 with both clathrins was evident in differentiated cultures when LHCNM2 cells had formed multinucleated myotubes and when lipid droplets were visible in primary adipocytes (Fig. 2, B and D, and fig. S3C). Both cell types were differentiated and treated with small interfering RNA (siRNA) to knock down CHC22 or CHC17 (Fig. 2, C and E, and fig. S3, D and E). CHC22 depletion was more efficient than CHC17 depletion (Fig. 2A and fig. S3B). In both cell types, CHC22 down-regulation led to strong reduction of GLUT4 staining and apparent loss of the GSC (Fig. 2E, fig. S3E, and fig. S4, D and F). Levels of GLUT4 protein were partially reduced in CHC22-depleted cells (Fig. 2A and fig. S3B), but this effect was not as dramatic as the reduction of intracellular staining, suggesting dispersion of GLUT4 protein as well as diversion to lysosomes. In contrast, the depletion of CHC17 had no clear effect on the level of intracellular GLUT4 staining or its localization (Fig. 2C, fig. S3D, and fig. S4, C and E), but for LHCNM2 cells, an increase of GLUT4 protein level was observed (Fig. 2A), consistent with some inhibition of GLUT4 endocytosis. Depletion of either CHC did not affect the localization or levels of the GLUT1 glucose transporter, which is constitutively expressed without intracellular sequestration and has a wider tissue distribution than GLUT4 (*21*) (fig. S4, E and F).

Differentiated LHCNM2 cells treated with siRNA were tested for uptake of radioactive glucose in response to insulin to assess how CHC22 depletion affected GSC function (Fig. 2F). In control-treated LHCNM2 cultures, insulin stimulation induced a 50% increase in glucose uptake relative to basal levels. This modest insulin response (compared to that of L6 rat myoblasts) is attributed to limited differentiation of LHCNM2 human myoblasts, assessed by the percentage of myonuclei (fig. S4G). Consistent with GSC loss,

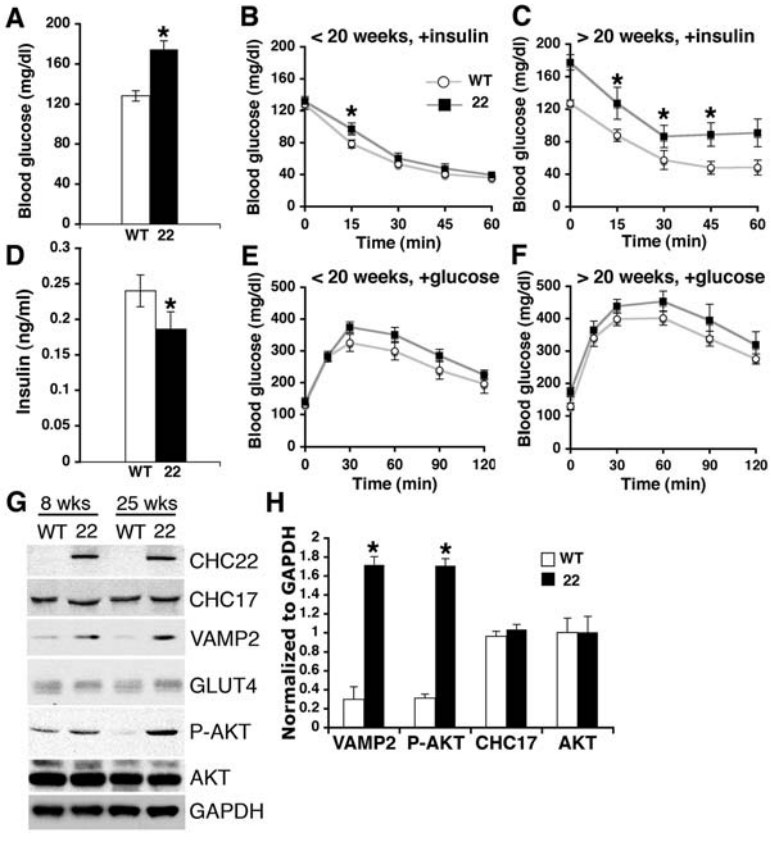

Fig. 3. Features of diabetes in CHC22 transgenic mice. (**A**) Fasting (16 hours) blood glucose levels of WT (n = 10) and CHC22 transgenic mice (22, n = 10, three strains). All mice were aged >25 weeks. Asterisks indicate statistical significance ($P < 0.01$). Error bars indicate ±SEM. (**B** and **C**) Blood glucose levels in CHC22 transgenic mice (solid squares, three strains) or WT littermates (open circles) (ages indicated) after insulin injection at time 0 (pre-fasted 6 hours). (**D**) Blood insulin levels of WT (n = 24) and CHC22 transgenic mice (n = 23, three strains), fasted 6 hours. All mice were aged >25 weeks. Asterisk indicates statistical significance ($P < 0.05$). (**E** and **F**) Blood glucose levels in CHC22 transgenic mice (solid squares, three strains) or WT littermates (open circles) (ages indicated) after glucose injection (2 g/kg body weight) at time 0 (pre-fasted 16 hours). The values in (B), (C), (E), and (F) are average glucose levels (n = 6 to 10) for each time point ± SEM. Asterisks indicate statistically significant differences ($P < 0.05$). (**G**) Skeletal muscle lysates (40 μg) from CHC22 transgenic strain 2 (22) or age-matched WT littermates (8 or 25 weeks old) were immunoblotted for the indicated proteins (P-AKT, phosphorylated AKT; GAPDH is a control). (**H**) Levels of proteins expressed as percentage of wild type and normalized to GAPDH detected as in (G) for mice aged >25 weeks (n = 4 of each type of mouse; error bars represent SD; asterisks indicate statistically significant differences; $P < 0.01$).

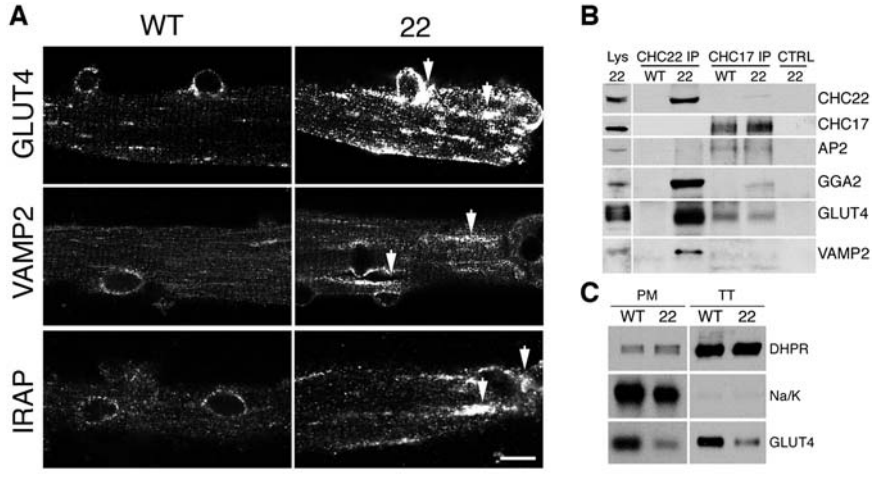

Fig. 4. GLUT4 membrane traffic in CHC22 transgenic mice. (**A**) Cultured skeletal muscle fibers from WT or CHC22 transgenic mice (22) (6 weeks old) analyzed by immunofluorescence for GLUT4, VAMP2, and IRAP. Scale bar, 10 μm. Arrows indicate expanded GSC compartments in CHC22 transgenic mouse muscle fibers. (**B**) Proteins associated with CHC22 or CHC17 immunoprecipitated (IP) from lysate of skeletal muscle from WT or CHC22 transgenic mice (22) (age > 25 weeks) were detected by immunoblotting. Input lysate (Lys, 1 to 5%) and IP with isotype-matched control (CTRL) antibody from CHC22 transgenic mouse muscle lysate were also analyzed. (**C**) PM and TT membrane from WT or CHC22 transgenic mice (22) (fed ad lib, age > 25 weeks) were purified, and equal amounts were analyzed by immunoblotting for GLUT4, the TT marker dihydropyridine receptor (DHPR), and the PM marker Na/K-ATPase (Na/K). These data represent results from all three CHC22 transgenic mouse strains.

CHC22-depleted LHCNM2 myotubes displayed no insulin-stimulated increase in glucose uptake (Fig. 2F). Myotubes depleted of CHC17 still responded to insulin, reflecting GSC persistence. Basal glucose uptake was increased upon the depletion of either clathrin, indicating redistribution of GLUT4 to the cell surface (Fig. 2F). In the case of CHC22 depletion, we propose that defective trafficking of newly synthesized GLUT4 to the GSC results in surface expression of the non-degraded GLUT4. For CHC17 depletion, increased surface expression is consistent with reduction in GLUT4 endocytosis. siRNA depletion of CHC17, but not CHC22, abrogated endocytosis of epidermal growth factor in LHCNM2 cells (fig. S4, H to J). Thus, CHC22 plays a role in intracellular biogenesis of the GSC independent from CHC17.

Mice have only a pseudogene for CHC22 and express no CHC22 protein (*12*), so the introduction of human CHC22 as a transgene provided a means to study the influence of CHC22 on glucose metabolism. CHC22 transgenic mice were produced with the use of a bacterial artificial chromosome (BAC) including the human gene CLTCL1 (formerly CLTD) encoding CHC22 under the control of its own promoter (fig. S5, A to D). CHC22 protein was detected in adipocytes and skeletal muscle of the transgenic mice and not in any other tissues that we tested (fig. S5, E to G). The three transgenic strains analyzed all showed features of diabetes. Older CHC22 mice were hyperglycemic compared with age-matched wild-type (WT) mice (Fig. 3A) and were not able to clear their excess blood glucose in response to insulin, though they were not completely insulin resistant (Fig. 3, B and C). For all ages of mice tested, clearance of injected glucose was slightly less efficient in the CHC22 mice compared with the WT mice (Fig. 3, E and F). Fasting blood insulin levels were mildly depressed in the older CHC22 mice, a feature characteristic of hyperglycemic patients with insulin resistance (*22*) (Fig. 3D). Adjacent to CLTCL1, the BAC used to produce the CHC22 mice included only one additional complete gene, SLC25A1, which encodes a citrate transporter already present in mice. Tissue from WT and CHC22 mice had comparable citrate levels (fig. S5H), indicating no detectable effect of the additional SLC25A1 human transgene. Thus, the presence of the CHC22 transgene in insulin-responsive tissues and its effect on GLUT4 trafficking is the most likely explanation for hyperglycemia and impaired glucose clearance in the CHC22 mice.

Analysis of proteins involved in GLUT4 transport and glucose metabolism revealed increases in phosphorylated AKT (pAKT, phosphoserine 473) and VAMP2 in the muscle of all three strains of CHC22 mice relative to WT mice (Fig. 3, G and H, and fig. S6A). The presence of CHC22 did not affect levels of GLUT4, IRAP, CHC17, or total AKT (Fig. 3, G and H, and fig. S6A). An increase in pAKT implies increased signaling in the GLUT4 export pathway (*23*, *24*) and has also been observed in some instances of diabetes (*25*, *26*).

VAMP2 is targeted to the GSC to mediate fusion with the PM (*17*). Elevated levels of VAMP2 suggest that normal trafficking out of the GSC might be altered in the CHC22 transgenic mice such that the routine turnover of VAMP2 was reduced. Immunofluorescence analysis of transgenic mouse muscle fibers showed that GLUT4, IRAP, and VAMP2 were indeed localized to swollen GSC-like structures, visible as extensive bright patches just underneath the PM that were not seen in WT mouse muscle fibers (Fig. 4A, fig. S6D, and movies S1 to S4). IRAP colocalized with GLUT4 and CHC22 in these compartments, and GLUT1 was excluded (fig. S6, D and E). In muscle of the CHC22 mice, the differential biochemical association of CHC22 or CHC17 with proteins involved in GLUT4 transport (Fig. 4B) was the same as was detected in human skeletal muscle (Fig. 1, C and D). Thus, CHC22 perturbs mouse GSC function by excessive intracellular sequestration of GLUT4 trafficking components, which, in the case of VAMP2, increases its stability (Fig. 3G and fig. S6A).

The PM and T-tubules (TT) are the major sites of GLUT4 release during an insulin response (*27*). To determine whether excessive sequestration of VAMP2 and GLUT4 in the CHC22 mice affected GLUT4 release, we assessed steady-state levels of GLUT4 in purified PM or TT membranes from feeding mice (Fig. 4C). Both membrane fractions from muscle of CHC22 mice had less GLUT4 relative to levels detected in the wild type, owing to intracellular retention of GLUT4 [41 ± 10.2% (SEM) of total GLUT4] by CHC22 (fig. S6, B and C). The reduced steady-state surface levels of GLUT4 could explain the hyperglycemia of the CHC22 mice.

Although much has been learned from mouse models about glucose metabolism that is relevant to human diabetes, we have observed a species-specific difference that should be considered for better understanding of the human disease. CHC22 clathrin, which is absent from mice, is involved in the intracellular generation of the GSC in human insulin-responsive tissues. Presumably through association with the AP1 and GGA2 adaptors, CHC22 participates in trafficking GLUT4 and other GSC components from endosomes and/or the TGN to the GSC, but CHC22 is not involved in GLUT4 endocytosis. In spite of this key role for CHC22 in GSC formation in humans, its artificial presence in mice sequesters GSC components and induces some features of diabetes in CHC22 transgenic mice. We propose that, in the transgenic mice, the presence of CHC22 disrupts the normal GLUT4 trafficking pathways that operate in mice, resulting in impaired release of GLUT4 in response to insulin. That the human GSC has at least one extra component contributing to its formation suggests the possibility that the human GSC in muscle and fat might be more robust than the equivalent compartment in mice, which is formed by a tenuous equilibrium between the biosynthetic and endocytic pathways (*1*, *28*). This difference between GLUT4 membrane traffic in human and mouse muscle could help to explain why 70 to 90% of insulin-stimulated glucose clearance depends on skeletal muscle in humans (*21*, *29*), but in mice, the liver is the most influential organ controlling insulin-responsive glucose reduction in the bloodstream (*30*, *31*). The ability of CHC22 to partially carry out its function in transgenic mice raises the possibility of rescuing the rest of its function and creating a better mouse model in which specific aspects of human glucose metabolism and diabetes can be studied.

References and Notes

1. N. J. Bryant, R. Govers, D. E. James, *Nat. Rev. Mol. Cell Biol.* **3**, 267 (2002).
2. C. B. Dugani, A. Klip, *EMBO Rep.* **6**, 1137 (2005).
3. J. C. Hou, J. E. Pessin, *Curr. Opin. Cell Biol.* **19**, 466 (2007).
4. S. Huang, M. P. Czech, *Cell Metab.* **5**, 237 (2007).
5. W. T. Garvey *et al.*, *J. Clin. Invest.* **101**, 2377 (1998).
6. L. Maianu, S. R. Keller, W. T. Garvey, *J. Clin. Endocrinol. Metab.* **86**, 5450 (2001).
7. F. M. Brodsky, C. Y. Chen, C. Knuehl, M. C. Towler, D. E. Wakeham, *Annu. Rev. Cell Dev. Biol.* **17**, 517 (2001).
8. D. J. Fazakerley, S. P. Lawrence, V. A. Lizunov, S. W. Cushman, G. D. Holman, *J. Cell Sci.* **122**, 727 (2009).
9. C. N. Antonescu, M. Diaz, G. Femia, J. V. Planas, A. Klip, *Traffic* **9**, 1173 (2008).
10. S.-H. Liu *et al.*, *EMBO J.* **20**, 272 (2001).
11. M. C. Towler *et al.*, *Mol. Biol. Cell* **15**, 3181 (2004).
12. D. E. Wakeham *et al.*, *Proc. Natl. Acad. Sci. U.S.A.* **102**, 7209 (2005).
13. Materials and methods are available as supporting material on *Science* Online.
14. M. S. Robinson, J. S. Bonifacino, *Curr. Opin. Cell Biol.* **13**, 444 (2001).
15. S. E. Miller, B. M. Collins, A. J. McCoy, M. S. Robinson, D. J. Owen, *Nature* **450**, 570 (2007).
16. L. V. Li, K. V. Kandror, *Mol. Endocrinol.* **19**, 2145 (2005).
17. V. K. Randhawa *et al.*, *Mol. Biol. Cell* **11**, 2403 (2000).
18. A. K. Gillingham, F. Koumanov, P. R. Pryor, B. J. Reaves, G. D. Holman, *J. Cell Sci.* **112**, 4793 (1999).
19. K. V. Kandror, P. F. Pilch, *Proc. Natl. Acad. Sci. U.S.A.* **91**, 8017 (1994).
20. C. H. Zhu *et al.*, *Aging Cell* **6**, 515 (2007).
21. P. R. Shepherd, B. B. Kahn, *N. Engl. J. Med.* **341**, 248 (1999).
22. S. E. Kahn, R. L. Hull, K. M. Utzschneider, *Nature* **444**, 840 (2006).
23. F. Koumanov, B. Jin, J. Yang, G. D. Holman, *Cell Metab.* **2**, 179 (2005).
24. Y. Ng, G. Ramm, J. A. Lopez, D. E. James, *Cell Metab.* **7**, 348 (2008).
25. J. M. Lizcano, D. R. Alessi, *Curr. Biol.* **12**, R236 (2002).
26. B. D. Manning, L. C. Cantley, *Cell* **129**, 1261 (2007).
27. P. Munoz *et al.*, *Biochem. J.* **312**, 393 (1995).
28. V. Blot, T. E. McGraw, *Mol. Biol. Cell* **19**, 3477 (2008).
29. C. Postic, R. Dentin, J. Girard, *Diabetes Metab.* **30**, 398 (2004).
30. M. D. Michael *et al.*, *Mol. Cell* **6**, 87 (2000).
31. J. C. Bruning *et al.*, *Mol. Cell* **2**, 559 (1998).

32. We thank N. Ohkoshi, A. Ishii, and A. Tamaoka for providing tissue samples from the archives of the Department of Neurology, Institute of Clinical Medicine, University of Tsukuba; P. Ursell for providing tissue samples from the Department of Pathology, UCSF; M. Birnbaum, J. Pessin, J. Bonifacino, and J. Hopwood for antibodies; E. Unger (UCSF Diabetes Center) and M. Yuneva (George Williams Hooper Foundation) for technical advice; and A. Klip (University of Toronto) for

helpful discussion. This work was supported by NIH grants GM038093 to F.M.B. and HD47863 to R.K.; a research grant and a career development award from the Muscular Dystrophy Association to W.E.W. and S.H., respectively; a grant from the Fondation Recherche Medicale, France to S.V.; and a Research Evaluation and Allocation Committee grant from the UCSF School of Medicine to F.M.B. Some images were acquired at the Nikon Imaging Center at UCSF.

Supporting Online Material
www.sciencemag.org/cgi/content/full/324/5931/1192/DC1
Materials and Methods
Figs. S1 to S6
References
Movies S1 to S4

28 January 2009; accepted 7 April 2009
10.1126/science.1171529

Proteasomal Regulation of the Hypoxic Response Modulates Aging in *C. elegans*

Ranjana Mehta,[1]* Katherine A. Steinkraus,[1]* George L. Sutphin,[2] Fresnida J. Ramos,[1] Lara S. Shamieh,[1] Alexander Huh,[1] Christina Davis,[1] Devon Chandler-Brown,[1] Matt Kaeberlein[1]†

The *Caenorhabditis elegans* von Hippel–Lindau tumor suppressor homolog VHL-1 is a cullin E3 ubiquitin ligase that negatively regulates the hypoxic response by promoting ubiquitination and degradation of the hypoxic response transcription factor HIF-1. Here, we report that loss of VHL-1 significantly increased life span and enhanced resistance to polyglutamine and β-amyloid toxicity. Deletion of HIF-1 was epistatic to VHL-1, indicating that HIF-1 acts downstream of VHL-1 to modulate aging and proteotoxicity. VHL-1 and HIF-1 control longevity by a mechanism distinct from both dietary restriction and insulin-like signaling. These findings define VHL-1 and the hypoxic response as an alternative longevity and protein homeostasis pathway.

Loss of protein homeostasis is increasingly becoming recognized as an important contributor to several age-associated diseases and may play a causal role in aging (*1*, *2*). A link between aging and protein homeostasis in the nematode *Caenorhabditis elegans* is supported by observations that increasing life span by reducing insulin and insulin-like signaling (ILS) or by dietary restriction (DR) also improves function in transgenic models of proteotoxic disease associated with aberrant protein aggregation (*3*, *4*).

A primary cellular mechanism for degrading damaged proteins is the ubiquitin-proteasomal system, which involves covalent attachment of ubiquitin to target proteins before degradation. RNA interference (RNAi) knockdown of proteasome components reduces resistance to polyglutamine toxicity and shortens life span in *C. elegans* (*5*, *6*), and we noted that proteasome inhibition led to accelerated paralysis in animals expressing a 35-residue polyglutamine repeat fused to yellow fluorescent protein (YFP) in body wall muscle cells (Q35YFP) (fig. S2). To further explore the relations between proteasomal function and protein homeostasis, we initiated an RNAi screen of known or predicted E3 ubiquitin ligases for altered resistance to polyglutamine toxicity (*7*) (table S1). Cullin-RING ubiquitin ligases (CULs) consist of multiple protein subunits that include a cullin protein, a RING finger protein, an adaptor protein, and a substrate recognition subunit (fig. S3) (*8*). Similar to proteasome inhibition, RNAi knockdown of genes encoding CUL1 or CUL2 core components accelerated paralysis in Q35YFP animals (fig. S3).

In contrast to knockdown of CUL core components, we identified an RNAi clone corresponding to a CUL2 substrate recognition subunit, VHL-1, that significantly delayed paralysis in Q35YFP animals (Fig. 1A). A similar increase in resistance to β-amyloid toxicity was also observed in response to *vhl-1(RNAi)* (Fig. 1B). VHL-1 is homologous to the mammalian von Hippel–Lindau tumor suppressor protein, which ubiquitinates the α subunit of the hypoxic response transcription factor, HIF-1 (*9*). Under normoxic conditions, ubiquitination of HIF-1 by VHL-1 represses the hypoxic response by targeting HIF-1 for proteasomal degradation (fig. S4). In order for VHL-1 to ubiquitinate HIF-1, HIF-1 must be hydroxylated by the EGL-9 prolyl hydroxylase (*10*). Similar to *vhl-1(RNAi)*, *egl-9(RNAi)* also enhanced resistance to both polyglutamine (Fig. 1C) and β-amyloid toxicity (Fig. 1D). Noting prior correlation between resistance to proteotoxicity and increased life span, we next determined whether *vhl-1* and *egl-9* also modulate aging by measuring the effect of RNAi knockdown of *vhl-1* or *egl-9* on life span in the RNAi-sensitive *rrf-3(pk1426)* background. Animals maintained on either *vhl-1 (RNAi)* or *egl-9(RNAi)* lived significantly longer than animals maintained on empty vector (EV) bacteria (Fig. 1, E and F).

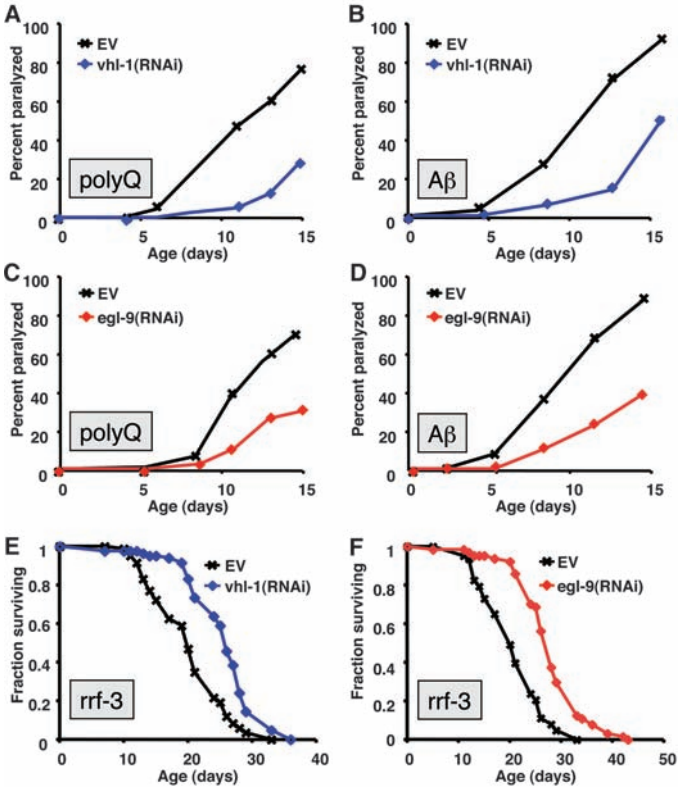

Fig. 1. VHL-1 and EGL-9 modulate proteotoxic stress and life span. RNAi knockdown of *vhl-1* significantly enhances resistance to (**A**) polyglutamine (polyQ) toxicity ($P < 1 \times 10^{-5}$) and (**B**) β-amyloid (Aβ) toxicity ($P < 1 \times 10^{-5}$) relative to animals fed EV bacteria. RNAi knockdown of *egl-9* significantly enhances resistance to (**C**) polyglutamine toxicity ($P < 1 \times 10^{-5}$) and (**D**) β-amyloid toxicity ($P < 1 \times 10^{-5}$) relative to animals fed EV bacteria. RNAi knockdown of (**E**) *vhl-1* ($P < 1 \times 10^{-5}$) or (**F**) *egl-9* ($P < 1 \times 10^{-5}$) significantly increased adult life span relative to the EV-fed control. Paralysis and life-span statistics are in tables S1 and S6.

[1]Department of Pathology, University of Washington, Seattle, WA 98195, USA. [2]Molecular and Cellular Biology Program, University of Washington, Seattle, WA 98195, USA.

*These authors contributed equally to this work.
†To whom correspondence should be addressed. E-mail: kaeber@u.washington.edu

To determine whether increased stability of HIF-1 could account for the enhanced longevity associated with *vhl-1* knockdown, we examined the life spans of animals deleted for *vhl-1*, *hif-1*, or both *vhl-1* and *hif-1* (*10*). The *hif-1(ia4)* allele removes exons 2, 3, and 4 of *hif-1*, including the DNA binding domain, and is believed to be a null allele (*11*) (Fig. 2A). The *vhl-1(ok161)* allele removes exons 1 and 2 of *vhl-1* and is also a putative null allele (Fig. 2B). As observed for *vhl-1(RNAi)* animals, deletion of *vhl-1* significantly increased life span (Fig. 2C). Deletion of *hif-1* alone did not substantially influence life span but completely suppressed the life-span extension imparted by deletion of *vhl-1* (Fig. 2C). Consistent with the observed longevity effects, the accumulation of autofluorescent age pigments, which has been proposed as a biomarker of aging and health span in *C. elegans* (*12*), was reduced in *vhl-1(ok161)* animals (Fig. 2D and fig. S5). This reduction was also fully suppressed by deletion of *hif-1*.

Given that deletion of *vhl-1* increased life span and resistance to proteotoxic stress, we speculated that there may be a fitness cost associated with constitutive expression of HIF-1 under normoxic conditions. One cost associated with many long-lived mutants is a decrease in fecundity. We quantified the number of eggs laid during adulthood (brood size) for N2, *vhl-1 (ok161)*, *hif-1(ia4)*, and *vhl-1(ok161); hif-1(ia4)* animals. A significant decrease in brood size was observed for *vhl-1(ok161)* animals but not for *hif-1(ia4)* animals (Fig. 2E). As observed for life span and age-pigment accumulation, deletion of *hif-1* suppressed the brood size defect of *vhl-1(ok161)* animals. Induction of HIF-1 by growth under hypoxic conditions also resulted in a significant decrease in brood size (figs. S6 and S7) and a corresponding increase in life span (fig. S8). These observations support the idea that repression of HIF-1 under normoxic conditions confers a fitness benefit in the form of enhanced fecundity.

We next examined the relations between DR and the hypoxic response. DR can be accomplished in *C. elegans* by reducing the availability of the bacterial food source, with complete removal of bacterial food during adulthood (bacterial deprivation) providing maximal life-span extension (*13*, *14*). If *vhl-1* and DR act in the same pathway to modulate longevity, then life-span extension from bacterial deprivation should require *hif-1* and not further extend the life span of *vhl-1* mutants. In contrast, bacterial deprivation extended the life span of *hif-1(ia4)* animals to an extent similar to that of controls (Fig. 3A) and further extended the long life span of *vhl-1(ok161)* animals (Fig. 3B). Bacterial deprivation also increased the life span of *hif-1(ia4)*; *vhl-1(ok161)* double mutants (Fig. 3C).

A common genetic model of DR in *C. elegans* is mutation of *eat-2*, which results in decreased food consumption because of a defect in pharyngeal pumping (*15*). Unlike *eat-2(ad465)* mutants, *vhl-1(ok161)* animals did not display a

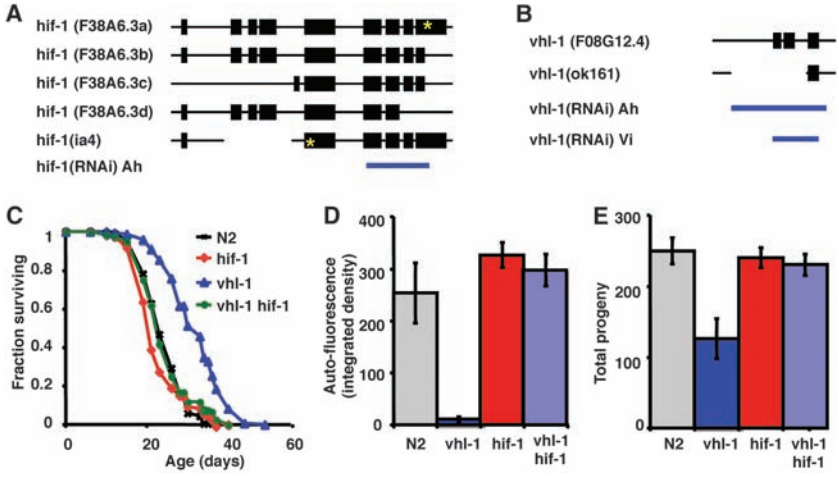

Fig. 2. VHL-1 modulates longevity, age-pigment accumulation, and reproduction in a HIF-1–dependent manner. Gene structures of (**A**) known *hif-1* splice variants, *hif-1 (ia4)* deletion, and *hif-1(RNAi)* and (**B**) known *vhl-1* splice variants, *vhl-1(ok161)* deletion, and *vhl-1(RNAi)*. Black boxes represent exons; yellow asterisk indicates a stop codon. Blue boxes indicate RNAi target sequences from Ahringer (Ah) or Vidal (Vi) library clones. The RNAi clones used to knock down *hif-1* and *vhl-1* target all known splice variants. (**C**) *Vhl-1(ok161)* animals are significantly longer-lived than wild-type (N2) animals ($P < 1 \times 10^{-5}$); *vhl-1(ok161); hif-1(ia4)* double-mutant animals are not longer-lived than N2 ($P = 0.66$). (**D**) Accumulation of autofluorescent age pigment is significantly reduced by deletion of *vhl-1* ($P < 1 \times 10^{-5}$). Autofluorescence is not significantly different in N2 versus *vhl-1(ok161); hif-1(ia4)* double-mutant animals ($P = 0.17$). (**E**) *Vhl-1(ok161)* animals produce significantly fewer progeny than N2 animals do ($P = 3.6 \times 10^{-3}$). No significant difference in brood size was observed for *vhl-1(ok161); hif-1(ia4)* double-mutant animals ($P = 0.69$) or *hif-1(ia4)* animals ($P = 0.43$), relative to N2 animals. Data in (D) and (E) are mean ± SD of at least nine animals per condition. Life-span statistics provided in table S6.

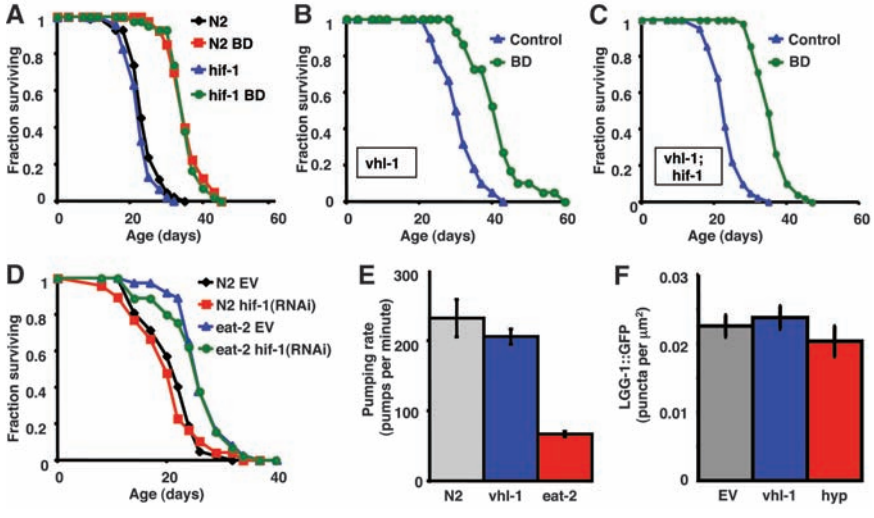

Fig. 3. VHL-1 and HIF-1 modulate longevity by a mechanism distinct from dietary restriction. (**A**) Life-span extension from bacterial deprivation (BD) is not significantly different in N2 and *hif-1(ia4)* animals ($P = 0.97$). (**B**) BD significantly increases the life span of *vhl-1(ok161)* animals ($P < 1 \times 10^{-5}$) and (**C**) *vhl-1(ok161)*; *hif-1(ia4)* double-mutant animals ($P < 1 \times 10^{-5}$). (**D**) *Hif-1(RNAi)* does not significantly alter the life-span extension of *eat-2(ad465)* animals ($P = 0.6$). (**E**) The *eat-2(ad465)* mutation significantly reduces pharyngeal pumping rate relative to rates in N2 ($P < 1 \times 10^{-5}$) or *vhl-1(ok161)* ($P < 1 \times 10^{-5}$) animals. Pharyngeal pumping rate is not significantly different in N2 and *vhl-1(ok161)* animals ($P = 0.06$). Data are mean ± SD. (**F**) Relative to animals fed EV bacteria under normoxic conditions, *vhl-1(RNAi)* under normoxia or growth on EV bacteria under hypoxia (hyp, 0.5% oxygen) failed to significantly increase autophagy, as indicated by the presence of LGG-1::GFP puncta ($P = 0.6$ and 0.5, respectively). Thirty-five animals per condition were imaged for EV and *vhl-1(RNAi)*. Seven animals were imaged for hypoxia. Data are mean ± SEM. Life-span statistics provided in table S6.

significant reduction in pumping rate (Fig. 3E), and, similar to the case for bacterial deprivation, knockdown of *hif-1* had no detectable effect on life-span extension from mutation of *eat-2* (Fig. 3D). Knockdown of *vhl-1* or growth under hypoxic conditions also failed to cause a significant increase in the abundance of autophagic vesicles (Fig. 3F and fig. S9), a phenotype reported to be required for life-span extension associated with DR (*16*, *17*). Thus, DR and the hypoxic response are likely to modulate longevity via distinct genetic pathways.

Decreased activity of the insulin-like receptor DAF-2 has been shown to increase life span (*18*, *19*) and promote resistance to hypoxia (*20*), leading us to consider whether *vhl-1* and *daf-2* act in the same genetic pathway to limit longevity. Like DR, however, *daf-2(RNAi)* further extended the already long life span of *vhl-1(ok161)* animals (Fig. 4A), and deletion of *hif-1* (Fig. 4B) or both *hif-1* and *vhl-1* (Fig. 4C) did not prevent life-span extension from *daf-2(RNAi)*. Life-span extension of animals with reduced ILS activity, including *daf-2* mutants, is dependent on the FOXO family transcription factor DAF-16, which acts downstream of DAF-2 to regulate gene expression (*21*, *22*). In order for DAF-16 to regulate target genes, it must be localized to the nucleus, a process that can be monitored by visualization of a DAF-16::GFP (green fluorescent protein) reporter (*23*). Transient heat shock or *daf-2(RNAi)* increased nuclear localization of DAF-16, whereas *vhl-1(RNAi)* had no detectable effect (Fig. 4D and fig. S10), suggesting that DAF-16 is not activated by loss of *vhl-1*. Consistent with this, *daf-16(RNAi)* did not fully suppress the increase in life span (Fig. 4E) or the reduced abundance of age pigment (Fig. 4F and fig. S11) associated with deletion of *vhl-1*, and *vhl-1(RNAi)* increased the life span of *daf-16* null animals (fig. S12). In contrast, *daf-16(RNAi)* fully suppressed the enhanced longevity of *daf-2(e1370)* animals (fig. S12), further phenotypically differentiating deletion of *vhl-1* from mutation of *daf-2*.

Our data support a model in which *vhl-1* and *daf-2* modulate longevity by different mechanisms, but it remains possible that ILS and the hypoxic response act through an overlapping set of target genes (fig. S1). Multiple DAF-16 target genes appear to be important for life-span extension in response to reduced ILS (*24*), and we speculate that multiple HIF-1 target genes may contribute to life-span extension in *vhl-1(ok161)* animals, some of which may be shared with DAF-16. Microarray studies have indicated that HIF-1 and DAF-16 have shared target genes (*25*, *26*), and mutation of *daf-2* can lead to increased resistance to hypoxic stress (*20*). In addition, reduced ILS and hypoxic response both induce resistance to heat stress (*27*), a phenotype often correlated with longevity. Like DAF-2, VHL-1 acts postdevelopmentally to modulate life span by a mechanism distinct from DR; however, unlike the case for *daf-2(e1370)* animals, *vhl-1(ok161)* animals did not show an enhanced frequency of dauer formation (table S2), suggesting that, if shared downstream effectors modulate aging and protein homeostasis, they are separable from the DAF-16 target genes involved in dauer formation.

Several features of the hypoxic response are highly conserved from nematodes to mammals, including regulation of mammalian HIF-1 by VHL-1 and the identity of many HIF-1 target genes. This high level of conservation suggests that induction of the hypoxic response is likely to have many similar physiological effects in nematodes and humans. Although inappropriate activation of the hypoxic response can promote tumorigenesis, therapeutically targeting specific components of this pathway may prove useful for treating age-associated diseases in people, particularly disorders associated with proteotoxicity in postmitotic cells, such as Huntington's disease, Alzheimer's disease, and other neurological disorders.

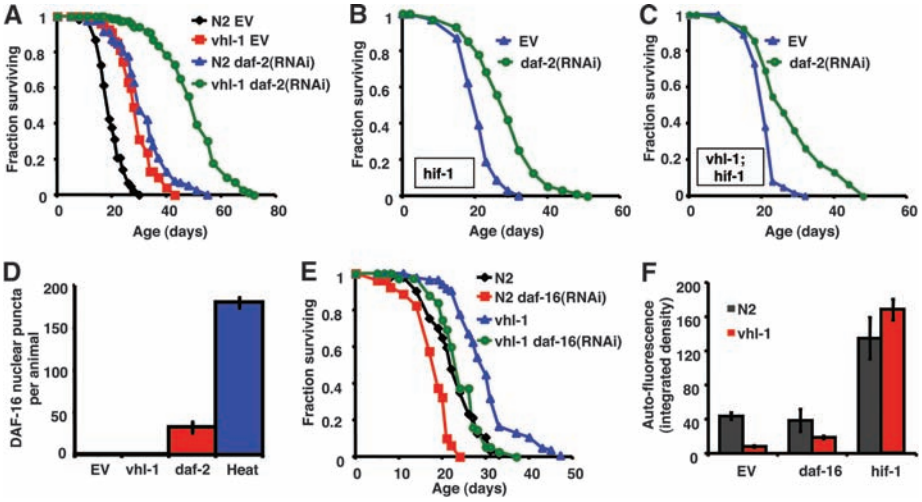

Fig. 4. ILS and VHL-1 modulate longevity by distinct mechanisms. *Daf-2(RNAi)* significantly increases the life span of (**A**) *vhl-1(ok161)* ($P < 1 \times 10^{-5}$), (**B**) *hif-1(ia4)* ($P < 1 \times 10^{-5}$), and (**C**) *hif-1(ia4); vhl-1(ok161)* animals ($P < 1 \times 10^{-5}$). (**D**) *Vhl-1(RNAi)* does not induce nuclear localization of DAF-16. *Daf-2(RNAi)* or heat shock significantly increases DAF-16 nuclear foci ($P < 1 \times 10^{-5}$ in each case). DAF-16 nuclear foci per animal was quantified for 10 animals per group. (**E**) *Daf-16(RNAi)* does not prevent life-span extension from deletion of *vhl-1* ($P < 1 \times 10^{-5}$). (**F**) Deletion of *vhl-1* significantly reduces autofluorescence in animals fed EV bacteria ($P < 1 \times 10^{-5}$) or *daf-16(RNAi)* ($P = 0.004$) but does not reduce autofluorescence in animals fed *hif-1(RNAi)* ($P = 0.9$). Median integrated pixel density shown for at least 10 randomly chosen animals per condition. Life-span statistics provided in table S6. Data in (D) and (F) are mean ± SEM.

References and Notes

1. E. Cohen, A. Dillin, *Nat. Rev. Neurosci.* **9**, 759 (2008).
2. M. Kaeberlein, B. K. Kennedy, *Aging Cell* **6**, 731 (2007).
3. E. Cohen, J. Bieschke, R. M. Perciavalle, J. W. Kelly, A. Dillin, *Science* **313**, 1604 (2006).
4. K. A. Steinkraus *et al.*, *Aging Cell* **7**, 394 (2008).
5. A. Ghazi, S. Henis-Korenblit, C. Kenyon, *Proc. Natl. Acad. Sci. U.S.A.* **104**, 5947 (2007).
6. C. Yun *et al.*, *Proc. Natl. Acad. Sci. U.S.A.* **105**, 7094 (2008).
7. Materials and methods are available as supporting material on *Science* Online.
8. D. R. Bosu, E. T. Kipreos, *Cell Div.* **3**, 7 (2008).
9. W. Kim, W. G. Kaelin Jr., *Curr. Opin. Genet. Dev.* **13**, 55 (2003).
10. A. C. Epstein *et al.*, *Cell* **107**, 43 (2001).
11. H. Jiang, R. Guo, J. A. Powell-Coffman, *Proc. Natl. Acad. Sci. U.S.A.* **98**, 7916 (2001).
12. B. Gerstbrein, G. Stamatas, N. Kollias, M. Driscoll, *Aging Cell* **4**, 127 (2005).
13. T. L. Kaeberlein *et al.*, *Aging Cell* **5**, 487 (2006).
14. G. D. Lee *et al.*, *Aging Cell* **5**, 515 (2006).
15. B. Lakowski, S. Hekimi, *Proc. Natl. Acad. Sci. U.S.A.* **95**, 13091 (1998).
16. M. Hansen *et al.*, *PLoS Genet.* **4**, e24 (2008).
17. K. Jia, B. Levine, *Autophagy* **3**, 597 (2007).
18. C. Kenyon, J. Chang, E. Gensch, A. Rudner, R. Tabtiang, *Nature* **366**, 461 (1993).
19. K. D. Kimura, H. A. Tissenbaum, Y. Liu, G. Ruvkun, *Science* **277**, 942 (1997).
20. B. A. Scott, M. S. Avidan, C. M. Crowder, *Science* **296**, 2388 (2002); published online 13 June 2002 (10.1126/science.1072302).
21. K. Lin, J. B. Dorman, A. Rodan, C. Kenyon, *Science* **278**, 1319 (1997).
22. S. Ogg *et al.*, *Nature* **389**, 994 (1997).
23. S. T. Henderson, T. E. Johnson, *Curr. Biol.* **11**, 1975 (2001).
24. C. T. Murphy *et al.*, *Nature* **424**, 277 (2003).
25. J. J. McElwee, E. Schuster, E. Blanc, J. H. Thomas, D. Gems, *J. Biol. Chem.* **279**, 44533 (2004).
26. D. Hoogewijs *et al.*, *BMC Genomics* **8**, 356 (2007).
27. M. Treinin *et al.*, *Physiol. Genomics* **14**, 17 (2003).

28. We would like to thank B. Kennedy and P. Kapahi for helpful discussion. Strains were provided by the Caenorhabditis Genetics Center. This work was supported by Alzheimer's Association grant IIRG-07-60158, a Glenn/AFAR (American Federation for Aging Research) Breakthroughs in Gerontology award, and NIH grant 1R01AG031108-01 to M.K. R.M. and K.A.S. were supported by postdoctoral fellowships from the Hereditary Disease Foundation. G.L.S., L.S.S., and F.J.R. were supported by NIH grant P30AG013280. M.K. is an Ellison Medical Foundation New Scholar in Aging.

Supporting Online Material

www.sciencemag.org/cgi/content/full/1173507/DC1
Materials and Methods
Figs. S1 to S12
Tables S1 to S6
References

13 March 2009; accepted 8 April 2009
Published online 16 April 2009;
10.1126/science.1173507
Include this information when citing this paper.

Synthetic Gene Networks That Count

Ari E. Friedland,[1*] Timothy K. Lu,[1,2*] Xiao Wang,[1] David Shi,[1]
George Church,[2,3] James J. Collins[1]†

Synthetic gene networks can be constructed to emulate digital circuits and devices, giving one the ability to program and design cells with some of the principles of modern computing, such as counting. A cellular counter would enable complex synthetic programming and a variety of biotechnology applications. Here, we report two complementary synthetic genetic counters in *Escherichia coli* that can count up to three induction events: the first, a riboregulated transcriptional cascade, and the second, a recombinase-based cascade of memory units. These modular devices permit counting of varied user-defined inputs over a range of frequencies and can be expanded to count higher numbers.

A counter is a key component in digital circuits and computing that retains memory of events or objects, representing each number of such as a distinct state. Counters would also be useful in cells, which often must have accurate accounting of tightly controlled processes or biomolecules to effectively maintain metabolism and growth. Counting mechanisms have been reportedly found in telomere length regulation (*1*, *2*) and cell aggregation (*3*). These system behaviors appear to be the result of a threshold effect in which some critical molecule number or density must be reached for the observed phenotypic change.

In this study, we first developed a counter, termed the riboregulated transcriptional cascade (RTC) counter, which is based on a transcriptional cascade with additional translational regulation. Two such cascades are illustrated in Fig. 1, A and C that can count up to two and three, respectively (hence, the designations RTC two-counter and RTC three-counter). For the RTC two-counter, the constitutive promoter $P_{Ltet0\text{-}1}$ drives transcription of T7 RNA polymerase (RNAP), whose protein binds the T7 promoter and transcribes the downstream gene, in this case, green fluorescent protein (GFP). Both genes are additionally regulated by riboregulators (*4*), whose cis and trans elements silence and activate posttranscriptional gene expression, respectively. The cis-repressor sequence [cr in Fig. 1] is placed between the transcription start site and the ribosome-binding site (RBS), and its complementarity with the RBS causes a stem-loop structure to form upon transcription. This secondary structure prevents binding of the 30*S* ribosomal subunit to the RBS, which inhibits translation. A short, transactivating, noncoding RNA (taRNA), driven by the arabinose promoter P_{BAD}, binds to the cis repressor in trans, which relieves RBS repression and allows translation. With this riboregulation, each node (i.e., gene) in the cascade requires both independent transcription and translation for protein expression. This cascade is able to count brief arabinose pulses [for pulse definition, see (*5*)] by expressing a different protein in response to each pulse (Fig. 1A). With cis-repressed T7 RNAP

[1]Howard Hughes Medical Institute, Department of Biomedical Engineering, Center for BioDynamics and Center for Advanced Biotechnology, Boston University, Boston, MA 02215, USA. [2]Harvard-MIT Division of Health Sciences and Technology, 77 Massachusetts Avenue, Room E25-519, Cambridge, MA 02139, USA. [3]Department of Genetics, Harvard Medical School, Boston, MA 02115, USA.

*These authors contributed equally to this work.
†To whom correspondence should be addressed. E-mail: jcollins@bu.edu

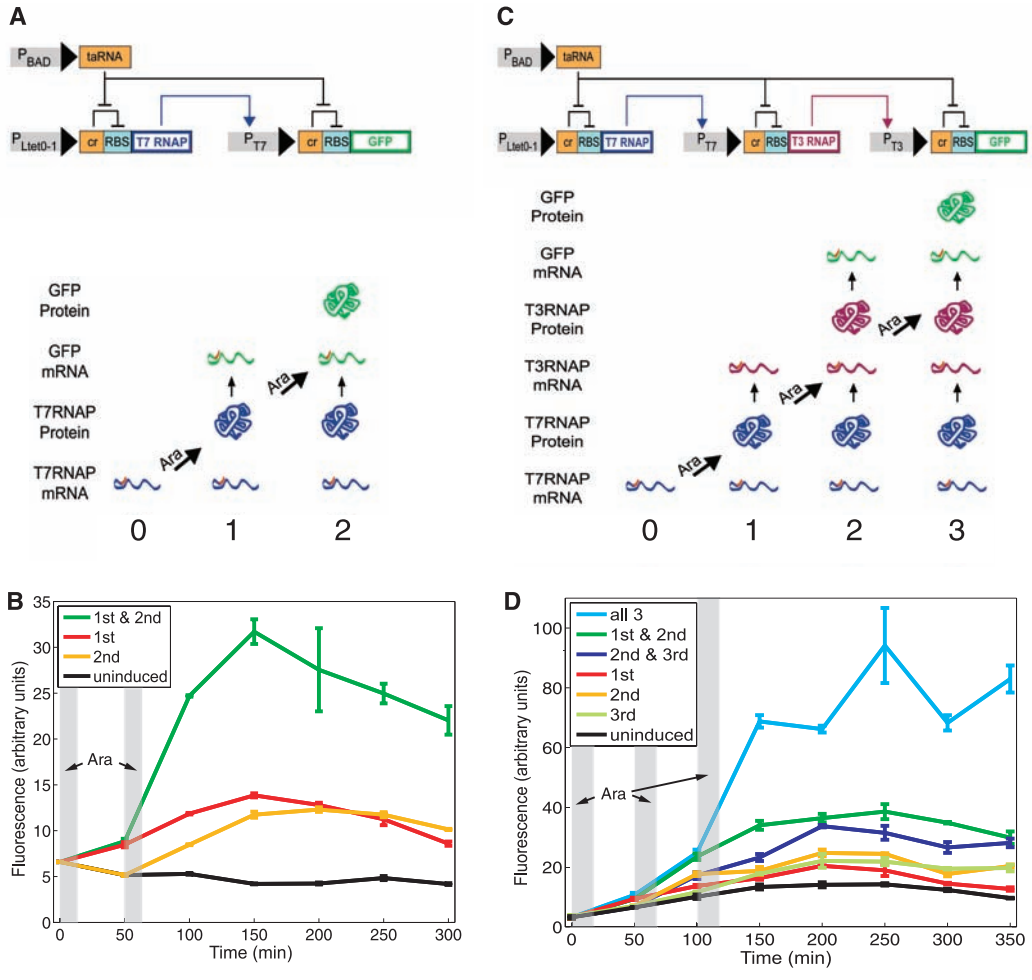

Fig. 1. The RTC two-counter and RTC three-counter construct designs and results. (**A**) The RTC two-counter is a transcriptional cascade with two nodes. Shown at the bottom are expected expression profiles after zero, one, and two arabinose (Ara) pulses. (**B**) Mean fluorescence of three replicates of RTC two-counter cell populations over time, measured by a flow cytometer. Shaded areas represent arabinose pulse duration. (**C**) The RTC three-counter is a transcriptional cascade with three nodes. Shown at the bottom are expected expression profiles after zero, one, two, and three arabinose pulses. (**D**) Mean fluorescence of three replicates of RTC three-counter cell populations over time, measured by a flow cytometer. Shaded areas represent arabinose pulse duration.

mRNAs in the cell, the first pulse of arabinose drives a short burst of taRNA production and, consequently, expression of T7 RNAP proteins. After the pulse is delivered, arabinose is removed from the cell environment, intracellular arabinose and taRNA are metabolized, and expression of T7 RNAP protein halts. The T7 RNAP proteins that have been translated then transcribe cis-repressed GFP transcripts, but few GFP proteins are made until the next arabinose pulse is delivered and translation is once again activated.

We built the RTC two-counter construct on a high-copy plasmid and transformed it into *Escherichia coli* strain K-12pro (*5*). Cells containing this construct were pulsed with the inducer arabinose, and fluorescence was measured over time (Fig. 1B). Uninduced cells show no increase in mean fluorescence, whereas cells that received either the first or second pulse show only small increases, indicating some degree of leakage—an effect in which the intended protein is expressed in each arabinose pulse, but also some unintended, downstream proteins are expressed as well. Cells that received both arabinose pulses show a substantial increase in fluorescence when the second pulse is delivered, precisely when the cells are expected to express GFP proteins.

To extend the RTC counter's capability to count to three, we built a second synthetic construct, the RTC three-counter, again with GFP as the quantitative readout. It is similar to the RTC two-counter but has three nodes in the cascade instead of two (Fig. 1C). T7 RNAP is the gene at the first node driving transcription of T3 RNAP, which ultimately drives transcription of GFP. All transcripts are likewise cis-repressed with the same riboregulator sequence. When pulsed with arabinose, this counter should primarily produce T7 RNAP proteins during the first pulse, T3 RNAP proteins during the second pulse, and GFP proteins during the third pulse (Fig. 1C).

Experimental results demonstrate that fluorescence increases substantially only when all three arabinose pulses are delivered (Fig. 1D). Flow cytometry measurements show this increase beginning at precisely the time of the third pulse, and the considerable slope at this juncture suggests that cells contain a high concentration of cis-repressed GFP transcripts ready for transactivation. The data also reveal slight leakage in cells that are pulsed only once or twice, but their fluorescence remains comparatively low. This result, in combination with the RTC two-counter evidence, shows that the temporal progression of RNA and protein species logically predicted by the counter network architecture is indeed responsible for the observed effect.

To further support these results, we constructed and analyzed a mathematical model based on the design of the RTC two-counter and three-counter constructs. This model, with fitted parameters [see section 6 of (*5*)], was able to match both the RTC two-counter and three-counter experimental results (Fig. 2, A and B). We used the model to investigate the effects of pulse frequency and pulse length on the performance of the RTC three-counter and to guide our experimental search for optimal combinations. The mathematical model predictions, shown as contour lines in Fig. 2C, indicate that maximum expression occurs with pulse lengths of ~20 to 30 min and pulse intervals of 10 to 40 min. The absolute difference in fluorescence after three pulses and two pulses is shown in Fig. 2D, with optimal counting behavior requiring similar pulse length and interval combinations noted above.

Experimentally, we sampled various pulse lengths and intervals, plotting these results as circles in Fig. 2, C and D. These results are consistent with the model predictions across a wide range of temporal conditions, and they confirm that the RTC three-counter has a sizable temporal region in which its counting behavior is robust. Within this region, the counter is also capable of counting irregular pulses; for example, it is able to distinguish between two short pulses followed by a long pulse and two long pulses, as predicted by the model (fig. S5). However, as indicated in Fig. 2, when pulse length or frequency is either too high or low, the RTC three-counter is unable to count properly, presumably because of the

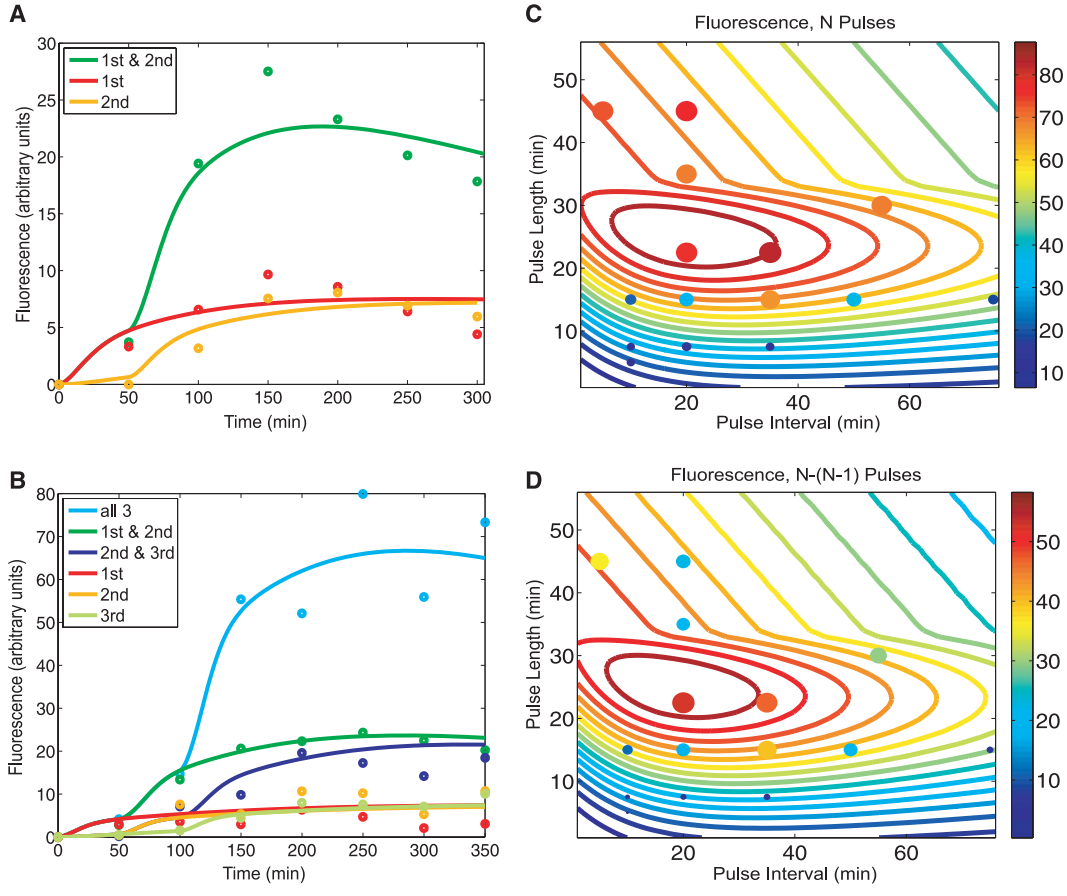

Fig. 2. Modeling predictions and RTC three-counter experimental characterization. (**A**) A model with fitted parameters captures the salient features of the normalized fluorescence results of the RTC two-counter. (**B**) An expanded model, again with fitted parameters, matches the normalized fluorescence results of the RTC three-counter. (**C**) On the basis of parameters fitted in (B), the model predicts expression output of the RTC three-counter (*N*) across a range of pulse lengths and intervals, and these calculations were used to generate the colored contour lines. Solid circles represent experimental results, with both color and size of circles indicating the level of expression. (**D**) Similar to (C), except that values shown are the difference in expression output after three (N) pulses and two ($N-1$) pulses.

intrinsic kinetic limits of the biochemical processes involved, such as transcription and mRNA degradation.

Our second counter design, termed the DNA invertase cascade (DIC) counter, was built by chaining together modular DNA-based counting units (Fig. 3A). The DIC counter uses recombinases, such as Cre and flp_e (*6*), which can invert DNA between two oppositely oriented cognate recognition sites, such as *loxP* and flp_e-recombination target (*FRT*) sites, respectively. Recombinases have been used for numerous applications, including the creation of gene knockouts and inducible expression systems (*7*, *8*). In our counter design, each recombinase gene (*rec*) is downstream of an inverted promoter (P_{inv}), fused to an *ssrA* tag that causes rapid protein degradation (*9*), and followed by a transcriptional terminator (Term) (fig. S7). The P_{inv}-*rec*-*ssrA*-Term DNA sequences are placed between forward and reverse recombinase recognition sites (R_f and R_r) (fig. S7), forming a single counting unit that we have named a single invertase memory module (SIMM) (Fig. 3A and fig. S7). Upon expression of recombinase by an upstream promoter, the entire SIMM is inverted between the recognition sites. Because the recombinase gene is inverted with respect to the upstream promoter, further expression of recombinase protein ceases, and DNA orientation is fixed.

We developed a single-inducer DIC two-counter (fig. S8) and three-counter (Fig. 3A and fig. S9), which are composed of one and two SIMMs, respectively, and placed them on pBAC plasmids that are maintained as single-copy episomes (*10*). These circuits utilize P_{BAD}, so that pulses of arabinose constitute inputs to the circuit. Each pulse of arabinose results in promoter activation and expression of the next recombinase in the cascade, which then inverts the SIMM in which it is located. This allows the inverted promoter contained within that SIMM to be placed in a forward orientation to drive expression of the next SIMM stage. The single-inducer DIC two-counter shows high GFP output after two pulses of arabinose but only low GFP output after one pulse of arabinose, which shows that a single SIMM can be inverted to count events (fig. S11). In the single-inducer DIC three-counter, some premature flipping of the Cre recombinase–based SIMM did occur, which resulted in a small amount of leakage, e.g., fluorescence increased after only two arabinose pulses (Fig. 3B and fig. S12). However, this leakage was small compared with the high GFP output exhibited in response to three pulses of arabinose (Fig. 3B). In order to probe the temporal characteristics of the single-inducer DIC three-counter, we varied the pulse lengths and intervals, calculating the ratio of GFP output for cells exposed to three, versus two, pulses of arabinose (Fig. 3C). This ratio was at least 1.5 for most conditions tested, which demonstrated that the single-inducer DIC three-counter is able to successfully count pulses whose lengths and intervals range from 2 to 12 hours (Fig. 3C).

We also developed a multiple-inducer DIC three-counter by replacing the P_{BAD} promoters in the single-inducer DIC three-counter with the inducible promoters $P_{Ltet0\text{-}1}$, P_{BAD}, and P_{A1lacO} (Fig. 4A and fig. S10). These promoters respond to anhydrotetracycline (aTc), arabinose, and isopropyl β-D-1-thiogalactopyranoside (IPTG), respectively (Fig. 4A). When exposed to aTc followed by arabinose, followed by IPTG, the multiple-inducer DIC three-counter produced a high GFP output (Fig. 4B). No other permutations of the three inducers produced a high output, although some did exhibit a small amount of leakage (Fig. 4, C and D). These results demonstrate that the circuit can be programmed to record only a desired sequence of events.

We have constructed and validated two complementary designs for synthetic counters that operate across a range of time scales. These counters are both highly modular and capable of functioning with multiple inducer-promoter pairs. In addition, the architectures of both counters allow for the tunable output expression of different protein species of interest at any number (up to three are shown) in the counting

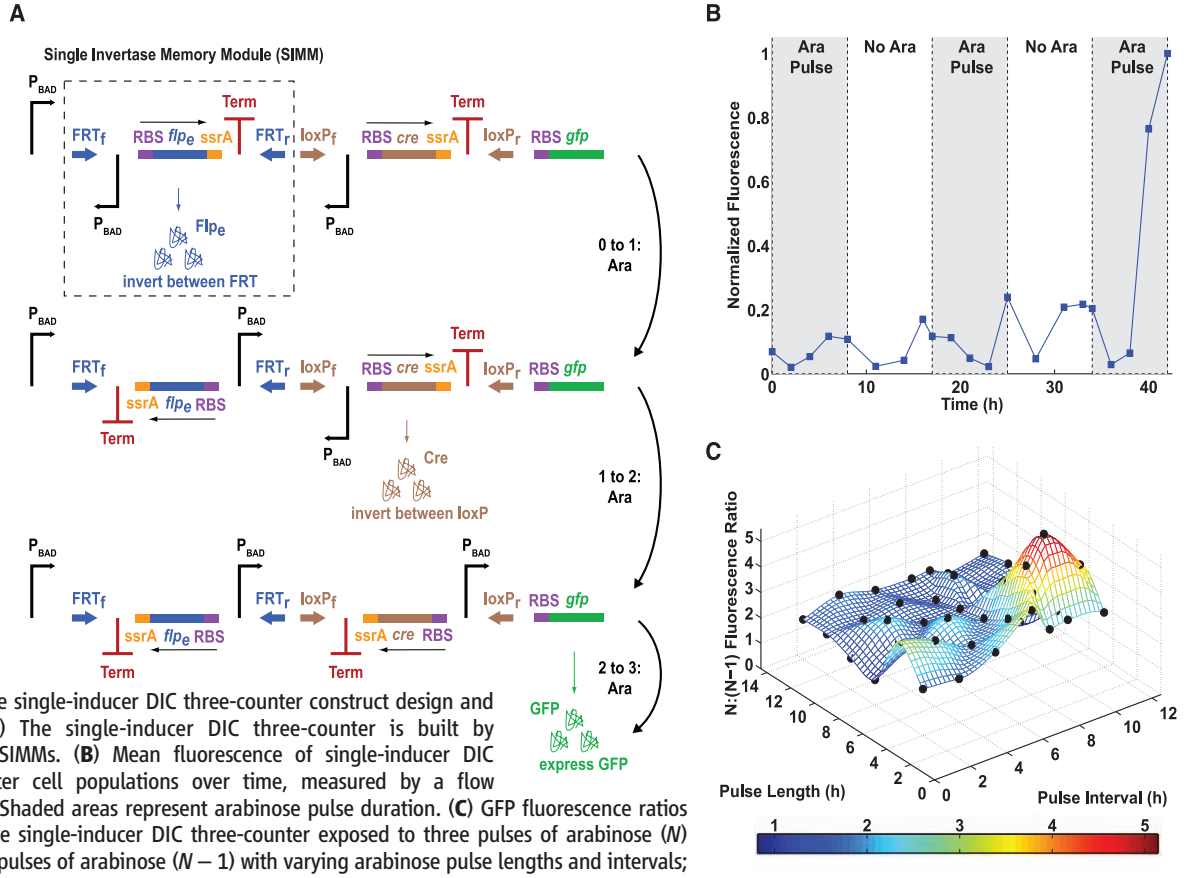

Fig. 3. The single-inducer DIC three-counter construct design and results. (**A**) The single-inducer DIC three-counter is built by cascading SIMMs. (**B**) Mean fluorescence of single-inducer DIC three-counter cell populations over time, measured by a flow cytometer. Shaded areas represent arabinose pulse duration. (**C**) GFP fluorescence ratios between the single-inducer DIC three-counter exposed to three pulses of arabinose (*N*) versus two pulses of arabinose ($N-1$) with varying arabinose pulse lengths and intervals; experimental results are represented by black dots.

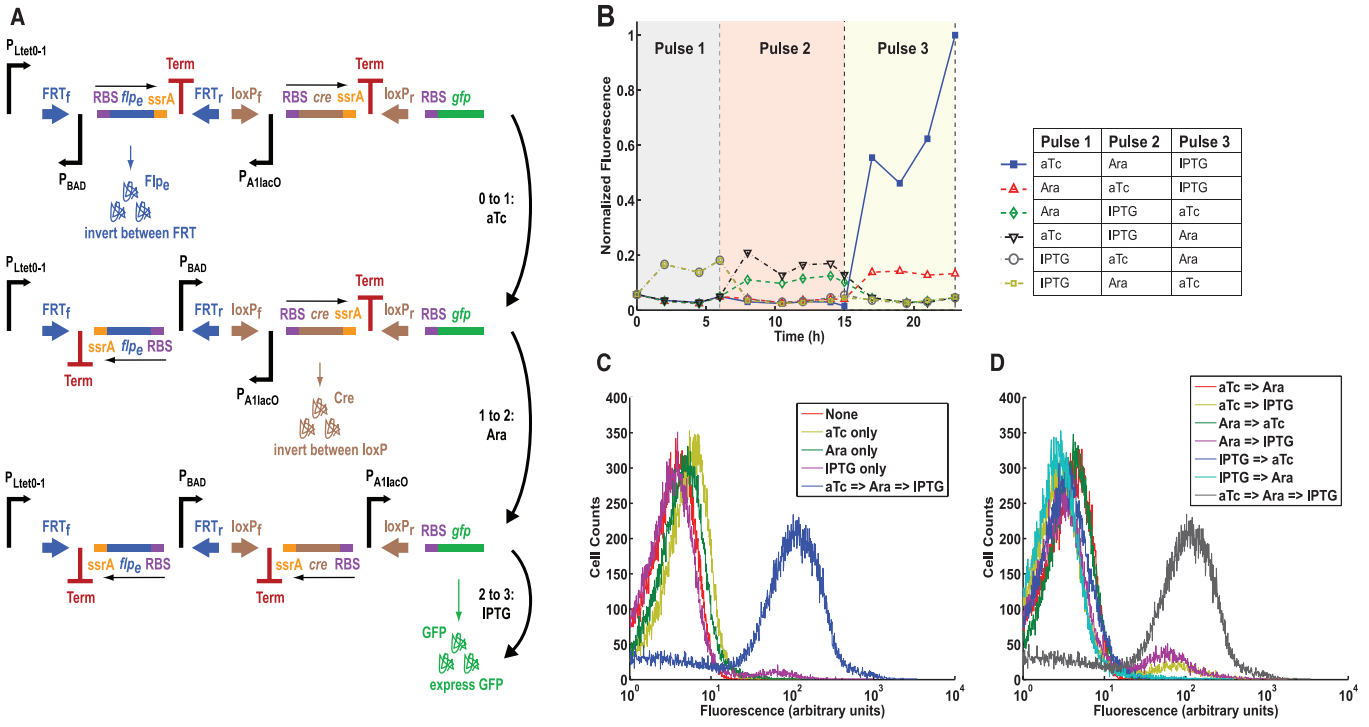

Fig. 4. The multiple-inducer DIC three-counter construct design and results. (**A**) The multiple-inducer DIC three-counter is similar to the single-inducer DIC three-counter in Fig. 3, except that each promoter is a unique inducible promoter: $P_{Ltet0\text{-}1}$, P_{BAD}, and P_{A1lacO}. These promoters respond to aTc, arabinose, and IPTG, respectively. (**B**) Mean fluorescence of multiple-inducer DIC three-counter cell populations over time, measured by a flow cytometer. Colored areas represent the durations of consecutive inducer pulses. (**C**) Flow cytometry population data showing the multiple-inducer DIC three-counter when exposed to the desired sequence of three inducers and to single inducers only. (**D**) Flow cytometry population data showing the multiple-inducer DIC three-counter when exposed to the desired sequence of three inducers and to all pairwise permutations of inducers.

process. Our constructs were built to count up to three events, but they both should be extensible with the use of other unique polymerases or recombinases, of which many are known (*5*). In addition to these shared qualities, each counter comes with its own set of properties. Our RTC counters demonstrate fast activation because of transcriptional and translational regulatory elements, which makes them useful for counting cellular events on the time scale of cell division. The DIC counters operate on time scales of hours (fig. S13) as a result of DNA recombination dynamics (*11*), and they are built with a novel SIMM design that retains counter state based on DNA orientation.

Synthetic gene circuits have enlarged the molecular tool set available to bioengineers and molecular biologists (*4*, *12*–*24*) and have enabled them to program novel cellular behaviors (*25*–*27*) and to construct therapeutic agents (*28*, *29*). Our synthetic counters represent complementary designs that can be used in different settings for a variety of purposes across a range of time scales. For example, if inputs to our RTC counter were coupled to the cell cycle, one might program cell death to occur after a user-defined number of cell divisions as a safety mechanism in engineered strains used for biosensing, bioremediation, or medical purposes. In addition, the multiple-inducer DIC counter might be used to study sequential events that occur in settings such as developmental biology and gene cascades; the single-inducer DIC counter could record events encountered in its environment (e.g., for biosensing); and our SIMM design could be used in other synthetic circuits to maintain genetic memory of low-frequency events, for therapeutic or other applications, such as studying neural circuits.

References and Notes

1. S. Marcand, E. Gilson, D. Shore, *Science* **275**, 986 (1997).
2. A. Ray, K. W. Runge, *Mol. Cell. Biol.* **19**, 31 (1999).
3. D. A. Brock, R. H. Gomer, *Genes Dev.* **13**, 1960 (1999).
4. F. J. Isaacs *et al.*, *Nat. Biotechnol.* **22**, 841 (2004).
5. Materials and methods are available as supporting material on *Science* Online.
6. F. Buchholz, P. O. Angrand, A. F. Stewart, *Nat. Biotechnol.* **16**, 657 (1998).
7. A. C. Groth, M. P. Calos, *J. Mol. Biol.* **335**, 667 (2004).
8. T. S. Ham, S. K. Lee, J. D. Keasling, A. P. Arkin, *Biotechnol. Bioeng.* **94**, 1 (2006).
9. J. B. Andersen *et al.*, *Appl. Environ. Microbiol.* **64**, 2240 (1998).
10. D. A. Wright *et al.*, *Nat. Protocols* **1**, 1637 (2006).
11. S. W. Santoro, P. G. Schultz, *Proc. Natl. Acad. Sci. U.S.A.* **99**, 4185 (2002).
12. M. B. Elowitz, S. Leibler, *Nature* **403**, 335 (2000).
13. T. S. Gardner, C. R. Cantor, J. J. Collins, *Nature* **403**, 339 (2000).
14. T. S. Bayer, C. D. Smolke, *Nat. Biotechnol.* **23**, 337 (2005).
15. D. Baker *et al.*, *Sci. Am.* **294**, 44 (2006).
16. O. Rackham, J. W. Chin, *Nat. Chem. Biol.* **1**, 159 (2005).
17. K. Rinaudo *et al.*, *Nat. Biotechnol.* **25**, 795 (2007).
18. Y. Yokobayashi, R. Weiss, F. H. Arnold, *Proc. Natl. Acad. Sci. U.S.A.* **99**, 16587 (2002).
19. N. J. Guido *et al.*, *Nature* **439**, 856 (2006).
20. J. M. Pedraza, A. van Oudenaarden, *Science* **307**, 1965 (2005).
21. T. L. Deans, C. R. Cantor, J. J. Collins, *Cell* **130**, 363 (2007).
22. E. Fung *et al.*, *Nature* **435**, 118 (2005).
23. B. P. Kramer *et al.*, *Nat. Biotechnol.* **22**, 867 (2004).
24. J. Stricker *et al.*, *Nature* **456**, 516 (2008).
25. S. Basu, Y. Gerchman, C. H. Collins, F. H. Arnold, R. Weiss, *Nature* **434**, 1130 (2005).
26. H. Kobayashi *et al.*, *Proc. Natl. Acad. Sci. U.S.A.* **101**, 8414 (2004).
27. A. Levskaya *et al.*, *Nature* **438**, 441 (2005).
28. T. K. Lu, J. J. Collins, *Proc. Natl. Acad. Sci. U.S.A.* **104**, 11197 (2007).
29. T. K. Lu, J. J. Collins, *Proc. Natl. Acad. Sci. U.S.A.* **106**, 4629 (2009).

30. Supported by the NIH Director's Pioneer Award Program, the NSF Frontiers in Integrative Biological Research program, and the Howard Hughes Medical Institute. Authors' contributions are in supporting online materials.

Supporting Online Material

www.sciencemag.org/cgi/content/full/324/5931/1199/DC1
Materials and Methods
SOM Text
Figs. S1 to S13
Tables S1 and S2
References

9 February 2009; accepted 31 March 2009
10.1126/science.1172005

Structural Basis of Transcription: Backtracked RNA Polymerase II at 3.4 Angstrom Resolution

Dong Wang, David A. Bushnell, Xuhui Huang, Kenneth D. Westover, Michael Levitt, Roger D. Kornberg*

Transcribing RNA polymerases oscillate between three stable states, two of which, pre- and posttranslocated, were previously subjected to x-ray crystal structure determination. We report here the crystal structure of RNA polymerase II in the third state, the reverse translocated, or "backtracked" state. The defining feature of the backtracked structure is a binding site for the first backtracked nucleotide. This binding site is occupied in case of nucleotide misincorporation in the RNA or damage to the DNA, and is termed the "P" site because it supports proofreading. The predominant mechanism of proofreading is the excision of a dinucleotide in the presence of the elongation factor SII (TFIIS). Structure determination of a cocrystal with TFIIS reveals a rearrangement whereby cleavage of the RNA may take place.

RNA polymerases catalyze rapid RNA chain growth [20 to 70 nucleotides (nt) per second for RNA polymerase II (pol II)] in a template-directed manner (*1*–*4*). They do not, however, move monotonously forward on the template. Rather, they oscillate between forward and backward movement at every step in the process (*5*). Three states of a transcribing complex are observed (Fig. 1): a pretranslocation state, in which the nucleotide just added to the growing RNA chain is still in the nucleotide addition site; a posttranslocation state, in which the enzyme has moved forward on the template, which makes the nucleotide addition site available for entry of the next nucleoside triphosphate (NTP); and a backtracked state, in which the enzyme has retreated on the template, extruding the 3′-end of the RNA (*6*, *7*). Forward movement is favored by NTP binding, which traps the complex in the posttranslocation state. Backtracking predominates when forward movement is impeded, for example, by damage in the template or by nucleotide misincorporation in the RNA (*8*, *9*). Backtracking by one or a few residues is reversible, whereas backtracking a greater distance leads to arrest, from which recovery is only possible by cleavage of the transcript in the polymerase active center, induced by transcription factor SII (TFIIS) in eukaryotes and GreA and/or Gre B in bacteria [reviewed in (*10*–*13*)]. Backtracking and cleavage enable proofreading of the transcript, through the excision of misincorporated nucleotides and resynthesis (*9*, *14*–*21*).

X-ray crystal structures of pol II transcribing complexes in the pre- and posttranslocation states have been obtained, illuminating the mechanisms of RNA synthesis and product release (*22*–*25*). Here, we report x-ray structures of backtracked complexes, showing that they are stable intermediates and completing the overall picture of the transcription process. Some of the backtracked structures include TFIIS, which reveals interactions responsible for transcript cleavage, proofreading, and recovery from arrest.

Backtracked complexes were produced by two approaches (*26*). DNA-RNA hybrids with mismatched nucleotides at the 3′-end of the RNA were bound to pol II, which directly recreated a backtracked state. Alternatively, DNA-RNA hybrids bearing DNA damage downstream of the 3′-end of the RNA were transcribed by pol II, with the expectation that the enzyme encountering the impediment would retreat to a backtracked state. In both cases, crystal structures were obtained showing extra electron density for the transcript downstream of the nucleotide addition site, indicative of an extruded 3′-end. The structures were, moreover, very similar (Fig. 2A and fig. S1).

In a complex with a hybrid containing one mismatched residue at the 3′-end of the RNA (12-nt oligomer RNA), the last matched residue, uridine 5′-monophosphate (UMP), was in the nucleotide addition site (designated +1) and the mismatched residue, guanosine 5′-monophosphate (GMP), was in a location downstream (+2) not observed in any previous transcribing complex structure (Fig. 2A). The UMP base was paired with its complement in the DNA template but tilted 15° to 20° out of the plane. Between the UMP and GMP, the backbone of the backtracked RNA was bent over 120° out of the path of the hybrid helix, which enabled the GMP base to hydrogen-bond with the adenosine 5′-monophosphate (AMP) base two residues away (position –1) in the RNA chain (Fig. 2C).

Interactions between the RNA and the bridge helix, trigger loop, and other pol II residues created a binding pocket for the backtracked GMP (Fig. 2, A and B) and caused the deviations from hybrid helix geometry observed. Bridge helix residue [RNA pol II subunit (Rpb)] Rpb1 Thr^{827}, Rpb2 Tyr^{769}, and Rpb2 529 to 531 contacted the GMP. These contacts are consistent with previous biochemical evidence that the base of GMP at the +2 position participates in polymerase interaction (*27*). The N-2 amino group of the base helps fix the location of GMP through pol II interaction. Although the precise positions of Mg^{2+} and associated water could not be determined at the resolution of our analysis, the proposal that N-7 of GMP base and/or Rpb2 Tyr^{769} coordinate Mg^{2+} and water for nucleophilic attack during intrinsic cleavage is at least consistent with the structure (*27*). Rpb 1 Asn^{479} and Arg^{446} contacted the UMP one nucleotide away from the GMP and the AMP two nucleotides away. The trigger loop was in a conformation intermediate between the "open" and "closed" conformations previously observed (*22*–*25*, *28*–*30*). Trigger loop residues Rpb1 Asn^{1082} and Gln^{1078} contacted the phosphate group between the UMP and GMP, whereas His^{1085}, believed to play a role in catalysis in the closed conformation (*25*), was directed away from the RNA and close to Rpb1 Ser^{769} and Gly^{772}.

In a complex with a hybrid containing two mismatched residues at the 3′-end (13-nt oligomer RNA), the last matched residue (UMP) and the first of the mismatched residues (GMP) were in locations similar to those for the complex with one mismatched residue (Fig. 2C).

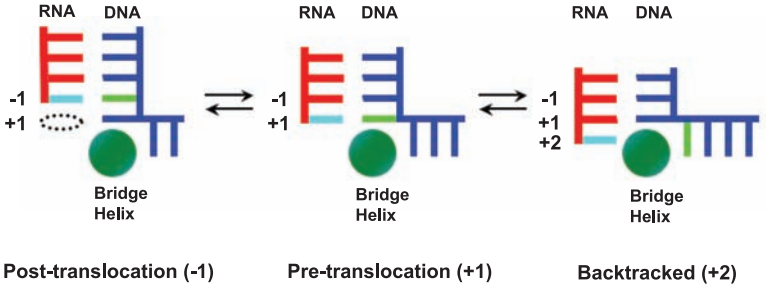

Fig. 1. The three states of a pol II transcription elongation complex. RNA transcript is red, DNA template is blue. The nucleotide base just added to the 3′-end of RNA and the complementary base in the DNA template are represented by cyan and green bars, respectively. The dashed oval represents the empty nucleotide addition site in the posttranslocation state. The green circle represents the pol II bridge helix.

Department of Structural Biology, Stanford University School of Medicine, Stanford, CA 94305, USA.

*To whom correspondence should be addressed. E-mail: kornberg@stanford.edu

The UMP base, paired with its complement in the DNA template, was tilted 20° to 30° out of the plane, and the backbone of the backtracked RNA was bent 80° to 90° out of the path of the hybrid helix (Fig. 2C). The next backtracked (second mismatched) residue was not revealed in the structure, because of motion or static disorder. In molecular dynamics simulations (Fig. 2D) [supporting online material (SOM) text (*26*)], this backtracked residue was highly mobile, which would argue in favor of motion rather than disorder.

Backtracked complexes containing additional mismatched residues and with different mismatched sequences showed the same conformation for the first mismatched residue. A complex with three mismatched residues (14-nt oligomer RNA) also showed no ordering of residues beyond position +2, but a complex with seven mismatched residues (18-nt oligomer RNA) produced more electron density downstream (Fig. 3A). Backtracked nucleotides at positions +3 and +4 could be built into this density, although the base and sugar at +4 were disordered. The backbone of the backtracked RNA was sharply bent between positions +2 and +3, owing to salt bridges of Rpb2 residues Gln^{763} and Arg^{766} with the phosphate between +2 and +3. Rpb1 Lys^{752}, Rpb2 Ser^{1019}, and Rpb2 Arg^{1020} appeared to form hydrogen bonds or salt bridges with the phosphate between +3 and +4 (Fig. 3B). Three regions of pol II interact with the backtracked RNA; bridge helix residues Rpb1 824 to 827 and Rpb2 regions 760 to 772 and 529 to 531 also interact with one another and form a network that probably enhances the stability of the backtracked state. In the more extensively backtracked complex structures, the trigger loop was in an "open" conformation, remote from the nucleotide-addition site. Part of the trigger loop (Rpb1 1078 to 1081), however, remained near enough to interact with the backtracked RNA.

To determine whether nucleotides other than GMP would be stably bound at the +2 position in the backtracked state, we also solved structures of backtracked complexes containing RNA of the same length (13-nt oligomer) but with UMP rather than GMP at this position. We observed significant electron density attributable to UMP in a similar location to that found for GMP. The UMP base was in the same binding pocket as the GMP base (between bridge helix residues Rpb1 824 to 827 and Rpb2 769), whereas the ribose sugar was in a different location, interacting with Rpb2 766 (fig. S5).

Cleavage of backtracked RNA in the presence of TFIIS depends on an Asp^{290}-Glu^{291} dipeptide in a hairpin loop of domain III of the protein (*31*), a zinc ribbon motif. Domain II, a three-helix bundle, and the linker between domains II and III are responsible for binding to pol II (*32*–*36*). Domain I, an N-terminal four-helix bundle, is nonessential in vitro (*34*, *37*, *38*), but appears to play a role in transcription initiation (*39*, *40*). A crystal structure of transcribing pol II in the posttranslocation state, complexed with TFIIS (*28*, *41*), showed domain III inserted in the pol II secondary channel (pore and funnel) but gave limited insight into the TFIIS mechanism, because of the absence of backtracked RNA. Superposition of this structure [Protein Data Bank (PDB) no. 1Y1V] with our backtracked complex structure reveals a steric clash of the hairpin loop of TFIIS domain III with backtracked RNA (Fig. 4). In particular, the

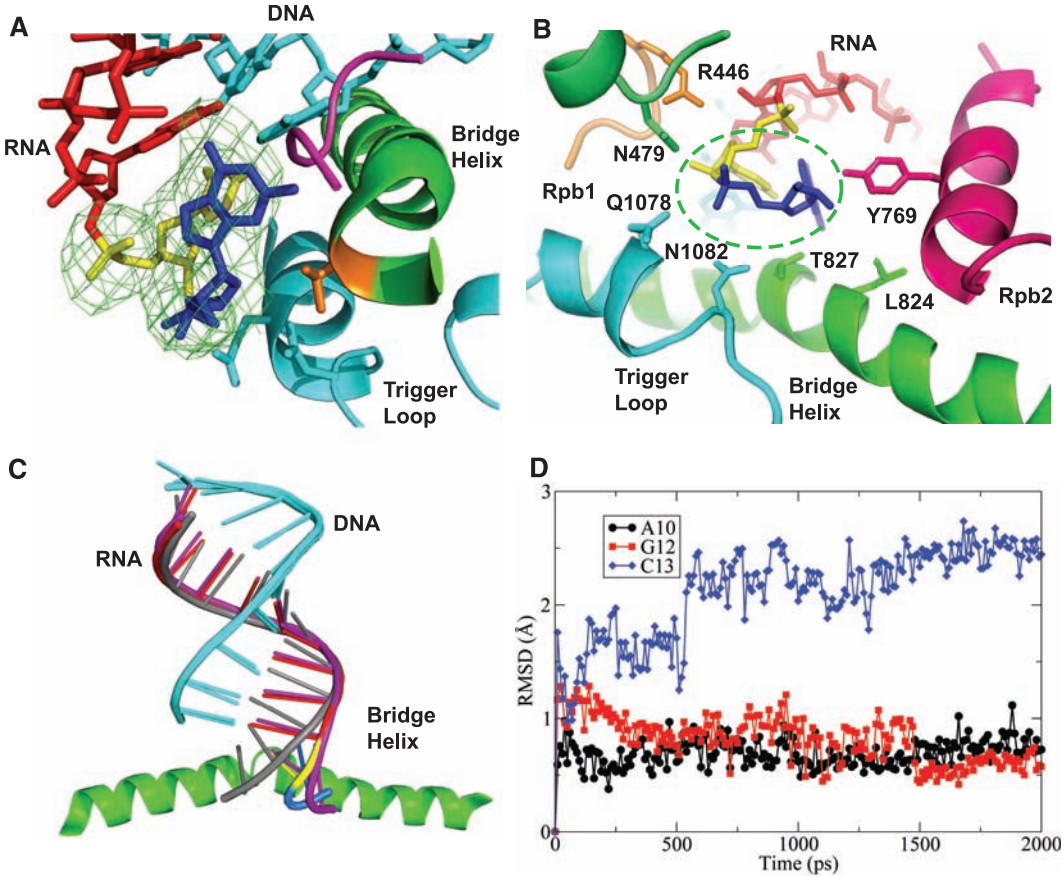

Fig. 2. Structure of pol II elongation complex in the backtracked state. (**A**) Complex with one mismatched residue at the 3′-end of the RNA (12-nt oligomer RNA). The view is a standard one, from the "Rpb2 side," as in the past (*22*–*25*). Difference electron density map ($F_{obs} - F_{calc}$ omit map, contoured at 3.0 sigma) between backtracked and posttranslocation complexes is shown in green mesh. RNA and DNA are red and cyan. Ribonucleotides at +1 and +2 positions in the RNA are yellow and blue. Parts of bridge helix (Rpb1 825 to 848) and trigger loop (Rpb1 1070 to 1100) are green and cyan. Rpb1 T827 is orange. Side chains of Rpb1 Q1078 and N1082 are also shown. Rpb2 527 to 532 is in light magenta. (**B**) The binding pocket for backtracked ribonucleotide at position +2. View is rotated from that in (A) to better reveal side-chain interactions. Rpb1 440 to 450, Rpb1 470 to 481, bridge helix (Rpb1 810 to 848), trigger loop (1070 to 1100), and Rpb2 760 to 776 are in orange, lime green, green, cyan, and hot pink, respectively. Side chains of Rpb1 (R446, N479, L824, T827, Q1078, and N1082) and Rpb2 (Y769) are shown. Other colors as in (A). The binding pocket is highlighted by a dashed green circle. (**C**) Backtracked RNA is kinked toward the bridge helix and differs from canonical A form RNA. Backbones of one-base–mismatch backtracked RNA (red, yellow, and blue) and canonical A form RNA (gray) are superimposed. The superimposed two-base–mismatch structure is shown in magenta. Color scheme as in (A). View is rotated 90° counterclockwise about a vertical axis from that in (A). (**D**) Molecular dynamics simulation of bases in the two-base–mismatch (13-nt oligomer RNA) complex. Deviations of bases three (A10) and one (G12) residues from the 3′-end, and of the 3′-terminal residue (C13). Root mean square deviation (RMSD) values with respect to the starting conformation were computed every 10 ps.

catalytic Asp[290] and Glu[291] residues of TFIIS come too close to the phosphate group between the –1 and +1 positions in the RNA (Fig. 4A) and clash with the side chain of Rpb2 Tyr[769] (Fig. 4B). This TFIIS structure might reflect the state following RNA cleavage, but to investigate interactions relevant to cleavage itself, we determined the structure of pol II in the backtracked state, with 13-nt oligomer RNA, complexed with a point mutant of TFIIS (E291H), in which Glu[291] is replaced by His, unable to cleave the RNA (*34*, *42*). Initial phases were obtained by molecular replacement with the previous structure (1Y1V), with the omission of TFIIS, Rpb 4/7, the trigger loop, and nucleic acids. The initial electron density map clearly showed the three-helix bundle of domain II of TFIIS, part of domain III, a long α helix of the interdomain linker, the pol II trigger loop, and nucleic acids. Trigger loop and nucleic acid models were manually built into the electron density. TFIIS was then manually docked, and rigid body refinement was performed, followed by manual adjustment of the conformation of the hairpin loop of domain III.

Parts of the electron density map were of sufficient quality that side chains could be placed and specific interactions between TFIIS and pol II identified (for example, the interdomain linker–pol II interaction). In the case of the hairpin loop, only the main chain could be built, because of limitations of resolution and less defined secondary structure. The structure clearly showed a different position of the hairpin loop from that seen previously (Fig. 4B). The position of the backtracked RNA was also affected, as the residue at +2 was disordered. There was no evidence of a 4 Å shift of the upstream RNA in the RNA-DNA hybrid region previously reported (*28*, *41*). The remainder of TFIIS was similar in conformation between the present and previous structures (*28*, *41*). The trigger loop was in an "open" conformation in both structures (*28*, *41*).

Superposition of our backtracked pol II–TFIIS complex structure with our structures of backtracked pol II alone revealed a steric clash of the hairpin loop with the RNA, but less severe than that observed with the previous posttranslocation complex–TFIIS structure. The clash was more pronounced for longer backtracked RNAs (15-nt, 18-nt, and 24-nt oligomer RNAs). Evidently, some rearrangement is required to accommodate both TFIIS and RNA in the complex, shown by the disorder of the residue at +2 in the 13-nt oligomer RNA cocrystal.

In the presence of wild-type TFIIS, backtracked complexes containing one, two, three, four, and seven mismatched residues were cleaved at positions two, three, four, five, and eight residues from the 3′-end of the RNA (fig. S6, A and C). On the basis of the structures of the complexes, we conclude that cleavage occurs between the addition site (–1) and the position preceding (+1 site). In effect, cleavage represents the reversal of nucleotide addition, except with water rather than pyrophosphate as the nucleophile (*43*, *44*).

The cleavage rates of mismatched complexes were 15- to 30-fold the rates of those of matched complexes (fig. S6A) (*26*), in keeping with results of previous studies (*9*). This preferential cleavage of mismatched complexes is the presumed basis for the error correction capability of TFIIS (*21*). Selective removal of mismatched residues has been observed for *E. coli* RNA polymerase stimulated by the TFIIS homolog GreA (*45*), *Archaeal* RNA polymerase stimulated by TFS (*46*, *47*), and pol III with its intrinsic counterpart of TFIIS (*48*).

Selective removal of mismatched residues has also been observed in the absence of GreA for *T. aquaticus* RNA polymerase (*27*). This "intrinsic" cleavage is much slower than the TFIIS-stimulated reaction (fig. S6). The half time for intrinsic cleavage of a backtracked complex with one mismatched residue (12-nt oligomer RNA) was about 440 s, compared with about 10 s for cleavage in presence of 100 nM TFIIS [equilibrium constant (K_e) for TFIIS–pol II interaction is about 100 nM] (fig. S6C) (*26*). Intrinsic cleavage of longer backtracked complexes was barely detectable. More rapid rates of intrinsic cleavage reported for *T. aquaticus* RNA polymerase (*27*) likely reflect differences in reaction conditions, such as higher Mg^{2+} concentration, pH, and temperature, as well as the different RNA polymerases involved.

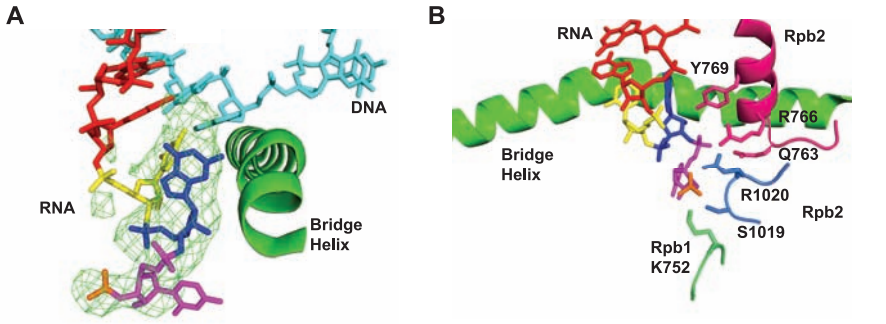

Fig. 3. Structure of backtracked complex with seven mismatched residues at the 3′-end of the RNA (18-nt oligomer RNA). (**A**) Same representation as Fig. 2A, except that ribonucleotide at +3 position is magenta and phosphate group at +4 position is orange. (**B**) Interactions of pol II with additional backtracked residues. Rpb1 750 to 754, Rpb2 760 to 772, and Rpb2 1018 to 1022 are lime green, hot pink, and marine blue, respectively. Other colors as in Fig. 2A, view as in Fig. 2C. Side chains of Rpb1 (K752) and Rpb2 (Q763, R766, Y769, S1019, and R1020) are shown.

Fig. 4. Structure of backtracked complex with TFIIS. (**A**) Clash of backtracked RNA with published structure of TFIIS. Backtracked complex with one mismatched base (12-nt oligomer RNA), depicted as in Fig. 2A, was superposed with TFIIS (1Y1V), with the use of Coot, on the basis of secondary-structure matching (ssm) of RPB1. The tip of domain III of TFIIS is light blue. Side chains of TFIIS residues 290 and 291 are shown. Parts of bridge helix and trigger loop of 1Y1V complex are wheat-colored. (**B**) Structure of backtracked complex with two mismatched bases (13-nt oligomer RNA) complexed with TFIIS. Backtracked complex is depicted as in Fig. 2A, except slightly rotated, and with Rpb2 760 to 776 in hot pink. The tip of domain III of TFIIS is magenta. Corresponding regions from 1Y1V are superimposed; pol II in wheat and TFIIS in light blue.

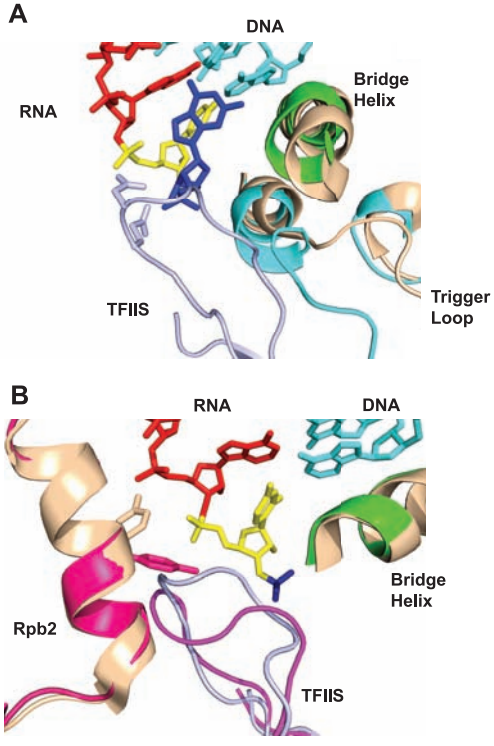

In our system, longer backtracked RNAs were also cleaved more slowly in the presence of TFIIS. The cleavage rates of backtracked 12-nt, 13-nt, and 14-nt oligomer were 1200-, 480-, and 60-fold faster than that for backtracked 18-nt oligomer (*26*). This trend presumably relates to the rearrangement required to accommodate both TFIIS and backtracked RNA in the pol II secondary channel. Longer RNA may undergo rearrangement less readily, because of more extensive interaction in the secondary channel.

To further investigate the influence of base mismatch on cleavage in the presence of TFIIS, we prepared a backtracked complex with a G<>U mismatch instead of a G<>G mismatch. Because G<>U can form a wobble base pair, it might occupy the nucleotide addition site at +1 rather than backtracking to +2. We observed two cleavage products, of two and three residues, instead of the single product of three residues found for a G<>G mismatch (fig. S6B). Evidently, a wobble base pair does form to a limited extent.

Our results lead to two conclusions. First, pol II backtracked by one residue represents a discrete, stable state of the transcribing enzyme. In the course of backtracking, pol II stalls at this position. The evidence is threefold: the observation of a defined structure of the 12-nt oligomer RNA complex, in which the backtracked nucleotide is revealed at full occupancy; the absence of density for additional nucleotides in 13-nt and 14-nt oligomer RNA complexes; and molecular dynamics simulations, showing that nucleotides beyond the first backtracked residue are expected to be highly mobile. The demonstration of a defined one-residue–backtracked state supports the long held, but largely conjectural, notion of polymerases in diffusional equilibrium between forward and retrograde motion during transcription. Backtracking by one residue is favorable, whereas backtracking by two or three more residues confers no greater energetic benefit. Longer backtracked RNAs do make additional interactions, possibly contributing to arrest (irreversible backtracking) and, by alteration of the RNA conformation, to the ability of TFIIS to rescue the complex from the arrested state (*49*).

The second conclusion concerns the significance of the one-residue–backtracked state. It is readily cleaved in the presence of TFIIS and releases a dinucleotide, which supports the previous ideas that cleavage occurs in the pol II active site, and that an important role of this cleavage is the removal of misincorporated nucleotides. The pol II structure is evidently well suited to the purpose. In the event of misincorporation, forward translocation is disfavored, because of distortion of the RNA-DNA hybrid helix, and the diffusional equilibrium of the enzyme is shifted towards the backtracked state. A significant lifetime in this state, due to binding of the misincorporated nucleotide in the +2 position, leads to cleavage. The stability of the one-residue–backtracked state thus underlies the proofreading capability of the pol II system. We refer to the nucleotide-binding site at +2, which defines the backtracked state, as the "P" site.

Cleavage in the one-residue–backtracked state can occur both in the presence of TFIIS and in its absence ("intrinsic cleavage"). Because the reaction with TFIIS is faster in vitro by more than 100-fold, it is likely the predominant mechanism in vivo. Intrinsic cleavage may nevertheless play an important role, as disruption of the gene for TFIIS causes at most an error rate 10 times as great in transcription (*50*–*53*).

References and Notes

1. P. B. Sehgal, E. Derman, G. R. Molloy, I. Tamm, J. E. Darnell, *Science* **194**, 431 (1976).
2. D. S. Ucker, K. R. Yamamoto, *J. Biol. Chem.* **259**, 7416 (1984).
3. S. Boireau *et al*., *J. Cell Biol.* **179**, 291 (2007).
4. X. Darzacq *et al*., *Nat. Struct. Mol. Biol.* **14**, 796 (2007).
5. F. Toulme, M. Guerin, N. Robichon, M. Leng, A. R. Rahmouni, *EMBO J.* **18**, 5052 (1999).
6. D. Reines, P. Ghanouni, W. Gu, J. Mote Jr., W. Powell, *Cell. Mol. Biol. Res.* **39**, 331 (1993).
7. N. Komissarova, M. Kashlev, *Proc. Natl. Acad. Sci. U.S.A.* **94**, 1755 (1997).
8. B. A. Donahue, S. Yin, J. S. Taylor, D. Reines, P. C. Hanawalt, *Proc. Natl. Acad. Sci. U.S.A.* **91**, 8502 (1994).
9. C. Jeon, K. Agarwal, *Proc. Natl. Acad. Sci. U.S.A.* **93**, 13677 (1996).
10. M. Wind, D. Reines, *Bioessays* **22**, 327 (2000).
11. R. N. Fish, C. M. Kane, *Biochim. Biophys. Acta* **1577**, 287 (2002).
12. R. J. Sims 3rd, R. Belotserkovskaya, D. Reinberg, *Genes Dev.* **18**, 2437 (2004).
13. A. Shilatifard, R. C. Conaway, J. W. Conaway, *Annu. Rev. Biochem.* **72**, 693 (2003).
14. M. G. Izban, D. S. Luse, *J. Biol. Chem.* **268**, 12874 (1993).
15. M. G. Izban, D. S. Luse, *J. Biol. Chem.* **268**, 12864 (1993).
16. M. G. Izban, D. S. Luse, *Genes Dev.* **6**, 1342 (1992).
17. D. Reines, *J. Biol. Chem.* **267**, 3795 (1992).
18. M. D. Rudd, M. G. Izban, D. S. Luse, *Proc. Natl. Acad. Sci. U.S.A.* **91**, 8057 (1994).
19. W. Gu, D. Reines, *J. Biol. Chem.* **270**, 30441 (1995).
20. W. Gu, W. Powell, J. Mote Jr., D. Reines, *J. Biol. Chem.* **268**, 25604 (1993).
21. M. J. Thomas, A. A. Platas, D. K. Hawley, *Cell* **93**, 627 (1998).
22. A. L. Gnatt, P. Cramer, J. Fu, D. A. Bushnell, R. D. Kornberg, *Science* **292**, 1876 (2001).
23. K. D. Westover, D. A. Bushnell, R. D. Kornberg, *Science* **303**, 1014 (2004).
24. K. D. Westover, D. A. Bushnell, R. D. Kornberg, *Cell* **119**, 481 (2004).
25. D. Wang, D. A. Bushnell, K. D. Westover, C. D. Kaplan, R. D. Kornberg, *Cell* **127**, 941 (2006).
26. Materials and methods are available as supporting material on *Science* Online.
27. N. Zenkin, Y. Yuzenkova, K. Severinov, *Science* **313**, 518 (2006).
28. H. Kettenberger, K. J. Armache, P. Cramer, *Mol. Cell* **16**, 955 (2004).
29. C. D. Kaplan, K. M. Larsson, R. D. Kornberg, *Mol. Cell* **30**, 547 (2008).
30. F. Brueckner, P. Cramer, *Nat. Struct. Mol. Biol.* **15**, 811 (2008).
31. C. Jeon, H. Yoon, K. Agarwal, *Proc. Natl. Acad. Sci. U.S.A.* **91**, 9106 (1994).
32. V. Booth, C. M. Koth, A. M. Edwards, C. H. Arrowsmith, *J. Biol. Chem.* **275**, 31266 (2000).
33. X. Qian *et al*., *Biochemistry* **32**, 9944 (1993).
34. D. E. Awrey *et al*., *J. Biol. Chem.* **273**, 22595 (1998).
35. X. Qian, C. Jeon, H. Yoon, K. Agarwal, M. A. Weiss, *Nature* **365**, 277 (1993).
36. P. E. Morin, D. E. Awrey, A. M. Edwards, C. H. Arrowsmith, *Proc. Natl. Acad. Sci. U.S.A.* **93**, 10604 (1996).
37. V. K. Olmsted *et al*., *J. Biol. Chem.* **273**, 22589 (1998).
38. M. Shimoaraiso, T. Nakanishi, T. Kubo, S. Natori, *J. Biol. Chem.* **272**, 26550 (1997).
39. B. Guglielmi, J. Soutourina, C. Esnault, M. Werner, *Proc. Natl. Acad. Sci. U.S.A.* **104**, 16062 (2007).
40. B. Kim *et al*., *Proc. Natl. Acad. Sci. U.S.A.* **104**, 16068 (2007).
41. H. Kettenberger, K. J. Armache, P. Cramer, *Cell* **114**, 347 (2003).
42. Single-letter abbreviations for the amino acid residues are as follows: A, Ala; C, Cys; D, Asp; E, Glu; F, Phe; G, Gly; H, His; I, Ile; K, Lys; L, Leu; M, Met; N, Asn; P, Pro; Q, Gln; R, Arg; S, Ser; T, Thr; V, Val; W, Trp; and Y, Tyr.
43. V. Sosunov *et al*., *EMBO J.* **22**, 2234 (2003).
44. E. Sosunova *et al*., *Proc. Natl. Acad. Sci. U.S.A.* **100**, 15469 (2003).
45. D. A. Erie, O. Hajiseyedjavadi, M. C. Young, P. H. von Hippel, *Science* **262**, 867 (1993).
46. W. Hausner, U. Lange, M. Musfeldt, *J. Biol. Chem.* **275**, 12393 (2000).
47. U. Lange, W. Hausner, *Mol. Microbiol.* **52**, 1133 (2004).
48. N. Alic *et al*., *Proc. Natl. Acad. Sci. U.S.A.* **104**, 10400 (2007).
49. E. A. Galburt *et al*., *Nature* **446**, 820 (2007).
50. H. Koyama, T. Ito, T. Nakanishi, N. Kawamura, K. Sekimizu, *Genes Cells* **8**, 779 (2003).
51. H. Koyama, T. Ito, T. Nakanishi, K. Sekimizu, *Genes Cells* **12**, 547 (2007).
52. N. K. Nesser, D. O. Peterson, D. K. Hawley, *Proc. Natl. Acad. Sci. U.S.A.* **103**, 3268 (2006).
53. R. J. Shaw, N. D. Bonawitz, D. Reines, *J. Biol. Chem.* **277**, 24420 (2002).

54. This research was supported by NIH grants GM049985 and GM036559 to R.D.K. D.W. was supported by a special fellow award from the Leukemia and Lymphoma Society and the NIH Pathway to Independence Award (K99 GM085136). X.H. and M.L. were supported by NIH Roadmap for Medical Research Grant U54 GM072970 and NIH grant GM041455. Portions of the research were carried out at the Stanford Synchrotron Radiation Laboratory, a national user facility operated by Stanford University on behalf of the U.S. Department of Energy (DOE), Office of Basic Energy Sciences. The SSRL Structural Molecular Biology Program is supported by the DOE, Office of Biological and Environmental Research, and by the National Institutes of Health, National Center for Research Resources, Biomedical Technology Program, and the National Institute of General Medical Sciences. Portions of this research were conducted at the Advanced Light Source, a national user facility operated by Lawrence Berkeley National Laboratory, on behalf of the DOE, Office of Basic Energy Sciences. The Berkeley Center for Structural Biology is supported in part by the DOE, Office of Biological and Environmental Research, and by the National Institutes of Health, National Institute of General Medical Sciences. We thank C. D. Kaplan for providing TFIIS E291H mutant for structural studies. PDB accession codes: 13-nt oligomer backtracked pol II, 3GTJ; 18-nt oligomer backtracked pol II, 3GTK; 12-nt oligomer backtracked pol II, 3GTG; and 13-nt oligomer backtracked pol II with TFIIS, 3GTM.

Supporting Online Material

www.sciencemag.org/cgi/content/full/324/5931/1203/DC1
Materials and Methods
SOM Text
Figs. S1 to S6
Tables S1 to S3
References

19 November 2008; accepted 9 April 2009
10.1126/science.1168729

High-Frequency, Long-Range Coupling Between Prefrontal and Visual Cortex During Attention

Georgia G. Gregoriou,[1]* Stephen J. Gotts,[2]* Huihui Zhou,[1] Robert Desimone[1]†

Electrical recordings in humans and monkeys show attentional enhancement of evoked responses and gamma synchrony in ventral stream cortical areas. Does this synchrony result from intrinsic activity in visual cortex or from inputs from other structures? Using paired recordings in the frontal eye field (FEF) and area V4, we found that attention to a stimulus in their joint receptive field leads to enhanced oscillatory coupling between the two areas, particularly at gamma frequencies. This coupling appeared to be initiated by FEF and was time-shifted by about 8 to 13 milliseconds across a range of frequencies. Considering the expected conduction and synaptic delays between the areas, this time-shifted coupling at gamma frequencies may optimize the postsynaptic impact of spikes from one area upon the other, improving cross-area communication with attention.

A typical crowded scene contains many objects that cannot be processed simultaneously, thus requiring attentional mechanisms to select the ones most relevant to behavior. Electrophysiological studies in monkeys have shown that attention leads to enhanced responses of neurons in ventral stream areas that are important for object recognition, at the expense of responses to distracting stimuli (*1*). Moreover, attention increases neural synchrony, often in the gamma frequency range (*2*–*5*). Given that cells have limited integration times, increases in synchrony and firing rates may together have a larger impact on downstream neurons and thus increase the effectiveness of behaviorally relevant stimuli (*6*, *7*). Areas in the prefrontal cortex (PFC) and parietal cortex may be sources of the top-down attentional feedback to ventral stream areas, which could enhance firing rates with attention (*1*, *4*, *8*). However, the mechanisms that cause increases in neural synchrony with attention in visual cortex are unknown.

We investigated whether the frontal eye field (FEF), an area within the PFC, is a source of enhanced neural synchrony effects in area V4 during attention. The FEF has reciprocal connections with V4 (*9*–*11*), and electrical stimulation of FEF enhances V4 neuronal responses to a stimulus in the receptive field (RF) (*12*, *13*). We recorded spikes (multi-unit) and local field potentials (LFPs) simultaneously from FEF and V4 in two monkeys trained in a covert attention task (Fig. 1A) (*14*). One grating stimulus appeared inside the shared RF, and two others appeared outside. After a variable delay, the spot at fixation changed color (which was the cue) so as to match the color of one of the three gratings, indicating the target stimulus to be attended. The monkey was rewarded for releasing a bar when the target stimulus changed color.

We first verified that attention caused enhanced firing rates in FEF and V4. We recorded from 292 sites with visual responses in FEF and 262 sites in V4. The results were qualitatively similar (and statistically significant) in both monkeys and were therefore combined. Figure 1, B and C, shows the average normalized response of the population of FEF and V4 neurons, respectively, for conditions with overlapping RFs. Neuronal responses were significantly increased by attention to the joint RF in both areas (average response in a window 100 to 800 ms after cue onset; Wilcoxon sign-rank test, $P < 0.001$) and remained significantly enhanced until the end of the trial (average response in a window 500 ms before the target's color change; Wilcoxon sign-rank test, $P < 0.001$) [for the distribution of attentional effects on firing rate, see the supporting online material (SOM) text].

Attentional effects on firing rates occurred significantly earlier in FEF than in V4 (at 80 ms after the cue in FEF, and 130 ms after the cue in V4) [Fig. 1, B and C dashed lines; $P = 0.017$ two-sided permutation test (SOM text)]. The distribution of attentional latencies is shown separately for FEF and V4 in Fig. 1, D and E, and was similarly shifted earlier for FEF (Wilcoxon rank-sum test, $P < 0.001$) (for a table of latency measurements, see table S1).

We next used multi-taper spectral methods to calculate the coherence between spikes and LFPs (*14*). Spike-field coherence in the gamma band significantly increased with attention within each area (coherence averaged between 40 and 60 Hz; paired t test, $P < 0.001$ in both areas), whereas low frequencies were desynchronized (average coherence between 5 and 20 Hz; paired t test, $P < 0.001$ in both areas) (Fig. 2, A and B). At the population level, gamma band coherence increased by 14% in V4 (*2*, *3*, *15*) and by 22% in the FEF (for distributions of effects, see SOM text).

If FEF is the source of enhanced synchrony in V4, the critical question is whether attention

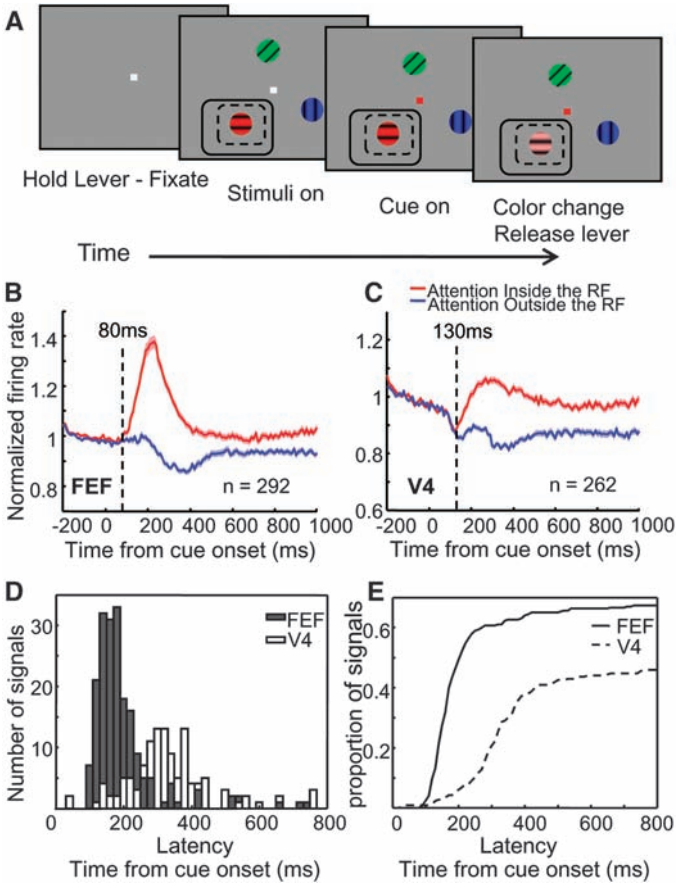

Fig. 1. (**A**) Illustration of behavioral task. Dashed- and solid-line rectangles indicate hypothetical overlapping RFs for V4 and FEF sites, respectively. (**B** and **C**) Normalized firing rates averaged across the population of cells in FEF and V4, respectively. SEM (±) at each time point is indicated by shading over the lines. Vertical dashed lines indicate latency of attentional effects at the population level. (**D**) Distribution of attentional latencies in the firing rates of FEF and V4 neurons. (**E**) Cumulative distribution of FEF and V4 latencies, represented as a proportion of recordings in which latencies could be reliably estimated.

[1]McGovern Institute for Brain Research, Massachusetts Institute of Technology, Cambridge, MA 02139, USA. [2]Laboratory of Brain and Cognition, National Institute of Mental Health, National Institutes of Health, Bethesda, MD 20892, USA.

*These authors contributed equally to this work.
†To whom correspondence should be addressed. E-mail: desimone@mit.edu

increases coupled oscillations between the two areas. We found that the attentional effect on gamma frequency spike-field coherence between areas was even larger than the effects within areas (Fig. 2, C and D). With attention, gamma coherence between V4 spikes and FEF LFPs increased by 26% at the population level (paired t test, $P < 0.001$), between FEF spikes and V4 LFPs increased by 37% (paired t test, $P < 0.001$), and remained enhanced through the end of the trial (paired t test, $P < 0.001$ for all pair types). All of these effects were highly dependent on RF overlap at the locus of attention. For pairs of recordings with nonoverlapping RFs, coherence in the two attention conditions did not differ from that in the pre-stimulus period (one-way analysis of variance, $P = 0.86$) (Fig. 2F and SOM text).

Gamma frequency coherence between LFPs recorded across the two areas was enhanced 63% by attention (Fig. 2E) (paired t test, $P < 0.001$), and gamma coherence between spike trains across areas was enhanced by 13% (paired t test, $P < 0.001$). In general, spike-spike coherence across electrodes is smaller than spike-field and field-field coherence for statistical reasons (*16*). Another probable factor is that connections between FEF and V4 are patchy (*9*, *10*), and LFPs sum signals over a wider area.

We considered whether the synchronous oscillations between V4 and FEF might have resulted from a common oscillatory input, which would be expected to result in zero phase-lag synchrony between the areas. To test for this, we computed the distribution of the coherence phase shifts within and across areas. Within areas, the distribution of the average (between 40 and 60 Hz) relative phase between the two recorded signals (Fig. 3) had a median close to zero (attend-in condition; Rayleigh test, FEF, $P < 0.001$, median = 7°, and V4, $P < 0.001$, median = –26°), corresponding to a time delay of 0.5 to 1.5 ms between spikes and the phase of maximum depolarization in the LFP at 50 Hz (Fig. 3A). By contrast, the phase of spike-field coherence across areas was shifted approximately half a gamma cycle [attend-in condition; Rayleigh test, FEF spikes–V4 LFPs, $P < 0.001$, median phase = –142° (or 218°), and V4 spikes–FEF LFPs, $P < 0.001$, median phase = 144° (or –216°)], corresponding to a time shift of ~8 (or 12) ms (Fig. 3A). Likewise, the median phase of spike-spike coherence pairs having a maximum gamma coherence peak of at least 0.1 was about 120°, which corresponds to a time shift of 7 ms. Similar results were found by com-

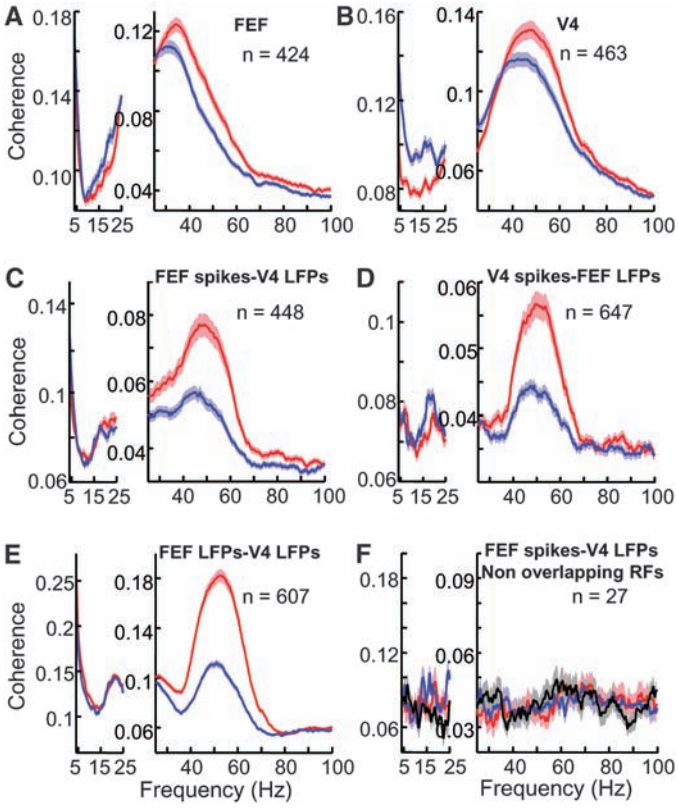

Fig. 2. Attentional enhancement of synchronization. (**A** to **D**) Spike-field coherence (A) within FEF, (B) within V4, (C) between spikes in FEF and LFPs in V4, and (D) between spikes in V4 and LFPs in FEF. (**E**) LFP-LFP coherence between FEF and V4 sites. Conventions are the same as in Fig. 1. (**F**) Spike-LFP coherence between FEF spikes and V4 LFPs from recording sites with nonoverlapping RFs (i) with attention inside the V4 RF during the post-stimulus period (red line), (ii) with attention in right hemifield, outside both V4 and FEF RFs during the post-stimulus period (blue line), and (iii) during the pre-stimulus period with no stimuli except for the fixation spot (black line). Tapers providing an effective smoothing of ±10 Hz were used for spectral estimation of higher frequencies [25 to 100 Hz, right part of (A) to (F)] and tapers providing smoothing of ±3 Hz were used for lower frequencies [<25 Hz, left part of (A) to (F)].

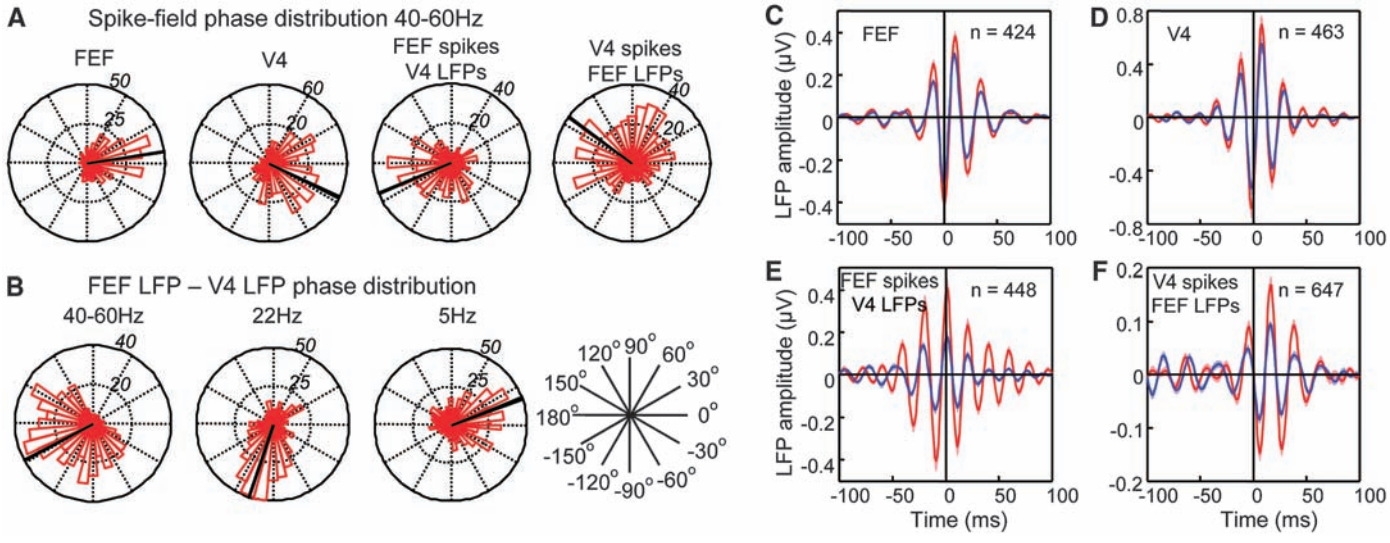

Fig. 3. Relative phase. (**A**) Distribution of average relative phase (40 to 60 Hz) between spikes and LFPs within and across areas. (**B**) Distribution of relative phases between FEF and V4 LFPs at different frequencies (40 to 60 Hz, 22 Hz, and 5 Hz). Shown are all phases from condition with attention inside the RF. (**C** to **F**) Spike-triggered averages of LFPs filtered between 35 and 80 Hz with (C) spikes and LFPs from FEF, (D) spikes and LFPs from V4, (E) spikes from FEF and LFPs from V4, and (F) spikes from V4 and LFPs from FEF. Conventions are the same as in Fig. 1.

paring spike-triggered averages of the LFP within and across areas (Fig. 3, C to F).

Although the peak coherence and largest attentional effects were in the gamma range, there was also coherence between FEF and V4 at other frequencies. We therefore tested whether the phase relationship at these other frequencies followed a fixed time shift of ~8 to 12 ms or a fixed phase shift of half a cycle. The medians of the distributions for the gamma, beta, and theta frequencies (40- to 60-Hz median = –152°, 22-Hz median = –105°, and 5-Hz median = 20°) correspond to time delays of –8, –13, and 11 ms, or a relatively fixed time shift of 8 to 13 ms in either direction rather than a fixed phase shift (Fig. 3B). A comparable (~10 ms) delay has been found between visual response latencies in anatomically connected areas along the ventral stream (*17*), suggesting that conduction times and synaptic delays account for the 8 to 13 ms shift in coupling.

The earlier latency of attentional effects on firing rates in FEF as compared with those in V4 suggests that FEF may initiate the coupled oscillations between the two areas. To further test this idea, we used Granger causality analysis to test the relative strength of influence of V4 on FEF LFPs and vice versa (*14*). Granger causality values for gamma increased with attention for both directions (paired *t* test, $P < 0.001$ for both directions) and were significantly above chance (FEF → V4 peak = 0.010 at 46 Hz and V4 → FEF peak = 0.025 at 55 Hz; permutation test, $P < 0.001$) (*14*), indicating that gamma activity in each area has a significant causal influence on the other area. However, the attentional effects on the Granger causality values appeared significantly earlier in the FEF-to-V4 direction than in the reverse direction (FEF to V4, 110 ms, and V4 to FEF, 160 ms; two-sided permutation test, $P < 0.05$) (Fig. 4, A and B), which is consistent with the idea that FEF initiates the gamma frequency oscillations in V4. The causality relationship reversed a short time later, with the Granger values becoming significantly larger in the V4-to-FEF direction around 300 ms after the cue onset (average 400 to 1000 ms after cue onset; paired *t* test, $P < 0.001$). In fact, the Granger values in the FEF-to-V4 direction greatly diminished across the trial.

We considered whether firing-rate changes with attention in FEF preceded the attentional effects on synchrony or vice versa. We used the Hilbert-Huang transform method (*18*) to calculate instantaneous LFP power over time in FEF and V4 (Fig. 4C). At the population level, significant attentional enhancement of gamma power in the LFP in FEF and V4 occurred at 120 ms and 100 ms, respectively (Fig. 4D), which was not a significant difference (two-sided permutation test, $P = 0.84$). To compare the relative latencies of attention effects on firing rate and LFP gamma power, we calculated the distribution of latencies for attentional effects across all individual sites in the first 300 ms after the cue onset. The distributions of attentional latencies in LFP gamma power in both FEF and V4 were significantly later than the distribution of latencies for attentional effects on firing rates in FEF (Wilcoxon rank-sum test, $P < 0.01$ for both comparisons) and significantly earlier than the distribution of latencies for attentional effects on V4 firing rates (Wilcoxon rank-sum test; V4 LFP gamma power, $P < 0.05$, and FEF LFP gamma power, $P < 0.001$) (table S2). Together, these results indicate that significant attentional effects on LFP gamma power in either area occur later than the earliest attentional effects on firing rates in the FEF. Rather than being caused by enhanced gamma oscillations, increases in firing rates in FEF with attention may initiate the coupled oscillations within and across areas. In contrast, firing-rate changes in area V4 occur later and might result at least in part from enhanced gamma oscillations.

In summary, the results suggest that FEF is a major source of the attentional effects on gamma frequency synchrony in V4 and probably other ventral stream areas. The Granger causality analyses suggest that top-down inputs from FEF to V4 predominate at the onset of spatially directed attention, but the bottom-up inputs from V4 to FEF come to predominate over the course of sustained attention. The coupled oscillations across areas are shifted in time by about 8 to 13 ms, which may be the optimal time shift to allow for spikes initiated in one area to affect cells at a peak depolarization phase in the coupled area (*17*). Tight coupling between the inputs and outputs of cells in V4 and FEF may also allow for enhanced spike timing–dependent plasticity of the connections between the two areas (*19*), which might mediate learning effects with attention. For distracting stimuli, or for sites with nonoverlapping RFs, these coupled oscillations are much smaller, which will reduce the impact of spikes in one area upon the other. We do not suggest that the attentional effects on gamma synchrony and firing rates in V4 are caused solely by inputs from FEF, because V4 receives inputs from several other structures that have been implicated in attention (*1*). However, these other inputs may also need to be synchronized at compatible frequencies and with the appropriate time shifts in order to support effective communication.

It has been suggested that low-frequency synchronization (for example, beta) is more suitable for long-range or polysynaptic communication across distant brain areas, with gamma rhythms being used for local computations (*20*). Although there is evidence for such low-frequency long-range synchronization (*21*–*25*), here we show that two distant but monosynaptically connected areas can be synchronized at gamma frequencies, which is probably not caused simply by common input (*21*). Enhanced oscillatory coupling has now been reported across several brain structures in monkeys (*4*, *23*, *26*) and other species (*21*, *24*, *27*) in association with attention and other behaviors, at a variety of frequencies, and may therefore be a general mechanism for regulating communication across brain structures (*6*, *28*).

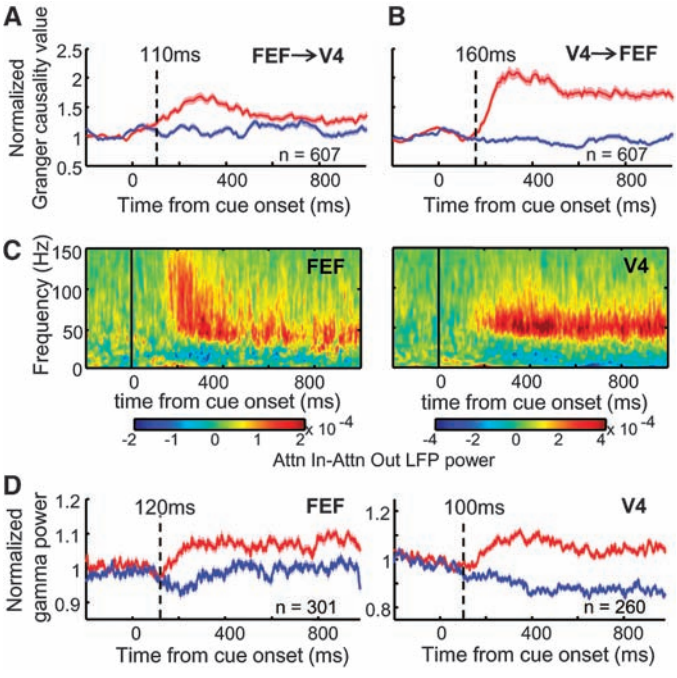

Fig. 4. Time-frequency synchrony measures and directional influences. (**A** and **B**) Population average of normalized Granger causality values averaged between 40 and 60 Hz across all pair-wise combinations of LFPs recorded in FEF and V4. Direction of influence is indicated by the arrows. (**C**) Population averages of attentional effects (attention inside RF–attention outside RF) on FEF and V4 power. (**D**) Normalized LFP gamma power in FEF and V4. Conventions are the same as in Fig. 1.

References and Notes

1. R. Desimone, J. Duncan, *Annu. Rev. Neurosci.* **18**, 193 (1995).
2. P. Fries, J. H. Reynolds, A. E. Rorie, R. Desimone, *Science* **291**, 1560 (2001).
3. N. P. Bichot, A. F. Rossi, R. Desimone, *Science* **308**, 529 (2005).
4. Y. B. Saalmann, I. N. Pigarev, T. R. Vidyasagar, *Science* **316**, 1612 (2007).
5. P. Lakatos, G. Karmos, A. D. Mehta, I. Ulbert, C. E. Schroeder, *Science* **320**, 110 (2008).
6. C. Borgers, S. Epstein, N. J. Kopell, *Proc. Natl. Acad. Sci. U.S.A.* **105**, 18023 (2008).
7. P. Tiesinga, J. M. Fellous, T. J. Sejnowski, *Nat. Rev. Neurosci.* **9**, 97 (2008).
8. E. K. Miller, J. D. Cohen, *Annu. Rev. Neurosci.* **24**, 167 (2001).
9. G. B. Stanton, C. J. Bruce, M. E. Goldberg, *J. Comp. Neurol.* **353**, 291 (1995).
10. J. D. Schall, A. Morel, D. J. King, J. Bullier, *J. Neurosci.* **15**, 4464 (1995).
11. L. G. Ungerleider, T. W. Galkin, R. Desimone, R. Gattass, *Cereb. Cortex* **18**, 477 (2008).

12. T. Moore, K. M. Armstrong, *Nature* **421**, 370 (2003).
13. L. B. Ekstrom, P. R. Roelfsema, J. T. Arsenault, G. Bonmassar, W. Vanduffel, *Science* **321**, 414 (2008).
14. Materials and methods are available as supporting material on *Science* Online.
15. P. Fries, T. Womelsdorf, R. Oostenveld, R. Desimone, *J. Neurosci.* **28**, 4823 (2008).
16. M. Zeitler, P. Fries, S. Gielen, *Neural Comput.* **18**, 2256 (2006).
17. L. G. Nowak, J. Bullier, in *Cerebral Cortex*, K. S. Rockland, J. H. Kaas, A. Peters, Eds. (Plenum, New York, 1997), vol. 12, pp. 205–241.
18. N. E. Huang *et al.*, *Proc. R. Soc. London Ser. A* **454**, 903 (1998).
19. Y. Dan, M. M. Poo, *Neuron* **44**, 23 (2004).
20. N. Kopell, G. B. Ermentrout, M. A. Whittington, R. D. Traub, *Proc. Natl. Acad. Sci. U.S.A.* **97**, 1867 (2000).
21. A. von Stein, C. Chiang, P. Konig, *Proc. Natl. Acad. Sci. U.S.A.* **97**, 14748 (2000).
22. A. Brovelli *et al.*, *Proc. Natl. Acad. Sci. U.S.A.* **101**, 9849 (2004).
23. B. Pesaran, M. J. Nelson, R. A. Andersen, *Nature* **453**, 406 (2008).
24. P. R. Roelfsema, A. K. Engel, P. Konig, W. Singer, *Nature* **385**, 157 (1997).
25. A. Sirota *et al.*, *Neuron* **60**, 683 (2008).
26. T. J. Buschman, E. K. Miller, *Science* **315**, 1860 (2007).
27. A. G. Siapas, E. V. Lubenov, M. A. Wilson, *Neuron* **46**, 141 (2005).
28. T. Womelsdorf, P. Fries, *Curr. Opin. Neurobiol.* **17**, 154 (2007).
29. We thank G. Pielli, D. Stock, and C. Alfes for help with the animal training and Z.-X. Liu for help with the Granger causality analysis. We also thank N. Bichot, R. Landman, G. Mulliken, and A. Mitz for helpful discussions. Supported by grants EY017292 and EY017921 to R.D. S.J.G. was supported in part by grant MH64445 from NIH (USA).

Supporting Online Material

www.sciencemag.org/cgi/content/full/324/5931/1207/DC1
Materials and Methods
SOM Text
Figs. S1 to S5
Table S1
References

26 January 2009; accepted 8 April 2009
10.1126/science.1171402

Genome-Wide Identification of Human RNA Editing Sites by Parallel DNA Capturing and Sequencing

Jin Billy Li,[1]* Erez Y. Levanon,[1]* Jung-Ki Yoon,[1]† John Aach,[1] Bin Xie,[2] Emily LeProust,[3] Kun Zhang,[1]‡ Yuan Gao,[2,4] George M. Church[1]§

Adenosine-to-inosine (A-to-I) RNA editing leads to transcriptome diversity and is important for normal brain function. To date, only a handful of functional sites have been identified in mammals. We developed an unbiased assay to screen more than 36,000 computationally predicted nonrepetitive A-to-I sites using massively parallel target capture and DNA sequencing. A comprehensive set of several hundred human RNA editing sites was detected by comparing genomic DNA with RNAs from seven tissues of a single individual. Specificity of our profiling was supported by observations of enrichment with known features of targets of adenosine deaminases acting on RNA (ADAR) and validation by means of capillary sequencing. This efficient approach greatly expands the repertoire of RNA editing targets and can be applied to studies involving RNA editing–related human diseases.

Adenosine-to-inosine (A-to-I) RNA editing converts a genomically encoded adenosine (A) into inosine (I), which in turn is read as guanosine (G), and increases transcriptomic diversity (*1*, *2*). It is critical for normal brain function (*3*–*7*) and is linked to various disorders (*8*). To date, a total of 13 edited genes have been identified within nonrepetitive regions of the human genome (table S1). The limiting factor in the identification of RNA editing targets has been the number of locations that could be profiled by the sequencing of DNA and RNA samples. Even with recent developments in massively parallel DNA sequencing technologies (*9*), it still remains expensive to sequence whole genomes and transcriptomes, both of which are required to identify RNA editing targets. Here, we report an efficient and unbiased genome-wide approach to identify RNA editing sites that uses tailored target capture followed by massively parallel DNA sequencing.

We first compiled a set of 59,437 genomic locations enriched with RNA editing sites, excluding repetitive regions such as *Alu* (fig. S1) (*10*). To reduce biases in detection, the key criteria for previous predictions of editing targets—conservation, coding potential, and RNA secondary structure (*11*–*15*)—were not taken into account. Over 90% of the previously identified editing targets are present in this data set (table S1). We designed padlock probes (*16*) for 36,208 sites that best satisfied our criteria for probe design (table S2) (*10*). Sites near splicing junctions required two different probes [targeting genomic DNA (gDNA) and cDNA], giving rise to a total of 41,046 probes designed for 36,208 sites (table S2).

To identify RNA editing sites, we used gDNA and cDNA from seven different tissues (cerebellum, frontal lobe, corpus callosum, diencephalon, small intestine, kidney, and adrenal), all derived from a single individual so as to rule out polymorphisms among populations. The pool of probes was hybridized to gDNA and cDNA in separate reactions (Fig. 1A and fig. S2). We sequenced the amplicons and identified sites where an A allele was observed in gDNA, whereas at least a fraction of G reads were present in the cDNA samples. A majority of sites were covered with multiple reads (Fig. 1B). Two independent

Table 1. Statistics of sequencing of samples used in this study.

Sample	Total reads	Mappable reads	Sites with ≥1 read	Fraction of sites with ≥1 read	RNA editing candidates*
gDNA (combined)	12,604,941	12,150,194	33,886	93.6%	N/A
Replicate 1	5,145,193	5,042,006	32,491	89.7%	N/A
Replicate 2	7,459,748	7,108,188	32,942	91.0%	N/A
cDNA					
Cerebellum	5,538,459	5,382,743	26,220	72.4%	126
Frontal lobe (combined)	14,065,388	13,360,868	28,382	78.4%	268
Replicate 1	6,950,660	6,563,630	26,617	73.5%	238
Replicate 2	7,114,728	6,797,238	26,628	73.5%	230
Corpus callosum	5,096,832	4,963,983	25,447	70.3%	180
Diencephalon	5,420,151	5,291,184	25,187	69.6%	172
Small intestine	6,516,258	6,172,901	26,845	74.1%	181
Kidney	6,354,025	5,984,709	26,299	72.6%	177
Adrenal	2,251,755	2,188,637	23,589	65.1%	121

*A site with evidence for RNA editing is required to have an editing level of ≥5% and a log-likelihood (LL) score of ≥2 (*10*).

[1]Department of Genetics, Harvard Medical School, 77 Avenue Louis Pasteur, Boston, MA 02115, USA. [2]Center for the Study of Biological Complexity, Virginia Commonwealth University, 1000 West Cary Street, Richmond, VA 23284, USA. [3]Genomics Solution Unit, Agilent Technologies, 5301 Stevens Creek Boulevard, Santa Clara, CA 95051, USA. [4]Department of Computer Science, Virginia Commonwealth University, 401 West Main Street, Richmond, VA 23284, USA.

*These authors contributed equally to this work.
†Present address: College of Medicine, Seoul National University, Seoul 110-799, Korea.
‡Present address: Department of Bioengineering, University of California, San Diego, CA 92093, USA.
§To whom correspondence should be addressed. E-mail: http://arep.med.harvard.edu/gmc/email.html

technical replicates were well correlated for both gDNA (Fig. 1C) and frontal lobe cDNA (Fig. 1D). In addition, the editing levels were highly correlated between the two replicates (Fig. 1E).

A total of 57.8 million reads were obtained, among which 55.5 million sequences were mapped to the target regions (Table 1) (*10*). To identify RNA editing sites, we searched for positions where a homozygous A was seen in gDNA and more than 5% of reads were G in at least two of the seven cDNA samples with a log likelihood score of ≥2 (*10*). A total of 239 such sites (in 207 targets) with stringent thresholds were identified and referred to as class I (table S3), including 10 of all 13 known edited genes (tables S1 and S3).

To validate the class I set, we randomly selected 18 different sites, successfully amplified them with polymerase chain reaction, and sequenced them using the dideoxynucleotide (Sanger) method. We also tested gDNA and frontal lobe cDNA from two additional donors (a total of 12 samples per site). Fourteen of the 18 sites were clearly edited, with a majority in all three donors (Fig. 2A and fig. S3). One of the

Table 2. Features of class I RNA editing sites.

Feature	36,208 set	Class I set	*P* value*
Double-stranded RNA (dsRNA) structure†	16%	41%	2.7×10^{-21}
Downstream of base G	34%	8%	1.1×10^{-21}
Coding sequence	52%	23%	2.0×10^{-19}
Conserved region‡	42%	21%	1.5×10^{-11}
MicroRNA target sequence§	33%	20%	4.6×10^{-6}

**P* values were calculated using Fisher's exact test. †Sequence centered on the site [4001 base pairs (bp) total] forms a dsRNA structure (*10*). ‡Sites in the "most conserved" track in the University of California Santa Cruz genome browser (http://genome.ucsc.edu). §Sequence centered on the site (13 bp total) contains 7 bp microRNA seeds (http://microrna.sanger.ac.uk) (*10*).

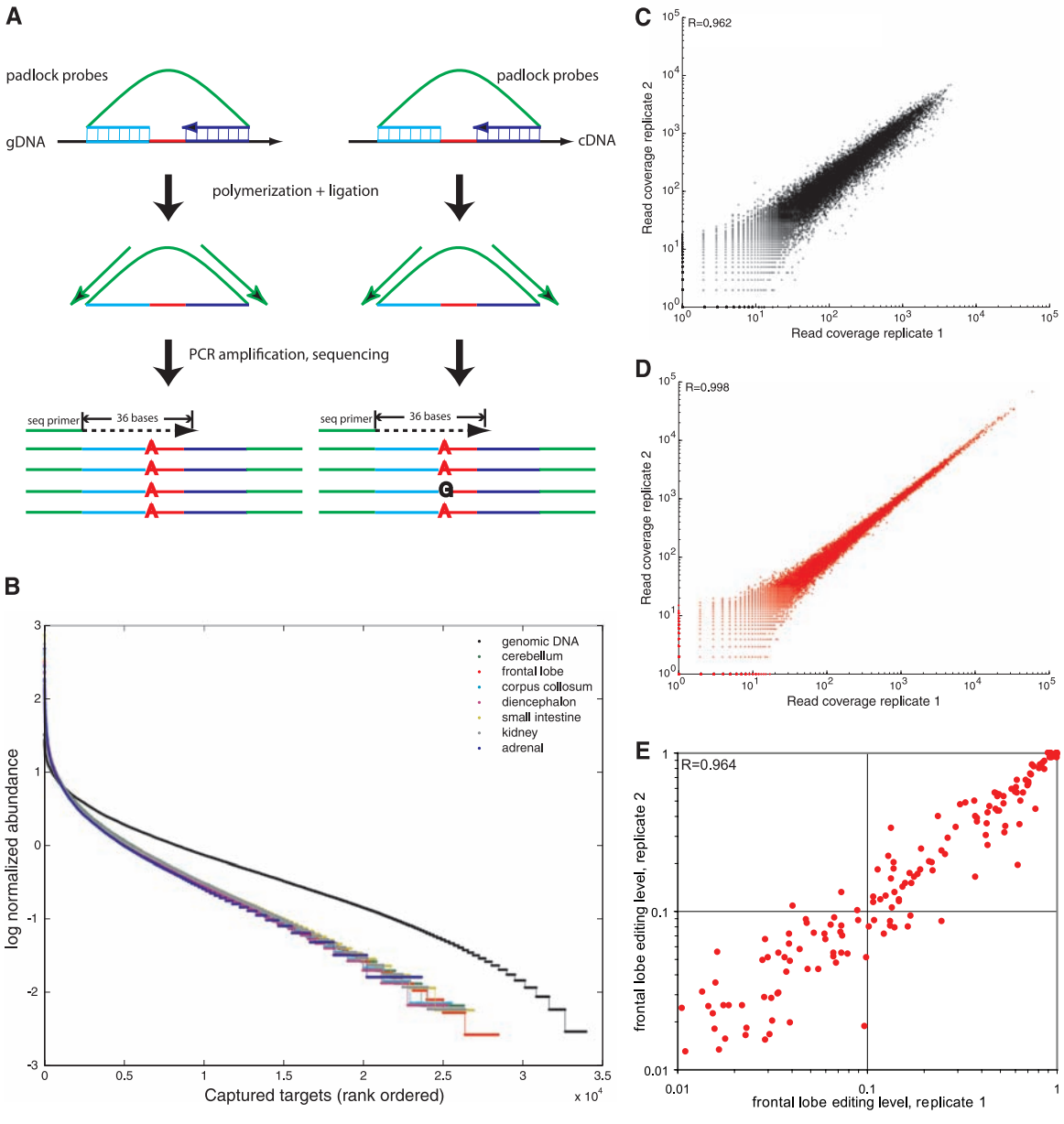

Fig. 1. Screening for RNA editing sites using padlock capture and massively parallel DNA sequencing technologies. (**A**) Schematic diagram of the padlock technology. The candidate RNA editing sites are specifically targeted by padlocks in both gDNA and cDNA samples from a single individual. Circles are formed when polymerase, deoxynucleotide triphosphate, and ligase are added, subsequently amplified, and sequenced with an Illumina genome analyzer (Illumina, San Diego, CA). (**B**) Uniformity of target abundance distributions in sequences obtained for all samples. Each graph shows the abundance of captured target sequences for each target over all samples, in which targets are given in ranked order. Abundance is represented by the $\log_{10}$ of the target coverage normalized to the mean of the target coverage for the sample. The abundance of different sites is nonuniform because of capturing biases and expression-level variations. The gDNA and frontal lobe replicates were combined in this analysis. (**C** to **E**) Target capture is highly reproducible for technical replicates. (C) Correlation of coverage of sites for gDNA replicates (Pearson correlation, $r = 0.962$); (D) correlation of coverage of sites for frontal-lobe cDNA replicates ($r = 0.998$); and (E) correlation of RNA editing level in frontal-lobe replicates ($r = 0.964$). Editing level is the number of G reads divided by the sum number of A and G reads when the sum is ≥10.

remaining sites, *ZNF7*, was edited at 1.1% level (2 of 187 individually sequenced clones). The false discovery rate of the set is thus up to 17% (3 of 18 sites).

RNA editing occurs when ADARs (adenosine deaminases acting on RNA) bind to an extended RNA duplex within target RNAs (*17*, *18*). Indeed, the class I set is significantly enriched, as compared with the 36,208-candidates set, with sites that are located in RNA double-stranded regions (Table 2 and table S4) (*10*). Previous studies have indicated that ADARs have a sequence preference for strong G depletion in the nucleotide 5′ to the editing site (*19*). This observation is in agreement with our findings (Table 2 and fig. S4).

Of the 239 class I sites, 55 (23%) are located in coding regions, 38 of which change amino acids (table S3), including one that adds an additional 29 amino acids by changing a stop codon (UAG) to a tryptophan (UGG) (Fig. 2B). There is a clear bias against the coding regions (Table 2), where changes are less likely to be tolerated. Similarly, possible microRNA target sequences are significantly reduced in our set (Table 2).

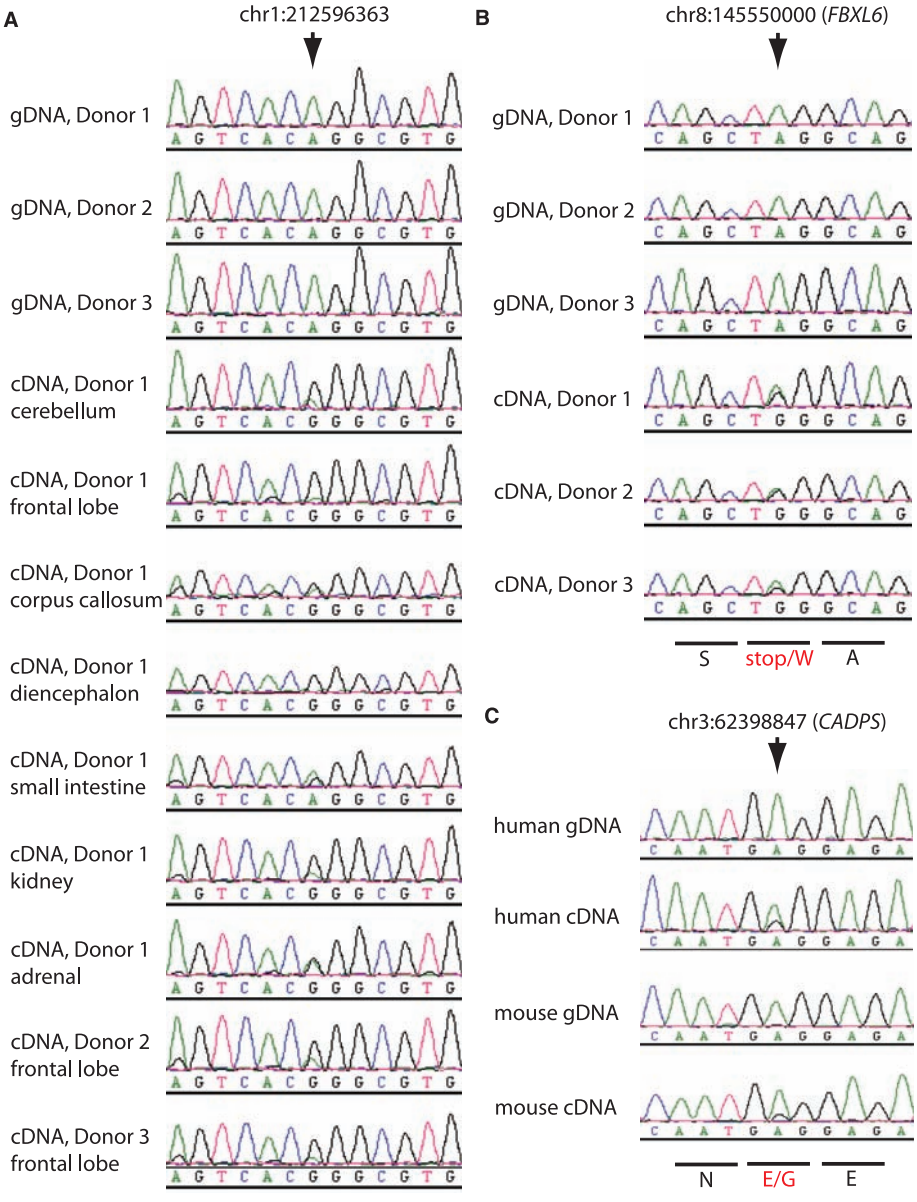

Fig. 2. Validation of RNA editing sites with conventional Sanger sequencing. (**A**) Sequencing chromatogram traces of an exemplary site, chr1:212596363, in gDNA and all seven tested cDNAs of the first donor and in gDNA and frontal lobe cDNA from two unrelated donors. Some nearby sites are also edited. A complete list of validated sites is in fig. S3. (**B**) At site chr8:145550000 [in *F-box and leucine-rich repeat protein 6* (*FBXL6*) gene], the genomic A in the stop codon (TAG) is highly edited, allowing the addition of 29 amino acids to the protein in all three donors. (**C**) The *CADPS* site, chr3:62398847, is edited in human (shown is the frontal-lobe cDNA), and the conserved site is edited in mouse as well (shown is the brain cDNA). The editing event leads to amino acid change from glutamic acid (GAG) to glycine (GGG).

Sequence conservation has been the main criterion in various attempts to identify new RNA editing sites. However, it has been shown that editing is enriched in the primate lineage, mainly because of widespread editing in *Alu* repetitive elements (*20*–*24*). In the class I set, the number of sites with flanking sequences conserved between human and mouse is significantly underrepresented (Table 2) (*10*). Of those sites that are highly conserved (fig. S5), we sequenced one located in the *CADPS* (Ca^{2+}-dependent secretion activator) gene in mouse gDNA and cDNA samples and observed an editing signal. This site is probably edited in all vertebrates based on A-to-G changes in supporting expressed sequence tags. Fourteen of the 50 editing sites located in conserved regions harbor a G in at least one of eight other vertebrate genomes (table S5), a phenomenon previously observed in flies (*25*). From an evolutionary perspective, RNA editing may thus play a role similar to genetic mutation in creating genetic diversity. In contrast to mutation, however, RNA editing provides a much wider spectrum of "genetic dosage"; our data demonstrate that the level ranges from very low to full editing (fig. S6).

In agreement with previous observations that targets of RNA editing are involved in nervous-system function (*7*, *11*–*15*, *26*–*28*), we found that the class I sites were enriched with functions such as synapse, cell trafficking, and membrane. Furthermore, many sites are located within genes that are implicated in human brain-related diseases (table S6). In addition to class I sites, many more sites are likely to be edited. When we relaxed our criteria to require only one tissue to be edited, we identified an additional set of 330 potential candidate editing sites as the class II set (table S7). We validated a selected candidate from this set, *GLI1* (Glioma-associated oncogene homolog 1, at site chr12:56150891), which was highly edited in the frontal lobe of all three donors (fig. S3). An additional set of 141 sites was identified as class III when the editing level threshold was reduced to 2% (table S8), which suggests that many targets may be edited at very low levels. By sequencing 118 clones of the class III site chr11:74994333 in *MAP6* (microtubule-associated protein 6), we found 13 clones with a G at the editing site.

Although it is unclear if the extensive editing of primate *Alu* sites has any biological role, it may require an increased expression of ADAR proteins in humans, which in turn may lead to the editing of non-*Alu* RNAs. In support of this scenario, most of the nonrepetitive sites we identified do not seem to be conserved beyond the primate lineage and may play roles in primate-specific functions. Many of the identified editing sites are located in noncoding RNAs that have recently been linked to brain function (*29*).

The approach described herein can be readily extended to a wider variety of tissues in normal and diseased individuals in order to identify additional RNA editing sites and measure their

editing levels. The enlarged set of nonrepetitive RNA editing targets may help unravel rules of RNA editing in human diseases and behavior.

References and Notes

1. B. L. Bass, *Annu. Rev. Biochem.* **71**, 817 (2002).
2. K. Nishikura, *Nat. Rev. Mol. Cell Biol.* **7**, 919 (2006).
3. M. Higuchi *et al.*, *Nature* **406**, 78 (2000).
4. R. Brusa *et al.*, *Science* **270**, 1677 (1995).
5. M. Singh *et al.*, *J. Biol. Chem.* **282**, 22448 (2007).
6. M. J. Palladino, L. P. Keegan, M. A. O'Connell, R. A. Reenan, *Cell* **102**, 437 (2000).
7. H. Lomeli *et al.*, *Science* **266**, 1709 (1994).
8. S. Maas, Y. Kawahara, K. M. Tamburro, K. Nishikura, *RNA Biol.* **3**, 1 (2006).
9. J. Shendure, H. Ji, *Nat. Biotechnol.* **26**, 1135 (2008).
10. Materials and methods are available as supporting material on *Science* Online.
11. E. Y. Levanon *et al.*, *Nucleic Acids Res.* **33**, 1162 (2005).
12. B. Hoopengardner, T. Bhalla, C. Staber, R. Reenan, *Science* **301**, 832 (2003).
13. W. M. Gommans *et al.*, *RNA* **14**, 2074 (2008).
14. D. R. Clutterbuck, A. Leroy, M. A. O'Connell, C. A. Semple, *Bioinformatics* **21**, 2590 (2005).
15. J. Ohlson, J. S. Pedersen, D. Haussler, M. Ohman, *RNA* **13**, 698 (2007).
16. G. J. Porreca *et al.*, *Nat. Methods* **4**, 931 (2007).
17. A. G. Polson, B. L. Bass, *EMBO J.* **13**, 5701 (1994).
18. K. Nishikura *et al.*, *EMBO J.* **10**, 3523 (1991).
19. K. A. Lehmann, B. L. Bass, *Biochemistry* **39**, 12875 (2000).
20. A. Athanasiadis, A. Rich, S. Maas, *PLoS Biol.* **2**, e391 (2004).
21. M. Blow, P. A. Futreal, R. Wooster, M. R. Stratton, *Genome Res.* **14**, 2379 (2004).
22. E. Eisenberg *et al.*, *Trends Genet.* **21**, 77 (2005).
23. D. D. Kim *et al.*, *Genome Res.* **14**, 1719 (2004).
24. E. Y. Levanon *et al.*, *Nat. Biotechnol.* **22**, 1001 (2004).
25. N. Tian, X. Wu, Y. Zhang, Y. Jin, *RNA* **14**, 211 (2008).
26. C. M. Burns *et al.*, *Nature* **387**, 303 (1997).
27. M. Kohler, N. Burnashev, B. Sakmann, P. H. Seeburg, *Neuron* **10**, 491 (1993).
28. B. Sommer, M. Kohler, R. Sprengel, P. H. Seeburg, *Cell* **67**, 11 (1991).
29. T. R. Mercer *et al.*, *Neuroscientist* **14**, 434 (2008).
30. We thank R. Emeson, M. P. Ball, and F. Isaacs for critical reading of the manuscript; P. Wang and Z. Liu (BioChain Institute) for helping collect human samples; M. Higuchi and P. Seeburg for providing *ADAR2*$^{-/-}$ mouse brain cDNA; Harvard Biopolymers Facility for help with Illumina sequencing; and A. Ahlford, H. Ebling, and J. Santosuosso for assistance with Sanger sequencing. E.Y.L. was supported by the Machiah foundation. Funding came from National Human Genome Research Institute Centers of Excellence in Genomic Science grant to G.M.C. The Illumina sequencing data are deposited at the National Center for Biotechnology Information Short Read Archive under accession number SRA008181.

Supporting Online Material

www.sciencemag.org/cgi/content/full/324/5931/1210/DC1
Materials and Methods
Figs. S1 to S10
Tables S1 to S12
References

15 January 2009; accepted 1 April 2009
10.1126/science.1170995

Unstable Tandem Repeats in Promoters Confer Transcriptional Evolvability

Marcelo D. Vinces,[1,2,3]* Matthieu Legendre,[1,4]* Marina Caldara,[1] Masaki Hagihara,[5] Kevin J. Verstrepen[1,2,3]†

Relative to most regions of the genome, tandemly repeated DNA sequences display a greater propensity to mutate. A search for tandem repeats in the *Saccharomyces cerevisiae* genome revealed that the nucleosome-free region directly upstream of genes (the promoter region) is enriched in repeats. As many as 25% of all gene promoters contain tandem repeat sequences. Genes driven by these repeat-containing promoters show significantly higher rates of transcriptional divergence. Variations in repeat length result in changes in expression and local nucleosome positioning. Tandem repeats are variable elements in promoters that may facilitate evolutionary tuning of gene expression by affecting local chromatin structure.

The genomes of most organisms are not uniformly prone to change because they contain hotspots for mutating events. An abundant class of sequences that mutate at higher frequencies than the surrounding genome is composed of tandem repeats (TRs, also known as satellite DNA), DNA sequences repeated adjacent to one another in a head-to-tail manner (*1*). Errors during replication make TRs unstable, generating changes in the number of repeat units that are 100 to 10,000 times more frequent than point mutations (*2*). Variable TRs are often dismissed as nonfunctional "junk" DNA. However, some TRs located within coding regions (exons) have demonstrable functional roles. For example, TR copy numbers in genes such as *FLO1* in *Saccharomyces cerevisiae* generate plasticity in adherence to substrates (*3*). In canines, variable repeats located in *Alx-4* and *Runx-2* confer variability to skeletal morphology, which may have facilitated the diversification of domestic dogs bred by humans (*4*). Thus, repeats located in coding regions may increase the evolvability of proteins.

There is also evidence that repeats influence expression of certain genes (*5*–*7*). To investigate the involvement of TRs in gene expression variation, we first mapped and classified all repeats in the S288C yeast genome (*8*) (data set S1). TRs are enriched in yeast promoters (table S1). Of the ~5700 promoters in the genome, 25% (1455) contain at least one TR. Many TRs in promoters consist of short, A/T-rich sequences (table S2, fig. S1, and data set S2). Comparison of orthologous regions in genomes of different *S. cerevisiae* strains showed that many of the TRs are variable (data set S1). For example, 24.1% of orthologous TR loci in promoters differ in the number of repeat units between the two fully sequenced strains, S288C and RM11 (*8*). To confirm this, we sequenced 33 randomly chosen promoter repeats in seven *S. cerevisiae* genomes (Fig. 1A, figs. S2 and S3, and data set S3). Twenty-five of the 33 TRs differed in repeat units in at least one of the seven strains. The repeat variation frequency is 40-fold higher than the frequency of insertions and deletions (indels) and of point mutations in the surrounding nonrepetitive sequence ($P < 10^{-15}$) (figs. S2 and S3).

To determine whether promoter TR variation affects gene expression, we compared repeat variablity to expression divergence (ED), which represents how fast the transcriptional activity of each gene evolves (*9*–*11*). Promoters containing TRs showed significantly ($P < 1.75 \times 10^{-4}$) higher amounts of ED than did promoters lacking TRs when comparing yeast species (*S. cerevisiae*, *S. paradoxus*, *S. mikatae*, and *S. kudriavzevii*) (Fig. 1, B to D, and fig. S4A) and *S. cerevisiae* strains (S288C and RM11) (Fig. 1, E to G, and fig. S4, B and C). This difference was independent of factors known to affect transcriptional divergence, for example, the presence of TATA boxes (fig. S5). Only promoters containing variable numbers of repeat units between strains or species showed the elevated ED (Fig. 1, D and G). Furthermore, when variable TRs were binned into variable and highly variable (10% most variable) groups, highly variable repeats displayed even higher ED. Hence, ED correlates not merely with TRs in promoters but more specifically with repeat number variation.

To directly test whether changes in promoter TRs affect transcriptional activity, we varied the TR repeat number in the promoters of yeast genes *YHB1*, *MET3*, and *SDT1* (Fig. 2 and fig. S6A). For each construct, expression increased as the length of the TR increased from zero, until a certain size was reached, after which expression dropped off. To determine whether natural variation between strains corresponded to similar changes in gene expression, we cloned promoters of several strains

[1]FAS Center for Systems Biology, Harvard University, 52 Oxford Street, Cambridge, MA 02138, USA. [2]Laboratory for Systems Biology, Flanders Institute for Biotechnology (VIB), Katholieke Universiteit Leuven (K.U. Leuven), B-3001 Heverlee, Belgium. [3]Genetics and Genomics Group, Centre of Microbial and Plant Genetics (CMPG), K.U. Leuven, Gaston Geenslaan 1, B-3001 Leuven (Heverlee), Belgium. [4]Structural and Genomic Information Laboratory, CNRS-UPR 2589, IFR-88, Université de la Méditerranée Parc Scientifique de Luminy, Avenue de Luminy, FR-13288 Marseille, France. [5]The Institute of Scientific and Industrial Research, Osaka University, 8-1 Mihogaoka, Ibaraki, 567-0047, Japan.

*These authors contributed equally to this work.
†To whom correspondence should be addressed. E-mail: Kevin.Verstrepen@biw.vib-kuleuven.be

into the respective promoters of strain S288C. These transformants indeed mirrored the expression-level patterns that we observed with the engineered TR strains (fig. S6, B to D). Moreover, TR-mediated changes in expression have functional consequences. *SDT1* encodes a pyrimidine nucleotidase that confers resistance to the nucleotide analog 6-azauracil (6AU) (*12*), and we observed that strains with various *SDT1* promoter TR constructs show differences in growth that match the *SDT1* expression changes (fig. S7).

Because promoter TR length variation affects transcription, we speculated that it should be possible to exploit promoter TR instability to quickly select for changes in gene expression. We used strains with a relatively long *SDT1* TR tract, because repeat mutation rates increase with increasing tract length (*13*), and selected for variants having higher gene expression. The *SDT1* open reading frame was replaced with selectable markers, either *URA3* or yellow fluorescent protein (YFP), for selection in SC-ura (medium requiring yeast to express *URA3* to grow in) or selection by sorting with flow cytometry, respectively. After a few rounds of selection, both regimes yielded mutants that showed increased growth on medium lacking uracil or increased YFP fluorescence. These mutants showed significant ($P < 1 \times 10^{-15}$) changes in the length of the TR tract in the *SDT1* promoter. The most common tract lengths yielded by both selections was 13 repeats (26 nucleotides), corresponding to a size close to that of the engineered TR constructs with the highest expression (Fig. 2B). Construction of a 13-unit TR revealed that it had the highest expression of all the engineered strains (Fig. 3A). When strains containing the long TR tract were grown without any selective pressure, most strains remained at the initial 48 units, and the few mutants that arose show a broader TR size distribution. We were unable to obtain strains with higher expression or TR size changes when the repeat sequence in the promoter was replaced by a randomized (no repeat) sequence of equal length as the 48-unit repeat tract (Fig. 3B).

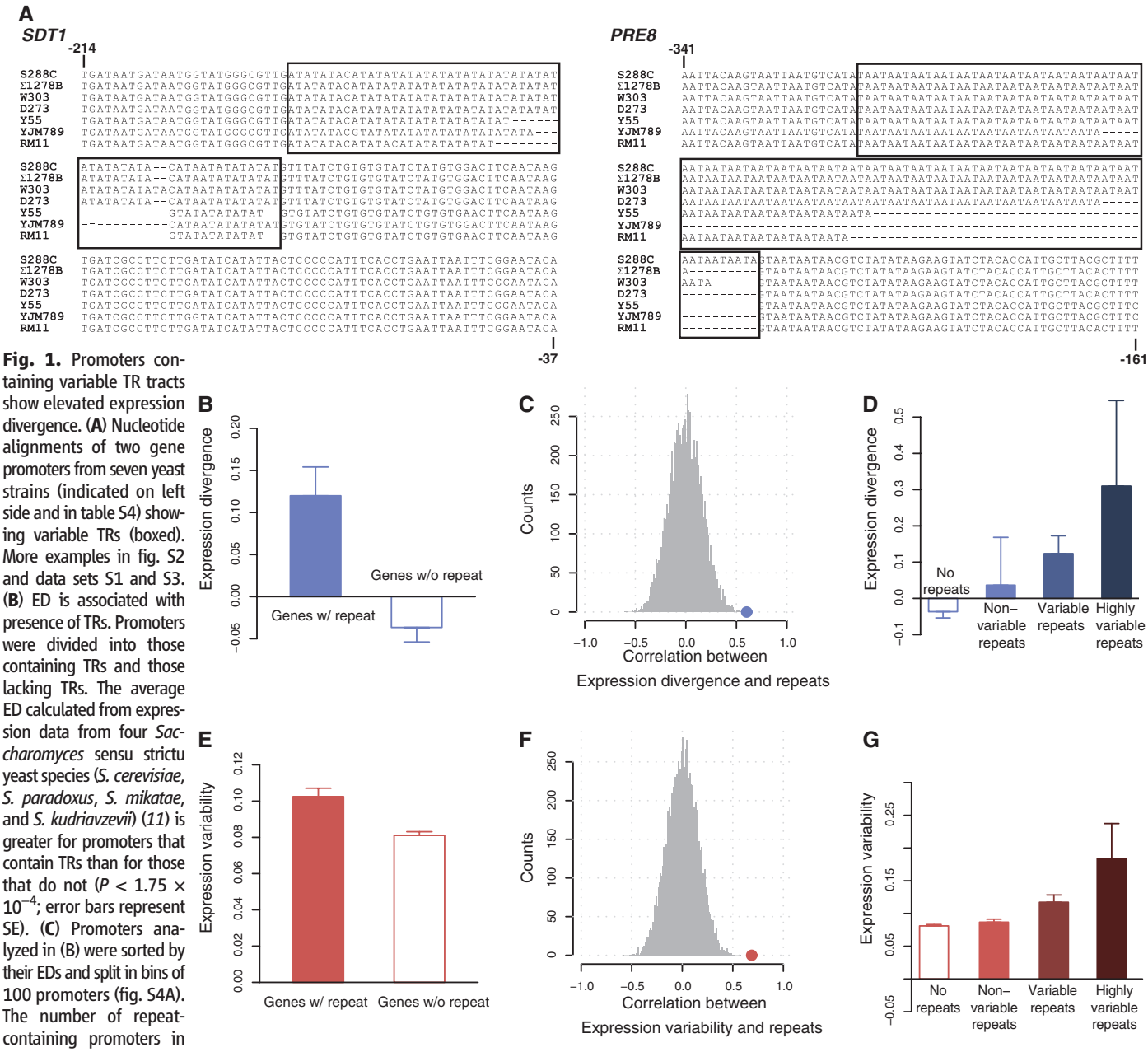

Fig. 1. Promoters containing variable TR tracts show elevated expression divergence. (**A**) Nucleotide alignments of two gene promoters from seven yeast strains (indicated on left side and in table S4) showing variable TRs (boxed). More examples in fig. S2 and data sets S1 and S3. (**B**) ED is associated with presence of TRs. Promoters were divided into those containing TRs and those lacking TRs. The average ED calculated from expression data from four *Saccharomyces* sensu strictu yeast species (*S. cerevisiae*, *S. paradoxus*, *S. mikatae*, and *S. kudriavzevii*) (*11*) is greater for promoters that contain TRs than for those that do not ($P < 1.75 \times 10^{-4}$; error bars represent SE). (**C**) Promoters analyzed in (B) were sorted by their EDs and split in bins of 100 promoters (fig. S4A). The number of repeat-containing promoters in each bin and ED were significantly correlated. Shown is the correlation coefficient of the data set (blue dot; Z score = 2.70, empirical P value = 6.75×10^{-3}) and of randomly shuffled data (gray histogram). (**D**) Only repeats that vary between the four yeast species show elevated ED. ED was calculated for promoters divided into four categories as shown (error bars represent SE). (**E** to **G**) Similar analyses as in (B) to (D), except that ED values were calculated by using data from two *S. cerevisiae* strains (S288c and RM11) (*9*). The results show a similar correlation of variable repeats and ED (all P values are $< 10^{-3}$). The data set for (F) is in fig. S4B.

TRs can contain transcription factor (TF) binding sites, so variation in the tract length may result in the removal or addition of binding sites. Of the 1455 TR-containing promoters, 113 contain known TF binding sites located within the repeats. Many of these TRs overlap stress-response TF binding sites (table S3). Investigation of one of these TRs, located in the promoter of *YKL107w*, indicated that, in this case, changes in the TR number may affect transcription through variation in the number of binding sites of the oxidative-stress-responsive TF, Yap1 (fig. S8).

Most promoter TRs, however, do not overlap known TF sites, indicating that another mechanism underlies repeat-related expression differences. To investigate whether distance between promoter elements affects transcription, we replaced the *SDT1* TR with different DNA sequences of the same length. These changes mostly led to severely reduced transcription, indicating that altered spacing alone is not sufficient to explain the effect of repeat variation on transcription (Fig. 4, A to C). Many promoter TRs are extremely A/T-rich, suggesting they may facilitate DNA melting. However, some of the constructs with the same high A/T content as the original repeat tract still show reduced transcription.

Most promoter TRs are located ~200 base pairs upstream from the translational start codon (Fig. 4D and fig. S9), corresponding to the nucleosome-free region of yeast promoters (*14*), suggesting a link between chromatin structure and TRs. We compared available genome-wide nucleosome positioning data with the positioning of TRs. Nucleosome density across promoter regions showed an inverse correlation with the presence of TRs (Fig. 4D and fig. S9A). Nucleosome depletion is especially pronounced around AT-rich repeats, which compose 80% of all repeats (fig. S9B). These results suggest either that TRs preferentially form in nucleosome-free regions or that nucleosomes cannot easily bind TRs. We also found that nucleosomes containing the histone variant H2AZ (*15*) tended to border the TRs (Fig. 4D and fig. S9). Although no simple rule governs nucleosome positioning, nucleosome positioning in the yeast genome is largely directed by DNA sequence (*15*–*18*), and a computational algorithm exists that uses DNA sequence information to predict where nucleosomes bind (*16*, *19*). This algorithm predicts that TR regions in promoters are nucleosome-free (fig. S10), suggesting that promoter TR sequences intrinsically bind poorly to nucleosomes, presumably because the repeats affect biophysical properties of DNA (e.g., bendability) (*20*). In line with these predictions, an analysis of a transcriptome data set for a large group of chromatin remodeling mutants (*21*) showed that the expression of repeat-containing promoters is strongly influenced by regulators of chromatin structure and activity (fig. S11).

If repeats control nucleosome positioning, changing the repeat sequence should influence the local nucleosome structure. Deletion of the TR of *SDT1* resulted in binding of nucleosomes to this region and also disturbed the positioning of downstream nucleosomes (Fig. 4E). Intermediate deletions of the TRs resulted in gradual changes in nucleosome occupancy (fig. S12), indicating that repeat variation directly affects the local chromatin structure. Replacing the repeat with a sequence predicted to have a high affinity for nucleosomes (*19*) resulted in a well-positioned nucleosome in the previously nucleosome-free region and in greatly reduced *SDT1* expression (Fig. 4, F and G).

Although several molecular mechanisms may underlie the effect promoter TRs have on gene expression, our data indicate that repeat-dependent changes in DNA sequence and chromatin structure play a role. Local chromatin structure is known to affect transcriptional activity (*22*). Most repeats in promoters do not contain the hallmark dinucleotide periodicities that are associated with nucleosome-binding DNA (*19*). As a result, these repeat tracts may help to establish variable nucleosome-free DNA structures and influence nucleosome positioning in nearby regions. Moreover, because of the high A/T content of most promoter TRs, it remains to be tested whether these nucleosome-free TRs may allow DNA melting for loading of the RNA polymerase.

Changes within coding regions and in protein sequence underlie much biological adaptation

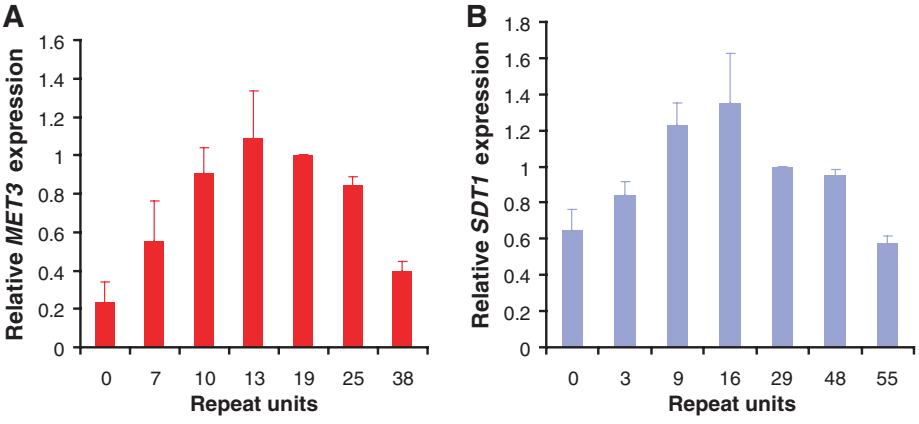

Fig. 2. Mutation of TRs in promoters alters gene expression. Sets of strains with varying numbers of repeat units were constructed for two yeast gene promoters: (**A**) *MET3* and (**B**) *SDT1*. Expression was determined by quantitative polymerase chain reaction (PCR). All values are normalized to transcript levels of housekeeping gene *ACT1* and to wild-type (WT) expression levels; error bars indicate SE, $n = 3$. Data for *YHB1* are in fig. S6A.

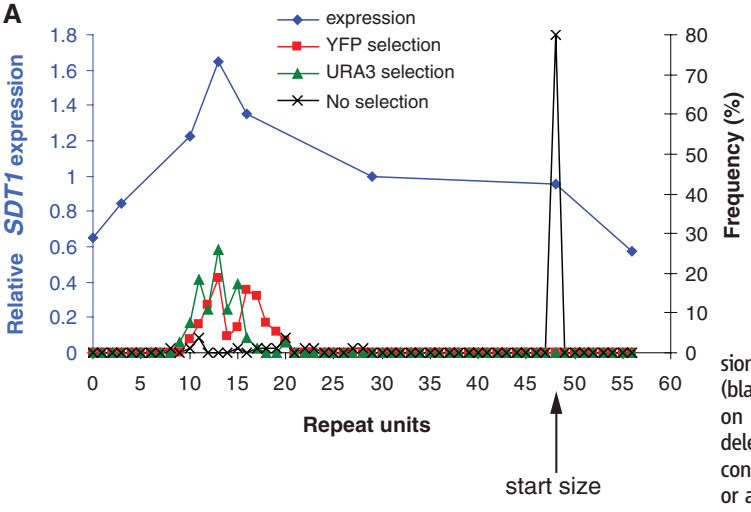

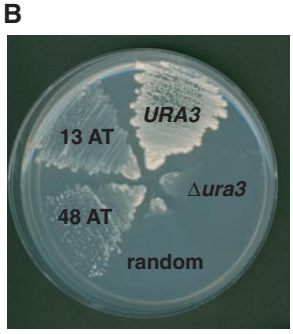

Fig. 3. Experimental evolution of gene expression mediated by TRs. (**A**) Selection for higher expression of the *SDT1* promoter results in changes in the number of TR units in the promoter. The starting strain (48 repeat units, indicated by arrow) has relatively low expression (blue line, left axis). The green (*URA3*) and red (YFP) lines represent the final size distributions of TRs after selection for higher expression by using *URA3* or YFP reporters. TR size distribution without selection (black line) remains mostly at the initial 48 units. See (*8*) for details. (**B**) Growth on SC-ura medium of strains with native *URA3* (positive control); with *ura3* deleted (negative control); and with *URA3* fused to the *SDT1* promoter containing a long nonrepetitive (scrambled, random) sequence, a 48-AT repeat, or a 13-AT repeat.

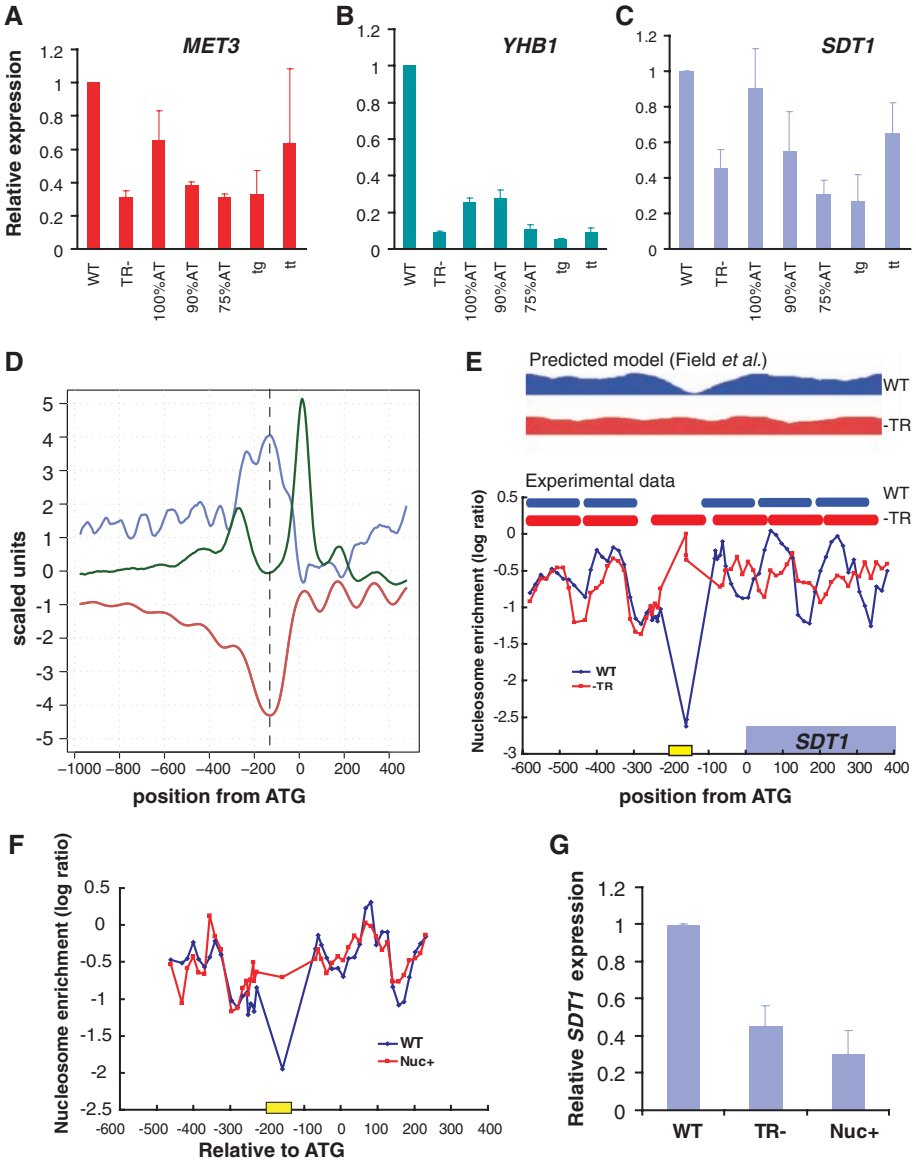

Fig. 4. TRs act as nucleosome positioning elements in promoters. Replacement of TRs with various sequences of the same size does not restore normal gene expression of (**A**) *MET3*, (**B**) *YHB1*, or (**C**) *SDT1*. TRs were replaced with other sequences of the same length: random (nonrepetitive) sequences (% A/T content indicated) and dinucleotide repeats (TG and TT repeats). The TR– strain lacks the entire TR. Error bars represent standard errors. (**D**) Genome-wide nucleosome position is largely anticorrelated with positions of TRs. Positions of the TR tracts are marked in blue; nucleosome positions, red (*18*); H2AZ nucleosome positions, green (*15*); and location of greatest TR enrichment, dashed vertical line. All repeat-containing promoters were aligned relative to the translational start site (ATG) or to the transcriptional start site (fig. S9A). (**E**) Deletion of TRs in the *SDT1* promoter interferes with maintenance of the nucleosome-free region. *SDT1* coordinates on the *x* axis are relative to the ATG. The *y* axis represents the signal from a PCR-based nucleosome positioning assay (*26*). The yellow box represents TR location. Inferred nucleosome positions based on our experimental data in the graph are depicted above (WT, blue ovals; –TR mutant, red ovals). Above these are the predicted nucleosome profiles (*16*). (**F**) Nucleosome positioning when *SDT1* promoter TRs are replaced with a sequence predicted to position nucleosomes (Nuc+). (**G**) *SDT1* expression in the Nuc+ strain compared with those of WT and TR– strains.

and innovation. However, changes in the regulation of genes may be equally important (*23*, *24*). Our results presented here are consistent with a role for TRs as ubiquitous and adjustable "evolutionary tuning knobs" (*25*) for transcription that mediate rapid evolution of gene expression. Genes that respond to changing environmental conditions would be particularly suited for such variable genetic elements. Indeed, genes driven by repeat-containing promoters show elevated responsiveness to changing environmental conditions (fig. S13).

A preliminary analysis of *Homo sapiens* promoters reveals a TR distribution comparable to that of yeast, suggesting that similar mechanisms are also at play in higher organisms (fig. S14).

References and Notes

1. O. J. Rando, K. J. Verstrepen, *Cell* **128**, 655 (2007).
2. M. Lynch *et al.*, *Proc. Natl. Acad. Sci. U.S.A.* **105**, 9272 (2008).
3. K. J. Verstrepen, A. Jansen, F. Lewitter, G. R. Fink, *Nat. Genet.* **37**, 986 (2005).
4. J. W. Fondon 3rd, H. R. Garner, *Proc. Natl. Acad. Sci. U.S.A.* **101**, 18058 (2004).
5. J. T. Streelman, T. D. Kocher, *Physiol. Genomics* **9**, 1 (2002).
6. P. Martin, K. Makepeace, S. A. Hill, D. W. Hood, E. R. Moxon, *Proc. Natl. Acad. Sci. U.S.A.* **102**, 3800 (2005).
7. M. V. Rockman, G. A. Wray, *Mol. Biol. Evol.* **19**, 1991 (2002).
8. Material and methods are available as supporting material on *Science* Online.
9. J. K. Choi, Y. J. Kim, *Nat. Genet.* **40**, 141 (2008).
10. J. Ronald, R. B. Brem, J. Whittle, L. Kruglyak, *PLoS Genet.* **1**, e25 (2005).
11. I. Tirosh, A. Weinberger, M. Carmi, N. Barkai, *Nat. Genet.* **38**, 830 (2006).
12. T. Nakanishi, K. Sekimizu, *J. Biol. Chem.* **277**, 22103 (2002).
13. M. Legendre, N. Pochet, T. Pak, K. J. Verstrepen, *Genome Res.* **17**, 1787 (2007).
14. G. C. Yuan *et al.*, *Science* **309**, 626 (2005); published online 16 June 2005 (10.1126/science.1112178).
15. I. Albert *et al.*, *Nature* **446**, 572 (2007).
16. Y. Field *et al.*, *PLOS Comput. Biol.* **4**, e1000216 (2008).
17. I. P. Ioshikhes, I. Albert, S. J. Zanton, B. F. Pugh, *Nat. Genet.* **38**, 1210 (2006).
18. W. Lee *et al.*, *Nat. Genet.* **39**, 1235 (2007).
19. E. Segal *et al.*, *Nature* **442**, 772 (2006).
20. H. R. Drew, A. A. Travers, *J. Mol. Biol.* **186**, 773 (1985).
21. I. Steinfeld, R. Shamir, M. Kupiec, *Nat. Genet.* **39**, 303 (2007).
22. F. H. Lam, D. J. Steger, E. K. O'Shea, *Nature* **453**, 246 (2008).
23. E. Pennisi, *Science* **321**, 760 (2008).
24. C. R. Landry, B. Lemos, S. A. Rifkin, W. J. Dickinson, D. L. Hartl, *Science* **317**, 118 (2007).
25. D. King, M. Soller, Y. Kashi, *Endeavour* **21**, 36 (1997).
26. E. A. Sekinger, Z. Moqtaderi, K. Struhl, *Mol. Cell* **18**, 735 (2005).

27. We thank B. Calderon, B. (Sze Ham) Chan, and B. Breaux for their contributions; B. Stern, E. O'Shea, A. Murray, A. Rowat, and A. New for critique of the manuscript; and the anonymous reviewers for their useful suggestions. Research in the lab of K.J.V. is supported by NIH National Institute for General Medical Studies grant P50GM068763, Human Frontier Science Program (HFSP) award RGY79/2007, the Flemish Institute for Biotechnology (VIB), and the Fonds Wetenschappelijk Onderzoek Vlaanderen–Odysseus program. M.D.V. acknowledges the Ford Foundation and the Belgian American Education Foundation.

Supporting Online Material

www.sciencemag.org/cgi/content/full/324/5931/1213/DC1
Materials and Methods
Figs. S1 to S14
Tables S1 to S6
References
Data Sets S1 to S3

22 December 2008; accepted 14 April 2009
10.1126/science.1170097

Nitrogen/Sulfur/Chlorine Analyzer

The Titan 4000 NSX analyzer for total nitrogen, sulfur, and chlorine analysis offers users in the refinery and petrochemical markets superior sample introduction and oxidative combustion performance. Its innovative detectors enable fast analysis speed with accuracy and reliability of results. Its range covers concentrations from low parts per billion to high parts per million. The incorporation of a powerful combustion method allows the analyzer to cater to a wide range of applications in refinery and chemical samples, including naphtha, aromatics, automotive fuels, biodiesel fuels, and LPG samples. The analyzer can process total nitrogen and total sulfur samples in two minutes and total chlorine samples in under four minutes.

ThermoFisher Scientific
For information +44-1606-548779
www.thermo.com/titan4000

DNA, RNA, and Protein Isolation

The illustra triplePrep kit is for rapid, simultaneous isolation of genomic DNA, RNA, and total denatured protein from a single undivided sample in less than one hour. The kit is a combination of two spin columns and six buffers optimized for use with mammalian cell culture or animal tissue. High quality and yield DNA, RNA, and protein can be successfully isolated from a range of tissue types, such as liver, kidney, spleen, brain, lung, and intestine, and the cell lines HeLa, NIH-3T3, CHO-K1, and HEK-293. Tissue amounts ranging from 1 to 20 mg and cell amounts ranging from 0.3 million to 5 million cells can be used for each preparation. Direct correlations of data derived from genomic DNA, RNA, and protein can be drawn with confidence because the data are obtained from the same undivided starting sample.

GE Healthcare
For information 262-501-0777
www.gelifesciences.com

Dispensing Device

The sciSwifter is a device for high-precision dispensing in 96-well, 384-well, and 1,536-well microplates. A drop-on-demand dispenser, it can dispense up to 16 different substances in parallel into various multiwell formats. The dispensing range is 100 pl to 100 µl with dead volumes close to zero. Each nozzle has online-drop-control and optical volume determination. The dispenser includes integrated touch-screen controls, a robotics shuttle, and external software for integration into automated robotics platforms. Its disposable pen technology enables preparation, storage, sonication, and dispensing of reagents to be performed in one integrated device. Substances can be stored directly in the dispensing pen, which serves as a closed container, eliminating the need for heat seals and ensuring sample integrity.

Scienion and Matrical Bioscience
For information +49-(0)30-6392-1700 and 509-343-6225
www.scienion.com and www.matrical.com

Positive Displacement Pipette

The Pos-D is a positive-displacement pipette with ergonomic features. Nonaqueous solutions that are viscous, dense, or high in vapor pressure are difficult to aspirate correctly with regular air-displacement pipettes. The Pos-D overcomes this problem by providing the pressure equalization needed to handle such solutions within the pipette tip. For example, a volatile liquid that would otherwise evaporate and force some of the sample out of the tip remains intact with the Pos-D because of the pressure equalization. The Pos-D's large handle fits comfortably in the hand. An ergonomic finger-hook eliminates the need to grip the pipette firmly. The volume control setting faces the user.

Mettler Toledo
For information 800-472-4646
www.mt.com/RAININ-Pipettes

Hepatocyte Isolation

The Hepatocyte Isolation System provides reliable, convenient, and consistent hepatocyte cell isolation. The kit contains an optimized combination of enzymes to minimize lot-to-lot variation and improve the quality of the isolated hepatocytes. Each kit includes single-use enzyme vials, balanced salt solution, buffer, culture media, and a protocol for five adult rat liver perfusions. A modified protocol for mouse applications is also available.

Worthington Biochemical Corp.
For information 800-445-9603
www.worthington-biochem.com

Reactor Master

The Reactor Master is for automating jacketed reactor systems and data logging without the need for any PC software. Designed for use with synthesis equipment in chemical laboratories, the system can automate circulators or chillers, stirrers, thermocouples, and resistance temperature detectors from virtually any manufacturer via an easy-to-use control knob. Data can be viewed in real-time and exported for offline analysis. The Reactor Master Basic is controlled using a multifunction knob that allows set points, ramps, or sophisticated profiles for temperature and stirring speed. Data are continually saved as a CSV file that can be exported with a USB stick. The Reactor Master Pro features closed loop control of the circulator for a uniform reaction temperature. A software upgrade enables graphs to be generated with the click of a button. Both models are compatible with a wide range of thermoregulators, temperature sensors, overhead stirrers, pH meters, and turbidity systems.

Syrris
For information 516-312-3028
www.syrris.com

Electronically submit your new product description or product literature information! Go to **www.sciencemag.org/products/newproducts.dtl** for more information.

Newly offered instrumentation, apparatus, and laboratory materials of interest to researchers in all disciplines in academic, industrial, and governmental organizations are featured in this space. Emphasis is given to purpose, chief characteristics, and availabilty of products and materials. Endorsement by *Science* or AAAS of any products or materials mentioned is not implied. Additional information may be obtained from the manufacturer or supplier.

Associate or Full Professor

The Institute of Human Virology (IHV) and the Institute for Genome Sciences (IGS), in conjunction with the Marlene and Stewart Greenebaum Cancer Center at the University of Maryland School of Medicine, are searching for a faculty candidate to direct a new Division of Oncological Genomics. The new division will be located in the IHV and, coupled with full appointments in IHV and IGS, will have the ability to recruit junior faculty to support its mission. The appointment will be either at the Associate or Full Professor level, commensurate with experience.

The successful candidate will have extramural funding and a track record of conducting independent and collaborative research using approaches that include genomics and bioinformatics, as well as an interest in the field of cancer. The candidate will work closely with tumor cell biologists, molecular biologists, immunologists, and epidemiologists in the IHV to identify high-risk individuals and cancers that may have an infectious etiology. Particular emphasis will be placed on cancer associated with adventitious agents, especially viruses, and the candidate will use appropriate genomics and bioinformatics approaches to identify such agents in tumors, in the tumor microenvironment, and in individuals at high risk for specific cancers. The qualified individual will have publications utilizing genomics that may be applicable to human cancer. The cancers of interest in this institute are those occurring in the context of HIV or Hepatitis C infection and include cancer of the lung, kidney, liver, ovary, prostate, brain, leukemia, lymphoma and epithelial cells. The qualified individual will have familiarity with genomic applications such as transcriptional profiling, genotyping, tiling arrays, exon throughput assays, methylation, real time PCR, microRNA analyses and automated high throughput assays, and be aware of technology leading to detection of other agents, including possibly novel ones.

IHV and IGS offer excellent laboratory facilities, competitive salary and startup packages, and access to numerous resources within the School of Medicine, including state-of-the-art BSL3/ABSL3 facilities and a large-scale DNA sequencing and analysis core in a strong academic environment.

The faculty search committee will be co-chaired by **Dr. Robert Gallo**, Director of IHV, and **Dr. Claire Fraser-Liggett**, Director of IGS.

Please submit a letter of interest, CV, and three references to: **Oncologic Genomics Faculty Search Committee, c/o Beth Peterson, Institute of Human Virology, 725 West Lombard Street, S307, Baltimore, MD 21201; bpeterson@ihv.umaryland.edu**.

The University of Maryland, Baltimore is an Equal Opportunity, Affirmative Action Employer. Minorities, women, veterans and individuals with disabilities are encouraged to apply.

OPPORTUNITY FOR INDIAN SCIENTISTS IN ENERGY BIOSCIENCES
DEPARTMENT OF BIOTECHNOLOGY
MINISTRY OF SCIENCE & TECHNOLOGY
INDIA

Applications are invited for National "Energy Bioscience Chairs" AND "Energy Bioscience Overseas Fellowships" for Indian Scientists desirous of working at the forefront of Energy Biosciences in Indian Institutes of repute.

(A) Energy Bioscience Chairs

"Energy Bioscience Chairs" scheme is designed to attract excellent team leaders to conduct and provide leadership in research in area of bioenergy. The applicants should have expertise in Academic or Industrial Research & Development, in areas of Plant Molecular Biology, Enzymology, Biochemistry, Genetic Engineering, Downstream processing, Fermentation, Synthetic Biology or other related areas that are directly or indirectly involved in Energy Biosciences. Applicants should be **Indians or of Indian origin**, and should possess a higher degree like Ph.D. with outstanding track record and proven leadership. Scientists in the age group of 50-65 years and desirous of working in a chosen Indian Institution of repute are eligible.

(B) Energy Bioscience Overseas Fellowship

"Energy Bioscience Overseas Fellowships" is a re-entry scheme aimed at bringing back **bright young scientists of Indian origin** working out side the country in areas related to energy biosciences and who are desirous of returning to India and pursuing research in energy biosciences area in an Indian institution. Applicants should possess a PhD in relevant area and should have an outstanding track record reflected in publications and other achievements/recognitions.

(C) Tenure Positions at DBT-ICT Centre for Energy Biosciences

Applications are also invited for the following Tenure Positions in the Institute of Chemical Technology, Mumbai at the DBT-ICT Centre for Energy Biosciences. Reader in Microbiology (1 post); Reader in Fermentation Technology (1 post); Reader in Biochemistry (1 post); Lecturer in Metabolic Engineering (1 post); Research Scientist in Fermentation Technology (1 post); Research Scientist in Molecular/Structural Biology (1 post); Instrument Engineer (Spectroscopy) (1 post). UGC prescribed qualifications shall be applicable for candidates with science degree and AICTE prescribed qualifications shall be applicable for candidates having degree in technology.

Details of the three schemes and their respective application requirements and prescribed formats are available on DBT, India website and www.udct.org. Applications should be sent to **Prof. Arvind M. Lali, Coordinator, DBT-ICT-Centre for Energy Biosciences, Institute of Chemical Technology, Nathalal Parikh Marg, Matunga, Mumbai 400 019** India (email: **dbt.uict.ceb@gmail.com**) latest by **15th July 2009**.

NANYANG TECHNOLOGICAL UNIVERSITY

The Nanyang Technological University, Singapore, invites applications for the following position:

DEAN, COLLEGE OF ENGINEERING

About Singapore

Singapore is a centre of new and exciting academic opportunities. Targets for the development of Singapore as a world centre for academic excellence have been set and this has been supported by major public sector investments which give traction to the further development of a vibrant environment for higher education and research. Singapore has also been able to establish lasting and synergistic business and academic relationships with China, India and other South East Asian countries.

About the University

Nanyang Technological University (NTU) is an internationally reputed research-intensive university with globally acknowledged strengths in Science, Engineering and Technology. Currently ranked 26th among technology universities, and well within the top 100 among the comprehensive universities by the Times Higher Education-QS World University Rankings, the university's academic and research programmes, with real-world relevance, have reaped dividends in the form of strong support from major corporations and industry leaders, in terms of both research funding and partnerships and global internship opportunities for the students.

The University provides a high-quality comprehensive and global education to more than 21,700 undergraduates and 9,400 graduate students. Together with the university's 2,700-strong faculty and research staff who bring international academic perspectives and depth of experience, the University's main 200-ha residential and garden campus, located at the south-western part of Singapore, is an international hub of academic vibrancy and endeavors.

About the College

NTU has four colleges - College of Engineering; College of Science; College of Business; College of Humanities, Arts and Social Sciences - with 12 component schools. The College of Engineering is one of the largest engineering colleges in the world, consisting of six schools, 16,000 students, 600 faculty and 1,200 staff. The six constituent schools are the School of Electrical and Electronic Engineering, School of Chemical and Biomedical Engineering, the School of Computer Engineering, the School of Civil and Environmental Engineering, the School of Materials Science and Engineering and the School of Mechanical and Aerospace Engineering.

The College enjoys a growing reputation for its multidisciplinary academic pursuits and research enterprises, achieved through constant diligence in striving for excellence and effective use of resources. Some of the research firsts and breakthroughs developed at the College include the World's Smallest Integrated Circuit Transformer, the World's First Diode pumped Yb:Y2O3 Ceramic Lasers and the World's First Multiple Drug-eluting Biodegradable Stent.

In 2008, the College won four prestigious Competitive Research Program grants from the Singapore National Research Foundation totalling USD24 million in Photonics, Clean Energy and EWT, Biomedical Devices and Printed Carbon Nanotubes. An institute in Environment & Water Technology has won USD55 million over a 3-year period. Another major strength in Nanoscience & Nanotechnology has garnered USD20 million since 2007. More information on the College can be accessed at the following website: http://coe.ntu.edu.sg/Pages/CoEHome.aspx.

About the Appointment

The University is seeking an accomplished, visionary and pragmatic academic leader for the position of the Dean of the College of Engineering, who will also be appointed as a tenured professor. This is an outstanding opportunity for an individual who is passionate about growing and strengthening a dynamic College, and taking it to greater heights of research and teaching excellence and scholarly achievements.

Reporting to the Provost, the Dean will provide foundational vision, leadership and oversight for the strategic, academic, intellectual and administrative affairs of the College and its constituent Schools. Essential responsibilities include sharpening and directing the College's focus to align with the University's mission and strategic directions, cultivating areas of academic and research excellence, providing leadership in fundraising through cooperation with the University's Development Office and strengthening ties with alumni, stakeholders, community partners, external organizations and industry to raise the College's profile and standing. The Dean is also a member of the University Cabinet, the highest decision making body of the faculty and a number of Provost and University's senior leadership committees and teams.

The appointee must have an outstanding record of academic leadership, research and teaching in a reputable University or academic institution. The appointee must demonstrate vision and the ability to raise the reputation of the College and to enhance its existing research and teaching strengths. Other essential attributes include, excellent ability to communicate and work collaboratively on inter-disciplinary research, with faculty and, students, both intra-university and externally, and a commitment to faculty-shared governance.

To apply, please send curriculum vitae, accompanied by a cover letter, to:

The Chairman of the Search Committee,
Professor Haresh Shah

c/o Office of Human Resources
Nanyang Technological University
Level 4, Administration Building
50, Nanyang Avenue
Singapore 639798

Fax: (65) 67919340
Email: CHRO@NTU.EDU.SG

Closing Date: 31 August 2009

All applications and materials submitted will be held in strict confidence.

STANFORD ENGINEERING

Department of Mechanical Engineering
Stanford University
Faculty Opening

The Department of Mechanical Engineering at Stanford University (**http://me.stanford.edu/**) invites applications for a tenure-track assistant and/or untenured associate professor faculty position opening. We give high priority to the overall originality and promise of the candidate's work rather than the candidate's area of specialization within mechanical engineering.

We seek applicants relevant to any area of mechanical engineering including, but not limited to, controls, energy systems and sciences, biomechanics and biological transport, propulsion systems and sciences, and nanotechnology. An earned Ph.D., evidence of the ability to pursue a program of research, and a strong commitment to graduate and undergraduate teaching are required. The successful candidate will be expected to teach courses at the graduate and undergraduate levels and to build and lead a team of graduate students in Ph.D. research.

Applications should include a curriculum vitae with a list of publications, a one-page statement each of research vision and teaching interests, and the names and addresses of five references. Please submit your application online at:

http://me.stanford.edu/research/open_positions.html

The review of applications will begin on **September 21, 2009**. However, applications will be accepted until the position is filled.

Stanford University is an Equal Opportunity Employer and is committed to increasing the diversity of its faculty. It welcomes nominations of and applications from women and members of minority groups, as well as others who would bring additional dimensions to the university's research and teaching missions.

BIOZENTRUM Universität Basel

UNI BASEL

OPPORTUNITIES FOR EXCELLENCE

International PhD program at the BIOZENTRUM University of Basel, Switzerland

The **Biozentrum** together with the **Werner Siemens - Foundation (WSF)** launches the **International PhD program** in **Molecular Life Sciences** and encourages excellent students to apply for one of the prestigious WSF fellowships.

The Biozentrum provides an internationally renowned research environment centered around three focal areas (Infection Biology, Growth and Development, Neurobiology) and two core programs (Structural Biology & Biophysics and Computational & Systems Biology) and is dedicated to basic molecular and biomedical research (http://www.biozentrum.unibas.ch/). We offer advanced Interdisciplinary training in the field of modern biology, a lively and interactive educational atmosphere, and competitive salaries with respect to European standards. University graduates admitted to the program receive theoretical and practical training and conduct a three-year research project under the supervision of a Biozentrum faculty member, monitored by a Thesis Advisory Committee.

Basel is an international center for biology research with major academic life science institutes and a high density of globally operating biotech companies.

Applications to the PhD fellowship program have to be submitted online. Application forms, requirements, and additional information can be found at: **http://www.biozentrum.unibas.ch/phd/.**

Application deadline: June 30, 2009.

The **Genomics Institute of the Novartis Research Foundation** (**GNF**), located in the Torrey Pines area of San Diego, CA, is funded by the Novartis Research Foundation and dedicated to the development and application of new methods and techniques for genome-wide biological discovery and biomedical research. GNF provides a unique and challenging opportunity to combine exploratory biomedical research with pharmaceutical drug development in a highly interactive, multidisciplinary environment and state-of-the-art facilities. GNF is expanding our drug discovery and research efforts in Type I diabetes and is seeking applicants with relevant experience to join our efforts to identify novel treatments for this disease.

Biology (*multiple positions available: Postdoctoral Fellows, Scientific Associates, and Research Investigators*); **Job Code:** JTBio: We are seeking self-motivated individuals with a Ph.D. or B.S./M.S. with a demonstrated record of scientific achievement in the field of pancreatic beta cell biology or autoimmunity to join our Diabetes research and drug discovery team. Successful candidates will play an important role in identifying and validating new approaches in beta cell protection, regeneration and proliferation, and/or autoimmune responses in Type I diabetes. An in-depth understanding of the biology of beta cells is required. Experience in preclinical drug discovery, animal models of autoimmune diseases, diabetes and/or cell transplantation are a plus.

Chemistry (*multiple positions available: Postdoctoral Fellows, Scientific Associates, and Research Investigators*): **Job Code:** JTChem: We are seeking self-motivated individuals with a Ph.D. or B.S./M.S. with 0 to 4 years drug discovery experience to join our Medicinal Chemistry group focusing on Diabetes and regenerative medicine applications. Preferred candidates will have a strong commitment to bench chemistry and will carry out SAR studies and compound optimization, scale up of lead molecules, and tool compound synthesis for target validation and identification. Must have experience in synthetic organic chemistry, and/or medicinal/pharmaceutical chemistry. Knowledge of pharmacokinetics and diabetes/regenerative medicine drug discovery is a plus.

Visit our website: **http://www.gnf.org** for complete list of employment opportunities. GNF offers excellent compensation and a great benefits package. **Fax 858/812-1670**, or submit online to **jobs@gnf.org**. Resumes must include a Job Code for consideration. **10675 John Jay Hopkins Drive, San Diego, CA 92121**.

Equal Opportunity Employer.

Full and Associate Professor Positions at Fudan School of Life Sciences

Fudan University School of Life Sciences (SLS; **http://life.fudan.edu.cn/english/**) at Shanghai, China, plans to recruit faculty members at the levels of **Full Professor** and **Associate Professor**. The current SLS faculty members conduct research in areas of Biochemistry, Bioinformatics and Evolution, Biophysics, Biostatistics, Cell and Developmental Biology, Ecology and Biodiversity, Genetics, Human Biology, Microbiology, and Plant Biology. SLS has the State Key Laboratory of Genetic Engineering, with support from the Chinese Central Government and two Key Laboratories of the Ministry of Education: one in Human Biology and another in Biodiversity and Ecology. In addition, several research institutes have been established to promote research and education, including the Institute of Genetics, the Institute of Biodiversity, and the recently established Institute of Plant Biology. Furthermore, the Institute of Developmental Biology and Molecular Medicine (IDM; **http://life.fudan.edu.cn/idm/index_%20En.html**) is affiliated with SLS, with joint faculty appointments and a shared graduate program. IDM has leading research programs and state-of-art facilities for mouse developmental genetics and other model organisms. SLS is in a major phase of expansion, with plans to recruit 10-20 faculty members in the next 3-5 years, in anticipation of a new Life Sciences Building of over 35 thousand square meters.

Candidates must have a Ph.D. or equivalent degree and have post-doctoral training, preferably in one or more of the current areas at SLS; experiences as faculty members and in teaching animal biology, biochemistry, cell biology, and/or plant biology are highly desirable. Salary and support will depend on experience and accomplishments in research, teaching and professional service. Established scientists/educators are especially encouraged to apply for positions with appointments of the "Cheung Kong Professorship" or the newly initiated "National Professorship" (so-called "1000 person" program). Applications will be reviewed as they are received. Applicants should first submit (1) a letter of application, (2) a detailed CV, and (3) research and teaching plans to **Ms. Lei Jiang** (**lifesciences@fudan.edu.cn**) and **Prof. Hong Ma** (**hongma@fudan.edu.cn**). Candidates in appropriate areas are welcome to apply for joint appointments in IDM, and should also contact **Ms. Lizhen Qiu** (**idm@fudan.edu.cn**).

AWARDS

Boehringer Ingelheim

Canadian Young Investigator Award

The recipient of the 2009 Boehringer Ingelheim Canadian Young Investigator Award in Biological Sciences is:

Dr. Anthony Gramolini
Department of Physiology
Heart and Stroke / Richard Lewar Centre
University of Toronto

anthony.gramolini@utoronto.ca

Dr. Gramolini's research currently centers on the cellular mechanisms that lead to the proper formation of the sarcoplasmic reticulum, and the involvement of the sarcoplasmic reticulum in heart failure. He uses molecular and cellular approaches, including advanced proteomic and genomic methods, to investigate the physiology and biochemistry of key calcium regulatory proteins in cardiac and skeletal muscle with the objective of identifying novel approaches to the diagnosis and treatment of cardiac disease.

The R&D division of Boehringer Ingelheim Canada Ltd. is one of Canada's largest pharmaceutical research centres. One of our important corporate policies is to support and encourage basic research in Canadian universities. To this end, we have established the Boehringer Ingelheim Young Investigator Award in Biological Sciences. The award is made annually to a new faculty member conducting biological research in a Canadian university, and consists of an unrestricted three-year research grant.

Previous recipients

2008 **Dr. Marie Kmita**, Université de Montréal
2007 **Dr. Zhong-Ping Feng**, Department of Physiology, University of Toronto
2006 **Dr. Hao Ding**, Department of Biochemistry and Medical Genetics, University of Manitoba
2005 **Dr. John H. Brumell**, University of Toronto

Visit our ENHANCED WEBSITE!

Revealing your vision to employers is our job. We're your source for connecting with top employers in industry, academia, and government. We're the experts and entry point to the latest and most relevant career information across the globe.

Our newly designed website offers a set of tools that reveal career opportunities and your personal potential. Whether you're seeking a new job, career advancement in your chosen field, or ways to stay current on industry trends, *Science* Careers is your window to a limitless future.

Improved Website Features:

- Relevant Job E-mail Alerts
- Improved Resume Uploading
- Content Specific Multimedia Section
- Facebook Profile

Job Search Functionality:

- Save and Sort Jobs
- Track Your Activity
- Search by Geography
- Enhanced Job Sorting

Your Future Awaits.

Science Careers

From the journal *Science* AAAS

ScienceCareers.org

POSITIONS OPEN

The University of Texas Health Science Center at Houston

BIOSTATISTICIAN
Tenure-Track Faculty Position

The University of Texas Health Science Center at Houston, Department of Neurosurgery, is seeking a faculty biostatistician for a position at the **ASSISTANT** or **ASSOCIATE PROFESSOR** level, commensurate with experience. Our Department is conducting several human clinical trials in a 32-bed neurological intensive care unit, and maintains laboratories studying neurological diseases utilizing genetic and proteomic analysis. We also test therapeutic approaches using animal models, and we have a significant effort utilizing stem cells. The successful candidate will provide statistical design and planning for experiments and clinical trials, then work with other faculty members in implementation. She/he will also analyze data. Join a department with 15-plus clinical faculty and 10-plus research faculty with programs affiliated with Memorial Hermann Hospital and Mischer Neuroscience Institute. Applicants should hold a Ph.D. in statistics, or a related field.

Candidates interested in applying should forward their curriculum vitae and three references to:

Dong H. Kim, M.D.
Professor and Chair
Department of Neurosurgery
6431 Fannin Street, MSB 7.146
Houston, TX 77030
E-mail: dann.voss@uth.tmc.edu

The University of Texas Health Science Center at Houston is an Equal Opportunity/Affirmative Action Employer, Minorities/Females/Persons with Disabilities/Veterans.

POSTDOCTORAL POSITIONS available for recent graduates with Ph.D. and/or M.D. degrees with a commitment to research careers in diabetes and related diseases. Studies are being conducted in the areas of islet biology and transplantation, beta cell proliferation, endodermally derived endocrine tissue, immune tolerance and histocompatibility molecules in type 1 diabetes, electrophysiology of ATP-sensitive potassium channels, insulin resistance in aging, diabetic neuropathy, insulin signaling, glucose transporters, lipid synthesis, metabolism, vascular diseases, pregnancy loss and malformations in diabetes. Send curriculum vitae to: **Dr. Michael L. McDaniel, Department of Pathology and Immunology, Campus Box 8118, Washington University School of Medicine, St. Louis, MO 63110. E-mail: mmcdaniel@wustl.edu.** *Affirmative Action/Equal Opportunity Employer.*

POSTDOCTORAL POSITION available in the laboratory of **Dr. Venigalla Rao,** Biology Department, The Catholic University of America, Washington, D.C., to work on the structure and mechanisms of virus assembly and DNA packaging in bacteriophage T4 (**website: http://faculty.cua.edu/rao/**). Research involves recombinant DNA construction, protein purification, and mutagenesis. Candidate will have Ph.D. in biological sciences and strong background in molecular biology and biochemistry. Send curriculum vitae and names of three references electronically to **e-mail: rao@cua.edu.** *Catholic University is an Equal Opportunity Employer.*

POSITIONS OPEN

The University of Texas Health Science Center at Houston

TWO TENURE-TRACK FACULTY POSITIONS
Stem Cell Biology

The University of Texas Health Science Center at Houston (UTHSC), Department of Neurosurgery, is seeking two faculty members working on stem cell biology, at the **ASSISTANT** or **ASSOCIATE PROFESSOR** level, commensurate with experience. We are recruiting for two outstanding scientists, working in two specific areas. The first faculty member will have extensive experience with induced pluripotent stem cells (IPS). Ideally, she/he will establish a research program using patient-derived IPS cells to study disease mechanisms and test therapeutic strategies. The second scientist will work on novel technologies to image the migration and differentiation of stem cells in vivo. The successful candidates will get excellent startup packages, and join the UT Center for Regenerative Medicine, collaborating with eight-plus faculty members already working on stem cell therapy for neurological and cardiac diseases. The candidates will also have access to a GMP facility and will work with clinicians already conducting human stem cell trials for stroke and neurotrauma at Memorial Hermann Hospital and the Mischer Neuroscience Institute.

Candidates interested in applying should forward their curriculum vitae and three references to:

Dong H. Kim, M.D.
Professor and Chair
Department of Neurosurgery
6431 Fannin Street, MSB 7.146
Houston, TX 77030
E-mail: dann.voss@uth.tmc.edu

The University of Texas Health Science Center at Houston is an Equal Opportunity/Affirmative Action Employer, Minorities/Females/Persons with Disabilities/Veterans.

The University of Texas Health Science Center at Houston

TWO TENURE-TRACK FACULTY POSITIONS
Cerebrovascular Biology

The University of Texas Health Science Center at Houston (UTHSC), Department of Neurosurgery, is seeking two faculty members working on cerebrovascular biology at the **ASSISTANT** or **ASSOCIATE PROFESSOR** level, commensurate with experience. We are recruiting for outstanding scientists, working in any area of cerebrovascular biology, from molecular approaches using in vitro models to physiological approaches using in vivo models. Vascular biologists working in clinical areas are also encouraged to apply. The successful candidates will get excellent startup packages, and have access to state-of-the-art technical resources within the Department and UTHSC and the various institutions of the Texas Medical Center. Examples include an advanced stem cell center, including a GMP facility. The successful candidates will also have access to human samples, from DNA to serum to cerebrospinal fluid, and collaborate with established clinicians treating a high volume of patients with cerebrovascular disease. Join a department with 15-plus clinical faculty and 10-plus research faculty with programs affiliated with Memorial Hermann Hospital and the Mischer Neuroscience Institute.

Candidates interested in applying should forward their curriculum vitae and three references to:

Dong H. Kim, M.D.
Professor and Chair
Department of Neurosurgery
6431 Fannin Street, MSB 7.146
Houston, TX 77030
E-mail: dann.voss@uth.tmc.edu

The University of Texas Health Science Center at Houston is an Equal Opportunity/Affirmative Action Employer, Minorities/Females/Persons with Disabilities/Veterans.

POSITIONS OPEN

The University of Texas Health Science Center at Houston

TWO TENURE-TRACK FACULTY POSITIONS
Cerebrovascular Imaging and Cerebrovascular Physiology

The University of Texas Health Science Center at Houston (UTHSC), Department of Neurosurgery, is seeking two faculty members focused on advanced neuroimaging techniques at the **ASSISTANT** or **ASSOCIATE PROFESSOR** level, commensurate with experience. We are recruiting for an expert using high-strength magnetic resonance imaging (MRI) to visualize small cerebral arteries. We are also looking for an expert working on novel methodologies to measure cerebral blood flow. The successful candidates will get excellent startup packages, and have access to outstanding technical resources. We have a state-of-the art, research-dedicated human 3T Philips scanner, with an 80 mT/m gradient system, 32-channel receiver, multichannel RF coils, and an In Vivo Eloquence System for functional MRI. We also have a Bruker 7T animal-dedicated MRI scanner.

These faculty members will work in the new six-story, 315,000-square-foot Center for Advanced Biomedical Imaging Research (CABIR). A collaboration between UTHSC, The University of Texas M. D. Anderson Cancer Center, and GE Healthcare, CABIR will house state-of-the-art research laboratories for synthetic and analytical chemistry, biochemistry, and molecular and cellular biology and facilities for production of clinical-grade imaging agents such as radiopharmaceuticals, nanoparticle-based agents, gene-reporter and cellular tracers. The facility will accommodate a translational imaging core that will include technologies supplied by GE Healthcare. The core will include a cyclotron, radiochemistry modules for production and labeling with radionuclides, a combination positron emission tomography (PET)/computed tomography (CT) unit, a volume CT unit, and an MRI unit. Join a department with 15-plus clinical faculty and 10-plus research faculty with programs affiliated with Memorial Hermann Hospital and the Mischer Neuroscience Institute.

Candidates interested in applying should forward their curriculum vitae and three references to:

Dong H. Kim, M.D.
Professor and Chair
Department of Neurosurgery
6431 Fannin Street, MSB 7.146
Houston, TX 77030
E-mail: dann.voss@uth.tmc.edu

The University of Texas Health Science Center at Houston is an Equal Opportunity/Affirmative Action Employer, Minorities/Females/Persons with Disabilities/Veterans.

POSTDOCTORAL POSITIONS
Infectious Disease Pathogenesis/Immunology
Yale University School of Medicine

Positions available to study the interactions between pathogens, arthropod vectors, and the mammalian host. *Borrelia burgdorferi, Anaplasma phagocytophilum,* West Nile virus, and *Plasmodium falciparum* will be among the model organisms. Experience in microbial pathogenesis, immunobiology, cell biology, or molecular biology necessary.

Send curriculum vitae and recent publications to: **Erol Fikrig, M.D., Investigator, Howard Hughes Medical Institute, Yale University School of Medicine, Section of Infectious Diseases, P.O. Box 208022, New Haven, CT 06520-8022. Or e-mail: erol.fikrig@yale.edu.** *Yale University is an Affirmative Action, Equal Opportunity Employer. Applications from women and minorities are encouraged.*

MARKETPLACE

Call for Papers

Submit your research now to be one of the first to be considered for publication in the **inaugural issue** of *Science Translational Medicine!*

Science Translational Medicine, to be published online weekly beginning in the fourth quarter 2009, focuses on the conversion of basic biomedical research into practical applications, thus bridging the research-to-application gap.

The editors of ***Science Translational Medicine*** are accepting manuscripts for review in the following areas:
cancer, cardiovascular disease, metabolism/diabetes/obesity, neuroscience/neurology/psychiatry, immunology/vaccines, infectious diseases, policy, behavior, bioengineering, physics, chemical genomics/drug discovery, imaging, applied physical sciences, medical nanotechnology, drug delivery, biomarkers, gene therapy/regenerative medicine, toxicology and pharmacokinetics, data mining, cell culture, animal, and human studies, medical informatics, and other interdisciplinary approaches to medicine.

Review the information for authors at http://sciencemag.org/marketing/stm/papers.dtl

Recommend a subscription to your library: www.sciencemag.org/cgi/recommend_subscription

Submit your research at www.submit2scitranslmed.org

For more information, contact Editor Katrina Kelner, Ph.D. at scitranslmededitors@aaas.org

Science Translational Medicine
AAAS

Integrating Medicine and Science

www.ScienceTranslationalMedicine.org

How can a bottle change your culture?

Angled neck makes pipetting and pouring easier

Wider mouth reduces chance of pipette touching sides

Narrower for easier storage and handling

Large label gives plenty of room to write

Make lab work less work with the new GIBCO® bottle. It's angled for comfort, built to fit in the fridge, and designed with plenty of room to make it your own. Change your culture at **www.invitrogen.com/gibcobottle**

invitrogen™ | GIBCO®